Fakultät für Physik und Astronomie

Ruprecht-Karls-Universität Heidelberg

Diplomarbeit

Im Studiengang Physik

vorgelegt von

Michael Lubasch

aus Bad Schwalbach

2009

Quantum chaos and entanglement in the Bose-Hubbard model

Die Diplomarbeit wurde von Michael Lubasch
ausgeführt am
Institut für Theoretische Physik in Heidelberg
unter der Betreuung von
Herrn Dr. Sandro Wimberger

Quantum chaos and entanglement in the Bose-Hubbard model:
This thesis presents a study of novel measures of quantum correlations for the standard Bose-Hubbard model. We investigate this model in the regime of finite fillings and system sizes, for which regular and quantum chaotic behaviour is known.

In the first place we review previously applied measures borrowed from quantum chaos theory, and we extend and discuss the usefulness of the fidelity measure (the scalar product of two identical states propagated by slightly different Hamiltonians) for the detection of avoided crossings and hence for distinguishing the different dynamical regimes.

The main part is devoted to the search for appropriate definitions of many-particle entanglement in the model. We propose several measures whose parameter and time dependence in the regular and the chaotic range is thoroughly studied, and which - as we hope - will help to clarify the lively discussion in the literature of characterizing quantum correlations for indistinguishable bosons by entanglement measures.

Quantenchaos und Verschränkung im Bose-Hubbard Modell:
Gegenstand der Arbeit ist die Untersuchung neuer Quantenkorrelationsmaße für das Bose-Hubbard Modell. Wir betrachten dieses Modell im Bereich endlicher Besetzung und Systemgröße, für welchen reguläres und quantenchaotisches Verhalten bekannt ist.

Zunächst einmal besprechen wir bereits verwendete Maße aus der Quantenchaostheorie, und wir erweitern und diskutieren die Nützlichkeit des Fidelity-Maßes (das Skalarprodukt zweier identischer Zustände, die mit zwei wenig unterschiedlichen Hamiltonians propagiert werden) für die Detektion von Avoided-Crossings und damit für die Unterscheidung der verschiedenen dynamischen Regime.

Der Hauptteil ist der Suche nach geeigneten Definitionen von Viel-Teilchen-Verschränkung in dem Modell gewidmet. Wir stellen mehrere Maße vor, deren Parameter- und Zeitabhängigkeit im regulären und im chaotischen Bereich ausgiebig untersucht wird, und welche - wie wir hoffen - zur Klärung der in der Literatur stattfindendenden Debatte bezüglich der Charakterisierung von Quantenkorrelationen bei ununterscheidbare Bosonen mittels Verschränkungsmaßen beitragen.

Contents

Chapter 1

Introduction

Since the first realization of a Bose-Einstein condensate in 1995 [1] ultracold atoms have turned into a common field of research. Owing to groundbreaking discoveries in cooling atoms down to the lowest accessible temperatures experimental groups are able to generate BECs within minutes, and by means of different kinds of traps they have almost perfect control over this quantum system [2, 3]. On the one hand it is the extremely low temperatures of the order of some nanokelvin that lead to the emergence of the fundamental quantum world and its nonclassical phenomena. On the other hand it is the high degree of control which allows a precise experimental probe of theoretical predictions. Among the numerous experiments carried out with BECs we chronologically want to mention the storing of the quantum state of a light pulse in a condensate [4], the realization of a BEC on an atom chip [5], the investigation of a quantum phase transition between a Mott insulating and a superfluid phase [6], the formation of Cooper pairs by fermionic atoms in the BCS-BEC crossover regime [7], the demonstration of the indistinguishability of ultracold atoms [8] and the observation of entanglement in a BEC [9].

The Bose-Hubbard model describes ultracold bosons in an optical lattice. It particularly well models ultracold bosons in sufficiently deep lattices since it neglects the intra-well dynamics in the lattice. The Bose-Hubbard model is a second quantized quantum many-body model in Fock formalism in contrast to the probably more prominent Gross-Pitaevskii equation, which is a wave equation for a many-particle wave function and a mean field approach. While the Bose-Hubbard model in a sense allows for an exact description of ultracold bosons in deep lattices because it is correct for all coupling strengths, the Gross-Pitaevskii equation is valid only in a limited regime of small coupling strength and semiclassically large fillings. The Bose-Hubbard model has a quantum phase transition between a superfluid and a Mott insulating phase [10]. A quantum phase transition is a phase transition that takes place at absolute zero which is why it is not driven by thermal but by quantum fluctuations. It was first pointed out by *Jaksch et al.* that all theoretical parameters of the Bose-Hubbard model can be tuned experimentally in a wide range [11]. Thus the model can be simulated by a real-life physical system, circumventing the numerical problems related to the exponentially growing state space with particle number. This

was termed quantum simulation by *Feynman* in 1982 [12] and so the Bose-Hubbard model is a paradigm for quantum simulation. Moreover the Bose-Hubbard model is a frequently discussed scheme for quantum computation [13, 14, 15, 16] due to the high degree of control achievable over ultracold bosons in optical lattices.

It was first shown by *Kolovsky* and *Buchleitner* that the Bose-Hubbard model exhibits quantum chaos in its spectral statistics [17], and we will search for further signatures of quantum chaos in this thesis. Quantum chaos denotes the quantum mechanics of classically chaotic systems [18]. One might now be misled to believe that quantum chaos can only be applied to quantum mechanical systems that have a clear classical counterpart. However today it can be used without ever thinking of the classical limit. This is due to remarkable theoretical and experimental discoveries in this fascinating field revealing universal laws that hold independently of the specific system. Both for the spectrum and for the dynamics indicators for the regular and the chaotic regime have been derived and experimentally confirmed.

Whether a classical system is chaotic or not determines if reliable predictions for its future evolution can be made. More formally classical chaos is defined in phase space [19]. Starting a propagation of the system at two nearby points, if the distance between the two resulting trajectories grows exponentially in time the system shows chaos. This exponential growth is characterized by the Lyapunov exponent.

The lack of a classical trajectory in quantum mechanics poses the question of how to assign chaos in these systems. At first glance one would propagate two slightly different wave functions $|\psi\rangle$ and $|\phi\rangle$ and look at their scalar product $|\langle\psi(t)|\phi(t)\rangle|^2$. However, if they evolve with the same Hamiltonian this scalar product is just constant over time,

$$|\langle\psi(t)|\phi(t)\rangle|^2 = |\langle\psi(0)|U^\dagger(t)U(t)|\phi(0)\rangle|^2 = |\langle\psi(0)|\phi(0)\rangle|^2 \quad ,$$

and so this approach does not work.

Surprisingly today one fundamental approach to quantum chaos is via random matrix theory, a method not applicable to classical systems in the same way that the classical notion of chaos is not applicable to quantum systems. Random matrices are matrices with randomly chosen entries that obey a certain probability distribution. Initially this theory was introduced by *Wigner* to compare spectra of atomic nuclei. Due to the complexity of the nucleus its spectrum cannot easily be computed directly. However, the spectral statistics of certain random matrices match the ones of atomic nuclei. More precisely the distribution of level spacings, i.e. the distance between neighbouring energy levels in the spectrum, of random matrices can be the same - in a statistical sense - as the distribution of level spacings of atomic nuclei. Random matrices also permit the distinction between regular and chaotic regimes in quantum systems by looking at the distribution of level spacings in the spectrum [20, 21]. In short, regular spectra are characterized by many vanishing level spacings, i.e. many crossing energy levels in the spectrum, and these are usually referred to as level crossings [22]. In contrast, chaotic spectra are characterized by the lack of

vanishing level spacings and the presence of many dense lying avoided crossings. Avoided crossings are energy levels that come very close to each other but never cross [22].

Nonintegrability is another property of classically chaotic systems and it allows for a much simpler connection between classical and quantum chaos. A classical system is called integrable if there exist as many constants of motion as there exist degrees of freedom. E.g. the classical 1-dimensional harmonic oscillator is integrable since energy is conserved and it has only one degree of freedom. The constants of motion of the problem can be found by separating the Hamilton-Jacobi equation, and if it is completely separable the problem is integrable. An alternative is to search for symmetries in the Lagrangian and then apply Noether's theorem. These considerations can be directly adopted to the quantum case. A quantum system is then called integrable if there exist as many quantum numbers as there are degrees of freedom [23]. Again separation of the Schrödinger equation or symmetries in the Lagrangian reveal the quantum numbers. Hence all energy levels of a quantum integrable system are independent of another.

Besides the spectrum the dynamics can also be used to differentiate between the regular and the chaotic regime. Here one looks at the time behaviour of the so-called fidelity which is the scalar product of two initially identical states that propagate under different Hamiltonians. Usually the Hamiltonian has one parameter λ and one wants to know for which values of λ the system is regular or chaotic. Then

$$F(t) \quad := \quad |\langle \psi_\lambda(t) | \psi_{\lambda+\epsilon}(t) \rangle|^2$$

for $\epsilon \ll 1$ is the studied fidelity. The decay of this fidelity might then allow the distinction of the two regimes [24]. The decay can be theoretically approximated for the regular and for the chaotic regime if a semiclassical limit exists. We finally want to emphasize that this fidelity represents a close link between classical and quantum chaos, and one would expect its decay to be exponential in the chaotic regime. Even though this can be the case, in general the decay of the fidelity in the chaotic regime is different and depends on the system under consideration. So the connection between classical and quantum chaos is much more intricate.

In this thesis we want to address the question if the regular and the chaotic regime of the Bose-Hubbard model can be separated by their entanglement properties. Quantum entanglement denotes genuinely non-classical quantum correlations between physical systems [25]. It is today widely believed that entanglement plays an important role in quantum phase transitions [26, 27, 28, 29]. Apart from that entanglement is also regarded to be an essential ingredient in quantum computation, quantum information and quantum cryptography [30]. As already mentioned the Bose-Hubbard model offers both a quantum phase transition and the possibility for quantum computation.

It was *Schrödinger* in 1935 who coined the term entanglement and gave a very farsighted definition:
"*When two systems, of which we know the states by their respective representatives, enter into temporary physical interaction due to known forces between*

them, and when after a time of mutual influence the systems separate again, then they can no longer be described in the same way as before, viz. by endowing each of them with a representative of its own. I would not call that one but rather the characteristic trait of quantum mechanics, the one that enforces its entire departure from classical lines of thought. By the interaction the two representatives have become entangled" - from [31].
This historical statement names quantum mechanical interaction to be the necessary ingredient for entanglement and foreshadows the philosophical debate that is going to follow its discovery.

In 1964 *Bell* presented his seminal Bell's equations [32], a set of inequalities that hold for local hidden variable theories and hence for the concept of local realism. Bell's inequalities finally provided a means of experimentally disproving local realism because experiments simply had to show that quantum mechanics can violate Bell's inequalities. To this day numerous experiments have proved that quantum mechanics violates Bell's inequalities and so either locality or realism or both are the wrong concept for nature. Entangled states are necessary for this violation to happen demonstrating again the outstanding role of entanglement. Indeed, Bell's inequalities are maximally violated by the *maximally entangled* Bell states

$$\begin{aligned} |\Phi^+\rangle &= \frac{1}{\sqrt{2}}(|00\rangle + |11\rangle) \\ |\Phi^-\rangle &= \frac{1}{\sqrt{2}}(|00\rangle - |11\rangle) \\ |\Psi^+\rangle &= \frac{1}{\sqrt{2}}(|01\rangle + |10\rangle) \\ |\Psi^-\rangle &= \frac{1}{\sqrt{2}}(|01\rangle - |10\rangle) \qquad . \end{aligned}$$

Bell's inequalities were the first attempt to *quantify entanglement*. Since then the quantification of entanglement has developed its own branch of physics as so-called entanglement theory. Entanglement theory is the theory of entanglement measures. The latter are mostly defined as scalar quantities that in the end shall be able to order all possible states with respect to their entanglement [33]. However, one single unique definition of entanglement does not exist. Rather there exist *many entanglement measures* that differ in their interpretation as well as in their computability and indeed these two aspects seem to counteract. Entanglement measures that have a highly reasonable interpretation turn out to be not computable efficiently, while other entanglement measures that are efficiently computable often lack a sensible interpretation. The current status of entanglement theory is that the entanglement properties of pure bipartite states of any finite dimension can be well managed interpretationally and computationally. This is also true for bipartite mixed states of lowest dimension, i.e. mixed states of two qubits. However, if one goes in either of the two directions of multipartite or higher-dimensional mixed states one still finds many open questions. We remark that always the decision of what the entangled entities shall be determines the proper entanglement measure. Another area of entanglement theory with many open questions is concerned with entanglement in

quantum many-body systems [34]. Here the particles are indistinguishable and the common description is the Fock formalism.

In this thesis we propose to introduce the term chaotic entanglement for entanglement properties of the chaotic regime. Chaotic entanglement links quantum chaos and entanglement. There is, however, a big conceptual difference between quantum chaos and entanglement. While the former strictly speaking only follows from classical chaos in the classical analogue to the system under consideration, the latter is a purely quantum mechanical phenomenon nonexistent in the classical analogue. In fact, as discussed above quantum entanglement is defined to be exactly the non-classical part of the total correlations. In this context a natural question is if chaotic entanglement is as valuable as regular entanglement, e.g. for practical use in a quantum computer.

We conclude our introduction with an outline of this diploma thesis. In **Chapter 2** we will thoroughly describe the Bose-Hubbard model. This chapter includes a derivation of the canonical representations of the model, a discussion of its symmetries and a brief introduction to its experimental realization. In **Chapter 3** we will investigate quantum chaos in the Bose-Hubbard model by means of the fidelity. First we will study its decay, second we will use the fidelity to define a new function for the unique quantification of avoided crossings, and third we will apply that new function to obtain the distribution of avoided crossings in the spectrum. In **Chapter 4** we will then be concerned with quantum entanglement in the Bose-Hubbard model. Since the notion of entanglement in quantum many-body systems is still controversely discussed, it is necessary to thoroughly introduce standard entanglement theory, which we will do in the first part of this chapter. There we will also work out the arising problems if the particles are indistinguishable or if the Fock formalism is used. In the second part we will briefly discuss the relation between single-copy and asymptotic entanglement. We will derive our own approach to entanglement in systems of indistinguishable bosons in the third part. This will enable us to investigate the quantum phase transition in the Bose-Hubbard model. In the final fourth part we will discuss the generation of practically useful entanglement in the Bose-Hubbard model. We will address chaotic entanglement in **Chapter 5**. There we will first look at the static entanglement properties of the eigenstates and then at the dynamic entanglement properties of propagating states. In **Chapter 6** we will discuss the obtained solutions and give an outlook to this vast field of research in the direction of complex quantum many-body systems.

Chapter 2

The Bose-Hubbard model

In the following we assume the second quantized Hamiltonian

$$\begin{aligned}\hat{H} &= \int \mathrm{d}x \hat{\Psi}^\dagger(x)\Big(-\frac{\hbar^2}{2m}\frac{\partial^2}{\partial x^2} + V_0 \sin^2(\frac{2\pi}{\lambda}x)\Big)\hat{\Psi}(x) + \\ & g\int \mathrm{d}x \hat{\Psi}^\dagger(x)\hat{\Psi}^\dagger(x)\hat{\Psi}(x)\hat{\Psi}(x)\end{aligned}$$

which may model a Bose-Einstein condensate in an optical lattice. We restrict ourselves to a potential $V_0 \sin^2(\frac{2\pi}{\lambda}x)$ arising from standing electromagnetic waves of wave length λ that form a lattice of lattice depth V_0 and the bosons interact with the dimensionless coupling constant g.

The Bose-Hubbard Hamiltonian is derived from the above Hamiltonian by imposing a discrete lattice on the potential, such that the bosons only sit in the minima of the potential. This models bosons which populate only the ground state of each harmonic well. Additionally the bosons are only allowed to tunnel to directly adjacent lattice points and one demands that the bosons only interact with each other if they are located in the same well, i.e. if they sit at the same lattice point. We will explain the Bose-Hubbard Hamiltonian in more detail soon.

In the context of quantum chaos, the Bose-Hubbard model has lately been extended to include an additional static force that tilts the lattice [35]. Although this tilt leads to very exciting effects, e.g. many-body Landau-Zener tunneling [36] and Bloch oscillations [37], we do not include it in our investigation. In order to obviate confusion we propose that the model without the tilt shall be called the pure Bose-Hubbard model. Whenever we talk about the Bose-Hubbard model then actually the pure Bose-Hubbard model is meant.

In this chapter we first rewrite the above Hamiltonian under the assumptions of the Bose-Hubbard model. Depending on the basis in which we express the field operator $\hat{\Psi}(x)$ we get a specific representation of the model. We will first choose highly localized Wannier functions as our one-particle eigenstates and by this obtain the standard form of the Bose-Hubbard model. Then we will write the Hamilonian with highly delocalized Bloch functions. As we will later see, these two representations are in some sense conjugate to each other, just as location and momentum observables are. Although the Wannier and Bloch

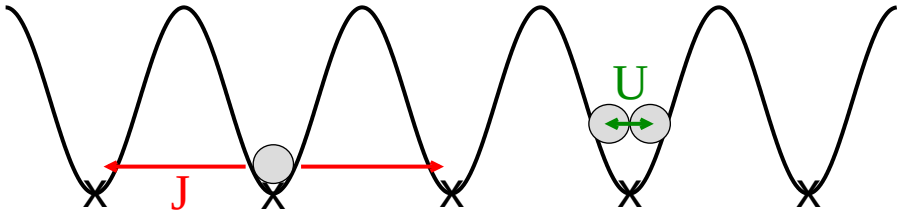

Figure 2.1: Schematic view of the Bose-Hubbard model. The **x** mark the discrete lattice points and emphasize that intra-well dynamics is neglected.

representation of the Bose-Hubbard model are frequently used in the literature we could not find a complete derivation, which is the reason why we present it here. We will then take a close look at the existing symmetries. To our knowledge the symmetries of the Bose-Hubbard model are nowhere discussed explicitly. We will do this discussion here because the symmetries are essential for us, from a theoretical and from a numerical point of view. Finally we briefly consider the experimental realization.

2.1 Representation

2.1.1 Wannier representation

We expand our field operator in a Wannier basis

$$\hat{\Psi}(x) \quad = \quad \sum_l \hat{a}_l \psi_l(x)$$

where $\psi_l(x) := w(x - x_l)$ is a Wannier function localized in the l-th well, i.e. at lattice point l. Under the assumptions that a boson can only tunnel from one well to a directly neighbouring well and that bosons interact only if they are in the same well the Bose-Hubbard Hamiltonian follows:

$$\hat{H} \quad = \quad -J \sum_l (\hat{a}_{l+1}^\dagger \hat{a}_l + \hat{a}_l^\dagger \hat{a}_{l+1}) + \frac{U}{2} \sum_l \hat{n}_l (\hat{n}_l - 1) \qquad . \tag{2.1}$$

Here we have defined the kinetic term

$$J \quad := \quad \int \mathrm{d}x \psi_l^*(x) \Big(-\frac{\hbar^2}{2m} \frac{\partial^2}{\partial x^2} + V_0 \sin^2(\frac{2\pi}{\lambda} x) \Big) \psi_{l+1}(x)$$

and the on-site interaction

$$U \quad := \quad g \int \mathrm{d}x |\psi_l(x)|^4 \qquad .$$

The assumptions that lead to our Bose-Hubbard Hamiltonian are justified experimentally if the bosons are ultracold and the lattice is sufficiently deep [11]. The above Bose-Hubbard Hamiltonian is a one band model which means here that in each well there is just one state that can be populated by bosons. So the bosons have to be ultracold such that they move only in the lowest band.

Additionally the lattice has to be sufficiently deep for the lowest band being sufficiently seperated from the higher bands. In the deep lattice limit where the lattice depth V_0 is big both integrals for J and U can be evaluated explicitly and we will give the result in the end of this chapter. There we will show how J and U depend on V_0, which is particularly interesting because the lattice depth is directly adjustable in the experiment and this is how the model is simulatable by the experiment.

Let us now explain the system of units used in this thesis. Since we will investigate spectral and dynamic properties, we have to define our unit of energy and our unit of time. As shown in [38] the proper energy scale in our problem is given by the recoil energy $E_R = \frac{\hbar^2 k^2}{2m}$. Here k is the wave vector of the laser field and m is the mass of a boson. Then the proper time scale of our system is given by $\frac{\hbar}{E_R}$ [39]. So the parameters J and U are expressed as multiples of E_R and this is also true for the energy given by our Hamiltonian, and the time t is expressed as a multiple of $\frac{\hbar}{E_R}$. However, we will be using different parametrizations of the Bose-Hubbard Hamiltonian in this thesis which summarize J and U in one dimensionless parameter, and we have to explain what this means for our system of units.

The Bose-Hubbard Hamiltonian effectively has only one parameter, in the following sense. If we factor out U,

$$\hat{H}_J = \Big(-\frac{J}{U} \sum_l (\hat{a}_{l+1}^\dagger \hat{a}_l + \hat{a}_l^\dagger \hat{a}_{l+1}) + \frac{1}{2} \sum_l \hat{n}_l(\hat{n}_l - 1) \Big) U \quad , \tag{2.2}$$

the energy is given in units of U. We can equally factor out J,

$$\hat{H}_U = \Big(-\sum_l (\hat{a}_{l+1}^\dagger \hat{a}_l + \hat{a}_l^\dagger \hat{a}_{l+1}) + \frac{U}{2J} \sum_l \hat{n}_l(\hat{n}_l - 1) \Big) J \quad , \tag{2.3}$$

and energy is measured in units of J. In practice this means that if we compute the spectrum of

$$\hat{H}' = -\frac{J}{U} \sum_l (\hat{a}_{l+1}^\dagger \hat{a}_l + \hat{a}_l^\dagger \hat{a}_{l+1}) + \frac{1}{2} \sum_l \hat{n}_l(\hat{n}_l - 1)$$

as a function of $\frac{J}{U}$ then this plot contains all the information necessary to determine the energy to arbitrary values of J and U. Given J and U (which are in units of E_R), one has to calculate the ratio $\frac{J}{U}$ (which is dimensionless), read out the energy in the plot (which is dimensionless), and finally multiply it by U (which is in units of E_R). Doing so we obtain the desired energy in units of E_R. Also any propagation can be described by $\hat{H}'$. Assume we want to propagate a state to arbitrary values of J and U. Then we have to determine the ratio $\frac{J}{U}$ (which is dimensionless), do the propagation with $\hat{H}'$ and finally have to multiply the time (which is dimensionless) by $\frac{\hbar}{U}$ to obtain the desired time in units of $\frac{\hbar}{E_R}$.

In this thesis we will apply three different kinds of parametrizations. If we parametrize by J, then actually Hamiltonian $\hat{H}_J$ (2.2) is meant and the true parametrization is given by the dimensionless parameter $\frac{J}{U}$. In this case, for

arbitrary values of J and U the dimensionless energy has to be multiplied by U and the dimensionless time has to be multiplied by $\frac{\hbar}{U}$. If we parametrize by U, then actually Hamiltonian $\hat{H}_U$ (2.3) is meant and the true parametrization is given by the dimensionless parameter $\frac{U}{J}$. In this case, for arbitrary values of J and U the dimensionless energy has to be multiplied by J and the dimensionless time has to be multiplied by $\frac{\hbar}{J}$. Our third parametrization is taken from [17]. There a parameter u is introduced such that $J = 1-u$, $U = u$ and u runs from 0 to 1 (in units of E_R). This parametrization is particularly appropriate for the presentation of quantum chaos in the Bose-Hubbard model, as we will see in Chapter 3. The corresponding Hamiltonian reads

$$\hat{H}_u \;=\; \Big(-\sum_l (\hat{a}_{l+1}^\dagger \hat{a}_l + \hat{a}_l^\dagger \hat{a}_{l+1}) + \frac{u}{2(1-u)} \sum_l \hat{n}_l(\hat{n}_l - 1) \Big)(1-u) \qquad (2.4)$$

So if we parametrize by u, then actually Hamiltonian $\hat{H}_u$ (2.4) is meant and the true parametrization is given by the dimensionless parameter $\frac{u}{1-u}$. In this case, for arbitrary values of J and U we first have to determine u by calculating

$$\frac{U}{J} = \frac{u}{1-u} \quad \Longleftrightarrow \quad u = \frac{\frac{U}{J}}{1+\frac{U}{J}} \quad ,$$

and then the dimensionless energy has to be multiplied by $1-u$ and the dimensionless time has to be multiplied by $\frac{\hbar}{1-u}$.

$\hat{H}$ acts on Fock states which are symmetrized products of one-particle Wannier functions. In fact, in the derivation we have to use Fock states to all particle numbers to ensure that the Hamiltonian is represented in a complete set of orthonormal functions. But from now on we will fix the particle number. This is of course possible because the Hamiltonian $\hat{H}$ and the particle number operator $\hat{N}$ commute,

$$[\hat{H}, \hat{N}] \;=\; 0 \quad ,$$

and we can therefore restrict our investigation to a subspace of any fixed particle number.

For fixed particle number N and fixed number of lattice sites L the dimension of the Hilbert space reads

$$\dim(L,N) \;=\; \binom{L+N-1}{N} \quad . \qquad (2.5)$$

This formula follows immediately from combinatorics because the problem can be mapped to the standard combinatorial question of how many possibilities there are to draw N balls out of a bowl filled with L different balls if one puts the ball back into the bowl after each draw and if one does not care for the order. Clearly the L different balls stand for the L possible lattice sites. For studies of quantum chaos, and also of the quantum phase transition, it is common to have unit filling, i.e. on average one particle per lattice site. Unit filling is interesting because the kinetic part and the interaction part of the Bose-Hubbard Hamiltonian are of comparable strength. In the case $\frac{N}{L} \to 0$ the hopping term J is

dominant, while in the case $\frac{N}{L} \to \infty$ the on-site interaction term U is dominant. The dimension of the Hilbert space to the Bose-Hubbard model with unit filling grows as $\dim(3,3) = 10$, $\dim(4,4) = 35$, $\dim(5,5) = 126$, $\dim(6,6) = 462$, $\dim(7,7) = 1716$, $\dim(8,8) = 6534$ and obviously any computation of big systems is numerically demanding. However taking symmetries of the Hamiltonian into account will ease the problem a little bit.

2.1.2 Boundary conditions

In the above Wannier representation of the Bose-Hubbard model (2.1) we did not specify how exactly the sums over l are supposed to be taken. We did this on purpose. The Bose-Hubbard model comes along with two different kinds of boundary conditions which are mathematically realized in these sums.

Hard wall boundary conditions are imposed if one lets the first sum over l run from 1 to $L-1$ and the second from 1 to L:

$$\hat{H} = -J \sum_{l=1}^{L-1} (\hat{a}_{l+1}^\dagger \hat{a}_l + \hat{a}_l^\dagger \hat{a}_{l+1}) + \frac{U}{2} \sum_{l=1}^{L} \hat{n}_l(\hat{n}_l - 1) \quad . \tag{2.6}$$

This Hamiltonian models a linear array of wells that has hard walls at both ends. We note that in solid-state physics hard wall boundary conditions are also referred to as open boundary conditions.

Periodic boundary conditions are imposed if one lets both sums over l run from 1 to L and identifies $L+1 := 1$:

$$\hat{H} = -J \sum_{l=1}^{L} (\hat{a}_{l+1}^\dagger \hat{a}_l + \hat{a}_l^\dagger \hat{a}_{l+1}) + \frac{U}{2} \sum_{l=1}^{L} \hat{n}_l(\hat{n}_l - 1) \quad . \tag{2.7}$$

This Hamiltonian models a ring of wells. If one wants to suppress boundary effects as much as possible, periodic boundary conditions and large system sizes should be adopted. In the experiment the lattice is usually much bigger than the sample of bosons which is why the bosons do not see a boundary. Hence we would choose periodic boundary conditions to model this experimental situation. Additionally the lack of boundaries can be interpreted as an infinitely extended lattice, where however the behaviour of the bosons repeats itself after each finite lattice length L. We will use periodic boundary conditions throughout this diploma thesis.

The choice of boundary conditions determines the symmetries of the model. We will soon see that the hard wall Bose-Hubbard Hamiltonian only shows invariance under parity while the periodic Bose-Hubbard Hamiltonian additionally turns out to be translationally invariant.

2.1.3 Bloch representation

One symmetry, translational invariance, is taken advantage of by using Bloch functions as the one-particle eigenstates. We want to do this basis change from Wannier to Bloch functions explicitly here. The above Bose-Hubbard Hamiltonian in Wannier representation is translationally invariant only if one demands

periodic boundary conditions. The symmetry manifests itself in the fact that the periodic Bose-Hubbard Hamiltonian (2.7) does not change under the transformation $l \to l+1$.

Expressed in terms of Wannier functions $\psi_l(x)$ the Bloch functions $\phi_\kappa(x)$ read

$$\phi_\kappa(x) \quad = \quad \frac{1}{\sqrt{L}} \sum_l e^{i\kappa l} \psi_l(x) \qquad .$$

Here $\kappa := \frac{2\pi k}{L}$ is the single-particle quasimomentum and k runs from 1 to L. Because of the one-to-one correspondence between κ and k we will also refer to k as the single-particle quasimomentum. In the Fock formalism a basis change of the one-particle eigenstates directly translates to a change of annihilation and creation operators. We have to substitute the $\hat{a}_l$ by

$$\hat{a}_l \quad := \quad \frac{1}{\sqrt{L}} \sum_l e^{-i\kappa l} \hat{b}_\kappa \qquad .$$

In the following derivation of the new Hamiltonian one relation will be particularly useful:

$$\sum_{m=1}^{L} e^{i\frac{2\pi k}{L}m} \quad = \quad 0 \qquad ,$$

which is why

$$\frac{1}{L} \sum_\kappa e^{i\kappa(l-l')} \quad = \quad \delta_{l,l'} \qquad .$$

We remark that, if not said explicitly, the sum over l always runs from 1 to L and the sum over κ always runs from $\frac{2\pi}{L}$ to 2π, i.e. k runs from 1 to L.

We rewrite our Wannier Bose-Hubbard Hamiltonian (2.1) as $\hat{H} = \hat{T} + \hat{V}$ where $\hat{T}$ is the kinetic part and $\hat{V}$ is the interaction part. Let us begin with the kinetic part:

$$\begin{aligned}
\hat{T} &= -J \sum_l (\hat{a}_{l+1}^\dagger \hat{a}_l + \hat{a}_l^\dagger \hat{a}_{l+1}) \\
&= -J \sum_l \Big(\frac{1}{L} (\sum_\kappa e^{i\kappa(l+1)} \hat{b}_\kappa^\dagger \sum_{\kappa'} e^{-i\kappa' l} \hat{b}_{\kappa'} + \sum_\kappa e^{i\kappa l} \hat{b}_\kappa^\dagger \sum_{\kappa'} e^{-i\kappa'(l+1)} \hat{b}_{\kappa'}) \Big) \\
&= -J \Big(\sum_{\kappa,\kappa'} \frac{1}{L} \sum_l e^{i(\kappa-\kappa')l} e^{i\kappa} \hat{b}_\kappa^\dagger \hat{b}_{\kappa'} + \sum_{\kappa,\kappa'} \frac{1}{L} \sum_l e^{i(\kappa-\kappa')l} e^{-i\kappa'} \hat{b}_\kappa^\dagger \hat{b}_{\kappa'} \Big) \\
&= -J \Big(\sum_{\kappa,\kappa'} \delta_{\kappa,\kappa'} e^{i\kappa} \hat{b}_\kappa^\dagger \hat{b}_{\kappa'} + \sum_{\kappa,\kappa'} \delta_{\kappa,\kappa'} e^{-i\kappa'} \hat{b}_\kappa^\dagger \hat{b}_{\kappa'} \Big) \\
&= -2J \sum_\kappa \frac{e^{i\kappa} + e^{-i\kappa}}{2} \hat{b}_\kappa^\dagger \hat{b}_\kappa \\
&= -2J \sum_\kappa \cos(\kappa) \hat{n}_\kappa \qquad .
\end{aligned}$$

For the interaction part we obtain

$$\begin{aligned}
\hat{V} &= \frac{U}{2}\sum_l \hat{n}_l(\hat{n}_l - 1) \\
&= \frac{U}{2}\sum_l \Big(\frac{1}{L}\sum_{\kappa_1,\kappa_2} e^{i(\kappa_1-\kappa_2)l}\hat{b}^\dagger_{\kappa_1}\hat{b}_{\kappa_2}\Big)\cdot\Big(\frac{1}{L}\sum_{\kappa_1,\kappa_2} e^{i(\kappa_1-\kappa_2)l}\hat{b}^\dagger_{\kappa_1}\hat{b}_{\kappa_2} - 1\Big) \\
&= \frac{U}{2L}\sum_{\kappa_1,\kappa_2,\kappa_3,\kappa_4}\frac{1}{L}\sum_l e^{i(\kappa_1-\kappa_2+\kappa_3-\kappa_4)l}\hat{b}^\dagger_{\kappa_1}\hat{b}_{\kappa_2}\hat{b}^\dagger_{\kappa_3}\hat{b}_{\kappa_4} - \\
&\quad \frac{U}{2}\sum_{\kappa_1,\kappa_2}\frac{1}{L}\sum_l e^{i(\kappa_1-\kappa_2)l}\hat{b}^\dagger_{\kappa_1}\hat{b}_{\kappa_2} \\
&= \frac{U}{2L}\sum_{\kappa_1,\kappa_2,\kappa_3,\kappa_4}\delta(\kappa_1-\kappa_2+\kappa_3-\kappa_4)\hat{b}^\dagger_{\kappa_1}\hat{b}_{\kappa_2}\hat{b}^\dagger_{\kappa_3}\hat{b}_{\kappa_4} - \frac{U}{2}\sum_{\kappa_1,\kappa_2}\delta_{\kappa_1,\kappa_2}\hat{b}^\dagger_{\kappa_1}\hat{b}_{\kappa_2} \\
&= \frac{U}{2L}\sum_{\kappa_1,\kappa_2,\kappa_3,\kappa_4}\hat{b}^\dagger_{\kappa_1}\hat{b}_{\kappa_2}\hat{b}^\dagger_{\kappa_3}\hat{b}_{\kappa_4}\delta(\kappa_1-\kappa_2+\kappa_3-\kappa_4) - \frac{UN}{2} \quad .
\end{aligned}$$

It is important to note here that the delta function $\delta(\kappa_1-\kappa_2+\kappa_3-\kappa_4)$ is meant to be modulo 2π or equivalently $\delta(k_1-k_2+k_3-k_4)$ should be understood modulo L, due to the way we sum over κ_1, κ_2, κ_3 and κ_4. Using

$$[\hat{b}_i, \hat{b}^\dagger_j] = \delta_{i,j} \quad ,$$

we can further simplify

$$\begin{aligned}
\hat{V} &= \frac{U}{2L}\sum_{\kappa_1,\kappa_2,\kappa_3,\kappa_4}\hat{b}^\dagger_{\kappa_1}\hat{b}^\dagger_{\kappa_3}\hat{b}_{\kappa_2}\hat{b}_{\kappa_4}\delta(\kappa_1-\kappa_2+\kappa_3-\kappa_4) + \\
&\quad \frac{U}{2L}\sum_{\kappa_1,\kappa_2,\kappa_3,\kappa_4}\hat{b}^\dagger_{\kappa_1}\hat{b}_{\kappa_4}\delta_{\kappa_2,\kappa_3}\delta(\kappa_1-\kappa_2+\kappa_3-\kappa_4) - \frac{UN}{2} \\
&= \frac{U}{2L}\sum_{\kappa_1,\kappa_2,\kappa_3,\kappa_4}\hat{b}^\dagger_{\kappa_1}\hat{b}^\dagger_{\kappa_3}\hat{b}_{\kappa_2}\hat{b}_{\kappa_4}\delta(\kappa_1-\kappa_2+\kappa_3-\kappa_4) + \frac{U}{2L}\sum_{\kappa_1,\kappa_2}\hat{b}^\dagger_{\kappa_1}\hat{b}_{\kappa_1} - \\
&\quad \frac{UN}{2} \\
&= \frac{U}{2L}\sum_{\kappa_1,\kappa_2,\kappa_3,\kappa_4}\hat{b}^\dagger_{\kappa_1}\hat{b}^\dagger_{\kappa_3}\hat{b}_{\kappa_2}\hat{b}_{\kappa_4}\delta(\kappa_1-\kappa_2+\kappa_3-\kappa_4) + \frac{U}{2L}\cdot L\sum_{\kappa_1}\hat{b}^\dagger_{\kappa_1}\hat{b}_{\kappa_1} - \\
&\quad \frac{UN}{2} \\
&= \frac{U}{2L}\sum_{\kappa_1,\kappa_2,\kappa_3,\kappa_4}\hat{b}^\dagger_{\kappa_1}\hat{b}^\dagger_{\kappa_3}\hat{b}_{\kappa_2}\hat{b}_{\kappa_4}\delta(\kappa_1-\kappa_2+\kappa_3-\kappa_4) \quad .
\end{aligned}$$

Renaming indices and evaluating the delta function yields

$$\hat{V} = \frac{U}{2L}\sum_{\kappa_1,\kappa_2,\kappa_3}\hat{b}^\dagger_{\kappa_1+\kappa_2-\kappa_3}\hat{b}^\dagger_{\kappa_3}\hat{b}_{\kappa_2}\hat{b}_{\kappa_1} \quad .$$

Finally our Bose-Hubbard Hamiltonian in Bloch representation reads

$$\hat{H} = -2J\sum_{k=1}^{L}\cos(\frac{2\pi k}{L})\hat{n}_k + \frac{U}{2L}\sum_{k_1,k_2,k_3=1}^{L}\hat{b}^\dagger_{k_1+k_2-k_3}\hat{b}^\dagger_{k_3}\hat{b}_{k_2}\hat{b}_{k_1} \quad , \quad (2.8)$$

where the index $k_1 + k_2 - k_3$ is calculated modulo L and secures conservation of quasimomentum.

This is actually the reason why the periodic Bose-Hubbard Hamiltonian can be decomposed into a direct sum,

$$\hat{H} \quad = \quad \oplus \hat{H}_\kappa \qquad ,$$

or equivalently that it can be block diagonalized where the different blocks of submatrices correspond to the different values of κ. Since $\kappa = \frac{2\pi k}{L}$ and $k = 1, 2, \ldots, L$ our energy spectrum consists of L parts which are totally independent of each other.

2.2 Symmetries

In this section we want to take a close look at the symmetries of the Bose-Hubbard model. In Chapter 2 we will be doing spectral analysis and for that have to be aware of all existing symmetries. By taking symmetries into account level crossings are removed from the spectrum and only avoided crossings remain. Thus the lack of level crossings is a good sign that all symmetries were considered.

A symmetry produces redundancy apparent in the fact that the corresponding Hamiltonian can be written as a direct sum. Let the Hermitian operator that is associated to the symmetry be called $\hat{O}$, then

$$[\hat{H}, \hat{O}] \quad = \quad 0$$

holds and $\hat{H}$ becomes block diagonal in the eigenbasis of $\hat{O}$. Let us remark that in terms of matrix representations a decomposition into a direct sum is equivalent to block diagonalization.

The shift operator $\hat{\mathcal{S}}$ [35] is responsible for the decomposition of the periodic Bose-Hubbard Hamiltonian (2.7) into the different κ-subspaces. It is defined by its action on a Wannier-Fock state:

$$\hat{\mathcal{S}}|n_1, n_2, \ldots, n_L\rangle \quad = \quad |n_L, n_1, \ldots, n_{L-1}\rangle \qquad .$$

Obviously a Wannier-Fock state of the form $|n_1, n_2, \ldots, n_L\rangle$ denotes a system of L wells and $N = n_1 + n_2 + \ldots + n_L$ bosons, where n_1 bosons are in well 1, n_2 bosons are in well 2, ...and n_L bosons are in well L. The shift operator commutes with the periodic Bose-Hubbard Hamiltonian (2.7),

$$[\hat{H}, \hat{\mathcal{S}}] \quad = \quad 0 \qquad .$$

The eigenvalues of $\hat{\mathcal{S}}$ are related to the different κ and the associated symmetry is a discrete translational invariance of the Hamiltonian due to periodic boundary conditions. This symmetry can be seen in the Wannier representation of the Bose-Hubbard model. Although in general the quest for symmetries might be very involved, the only other symmetry of our problem can be easily discovered too. It is parity, which we define by

$$\hat{\mathcal{P}}|n_1, n_2, \ldots, n_L\rangle \quad = \quad |n_L, n_{L-1}, \ldots, n_1\rangle \qquad ,$$

and it commutes both with the hard wall Bose-Hubbard Hamiltonian (2.6) and with the periodic Bose-Hubbard Hamiltonian (2.7),

$$[\hat{H}, \hat{\mathcal{P}}] \;=\; 0 \qquad .$$

Unfortunately

$$[\hat{\mathcal{S}}, \hat{\mathcal{P}}] \;\neq\; 0 \qquad ,$$

which is why $\hat{H}$, $\hat{\mathcal{S}}$ and $\hat{\mathcal{P}}$ do not form a set of commuting observables and so in general there is no further decomposition of our Hamiltonian. We can either decompose it into L block matrices by representing it in the eigenbasis of the shift operator $\hat{\mathcal{S}}$ or into 2 block matrices by representing it in the eigenbasis of the parity operator $\hat{\mathcal{P}}$. However it follows from group theory that in the former case the subspace $\kappa = 2\pi$ for an odd number of wells and the subspaces $\kappa = 2\pi$ and $\kappa = \pi$ for an even number of wells can be decomposed further due to parity.

The hard wall Bose-Hubbard Hamiltonian (2.6) has the same symmetries as the symmetry group $\mathbb{Z}_2$. Group theory teaches us that parity alone generates all elements of $\mathbb{Z}_2$ [40]. Hence parity is the only symmetry of the hard wall Bose-Hubbard Hamiltonian (2.6). The symmetries of the periodic Bose-Hubbard Hamiltonian (2.7) are the same as the ones of the so-called Dihedral Group D_n which is the symmetry group of rotations of a regular polygon with n sides. Interpreting n as the number of edges of the polygon we can identify each edge of the polygon with a well. E.g. D_3, being the symmetry group of an equilateral triangle, should describe a system of 3 wells. But it follows from group theory that we can generate all elements of D_n with only two symmetry operators which are the ones we call shift and parity. So we have found all the symmetries inherent to the periodic Bose-Hubbard Hamiltonian (2.7).

In order to take advantage of both existing symmetries we have to find a representation of D_n that is also one of $\mathbb{Z}_2$. One such representation is the trivial one and that's why the subspace to $k = L$ always decomposes further. The only other representation is the one to $k = \frac{L}{2}$ for even L. With this discussion we also proved the non-integrability of the Bose-Hubbard model because referring to group theory we showed that it is not possible to find a complete set of commuting observables.

We believe that an example should show how the above formalism is applied in practice, i.e. how a new basis is chosen that makes use of both discrete translational and parity invariance. Let us consider a system made up of $N = 3$ atoms in $L = 3$ wells and let us use the periodic Bose-Hubbard Hamiltonian in Wannier representation (2.7). Clearly the Wannier-Fock states have the form $|n_1, n_2, n_3\rangle$ where $n_1 + n_2 + n_3 = 3$. The complete set of Fock states for this subspace of fixed particle number reads:

$$\begin{array}{ccc} |3,0,0\rangle, & |0,3,0\rangle, & |0,0,3\rangle, \\ |2,1,0\rangle, & |0,2,1\rangle, & |1,0,2\rangle, \\ |2,0,1\rangle, & |1,2,0\rangle, & |0,1,2\rangle, \\ & |1,1,1\rangle & . \end{array}$$

Now the action of the shift operator $\hat{\mathcal{S}}$ is:

$$\hat{\mathcal{S}}|n_1, n_2, n_3\rangle \quad = \quad |n_3, n_1, n_2\rangle \qquad .$$

We construct 10 orthonormal eigenstates to $\hat{\mathcal{S}}$ from the above Fock states:

$$\begin{aligned}
|1\rangle &:= \frac{1}{\sqrt{3}}(e^{i\kappa_1\cdot 1}|3,0,0\rangle + e^{i\kappa_1\cdot 2}|0,3,0\rangle + e^{i\kappa_1\cdot 3}|0,0,3\rangle) \qquad , \\
|2\rangle &:= \frac{1}{\sqrt{3}}(e^{i\kappa_1\cdot 1}|2,1,0\rangle + e^{i\kappa_1\cdot 2}|0,2,1\rangle + e^{i\kappa_1\cdot 3}|1,0,2\rangle) \qquad , \\
|3\rangle &:= \frac{1}{\sqrt{3}}(e^{i\kappa_1\cdot 1}|2,0,1\rangle + e^{i\kappa_1\cdot 2}|1,2,0\rangle + e^{i\kappa_1\cdot 3}|0,1,2\rangle) \qquad , \\
|4\rangle &:= \frac{1}{\sqrt{3}}(e^{i\kappa_2\cdot 1}|3,0,0\rangle + e^{i\kappa_2\cdot 2}|0,3,0\rangle + e^{i\kappa_2\cdot 3}|0,0,3\rangle) \qquad , \\
|5\rangle &:= \frac{1}{\sqrt{3}}(e^{i\kappa_2\cdot 1}|2,1,0\rangle + e^{i\kappa_2\cdot 2}|0,2,1\rangle + e^{i\kappa_2\cdot 3}|1,0,2\rangle) \qquad , \\
|6\rangle &:= \frac{1}{\sqrt{3}}(e^{i\kappa_2\cdot 1}|2,0,1\rangle + e^{i\kappa_2\cdot 2}|1,2,0\rangle + e^{i\kappa_2\cdot 3}|0,1,2\rangle) \qquad , \\
|7\rangle &:= \frac{1}{\sqrt{3}}(e^{i\kappa_3\cdot 1}|3,0,0\rangle + e^{i\kappa_3\cdot 2}|0,3,0\rangle + e^{i\kappa_3\cdot 3}|0,0,3\rangle) \qquad , \\
|8\rangle &:= \frac{1}{\sqrt{3}}(e^{i\kappa_3\cdot 1}|2,1,0\rangle + e^{i\kappa_3\cdot 2}|0,2,1\rangle + e^{i\kappa_3\cdot 3}|1,0,2\rangle) \qquad , \\
|9\rangle &:= \frac{1}{\sqrt{3}}(e^{i\kappa_3\cdot 1}|2,0,1\rangle + e^{i\kappa_3\cdot 2}|1,2,0\rangle + e^{i\kappa_3\cdot 3}|0,1,2\rangle) \qquad , \\
|10\rangle &:= |1,1,1\rangle \qquad ,
\end{aligned}$$

where

$$\kappa_1 := \frac{2\pi}{3} \qquad , \quad \kappa_2 := \frac{4\pi}{3} \qquad , \quad \kappa_3 := \frac{6\pi}{3} = 2\pi \qquad .$$

Obviously $|1\rangle$, $|2\rangle$ and $|3\rangle$ are eigenstates to $\hat{\mathcal{S}}$ with eigenvalue $e^{i\kappa_1}$, $|4\rangle$, $|5\rangle$ and $|6\rangle$ are eigenstates to $\hat{\mathcal{S}}$ with eigenvalue $e^{i\kappa_2}$ and $|7\rangle$, $|8\rangle$, $|9\rangle$ and $|10\rangle$ are eigenstates to $\hat{\mathcal{S}}$ with eigenvalue $e^{i\kappa_3}$.

Written in the states $|1\rangle$ to $|10\rangle$ our Wannier Hamiltonian (2.7) is block diagonal with a 3-by-3-matrix associated to $k = 1$ in the upper left corner, a 3-by-3-matrix associated to $k = 2$ in the middle part and a a 4-by-4-matrix associated to $k = 3$ in the lower right corner. The spectra of these three matrices are totally equivalent to the spectra of the corresponding three submatrices in the Bloch Hamiltonian (2.8). One might now ask what we have gained then. Well, starting from the Bloch Hamiltonian it is hard to see its invariance under parity and it is difficult to construct an eigenbasis to the parity operator from Bloch Fock states. Starting from the Wannier Hamiltonian (2.7), however, its parity invariance is obvious and it is straightforward to construct an eigenbasis to the parity operator from its Wannier Fock states.

Now the action of parity on a Wannier-Fock state has to be:

$$\hat{\mathcal{P}}|n_1, n_2, n_3\rangle \quad = \quad |n_3, n_2, n_1\rangle \qquad .$$

Taking a close look at the eigenstates of $\hat{\mathcal{S}}$ one finds out that only the ones to $\kappa_3 = 2\pi$ can be eigenstates to $\hat{\mathcal{P}}$ if one declares

$$\begin{aligned} |7'\rangle &:= |7\rangle \quad , \quad |8'\rangle := \frac{1}{\sqrt{2}}(|8\rangle + |9\rangle) \quad , \\ |9'\rangle &:= |10\rangle \quad , \quad |10'\rangle := \frac{1}{\sqrt{2}}(|8\rangle - |9\rangle) \quad . \end{aligned}$$

Clearly $|7'\rangle$, $|8'\rangle$ and $|9'\rangle$ are eigenstates to $\hat{\mathcal{P}}$ with eigenvalue $+1$, and $|10'\rangle$ is an eigenstate to $\hat{\mathcal{P}}$ with eigenvalue -1. Therefore the 4-by-4-matrix in the lower right corner decomposes further into a 3-by-3-matrix to even parity and a single element to odd parity.

We want to check our thoughts by numerical calculations. Let us plot the energy spectra depending on one parameter u as explained above. Thus we set $J = 1 - u$, $U = u$ and let u run from 0 to 1. First we look at a system of $L = 3$ wells and $N = 3$ bosons. The total Hilbert space has dimension 10 and so we would expect to see 10 energy levels in the full spectrum. In Figure 2.2 we only count 7 energy levels and Figure 2.3 reveals that this is due to the fact that the spectra to the quasimomenta $k = 1$ and $k = 2$ are equivalent. Doing spectral analysis it is therefore sufficient to investigate the subspaces to $k = 1$ and $k = 3$. However the subspace to quasimomentum $k = 3$ can be further decomposed due to parity. Finally we should not be able to find level crossings in the decomposed spectrum anymore and this is indeed the case, as we conclude from Figure 2.4.

Additionally we want to look at a system of $L = 4$ wells and $N = 4$ bosons because we expect the subspace to quasimomentum $k = 2$ to be further decomposable due to parity. Now the dimension of the total Hilbert space is 35 and again the full spectrum has many energy levels that lie on top of each other as can be seen in Figure 2.5. We conclude from Figure 2.6 that the subspaces to the quasimomenta $k = 1$ and $k = 3$ have the same spectra. As shown in Figure 2.7 the subspace to quasimomentum $k = 2$ can indeed be further decomposed due to parity. Here no level crossings are left after the decomposition of the spectrum, too. We remark that on the scale of Figure 2.8 one avoided crossing cannot be resolved.

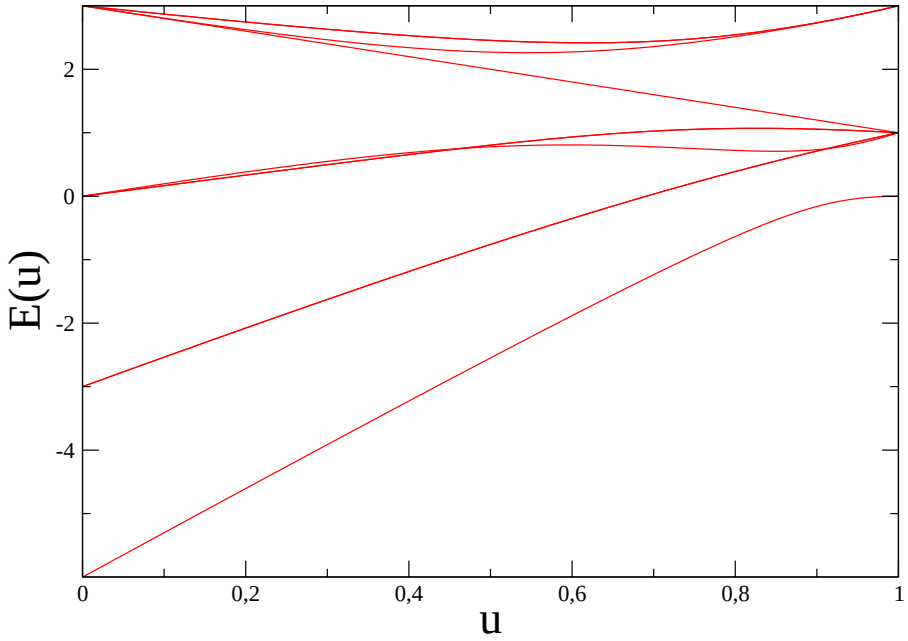

Figure 2.2: Full spectrum of the periodic Bose-Hubbard Hamiltonian with $L = 3$ wells and $N = 3$ bosons. We only count 7 energy levels instead of 10 because the spectra to the quasimomenta $k = 1$ and $k = 2$ are equivalent.

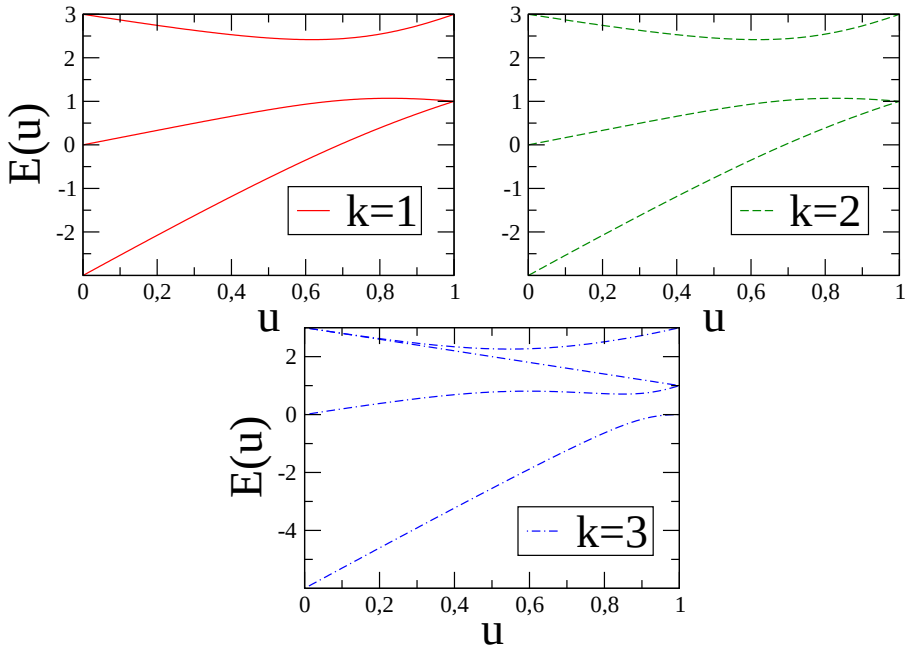

Figure 2.3: Decomposed spectrum of the periodic Bose-Hubbard Hamiltonian with $L = 3$ wells and $N = 3$ bosons. Here we directly see that the spectra to the quasimomenta $k = 1$ and $k = 2$ are equivalent.

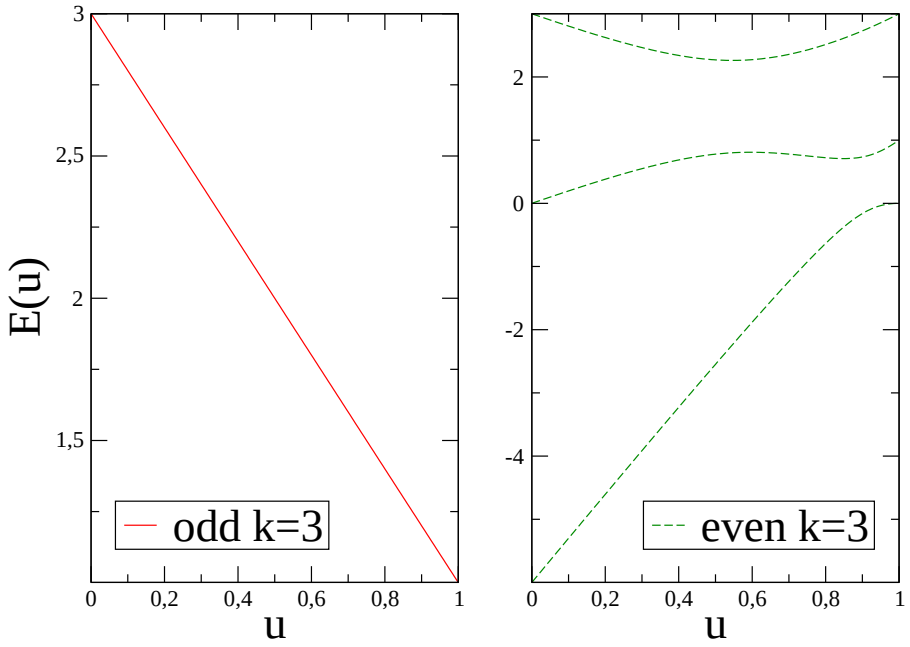

Figure 2.4: Decomposed spectrum of the periodic Bose-Hubbard Hamiltonian with $L = 3$ wells, $N = 3$ bosons and quasimomentum $k = 3$. This subspace can be further decomposed into a part to odd parity and into a part to even parity.

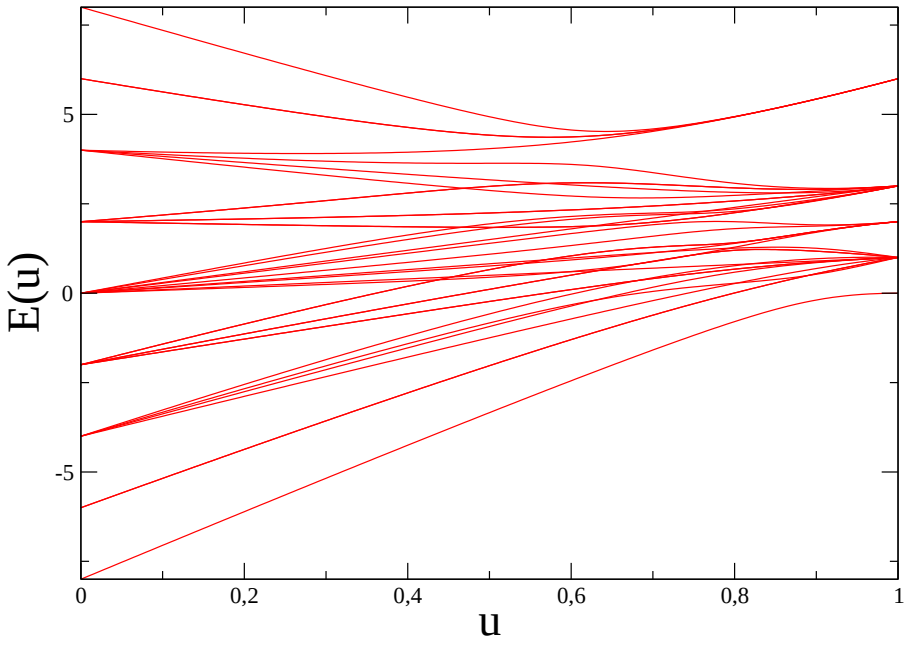

Figure 2.5: Full spectrum of the periodic Bose-Hubbard Hamiltonian with $L = 4$ wells and $N = 4$ bosons. Again many energy levels lie on top of each other and we find level crossings.

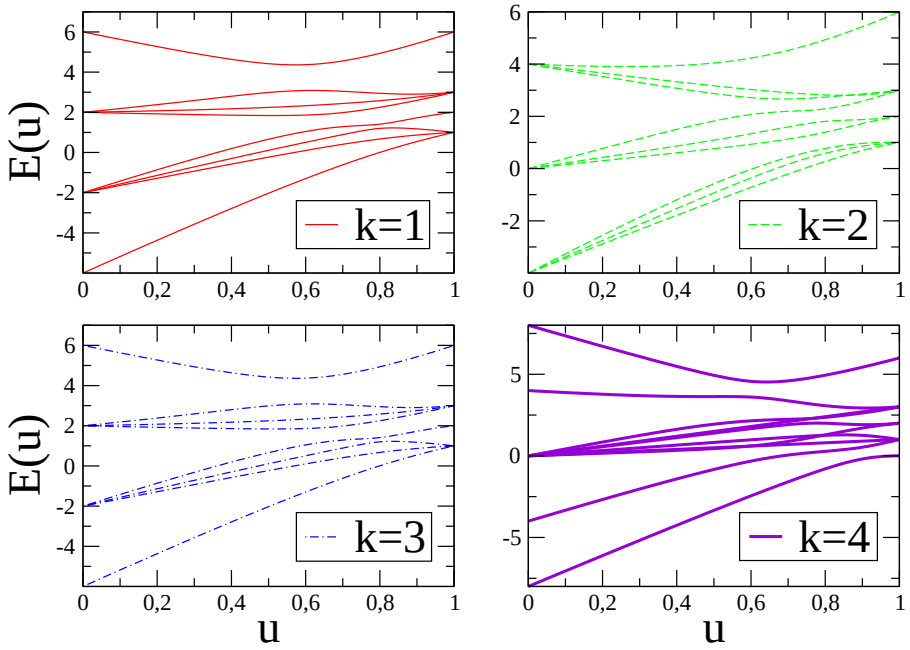

Figure 2.6: Decomposed spectrum of the periodic Bose-Hubbard Hamiltonian with $L = 4$ wells and $N = 4$ bosons. We conclude that the subspaces to the quasimomenta $k = 1$ and $k = 3$ have the same spectra.

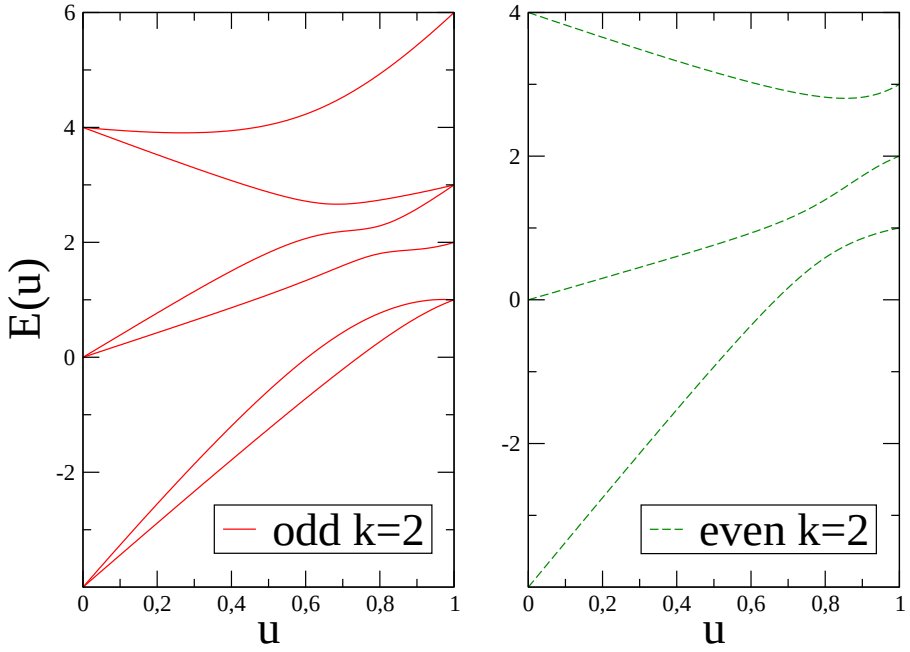

Figure 2.7: Decomposed spectrum of the periodic Bose-Hubbard Hamiltonian with $L = 4$ wells, $N = 4$ bosons and quasimomentum $k = 2$. This subspace can be further decomposed into a part to odd parity and into a part to even parity.

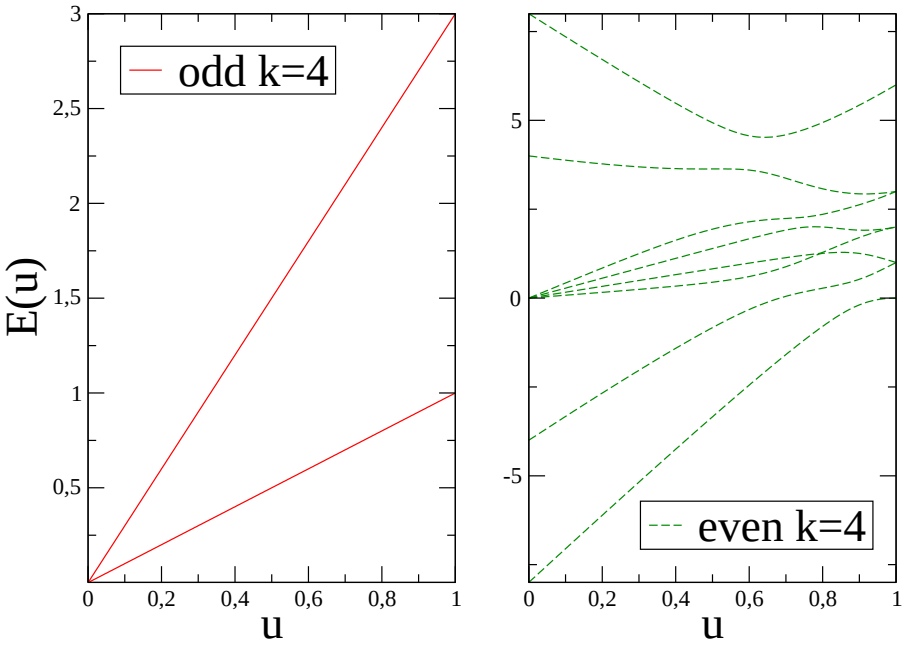

Figure 2.8: Decomposed spectrum of the periodic Bose-Hubbard Hamiltonian with $L = 4$ wells, $N = 4$ bosons and quasimomentum $k = 4$. This subspace can be further decomposed into a part to odd parity and into a part to even parity.

2.3 Experimental realization

The experimental realization is a very fascinating subject itself. Nevertheless we do not want to go into detail here. It is the intention of this section to sketch a simple picture of the experimental setup for a better understanding of the Bose-Hubbard model and our later studies.

The cooling of the atoms is done in two steps. First laser cooling is used to reach temperatures of the order of millikelvin. However, this is not cold enough yet for the creation of a Bose-Einstein condensate. That's why secondly, evaporative cooling has to be applied to cool down the atoms to temperatures of a few hundreds of nanokelvin. These ultralow temperatures are necessary for the formation of a BEC. E.g. the critical temperature of Rubidium-87 is around 300 nanokelvin [41].

Probably the most prominent tool for laser cooling is the magneto-optical trap. Here the atoms get trapped in a strong magnetic field due to their magnetic moments and additionally they are slowed down by scattering from photons. This last process is the actual laser cooling. It can be explained with the Doppler effect, i.e. atoms moving against a source of laser light see a smaller wavelength, a blueshift, while atoms moving away from the source of laser light see a larger wavelength, a redshift. Thus if one shines in laserlight that is slightly red-detuned to an electronic transition of the atoms in the trap and that is aimed at the middle of the trap then atoms moving in the direction out of the trap to the source of the laser light may absorb a photon and its momentum. The atom is then slowed down in this direction. The subsequent spontaneous emission of

a photon happens in a random direction. If one shines in this red-detuned laser light from around the trap the atoms are laser cooled and confined in the trap. In fact the inventors of laser cooling *Chu* (the current US Secretary of Energy), *Cohen-Tannoudji*, and *Phillips* were awarded the Nobel Prize in 1997.

Evaporative cooling is best explained by using the analogue of how a hot cup of coffee cools. One removes the fast atoms out of the trap by lowering its walls. Experimentally the speed of lowering is crucial for retaining an ensemble of ultracold atoms. For the creation of the first BEC *Cornell*, *Wieman*, and *Ketterle* got the Nobel Prize in 2001.

Optical lattices are created by counterpropagating laser beams that form standing electromagnetic waves. The ultracold atoms are confined to the lattice due to a dipole force coming from a spatially varying ac-Stark shift [3]. We note that the validity of the Bose-Hubbard model is limited to bosonic atoms sitting in the lowest band of each well and so the wells have to be sufficiently deep. The depth of the lattice is adjusted by the power of the laser.

Assume we have a 3-dimensional lattice

$$V(x,y,z) \quad = \quad V_0\Big(\sin^2(kx)+\sin^2(ky)+\sin^2(kz)\Big)$$

with lattice depth V_0. As already explained in Section 2.1.1, a proper energy scale for this setting is the recoil energy $E_R = \frac{\hbar^2 k^2}{2m}$ where k denotes the wave vector of the laser light and m is the mass of an atom. In the deep lattice limit $V_0 \gg E_R$ the parameters J and U of the Bose-Hubbard model can be calculated explicitly [38]. The kinetic term reads

$$\frac{J}{E_R} \quad = \quad \frac{4}{\sqrt{\pi}}\Big(\frac{V_0}{E_R}\Big)^{\frac{3}{4}} e^{-2\sqrt{\frac{V_0}{E_R}}} \tag{2.9}$$

and the onsite interaction becomes

$$\frac{U}{E_R} \quad = \quad \sqrt{\frac{8}{\pi}} k a_s \Big(\frac{V_0}{E_R}\Big)^{\frac{3}{4}} \tag{2.10}$$

where a_s denotes the s-wave scattering length.
As physically sensible parameters from the experiment we choose an optical lattice with periodicity $\lambda = 825\,\text{nm}$ and the s-wave scattering length of the hyperfine splitting of Rubidium-87 $a_s = 5.45\,\text{nm}$ [39] and obtain the relation shown in Figure 2.9.

The above considerations are for a 3-dimensional lattice. In this thesis we restrict ourselves to the 1-dimensional Bose-Hubbard model. The reason for this restriction is that the state space grows very fast already in the 1-dimensional case, as can be seen in (2.5). Studying experimentally interesting large systems is numerically demanding and, of course, the effort grows with the dimensionality of the lattice. E.g. the dimension of the state space to a square 2-dimensional lattice with side length of 3 lattice sites and unit filling is the same as the dimension of the state space to a linear 1-dimensional lattice with length of 9 lattice sites and unit filling, and this is according to (2.5) $\dim(9,9) = 24310$. We want to remark that the 1-dimensional Bose-Hubbard model can be realized in

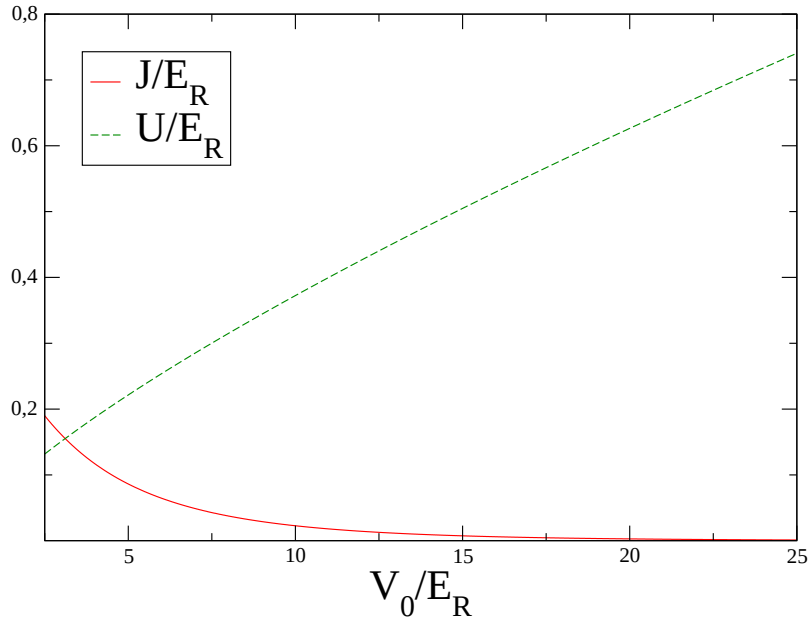

Figure 2.9: Dependence of J (red, solid line) and U (green, dashed line) on V_0 in units of E_R. We choose the realistic parameters $\lambda = 825\,\text{nm}$ for the optical lattice and $a_s = 5.45\,\text{nm}$ as s-wave scattering length of the hyperfine splitting of Rubidium-87.

the experiment very well by using traps that confine the movement of the atoms to one dimension [3]. We will be using the above formulas when we present an experimentally realizable scheme for the generation of practical entanglement in Chapter 4. There we will have to take the restriction of our model to one dimension into account and will therefore adapt the equations (2.9) and (2.10).

Chapter 3

Quantum chaos in the Bose-Hubbard model

Quantum chaos was for the first time investigated in the Bose-Hubbard model by *Kolovsky* and *Buchleitner* in [17]. There they applied the very useful parametrization $U = u$ and $J = 1 - u$ where u runs from 0 to 1. As we have argued in the above chapter on the Bose-Hubbard model, the spectrum of our pure Bose-Hubbard model effectively can be parametrized by one parameter. While u runs from 0 to 1 all possible ratios $\frac{J}{U}$ are covered. This parametrization is particularly useful with respect to quantum chaos because, as we will soon see, the chaotic regime is always around $J = U$, which corresponds to $u = 0.5$ and this is exactly the center of a plot parametrized by u. Additionally, plots over u are bounded by 0 and 1 in contrast to plots over J or U which are unbounded in one direction. That's why we will mostly use their plotting scheme in this thesis.

Kolovsky and *Buchleitner* showed that the Bose-Hubbard model can have quantum chaos in its spectral statistics. More precisely they chose the point $u = 0.3$ of the system $L = 8$ and $N = 8$ and concluded that the level spacing distribution is very well approximated by a Wigner-Dyson distribution by explicitly looking at the integrated level spacing distribution.

At this point let us recapitulate how the chaotic regime is detected in spectral statistics by means of random matrix theory. As already mentioned in the introduction to this thesis, random matrices have randomly chosen entries that follow a certain probability distribution. Initially *Wigner* introduced random matrix theory to describe energy spectra of atomic nuclei and it turned out that the distribution of energy level spacings $s := E_{j+1} - E_j$, between adjacent energy levels in the spectrum, of a specific random matrix ensemble is the same as the distribution of energy level spacings in atomic nuclei. Fortunately, the distribution of level spacings also allows to distinguish the regular and the chaotic regime. Quantum chaos arises in the quantum counterpart of a classically chaotic system. It was found that the probability density P of energy level spacings s in the spectrum of the quantum analogue to a classically regular system obeys a Poisson distribution

$$P(s) \quad = \quad e^{-s} \qquad ,$$

and the Berry-Tabor conjecture states that this shall be true for all classically regular systems [20]. In practice, a Poisson distribution of a regular spectrum is characterized by many vanishing level spacings, i.e. by level crossings. On the other hand it was observed that the probability density P of energy level spacings s in the spectrum of the quantum analogue to a classically chaotic system conforms to a Wigner distribution of either the Gaussian orthogonal ensemble

$$P_{GOE}(s) = \frac{\pi}{2} s e^{-\frac{\pi}{4}s^2} \quad ,$$

the Gaussian unitary ensemble

$$P_{GUE}(s) = \frac{32}{\pi^2} s^2 e^{-\frac{4}{\pi}s^2} \quad ,$$

or the Gaussian symplectic ensemble

$$P_{GSE}(s) = \frac{2^{18}}{3^6\pi^3} s^4 e^{-\frac{64}{9\pi}s^2} \quad ,$$

and the Bohigas-Giannoni-Schmit conjecture states that this shall hold for any classically chaotic system [21]. In contrast to regular spectra, chaotic spectra have no vanishing level spacings, i.e. they are characterized by level repulsion. These repelling energy levels, that come very close to each other but never cross, are called avoided crossings. Their presence is a clear sign for a strong coupling regime and hence for a chaotic spectrum. To which random matrix ensemble a given Hamiltonian belongs is completely determined by its symmetries. The three ensembles differ in their degree of level repulsion specified in the power of the first s in the formula, i.e. the GOE exhibits linear, the GUE quadratic and the GSE quartic level repulsion. Experimentally linear level repulsion has been confirmed by atomic nuclei and micro waves, quadratic level repulsion by Rydberg atoms in strong inhomogeneous magnetic fields and quartic level repulsion has not been observed yet [22]. Our Bose-Hubbard Hamiltonian belongs to the GOE and so we expect linear level repulsion.

However, before we can compare numerically obtained level spacings with the above distributions we have to normalize the level spacings in a proper way, a procedure called unfolding the spectrum [22]. The main goal of unfolding a spectrum is to get a mean level spacing of $\langle s \rangle = 1$. *Kolovsky* and *Buchleitner* unfold their spectrum by fitting a Gaussian to their numerically obtained probability density $\rho(E)$ of energy levels, i.e.

$$\rho(E) = \frac{1}{\sqrt{2\pi}\sigma} e^{-\frac{(E-\mu)^2}{2\sigma^2}}$$

with expectation value μ and standard deviation σ. It can be shown [22] that the new energy levels e_j of the properly unfolded spectrum are then given in terms of the so-called levelstaircase function

$$\sigma(E) = \int_{-\infty}^{E} \mathrm{d}E' \rho(E')$$

as

$$e_j \quad = \quad \sigma(E_j)N \qquad .$$

While for small on-site interation U the data can be well approximated by a Gaussian, it is difficult to fit the data for large on-site interaction U because there the distribution of energy levels is not Gaussian anymore. So their method of unfolding the spectrum is applicable only for small values of u.

Let us look at an example. The Bose-Hubbard Hamiltonian belongs to the GOE and so we expect the probability density P of level spacings s to be a Poisson distribution

$$P_P(s) \quad = \quad e^{-s} \tag{3.1}$$

in the regular regime and a Wigner-Dyson distribution

$$P_{WD}(s) \quad = \quad \frac{\pi}{2} s e^{-\frac{\pi}{4}s^2} \tag{3.2}$$

in the chaotic regime. In order to obtain the level spacing distribution $P(s)$ for numerical data the data has to be binned. This binning, however, is artificial because the underlying data is continuous [42]. Especially for a statistical test binning should be avoided because it enters as an additional optimization. So it is advisable to look at the integrated level spacing distribution

$$I(s) \quad = \quad \int_0^s \mathrm{d}s' P(s')$$

instead. The integrated Poisson distribution is

$$I_P(s) \quad = \quad 1 - e^{-s}$$

and the integrated Wigner-Dyson distribution is

$$I_{WD}(s) \quad = \quad 1 - e^{-\frac{\pi}{4}s^2} \qquad .$$

As one can see in the two Figures 3.1 and 3.2 the integrated level spacing distribution $I(s)$ allows a much better mapping of the regimes than it is possible with binned data because in the latter case the correct assignment of the regime depends on the bin width. We emphasize that the actual numerical integrated level spacing distribution $I_{act.}(s)$ can be directly compared with the expected integrated level spacing distribution $I_{exp.}(s)$, while the actual numerical level spacing distribution $P_{act.}(s)$ additionally has to be optimized in the bin width before it can be compared with the expected level spacing distribution $P_{exp.}(s)$.

Tomadin et al. also investigated spectral statistics in the Bose-Hubbard model with a tilt in [36]. More precisely they determined for which values of the tilting force F the numerical level spacing distribution matches the Wigner-Dyson distribution by making a χ^2 test for binned data.

Kolovsky and *Buchleitner* in [17] additionally studied the nonintegrability of the Bose-Hubbard model via the Shannon entropy of the eigenstates in the Wannier basis,

$$\langle H_W(u) \rangle \quad = \quad \langle - \sum_j |c_j^W(u)|^2 \log(|c_j^W(u)|^2) \rangle \qquad ,$$

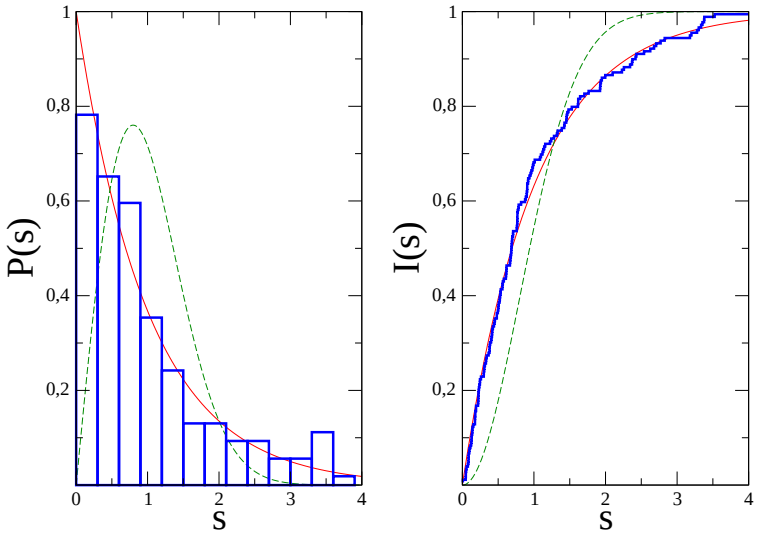

Figure 3.1: Level spacing distribution $P(s)$ (left) and integrated level spacing distribution $I(s)$ (right) for the periodic Bose-Hubbard Hamiltonian with $L = 7 = N$, $J = 5.5$ and $U = 1$, where our numerical data (blue, thick bars) is compared to Poisson (red, thin line) and Wigner-Dyson (green, thin dashed line). Our numerical data very well follows the Poisson distribution and so we conclude that the periodic Bose-Hubbard Hamiltonian of $L = 7$ wells and $N = 7$ bosons is regular for the parameters $J = 5.5$ and $U = 1$.

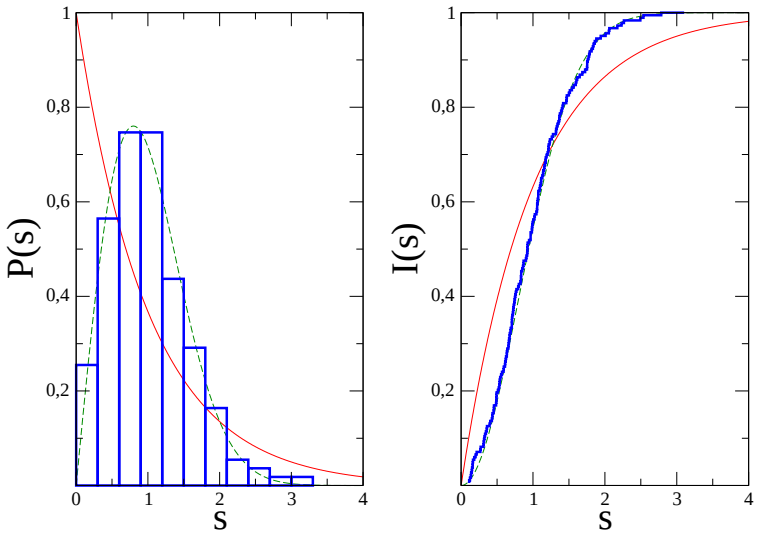

Figure 3.2: Level spacing distribution $P(s)$ (left) and integrated level spacing distribution $I(s)$ (right) for the periodic Bose-Hubbard Hamiltonian with $L = 7 = N$, $J = 1$ and $U = 1$, where our numerical data (blue, thick bars) is compared to Poisson (red, thin line) and Wigner-Dyson (green, thin dashed line). Our numerical data very well follows the Wigner-Dyson distribution and so we conclude that the periodic Bose-Hubbard Hamiltonian of $L = 7$ wells and $N = 7$ bosons is chaotic for the parameters $J = 1$ and $U = 1$.

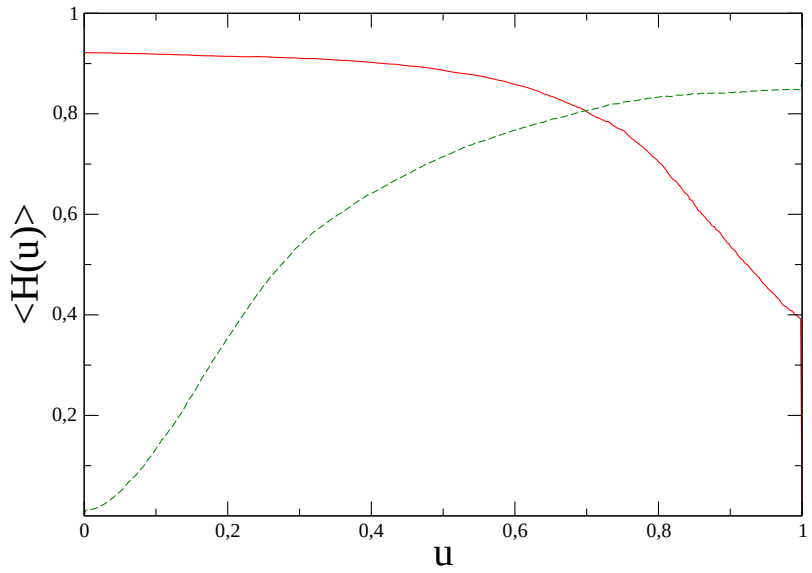

Figure 3.3: Wannier Shannon entropy $\langle H_W(u)\rangle$ (red, thin line) and Bloch Shannon entropy (green, thin dashed line) of the eigenstates of the periodic Bose-Hubbard Hamiltonian with $L = 7 = N$ and quasimomentum $k = 1$ averaged over all eigenstates. We conclude that for $u = 0$ the system is integrable and the proper basis is the Bloch basis, for $u = 1$ the system is integrable and the proper basis is the Wannier basis, and for all other values $u \in (0, 1)$ the system is nonintegrable.

and in the Bloch basis,

$$\langle H_B(u)\rangle \quad = \quad \langle -\sum_j |c_j^B(u)|^2 \log(|c_j^B(u)|^2)\rangle \qquad .$$

Here the c_j^W are the expansion coefficients of a specific eigenstate in the Wannier basis, the c_j^B are the expansion coefficients of a specific eigenstate in the Bloch basis and the brackets denote an average over all eigenstates. As already stated in the introduction to this thesis a quantum system is integrable if there exist as many quantum numbers as degrees of freedom [23]. The canonical quantum numbers of the Bose-Hubbard model are the Wannier occupation numbers of the single-particle Wannier functions and the Bloch occupation numbers of the single-particle Bloch functions. They are canonical because our periodic Bose-Hubbard Hamiltonian has a diagonal interaction part if it is written in Wannier Fock states and it has a diagonal kinetic part if it is written in Bloch Fock states. The averaged Shannon entropy is a good measure for nonintegrability because it vanishes if and only if all eigenstates belong to the expected quantum number, otherwise it is greater than zero.

From Figure 3.3 we conclude that for $u = 0$ the proper basis is the Bloch basis and for $u = 1$ it is the Wannier basis, as expected. But obviously any small interaction U, if one comes from $u = 0$, or respectively any small tunneling J, if one comes from $u = 1$, causes a discontinuous jump in the averaged Shannon

entropy. This discontinuous jump is due to the immediate splitting up of degenerate energy levels at $u > 0$ compared to $u = 0$ and at $u < 1$ compared to $u = 1$. We infer from our measure of nonintegrability that the periodic Bose-Hubbard model is integrable for $u = 0$ and for $u = 1$, and it is nonintegrable for all other values of u.

Apart from static analysis, in the form of spectral statistics and nonintegrability, dynamic properties can also separate the regular and the chaotic regime. *Gorin et al.* explain in [24] how the decay of the fidelity

$$F(t) \quad = \quad |\langle \psi_{\lambda,0}(t) | \psi_{\lambda,\epsilon}(t) \rangle|^2$$

can be used to differentiate between the regular and chaotic regime. Here we propagate the same initial state $|\psi(0)\rangle$ with two slightly different Hamiltonians. In fact we only have one possibly time-dependent Hamiltonian

$$H_{\lambda,\epsilon}(t) \quad = \quad H_\lambda(t) + \epsilon V(t)$$

and evolve the bra with $H_{\lambda,0}(t) = H_\lambda(t)$ and the ket with $H_{\lambda,\epsilon}(t) = H_\lambda(t) + \epsilon V(t)$. As explained in [24], very often the decay of the fidelity is calculated analytically in the semiclassical limit of the system under consideration and then a prediction for the quantum limit is made. The semiclassical limit of the Bose-Hubbard model is given by $\frac{N}{L} \to \infty$ [43], i.e. if the filling goes to infinity. However, predictions for the Bose-Hubbard model with an arbitrary number of L wells are difficult to obtain as can be seen in [44] where calculations for a two-component BEC are presented.

We want to remark that the fidelity is an outstandingly powerful tool that is employed in completely different fields of physics. *Zanardi et al.* developed an elaborate theory for the inspection of quantum phase transitions based on the fidelity [45]. The fidelity is also an important tool in quantum information theory [30].

We believe that avoided crossings are a clear indicator of quantum chaos in all the above aspects. In spectral statistics, avoided crossings are the fundamental reason for the lack of vanishing level spacings. At an avoided crossing of two energy levels the corresponding two wave functions swap, which is why there cannot exist a reasonable quantum number attached to each of them, and so nonintegrability follows. The study of avoided crossings also allows to merge two core disciplines of quantum chaos, namely spectral and dynamic investigations. Because the wave function changes at an avoided crossing the fidelity can locate avoided crossings in the spectrum.

Additionally avoided crossings are responsible for the so-called diffusion in energy space [46]. Here the nonintegrable Hamiltonian under consideration depends on one parameter λ that is changed in time such that we have $\hat{H}(\lambda(t))$. If one starts with a highly excited eigenstate $|\psi(0)\rangle$ to $\hat{H}(\lambda(0))$ at a specific time $t = 0$, propagates it with the time-dependent Hamiltonian $\hat{H}(\lambda(t))$ and looks at the occupation probability $|\langle \psi(t) | n(t) \rangle|^2$ with the instantaneous eigenstates $|n(t)\rangle$ to $\hat{H}(\lambda(t))$, then this occupation probability spreads diffusively away from the initial state. This diffusion can indeed be described with a diffusion constant.

In the first section of this chapter we will investigate the spectral statistics of the Bose-Hubbard model with different filling. We will explain our own unfolding procedure that will allow the investigation of a bigger range of u than it is possible with the unfolding procedure of *Kolovsky* and *Buchleitner*. Additionally we will discuss and apply a statistical test for continuous data, the Kolmogorov-Smirnov test, that is much better suited to our problem than the χ^2 for binned data. In this first section we will show the limitations of the approach via spectral statistics for the determination of the chaotic regime. We do a dynamic analysis by means of the fidelity in the second section. There we will begin with studies of the decay of the fidelity. Then we will redefine the fidelity for the quantification of avoided crossings. Finally we will use this redefined fidelity to compute the distribution of avoided crossings in the spectrum of the Bose-Hubbard model with different filling and compare these results to spectral statistics in the first section.

3.1 Spectral statistics

In this section we will first explain our own unfolding procedure that allows the investigation of a bigger range of u than the unfolding procedure used by *Kolovsky* and *Buchleitner* in [17]. Then we will present a statistical test, the Kolmogorov-Smirnov test, that allows an unambiguous detection of the regular and of the chaotic regime. This test is much better suited for the classification of the regular and the chaotic regime than the χ^2 test for binned data used by *Tomadin et al.* in [36] because this χ^2 test for binned data additionally has to optimize over the bin width. We emphasize that their binning is completely artificial because the investigated data is continuous [42]. It is our intention in this section to work out the limitations of the approach via spectral statistics for the determination of the regular and chaotic regime. These limitations can be circumvented with a novel method for the detection of the chaotic regime that we derive in the end of the second section. We want to compare the two approaches by looking at systems of different filling. That's why in this first section, finally, we will apply the Kolmogorov-Smirnov test to systems of different filling.

3.1.1 Unfolding the spectrum

In the introduction to this chapter we explained the unfolding procedure used by *Kolovsky* and *Buchleitner* in [17]. Because their approach of unfolding is not applicable to the whole parameter range of u we take an alternative path.

We proceed in three steps. First we normalize all energy levels E_j by defining new energies

$$e_j = \frac{E_j}{E_{max} - E_{min}} \quad .$$

Second we calculate all level spacings

$$s'_j = e_{j+1} - e_j$$

of these new energies and third we derive the final level spacings s_j by locally normalizing the s'_j to 1,

$$s_j \;=\; \frac{s'_j}{\langle s'_j \rangle_{local}} \qquad .$$

In the third step the local average $\langle s'_j \rangle_{local}$ is obtained by averaging over a specific number $n_{s'}$ of neighbouring level spacings. $n_{s'}$ is the only free parameter in our statistical test. In order to get a continuous function of the level spacings, $n_{s'}$ has to be chosen small enough to be infinitesimal on the whole scale and on the other hand, $n_{s'}$ has to be chosen big enough such that local fluctuations are smeared out [22]. Having that in mind we decide to let $n_{s'}$ run from 1 energy level, where there is no local normalization, up to $\frac{1}{10}$ of all energy levels. In fact, we will optimize our statistical test only over $n_{s'}$ and only within this range. Figures 3.1 and 3.2 show results obtained from our unfolding procedure for the periodic Bose-Hubbard model with $L = 7$ wells and $N = 7$ bosons at $J = 5.5$ and $U = 1$ and at $J = 1$ and $U = 1$.

3.1.2 Kolmogorov-Smirnov test

We now need a statistical test that enables us to classify the regular and chaotic regime with certain probabilities. The simplest test of this kind is the χ^2 test for binned data and it was used by *Tomadin et al.* in [36]. But our data is continuous and not binned [42]. Applying the χ^2 test for binned data would mean that we would have to artificially bin the data. Then, additionally, our statistical test would have to optimize over the bin width. These two problematic points can be avoided if we use the Kolmogorov-Smirnov test, which is a statistical test for continuous data. In short, the Kolmogorov-Smirnov test compares the cumulative function of the actual distribution with the cumulative function of the expected distribution [42]. The cumulative function is just the integral over the distribution. So instead of a direct comparison with the Poisson level spacing distribution $P_P(s)$ (3.1) or with the Wigner-Dyson level spacing distribution $P_{WD}(s)$ (3.2) the integrated level spacing distribution $I(s)$ is considered. The integrated Poisson distribution is

$$I_P(s) \;=\; 1 - e^{-s}$$

and the integrated Wigner-Dyson distribution is

$$I_{WD}(s) \;=\; 1 - e^{-\frac{\pi}{4}s^2} \qquad .$$

As we already concluded from the two Figures 3.1 and 3.2 the integrated level spacing distribution $I(s)$ also allows a simpler assignment of the regular or the chaotic regime than the level spacing distribution $P(s)$, where the data has to be binned and the correct classification of the regimes depends on the bin width.

Another great advantage of the Kolmogorov-Smirnov test is that the significance that the actual distribution $I_{act.}$ matches the expected distribution $I_{exp.}$ can be calculated explicitly [42]. The significance tells us the probability p that

the actual distribution $I_{act.}$ originates from the expected distribution $I_{exp.}$. In the following plots we choose a significance level of 0.05. This means we reject that our actual distribution $I_{act.}$ comes from the expected distribution $I_{exp.}$ if the probability p for that is less than 5 percent.

In Figure 3.4 we study the applicability of spectral statistics depending on the number of energy levels. Since the expected distribution is derived from a random matrix ensemble in the limit of infinitely many energy levels [22], we expect that spectral statistics is useful only if at least some lower bound of energy levels are considered. We investigate the $k = 1$-subspace of the periodic Bose-Hubbard Hamiltonian with $L = 7$ wells and fill these with particles. We read off from the plot that a clear distinction between the regular and the chaotic regime is not possible until we have at least 132 energy levels in the system of $N = 6$ bosons. Moreover, we conclude that in general the inner part of u is chaotic and the outer parts are regular.

It is conspicuous that the outer parts of u, i.e. the regimes $\frac{J}{U} \gg 1$ and $\frac{U}{J} \gg 1$ seem to be neither regular nor chaotic. This is due to degeneracy in the spectrum. In these limits the degeneracy becomes noticeable such that there are many small and few large level spacings. So the distribution of level spacings is not determined by the absence or presence of avoided crossings but by the degree of degeneracy, an effect we are not interested in. We believe that degeneracy is a fundamental problem in the analysis of level spacings and that it limits the use of this technique for the distinction between the regular and the chaotic regime. Of course, the outer parts of u have to be regular as we infer for example from the aspect of nonintegrability in Figure 3.3.

Figure 3.5 shall serve as a reference, throughout this thesis, for the position of the regular and the chaotic regime in the periodic Bose-Hubbard Hamiltonian with unit filling, i.e. $\frac{N}{L} = 1$. The plots for $L = 5 = N$, $L = 6 = N$ and $L = 8 = N$ qualitatively look the same and so we decided to show the system $L = 7 = N$. We remark that also the different k-subspaces qualitatively give the same results. We investigated all different k-subspaces for $L = 7 = N$ and then chose $k = 1$ for this presentation.

Finally we want to apply spectral statistics to systems of different filling. The results obtained here shall be later compared with the results obtained from our novel method for the detection of the chaotic regime in the end of the second section.

In order to be able to compare the spectral statistical analysis of systems with different filling, their spectra must have approximately the same number of energy levels. Because we chose the $k = 1$-subspace of $L = 7 = N$ as our reference and because it comprises 245 energy levels, we will choose systems like that. Our considered systems have 250 ± 25 energy levels. We conclude from our spectral statistical analysis in Figure 3.6 that for small filling, $L = 37$ and $N = 3$, the periodic Bose-Hubbard Hamiltonian is regular throughout the whole spectrum. Already at half filling, $L = 11$ and $N = 5$, a clear chaotic regime shows up. For big filling, $L = 3$ and $N = 37$, the chaotic regime gets smaller and wanders to small values of u. We note that we applied the Kolmogorov-Smirnov test to many more different systems and qualitatively obtained exactly these results, which is why we only plotted the selected systems in Figure 3.6. We

will further discuss these results at the end of the second section of this chapter.

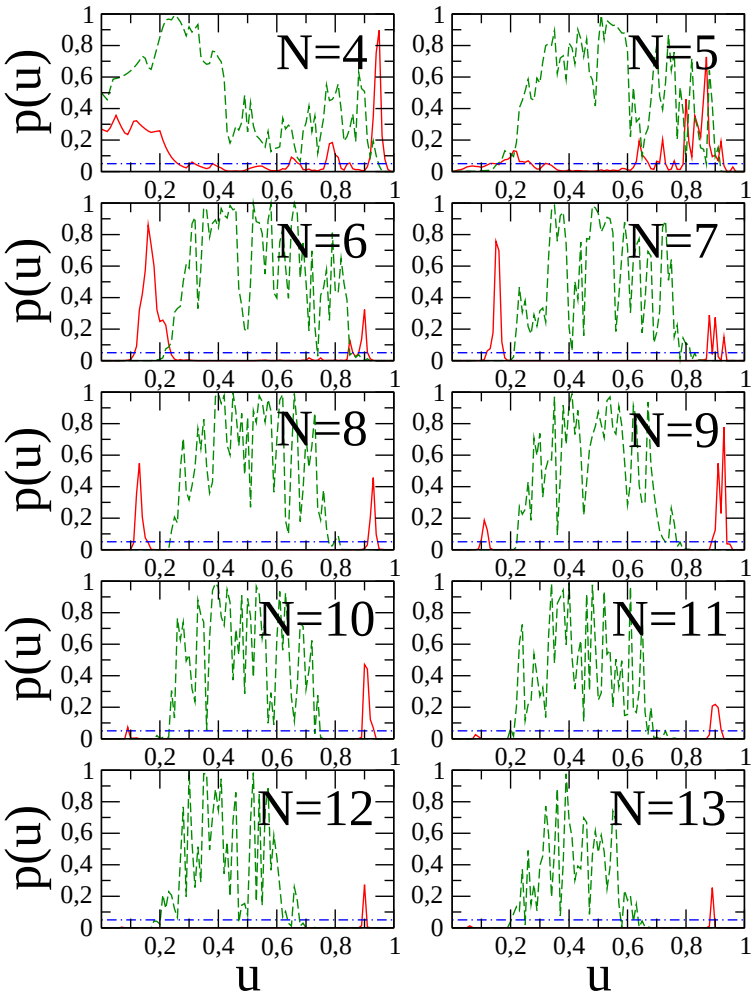

Figure 3.4: Kolmogorov-Smirnov Poisson test (red, thin line) and Wigner-Dyson test (green, thin dashed line) applied to the periodic Bose-Hubbard Hamiltonian with $L = 7$ wells, quasimomentum $k = 1$ and different particle numbers (the significance level is set to 5 percent (blue, thin dash dotted line)), revealing the validity of spectral statistics depending on the number of energy levels because $N = 4$ has 30 energy levels, $N = 5$ has 66 energy levels, $N = 6$ has 132 energy levels, $N = 7$ has 245 energy levels, $N = 8$ has 429 energy levels, $N = 9$ has 715 energy levels, $N = 10$ has 1144 energy levels, $N = 11$ has 1768 energy levels, $N = 12$ has 2652 energy levels and $N = 13$ has 3876 energy levels. We conclude that at least 132 energy levels have to be considered for a clear separation of the regular and the chaotic regime by means of spectral statistics. Moreover we see that in general the middle part of u is chaotic and the outer parts are regular. However, spectral statistics does not work well in the outer parts of u due to the beginning degeneracy.

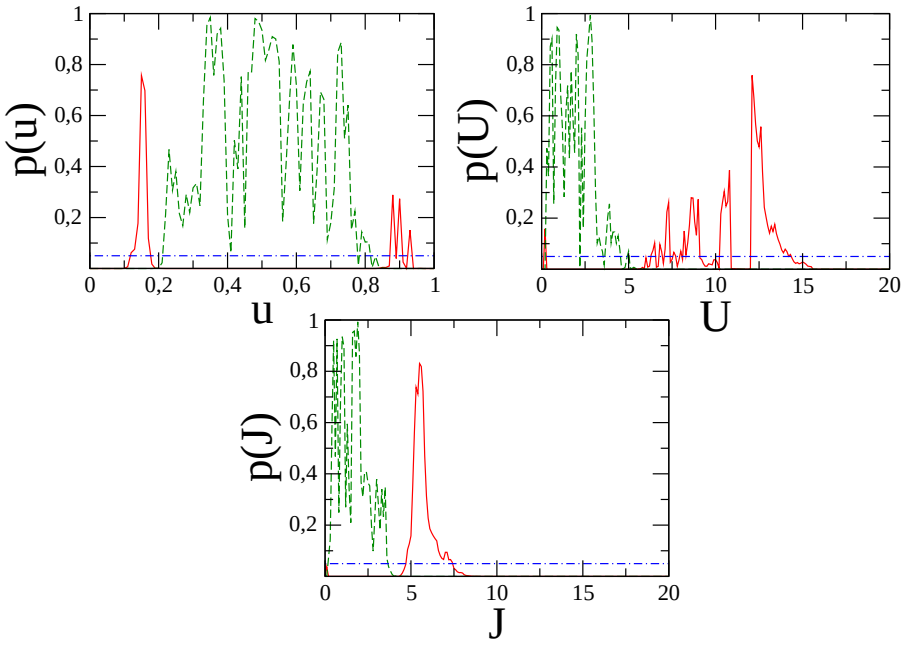

Figure 3.5: Kolmogorov-Smirnov Poisson test (red, thin line) and Wigner-Dyson test (green, thin dashed line) applied to the periodic Bose-Hubbard Hamiltonian with $L = 7$ wells, $N = 7$ bosons, quasimomentum $k = 1$ and different parametrizations (the significance level is set to 5 percent (blue, thin dash dotted line)), as a reference for the location of the regular and the chaotic regime in the periodic Bose-Hubbard Hamiltonian with unit filling. Clearly spectral statistics does not work in the outer parts of u due to degeneracy.

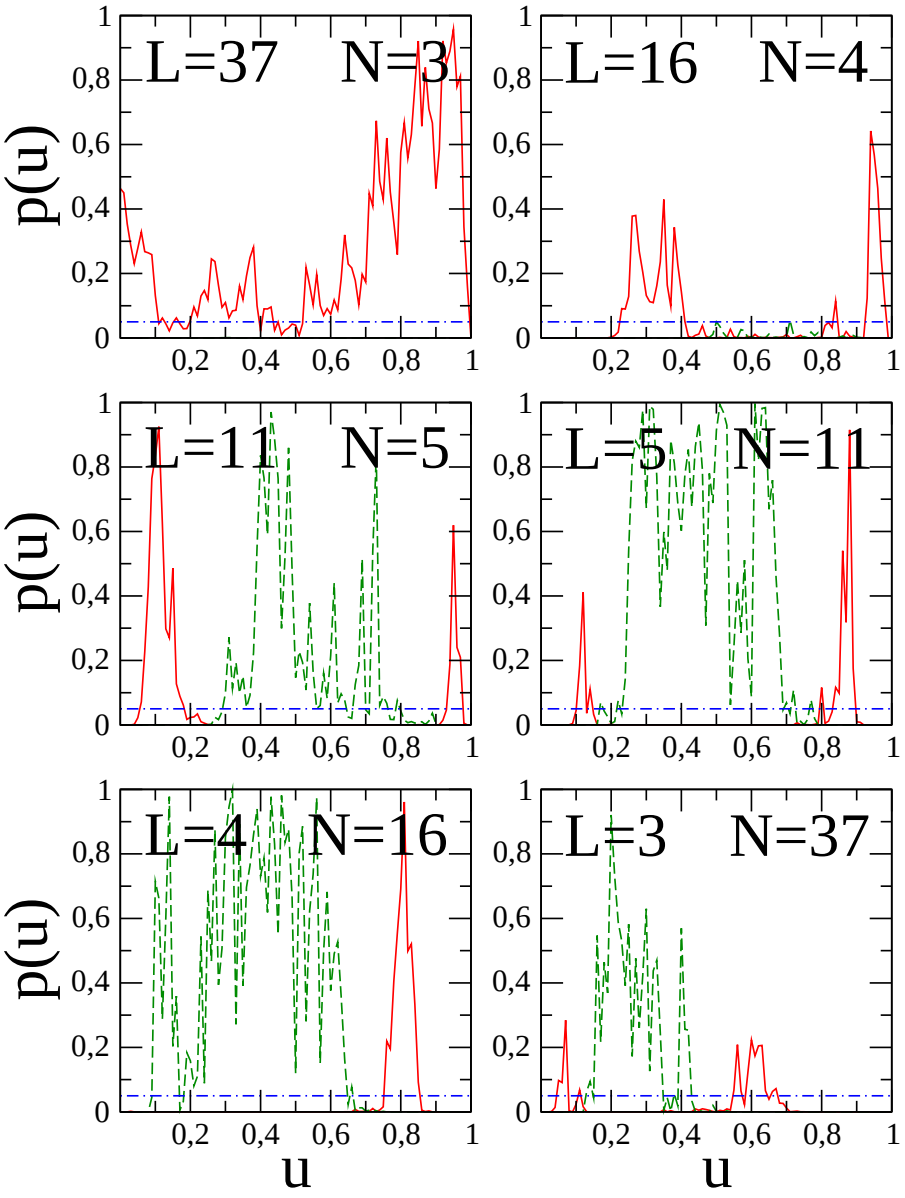

Figure 3.6: Kolmogorov-Smirnov Poisson test (red, thin line) and Wigner-Dyson test (green, thin dashed line) applied to the periodic Bose-Hubbard Hamiltonian with quasimomentum $k = 1$ and different fillings but with the same number of 250 ± 25 energy levels because $L = 37$ and $N = 3$ has 247 energy levels, $L = 16$ and $N = 4$ has 240 energy levels, $L = 11$ and $N = 5$ has 273 energy levels, $L = 5$ and $N = 11$ has 273 energy levels, $L = 4$ and $N = 16$ has 240 energy levels and $L = 3$ and $N = 37$ has 247 energy levels. This Figure has to be compared with the result at the end of the second section. As expected, systems of very small filling are regular throughout the spectrum. With increasing filling the chaotic regime gets smaller and wanders to the region of small values of u.

3.2 Fidelity

After we have done spectral analysis we now want to address the determination of the regular and of the chaotic regime from a dynamic point of view. As we have argued in the introduction to this diploma thesis classical chaos is examined in classical phase space [19]. If a classical system evolves from two initially very close points in phase space such that the distance between the two resulting trajectories grows exponentially in time, then the system is called chaotic. More precisely the definition of classical chaos additionally includes the requirement that the trajectories have to be spatially delimited. The exponential growth in the distance between the two classical trajectories is characterized by the Lyapunov exponent.

In quantum chaos a close link to this classical dynamic definition of chaos is given in terms of the fidelity. In this context a highly excited state, i.e. a state of high energy, is propagated with two slightly different Hamiltonians. These actually emerge from the same single possibly time-dependent Hamiltonian

$$\hat{H}_{\lambda,\epsilon}(t) \quad = \quad \hat{H}_{\lambda}(t) + \epsilon \hat{V}(t)$$

such that the state evolves once with the unperturbed Hamiltonian $\hat{H}_{\lambda,0}(t) = \hat{H}_{\lambda}(t)$ and once with the slightly perturbed Hamiltonian $\hat{H}_{\lambda,\epsilon}(t) = \hat{H}_{\lambda}(t)+\epsilon\hat{V}(t)$. The distance between these two propagations is then measured with the fidelity

$$F_{\lambda,\epsilon}(t) \quad = \quad |\langle \psi_{\lambda,0}(t) | \psi_{\lambda,\epsilon}(t) \rangle|^2 \tag{3.3}$$

where the bra denotes the time evolution of the initial state $|\psi(0)\rangle$ with the unperturbed Hamiltonian $\hat{H}_{\lambda,0}(t)$ and the ket is the time evolution of the initial state $|\psi(0)\rangle$ with the perturbed Hamiltonian $\hat{H}_{\lambda,\epsilon}(t)$. This dynamic fidelity can then have signatures of quantum chaos in its decay behaviour [24].

Expressed in a different form the fidelity can also be used for static investigations of eigenstates,

$$F(\lambda,\epsilon) \quad = \quad |\langle \psi(\lambda) | \psi(\lambda+\epsilon) \rangle|^2 \qquad . \tag{3.4}$$

Here we consider a Hamiltonian $\hat{H}(\lambda)$ that depends on a parameter λ. $|\psi(\lambda)\rangle$ is a specific eigenstate to $\hat{H}(\lambda)$ and $|\psi(\lambda+\epsilon)\rangle$ is the same specific eigenstate to $\hat{H}(\lambda+\epsilon)$. In order to be able to distinguish the two above fidelities we will refer to (3.3) as the dynamic fidelity and to (3.4) as the static fidelity. The idea of the static fidelity goes back to *Zanardi et al.* when they used this quantity to run through a quantum phase transition in [45, 47]. Then the specific eigenstate $|\psi\rangle$ in the static fidelity is the ground state. For our periodic Bose-Hubbard Hamiltonian this investigation of the ground state via the static fidelity has already been done by *Buonsante* and *Vezzani* in [28]. There they pinpointed the quantum critical point of the superfluid to Mott insulating quantum phase transition to $(\frac{J}{U})_{crit.} = 0.257 \pm 0.001$ with the help of finite size scaling.

In this section we will first investigate the fidelity decay of the dynamic fidelity of highly excited states. Then we will define a new measure for the unique quantification of avoided crossings from the static fidelity. Finally we

will use this new measure to obtain the distribution of avoided crossings in the periodic Bose-Hubbard model with different filling. This determination of the distribution of avoided crossings is a novel technique for the specification of the quantum chaotic regime. We will compare our new method with the spectral statistics approach by comparing the predictions for systems of different filling in the end of this section.

3.2.1 Fidelity decay

Our periodic Bose-Hubbard Hamiltonian depends linearly on J and U and so the above definition (3.3) of the dynamic fidelity can be directly used for either of the two parameters by setting the other equal to 1. Additonally our Hamiltonian is time-independent. We want to begin with $U = 1$ and J being the varying parameter. So we set $\lambda = J$, $\epsilon = \delta J$ and

$$\begin{aligned}\hat{H}_{J,\delta J} &:= \frac{1}{2}\sum_{l=1}^{L}\hat{n}_l(\hat{n}_l - 1) - J\sum_{l=1}^{L}(\hat{a}_{l+1}^{\dagger}\hat{a}_l + \hat{a}_l^{\dagger}\hat{a}_{l+1}) - \\ &\qquad \delta J\sum_{l=1}^{L}(\hat{a}_{l+1}^{\dagger}\hat{a}_l + \hat{a}_l^{\dagger}\hat{a}_{l+1}) \qquad .\end{aligned}$$

We choose a system of $L = 5$ wells and $N = 5$ bosons. The initial state shall be the state of highest energy in the Wannier basis, which is $|\psi(0)\rangle = |50000\rangle_W$ where all the bosons sit in the same well. We propagate this state with $H_{J,0}$ to get the bra and propagate it with $H_{J,\delta J}$ to obtain the ket for the dynamic fidelity

$$F_{J,\delta J}(t) = |\langle\psi_{J,0}(t)|\psi_{J,\delta J}(t)\rangle|^2$$

and set $\delta J = 0.001$. Figure 3.7 depicts the time evolution of this dynamic fidelity for the ratios $\frac{J}{U} = \frac{1}{10}$, $\frac{J}{U} = \frac{1}{2}$, $\frac{J}{U} = 1$, $\frac{J}{U} = 2$ and $\frac{J}{U} = 10$. Let us note that the precise units of time are discussed in Section 2.1.1. From Figure 3.7 we see that the initial state remains constant on this time scale for $J \ll U$ while for $J \gg U$ the curves seem to converge to a decay independent of J. This makes sense because for J much smaller than U the initial state $|50000\rangle_W$ is very close to an eigenstate of $\hat{H}_{J,\delta J}$ and an eigenstate, of course, is stationary. However, that the decay becomes independent of J for $J \gg U$ is unexpected and can be interpreted as a manifestation of the regular regime.

Let us remind ourselves of the reference Figure 3.5 for the precise position of the regular and of the chaotic regime in the periodic Bose-Hubbard Hamiltonian with unit filling. From this figure we read off that $J = 10$ and $U = 1$ is in the regular regime and that $J = 1$ and $U = 1$ is in the chaotic regime. Hence it seems plausible that the decay becomes independent of J in the regular regime.

We are now interested in the question of what happens if we propagate slightly different highly excited initial states, i.e. initial states of slightly different high energy. Thinking of classical chaos, we would expect the propagation of slightly different initial states to be only slightly different in the regular regime and to be significantly different in the chaotic regime. For that we take the

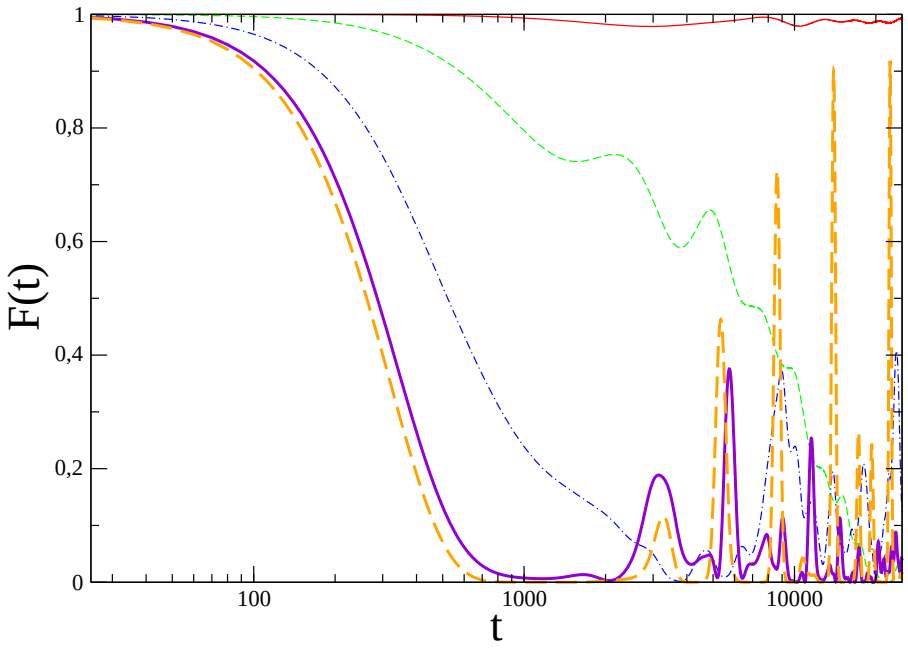

Figure 3.7: Time evolution of the dynamic fidelity $F_{J,\delta J}$ with $\delta J = 0.001$ and the highly excited initial state $|50000\rangle_W$ propagated with the periodic Bose-Hubbard Hamiltonian with $U = 1$ and $J = 0.1$ (red, thin line), $J = 0.5$ (green, thin dashed line), $J = 1$ (blue, thin dash dotted line), $J = 2$ (violet, thick line) and $J = 10$ (orange, thick dashed line); see Section 2.1.1 for our definition of the units of time. We see that if J is much smaller than U, the red curve corresponds to $\frac{J}{U} = 0.1$, the initial state remains unchanged on this time scale. This is expected to happen because then the initial state is very close to an eigenstate of $\hat{H}_{J,\delta J}$. But if J is much larger than U, the orange curve corresponds to $\frac{J}{U} = 10$, the initial state decays comparably on the same time scale independent of J, and this can be interpreted as a manifestation of the regular regime.

initial states $|50000\rangle_W$, $|41000\rangle_W$ and $|32000\rangle_W$. They evolve in the regular regime for $J = 10$ and $U = 1$ and in the chaotic regime for $J = 1$ and $U = 1$ in Figure 3.8. Figure 3.9 is a close-up of the decay.

Remarkably the propagation of the three slightly different states is only slightly different in the regular regime and significantly different in the chaotic regime. It is even more remarkable that the fidelity has these very high maxima, which are referred to as revivals, in the regular regime and they do not show up in the chaotic regime. We believe that these maxima are finite size effects, but we certainly will investigate that in the near future. Figure 3.9 reveals that the short time scale of the decay does not allow a separation of the regular and the chaotic regime, and we conclude from the insets that the decay is neither exponential nor power-law.

Until now we have always used a fix perturbation strength $\delta J = 0.001$. Let us analyze the dependence of the fidelity decay on δJ. It can be shown [24] that

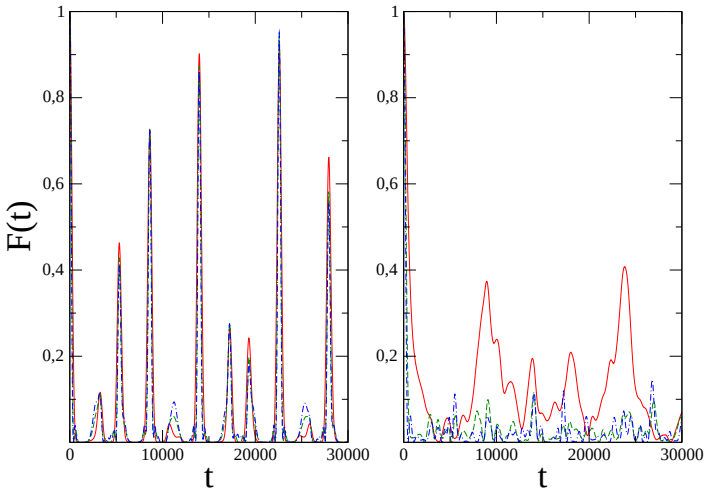

Figure 3.8: Time evolution of the dynamic fidelity $F_{J,\delta J}$ with $\delta J = 0.001$ and the slightly different highly excited initial states $|50000\rangle_W$ (red, thin line), $|41000\rangle_W$ (green, thin dashed line) and $|32000\rangle_W$ (blue, thin dash dotted line) propagated with the periodic Bose-Hubbard Hamiltonian with $U = 1$ and $J = 10$ in the regular regime (left) and with $U = 1$ and $J = 1$ in the chaotic regime (right) (c.f. Section 2.1.1 for the units of time). Remarkably the slightly different initial states feature only a slightly different propagation in the regular regime and a significantly different propagation in the chaotic regime, as one would expect from the analogy to classical chaos.

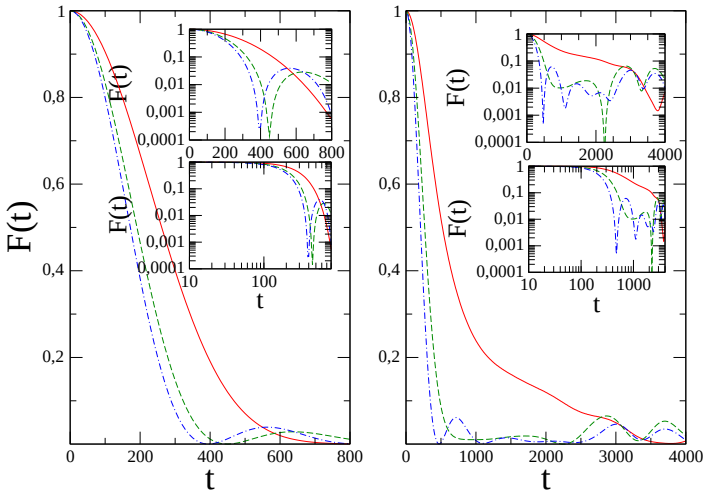

Figure 3.9: Decay of the dynamic fidelity $F_{J,\delta J}$ with $\delta J = 0.001$ and the slightly different highly excited initial states $|50000\rangle_W$ (red, thin line), $|41000\rangle_W$ (green, thin dashed line) and $|32000\rangle_W$ (blue, thin dash dotted line) propagated with the periodic Bose-Hubbard Hamiltonian with $U = 1$ and $J = 10$ in the regular regime (left) and with $U = 1$ and $J = 1$ in the chaotic regime (right); note the logarithmic and the double-logarithmic insets. Compared with the previous Figure 3.8, the short time scale of the decay does not allow for a distinction of the regular and the chaotic regime.

for a time-independent Hamiltonian the dynamic fidelity (3.3) behaves like

$$F_{\lambda,\epsilon}(t) \quad = \quad 1 - C \cdot \epsilon^2 t^2$$

at the beginning of the decay, where C is a constant, and hence if we plot the dynamic fidelity over ϵt we should always observe a quadratic decrease at the beginning of the decay. From now on we will examine the dynamic fidelity as a function of ϵt. Here λ and J are used interchangeably, and this is also the case with ϵ and δJ.

So we have $|50000\rangle_W$ as the initial state and look at the time evolution of the dynamic fidelity $F_{J,\delta J}(t)$ for $\delta J = 0.5$, $\delta J = 0.1$, $\delta J = 0.01$, $\delta J = 0.001$, and $\delta J = 0.0001$. We propagate this initial state in the regular regime for $J = 10$ and $U = 1$ and in the chaotic regime for $J = 1$ and $U = 1$. Surprisingly Figure 3.10 shows that the time evolution of the dynamic fidelity is completely independent of the perturbation strength δJ in the regular regime and this is not the case in the chaotic regime. In the chaotic regime the curves converge only for $\delta J < 0.001$ on the long time scale.

So we have another correspondence between classical and quantum chaos. If we interpret the perturbation strength δJ to be the initial distance of the two

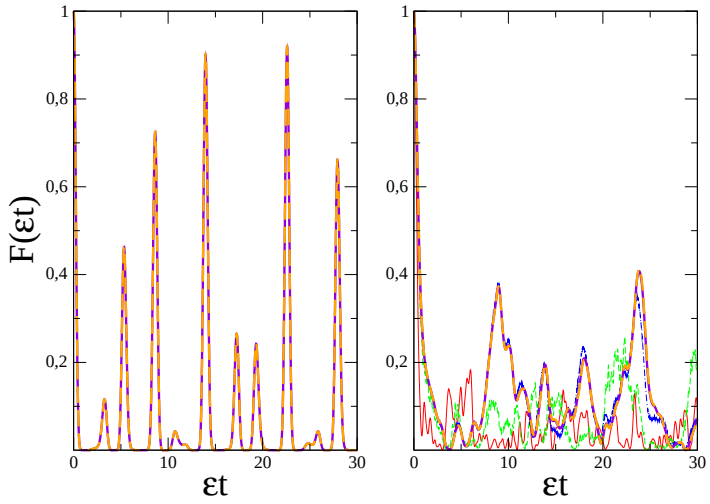

Figure 3.10: Time evolution of the dynamic fidelity $F_{J,\delta J}$ with $\delta J = 0.5$ (red, thin line), $\delta J = 0.1$ (green, thin dashed line), $\delta J = 0.01$ (blue, thin dash dotted line), $\delta J = 0.001$ (violet, thick line) and $\delta J = 0.0001$ (orange, thick dashed line) and the highly excited initial state $|50000\rangle_W$ propagated with the periodic Bose-Hubbard Hamiltonian with $U = 1$ and $J = 10$ in the regular regime (left) and with $U = 1$ and $J = 1$ in the chaotic regime (right). Obviously there is no dependence of the time evolution of the dynamic fidelity on the perturbation strength δJ in the regular regime and this is not the case in the chaotic regime. We get a correspondence to classical chaos if we interpret δJ to be the distance of two classical starting points in classical phase space because classically we would also expect there to be no dependence on this initial distance in the regular regime.

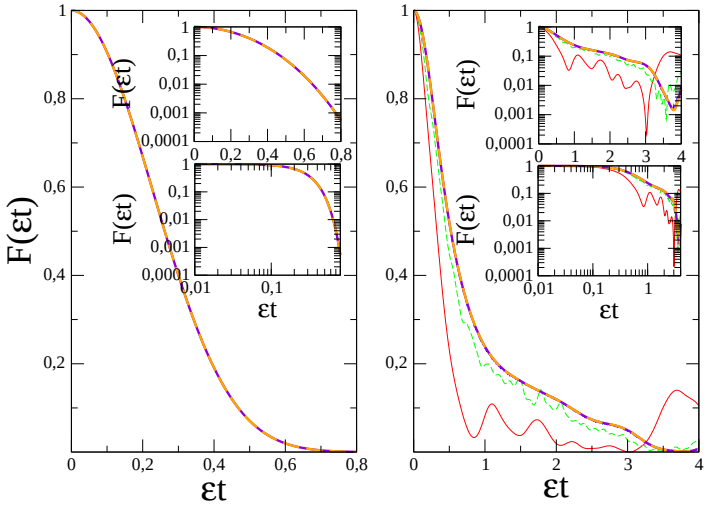

Figure 3.11: Decay of the dynamic fidelity $F_{J,\delta J}$ with $\delta J = 0.5$ (red, thin line), $\delta J = 0.1$ (green, thin dashed line), $\delta J = 0.01$ (blue, thin dash dotted line), $\delta J = 0.001$ (violet, thick line) and $\delta J = 0.0001$ (orange, thick dashed line) and the highly excited initial state $|50000\rangle_W$ propagated with the periodic Bose-Hubbard Hamiltonian with $U = 1$ and $J = 10$ in the regular regime (left) and with $U = 1$ and $J = 1$ in the chaotic regime (right). Compared to the previous figure 3.10 the time scale of the decay suffices to separate the regular and the chaotic regime.

classical starting points in the classical phase space, then in the regular regime we do not have any dependence of the propagation on this initial distance, in contrast to the chaotic regime. This is exactly what one would expect from classical chaos.

Further analysis showed that as soon as U gets bigger than J another time scale has to be used. As already mentioned the initial state $|50000\rangle_W$ of all bosons in one well just doesn't change for big ratios $\frac{U}{J}$ because it is close to an eigenstate to $\hat{H}_{J,\delta J}$. Numerically we find that scaling the time with U^4 gives comparable curves, and the dynamic fidelity also decays on a much larger time scale.

A much nicer way of investigating the regime $\frac{U}{J} > 1$ is given by simply swapping the appearance of Wannier and Bloch in the above calculations. This means that we put $J = 1$, $\lambda = U$, $\epsilon = \delta U$ and

$$\hat{H}_{U,\delta U} := -\sum_{l=1}^{L}(\hat{a}_{l+1}^{\dagger}\hat{a}_l + \hat{a}_l^{\dagger}\hat{a}_{l+1}) + \frac{U}{2}\sum_{l=1}^{L}\hat{n}_l(\hat{n}_l - 1) + \frac{\delta U}{2}\sum_{l=1}^{L}\hat{n}_l(\hat{n}_l - 1) \quad .$$

For the propagation we need a highly excited Bloch Fock state. We choose the Bloch Fock state of highest energy $|05000\rangle_B$ as $|\psi(0)\rangle$. With this change all the above results can now be obtained for $\frac{U}{J} > 1$, as we checked explicitly, and

the correspondence between classical and quantum chaos exists in the same way for the regular regime of $J = 1$ and $U = 10$ and the chaotic regime of $J = 1$ and $U = 1$ as above. In fact, the same analogies between classical and quantum chaos can be derived. Here we only want to show Figure 3.12 and 3.13 which confirm the independence of the time evolution of the dynamic fidelity from the perturbation strength δU.

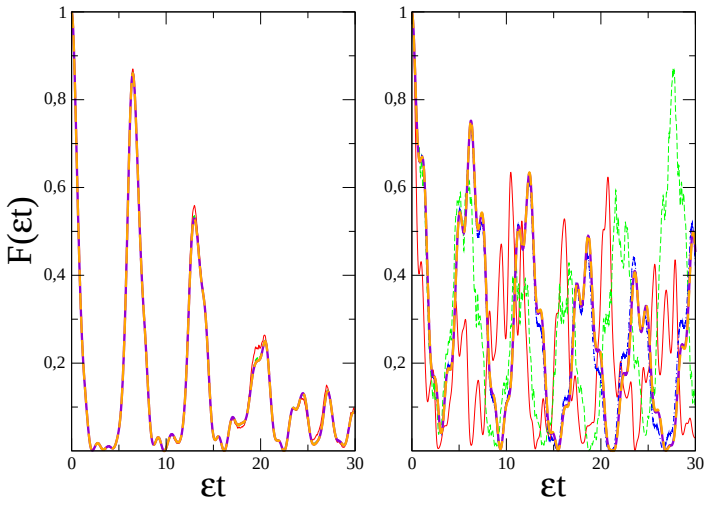

Figure 3.12: Time evolution of the dynamic fidelity $F_{U,\delta U}$ with $\delta U = 0.5$ (red, thin line), $\delta U = 0.1$ (green, thin dashed line), $\delta U = 0.01$ (blue, thin dash dotted line), $\delta U = 0.001$ (violet, thick line) and $\delta U = 0.0001$ (orange, thick dashed line) and the highly excited initial state $|05000\rangle_B$ propagated with the periodic Bose-Hubbard Hamiltonian with $J = 1$ and $U = 10$ in the regular regime (left) and with $J = 1$ and $U = 1$ in the chaotic regime (right). This figure is completely analogous to Figure 3.10 and one can infer the same interpretation.

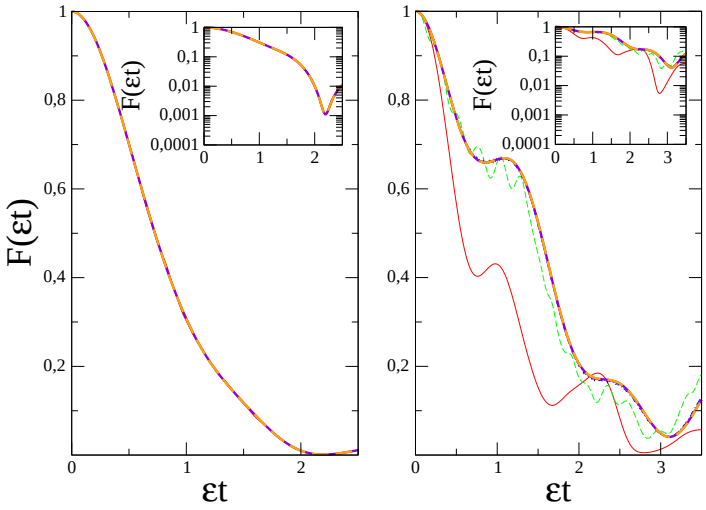

Figure 3.13: Decay of the dynamic fidelity $F_{U,\delta U}$ with $\delta U = 0.5$ (red, thin line), $\delta U = 0.1$ (green, thin dashed line), $\delta U = 0.01$ (blue, thin dash dotted line), $\delta U = 0.001$ (violet, thick line) and $\delta U = 0.0001$ (orange, thick dashed line) and the highly excited initial state $|05000\rangle_B$ propagated with the periodic Bose-Hubbard Hamiltonian with $J = 1$ and $U = 10$ in the regular regime (left) and with $J = 1$ and $U = 1$ in the chaotic regime (right). This figure is completely analogous to Figure 3.11 and implies the same interpretation.

3.2.2 Quantifying avoided crossings by means of the fidelity

The mere presence of a large number of dense lying avoided crossing is a clear sign for quantum chaos. In spectral analysis it is level repulsion, manifest in the existence of avoided crossings, that causes level spacings to obey a Wigner distribution. And the fact that the wave function changes at an avoided crossing implies nonintegrability. So the detection of avoided crossings is a fundamentally useful tool for the determination of the chaotic regime.

This detection of avoided crossings can be achieved by making use of the static fidelity 3.4. From now on we will again parametrize our periodic Bose-Hubbard Hamiltonian with u, i.e. $J = 1 - u$, $U = u$ and u runs from 0 to 1. Thus we set $\lambda = u$ and $\epsilon = \delta u$. In this case the static fidelity reads

$$F(u, \delta u) \quad = \quad |\langle \psi(u) | \psi(u + \delta u) \rangle|^2 \tag{3.5}$$

for a specific eigenstate $|\psi(u)\rangle$ of our Hamiltonian $\hat{H}(u)$. This static fidelity is constant of value 1 everywhere except for the vicinity of an avoided crossing. It is minimal exactly at the position of an avoided crossing and can therefore be used to locate them.

In Figure 3.14 we plot $1 - F(u, \delta u)$ with $\delta u = 0.001$ for the eigenstate 22 of the spectrum to $L = 5$ wells, $N = 5$ bosons and quasimomentum $k = 1$. This function pinpoints the two avoided crossings and additionally quantifies the right one to be narrower than the left one.

Our intention is to apply this static fidelity to the whole spectrum. This means that we extend the applicability of the static fidelity from the ground

state, as it was introduced by *Zanardi et al.* in [45, 47], to the complete spectrum. A first attempt in the direction of this extension to the whole spectrum is given by analyzing the average of the function $\langle 1 - F(u, \delta u)\rangle$ over all eigenstates. In Figure 3.15 this average is performed over all eigenstates of the spectrum to $L = 7$ wells, $N = 7$ bosons and quasimomentum $k = 1$. We conclude that the spectrum around $u = 0.8$ is characterized by either many or by strong avoided crossings. We note that the quantum phase transition takes place at $(\frac{J}{U})_{crit.} = 0.26$ which corresponds to $u_{crit.} = 0.79$, but of course this quantum phase transition affects only the ground state.

The main disadvantage of the function $1 - F(u, \delta u)$ is its dependence on δu. We would like to have a quantity that locates and measures avoided crossings independent of δu. The form of the static fidelity 3.4,

$$F(\lambda, \epsilon) \quad = \quad |\langle \psi(\lambda) | \psi(\lambda + \epsilon)\rangle|^2 \qquad ,$$

suggests that it can be well treated with standard quantum mechanical perturbation theory for small values of ϵ [48, 49]. In fact, in [49] the lowest order correction to the fidelity is presented but without derivation, which is why we want to do this derivation here. Consider the Hamiltonian

$$\hat{H} \quad = \quad \hat{H}_0 + \epsilon \hat{V} \qquad .$$

In order to solve the eigenproblem

$$\hat{H}|n\rangle \quad = \quad E_n|n\rangle \qquad ,$$

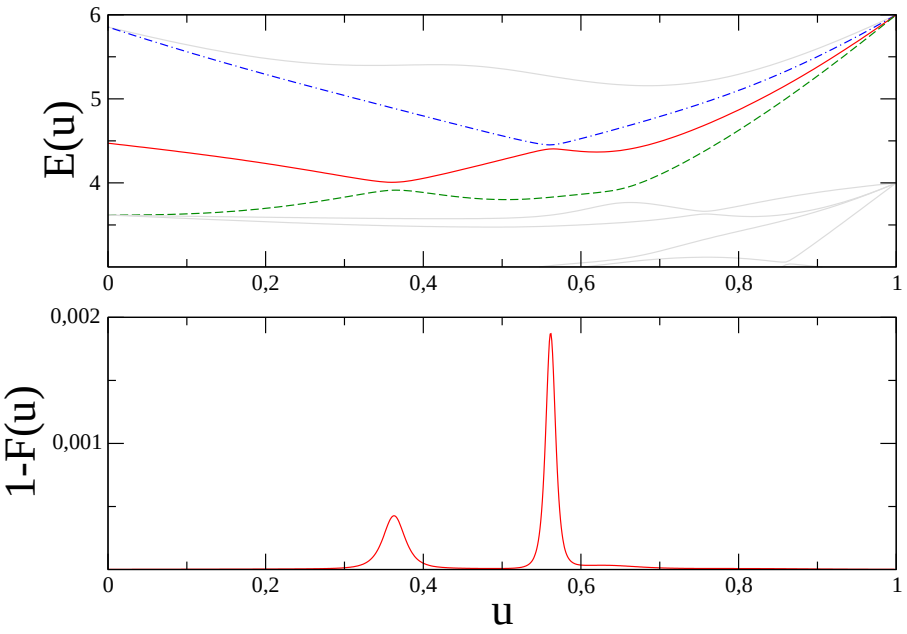

Figure 3.14: Static fidelity $1 - F(u, \delta u)$ with $\delta u = 0.001$ applied to eigenstate 22 of the periodic Bose-Hubbard Hamiltonian with $L = 5$ wells, $N = 5$ bosons and quasimomentum $k = 1$. The static fidelity very well locates the two avoided crossings and also quantifies the right one to be narrower than the left one.

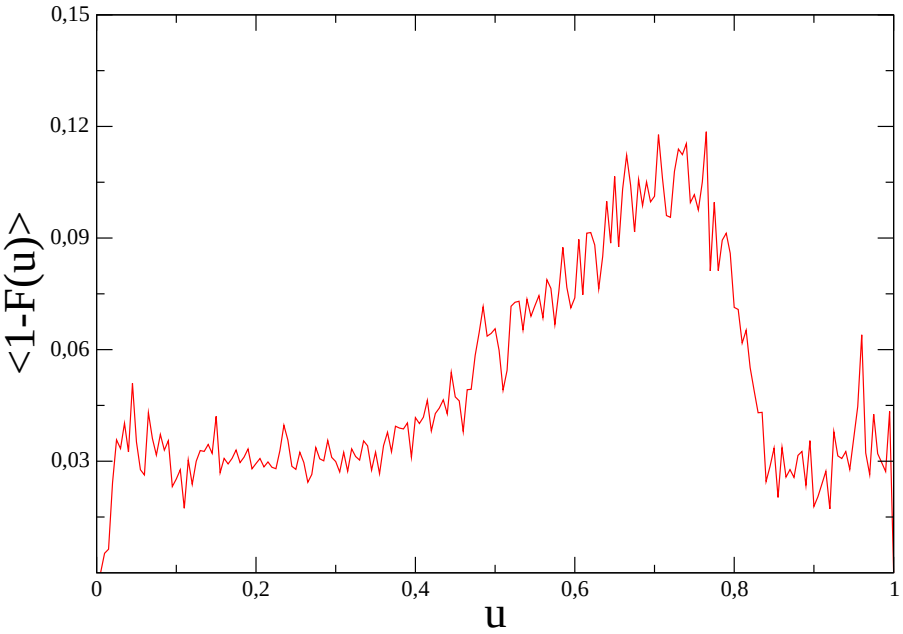

Figure 3.15: Averaged static fidelity $F(u, \delta u)$ with $\delta u = 0.005$ of all eigenstates to the periodic Bose-Hubbard Hamiltonian with $L = 7$ wells, $N = 7$ bosons and quasimomentum $k = 1$. The most or the narrowest avoided crossings are located around $u = 0.8$.

with eigenvalue E_n to the nth eigenstate $|n\rangle$, we make the standard ansatz of non-degenerate quantum mechanical perturbation theory by expanding E_n and $|n\rangle$ as power series in ϵ,

$$\begin{aligned}(\hat{H}_0 + \epsilon\hat{V}) \cdot (|n_0\rangle + \epsilon|n_1\rangle + \epsilon^2|n_2\rangle + \ldots) &= (E_n^0 + \epsilon E_n^1 + \epsilon^2 E_n^2 + \ldots) \cdot \\ &\quad (|n_0\rangle + \epsilon|n_1\rangle + \epsilon^2|n_2\rangle + \ldots) \quad .\end{aligned}$$

With the standard assumptions, as they are discussed in any elementary course on quantum mechanics, we calculate the pth order correction to the energy,

$$E_n^p = \langle n_0|\hat{V}|n_{p-1}\rangle - \sum_{j=1}^{p-1} E_n^j \langle n_0|n_{p-j}\rangle \quad ,$$

and the pth order correction to the eigenstate,

$$\begin{aligned}|n_p\rangle = \sum_{m\neq n} \frac{\langle m_0|\hat{V}|n_{p-1}\rangle - \sum_{j=1}^{p-1} E_n^j \langle m_0|n_{p-j}\rangle}{E_n^0 - E_m^0}|m_0\rangle - \\ \frac{1}{2}\sum_{j=1}^{p-1}\langle n_j|n_{p-j}\rangle|n_0\rangle \quad .\end{aligned}$$

The above two formulas allow the recursive, or numerically better the iterative, computation of all corrections of any order.

If we are interested in the nth eigenstate, the static fidelity (3.4) can be rewritten as

$$F(\lambda,\epsilon) \quad = \quad |\langle n(\lambda)|n(\lambda+\epsilon)\rangle|^2 \qquad .$$

Now we artificially split our Hamiltonian $\hat{H}(\lambda+\epsilon)=\hat{H}_0(\lambda)+\epsilon\hat{V}$ and see that $|n(\lambda)\rangle$ is the nth eigenstate to the unperturbed Hamiltonian $\hat{H}(\lambda)=\hat{H}_0(\lambda)$ while $|n(\lambda+\epsilon)\rangle$ is the nth eigenstate to the perturbed Hamiltonian $\hat{H}(\lambda+\epsilon)=\hat{H}_0(\lambda)+\epsilon\hat{V}$. This shows how we can simply apply our result from non-degenerate quantum mechanical perturbation theory by identifying $|n(\lambda)\rangle=|n_0\rangle$.

Doing this, our static fidelity with all corrections up to pth order reads

$$F(\lambda,\epsilon) \quad = \quad |1-\frac{1}{2}\sum_{j=2}^{p}\epsilon^j\sum_{k=1}^{j-1}\langle n_k|n_{j-k}\rangle|^2 \qquad .$$

Writing out the first terms explicitly yields

$$\begin{aligned} F(\lambda,\epsilon) \quad = \quad & 1-\epsilon^2\langle n_1|n_1\rangle-\epsilon^3(\langle n_1|n_2\rangle+\langle n_2|n_1\rangle)- \\ & \epsilon^4(\langle n_1|n_3\rangle+\langle n_2|n_2\rangle+\langle n_3|n_1\rangle-\frac{\langle n_1|n_1\rangle^2}{4})-\ldots \end{aligned}$$

We are now in a position to define a function that we want to call "level correlation fidelity":

$$f(n,\lambda) \quad = \quad \lim_{\epsilon\to 0}\frac{1-|\langle n(\lambda)|n(\lambda+\epsilon)\rangle|^2}{\epsilon^2} \qquad . \tag{3.6}$$

If non-degenerate quantum mechanical perturbation theory can be applied, then this quantity is strictly equal to

$$\begin{aligned} f(n,\lambda) \quad &= \quad \langle n_1|n_1\rangle(\lambda) \\ &= \quad \sum_{m\neq n}\frac{|\langle m_0|\hat{V}|n_0\rangle|^2}{(E_n^0-E_m^0)^2}(\lambda) \qquad . \end{aligned}$$

But of course our definition of the level correlation fidelity (3.6) can also be used for degenerate energy levels, in contrast to the function $\langle n_1|n_1\rangle(\lambda)$.

We denote the level correlation fidelity by a small letter f such that we can distinguish it from the static fidelity (3.4). In the following we will always use a sufficiently small ϵ, i.e. δu, such that the numerical level correlation fidelity converges. Numerically it mostly suffices to put $\delta u=0.001$.

Figure 3.16 shows the level correlation fidelity applied to eigenstate 22 of the spectrum to $L=5$ wells, $N=5$ bosons and quasimomentum $k=1$. This figure has to be compared with Figure 3.14 because we have finally obtained the desired unique quantification of avoided crossings.

3.2.3 Distribution of avoided crossings

Of course the level correlation fidelity (3.6) can also be used, apart from the quantification of avoided crossings, to simply locate avoided crossings in the

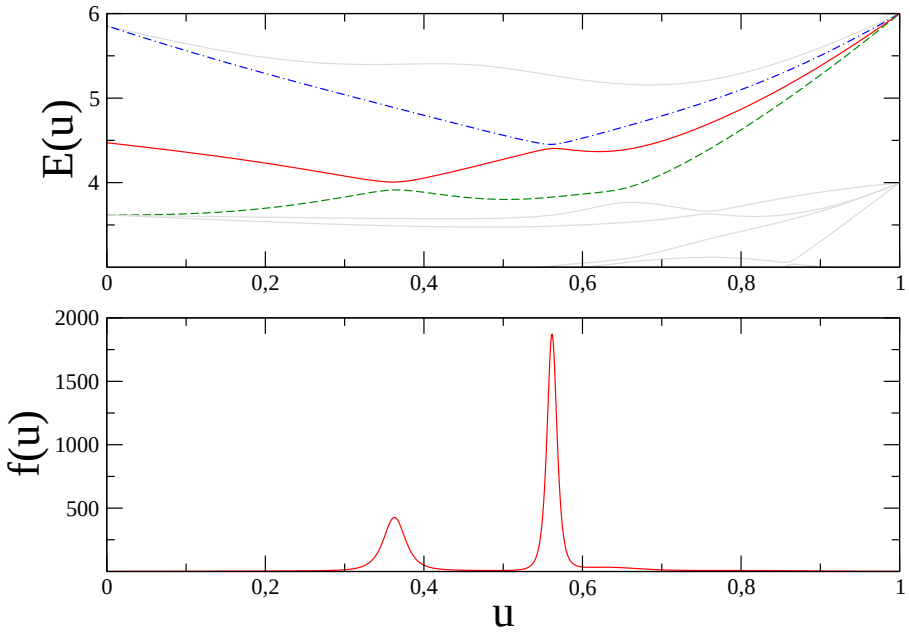

Figure 3.16: Level correlation fidelity $f(n,u)$ applied to eigenstate $n = 22$ of the periodic Bose-Hubbard Hamiltonian with $L = 5$ wells, $N = 5$ bosons and quasimomentum $k = 1$. This figure should be compared with Figure 3.14, since here we have a unique quantification of the two avoided crossings.

spectrum. In this last part we want to present a novel method for the detection of the chaotic regime by determining the distribution of avoided crossings in the spectrum.

In practice we follow each energy level with the level correlation fidelity. An avoided crossing is detected and counted if the level correlation fidelity is maximal and greater than a lower bound. The lower bound shall assure that only avoided crossings having at least a certain minimal strength are considered. We note that the avoided crossings have to be counted into a bin, i.e. their location is then given with an uncertainty of the bin width. In the following plots this bin width is set to $\delta u = 0.02$.

In Figure 3.17 we apply this method to the spectrum of $L = 5$ wells, $N = 5$ bosons and quasimomentum $k = 1$. The number and location of maxima of the level correlation fidelity in the lower part of the figure reliably reflect the distribution of avoided crossings, as we convinced ourselves by directly counting avoided crossings in the spectrum in the upper part of the figure.

Instead of plotting the absolute number of avoided crossings, it makes more sense to look at the number of avoided crossings per energy level, i.e. we divide the number of avoided crossings that we detect in a bin by the total number of energy levels. So what we are exactly studying here is the number of avoided crossings per energy level per bin. Figure 3.18 shows the distribution of avoided crossings in the spectrum of the periodic Bose-Hubbard model of $L = 7$ wells, $N = 7$ bosons and quasimomentum $k = 1$. If we compare this plot with our reference Figure 3.5 we conclude that the regular regime arises when the number

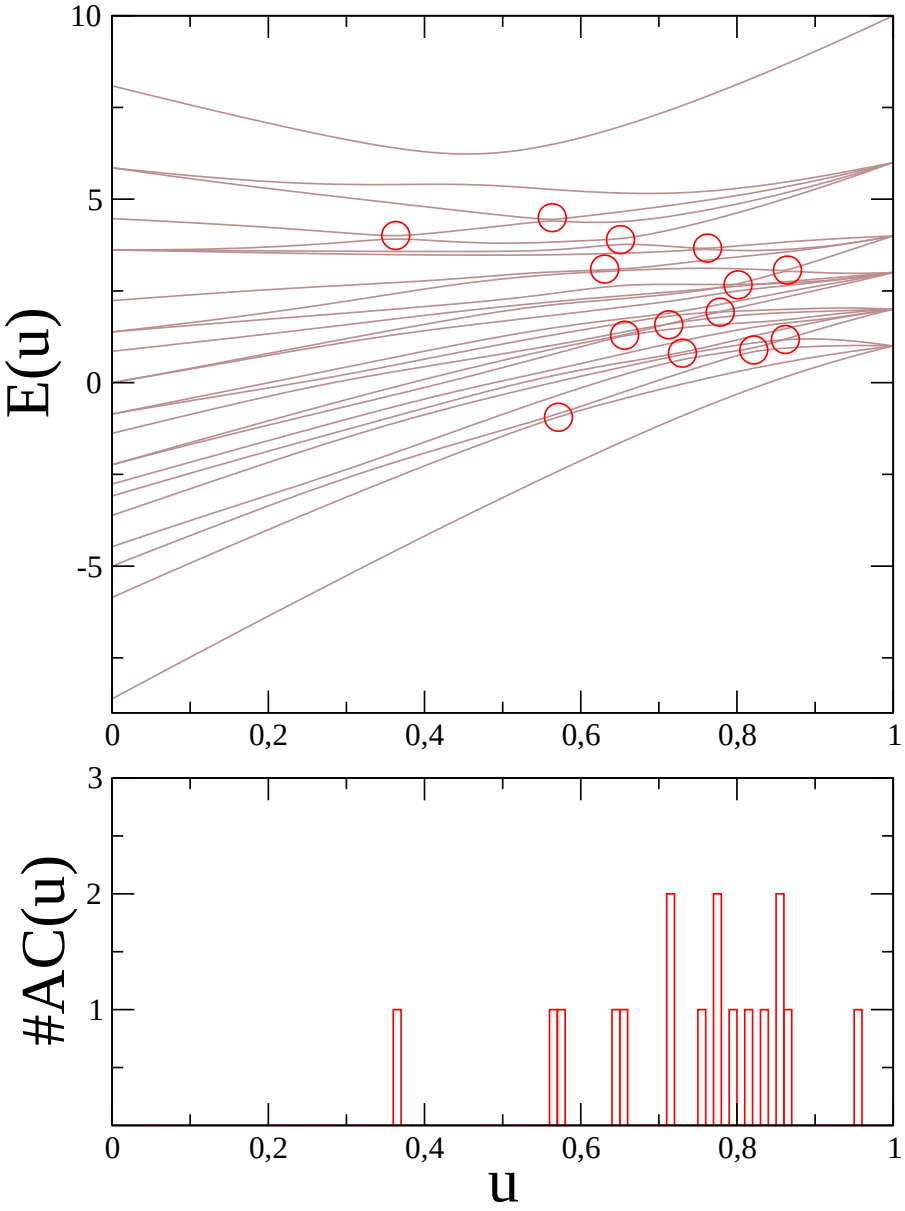

Figure 3.17: Spectrum and number of avoided crossings obtained from the level correlation fidelity, as the number of its maxima, for the periodic Bose-Hubbard Hamiltonian with $L = 5$ wells, $N = 5$ bosons and quasimomentum $k = 1$. In the upper plot we have highlighted the avoided crossings that we could find by explicitly looking at the spectrum. The level correlation fidelity correctly counts them, as one can convince oneself in the lower plot.

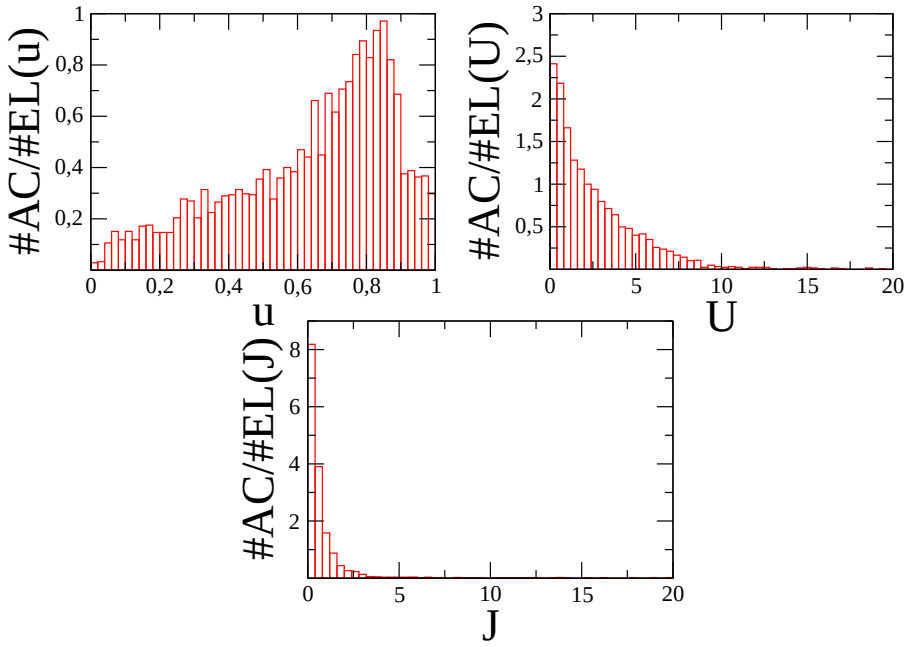

Figure 3.18: Number of avoided crossings per energy level for the periodic Bose-Hubbard Hamiltonian with $L = 7$ wells, $N = 7$ bosons and quasimomentum $k = 1$. This plot has to be compared with Figure 3.5. The comparison reveals that the regular regime sets in if the number of avoided crossings per energy level is sufficiently low.

of avoided crossings per energy level is sufficiently low.

In Figure 3.19 we investigate the distribution of avoided crossings in the spectra of systems with different filling but with the same number of 250 ± 25 energy levels. In fact, we use the same setting as in Figure 3.6 such that we can now compare the results of spectral statistics with the results of our novel method. As we clearly see in Figure 3.19 the system with lowest filling of $L = 37$ and $N = 3$ still has a significant number of avoided crossings per energy level which is why the spectrum cannot be regular. Looking at Figure 3.6 we see that spectral statistics wrongly assigns the whole spectrum to be regular. So the determination of the distribution of avoided crossings in the spectrum is a necessary new technique for the correct classification of the regular and the chaotic regime.

We also tried to make out a quantity that is independent of the system size, i.e. the number of energy levels considered, and we propose the probability density of avoided crossings

$$P_{AC}(u) \quad = \quad \frac{N_{AC}(u)}{N_{AC}^{total} \mathrm{d}u} \tag{3.7}$$

where $N_{AC}(u)$ is the number of avoided crossings in $[u - \frac{\mathrm{d}u}{2}, u + \frac{\mathrm{d}u}{2}]$, i.e. in a bin of width $\mathrm{d}u$ around u, and N_{AC}^{total} is the total number of avoided crossings in the spectrum for all values of u, i.e. in $[0, 1]$. This density of avoided crossings

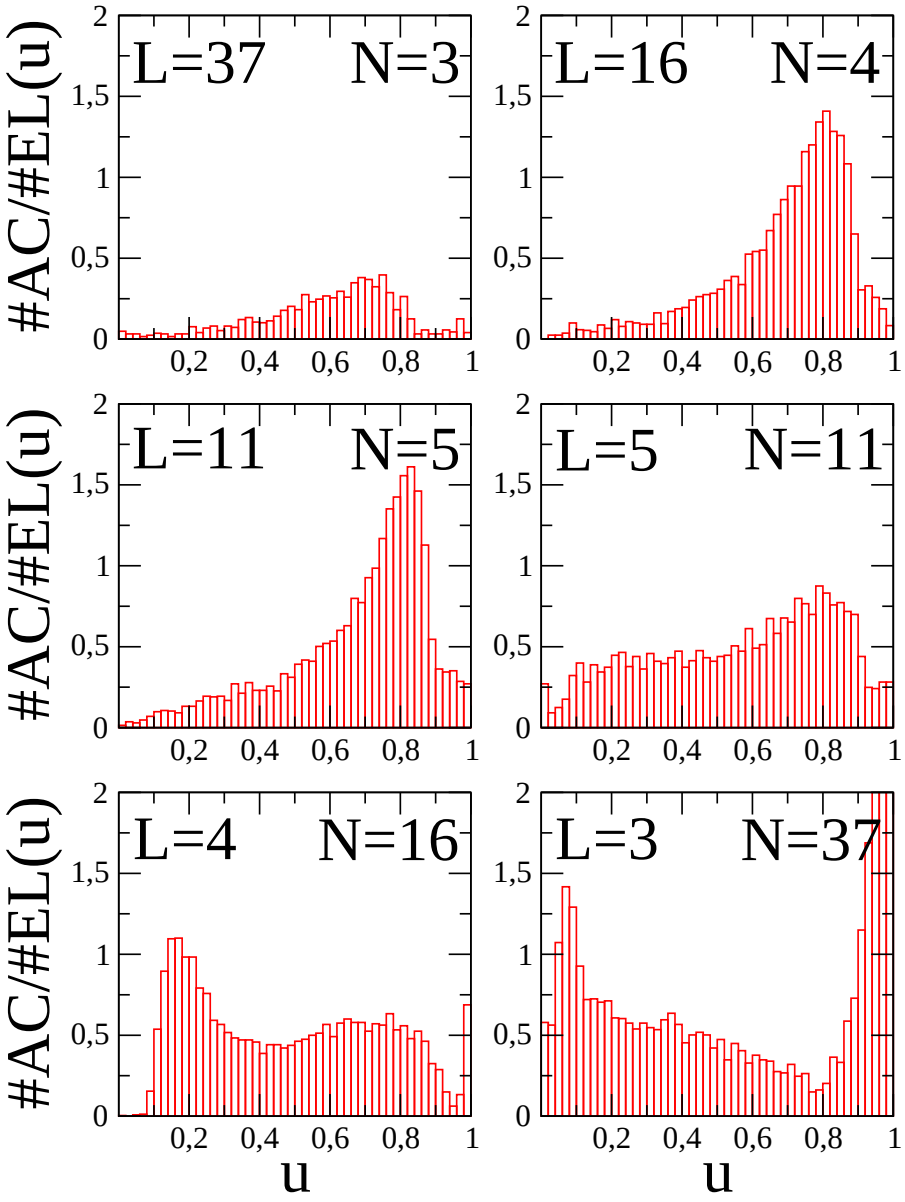

Figure 3.19: Number of avoided crossings per energy level for the Bose-Hubbard Hamiltonian with different fillings but with the same number of 250 ± 25 energy levels and quasimomentum $k = 1$. This plot has to be compared with Figure 3.6. Surprisingly spectral statistics assigns a regular spectrum to the system of $L = 37$ wells and $N = 3$ bosons where the level correlation fidelity detects a big number of avoided crossings per energy level. Hence the spectrum of $L = 37$ and $N = 3$ can not be regular.

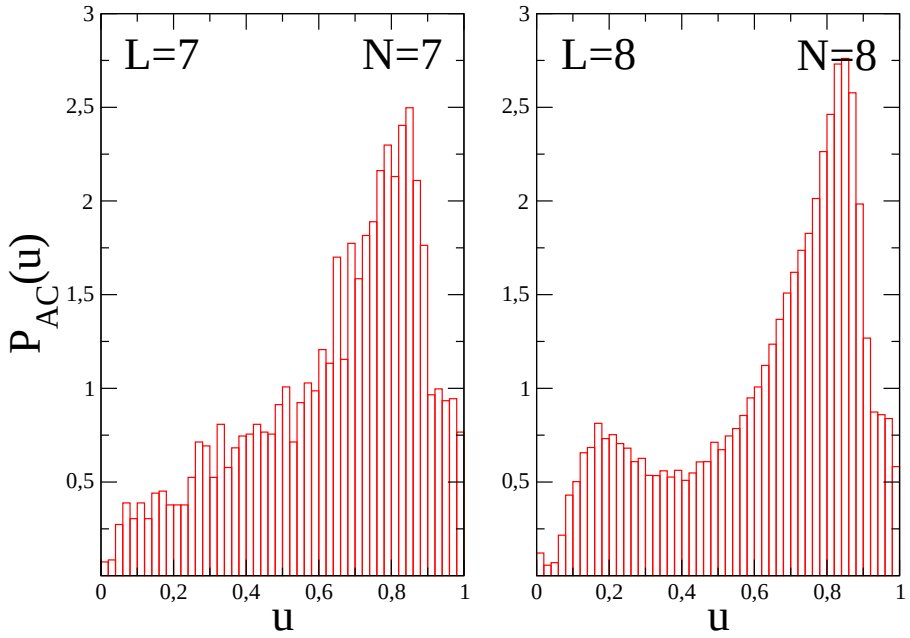

Figure 3.20: Probability density of avoided crossings $P_{AC}(u)$ applied to the periodic Bose-Hubbard Hamiltonian with quasimomentum $k = 1$ and $L = 7 = N$ (left) and $L = 8 = N$ (right). Indeed the distribution of avoided crossings looks similar, although the systems considered have a different number of energy levels.

indeed looks similar for the spectrum of the $k = 1$-subspace to $L = 7 = N$ and to $L = 8 = N$ as can be seen in Figure 3.20.

Chapter 4

Quantum entanglement in the Bose-Hubbard model

There exist many nice introductions to entanglement theory, but sadly all of them lack a beautiful treatment of the important computable entanglement measures. *Nielsen* and *Chuang* present entanglement only very briefly in their book [30]. In contrast, *Horodecki et al.* have worked out an extremely thorough, but lengthy, discussion of almost all aspects of quantum entanglement [25], however without explaining how entanglement measures are computed in practice. This is also true for the introduction to entanglement measures by *Plenio* and *Virmani* [33]. A quantum information theory lecture of *Wolf* has a particularly nice treatment of the entropy of entanglement, but does not explain other measures [50]. Fortunately a lecture given by *Mintert* mostly concentrates on computable entanglement measures [51]. Nevertheless we could not find any introduction to entanglement theory that additionally highlights the problems of standard entanglement theory in quantum many-body systems. There the particles are indistinguishable and the common description is the Fock formalism.

Recently the most important results concerning entanglement in quantum many-body systems were reviewed by *Amico et al.* in [34]. This work, most of all, demonstrates the enormous complexity of the subject. *Amico et al.* make clear that many different notions of entanglement have been developed in the context of quantum many-body systems and that the correct notion of entanglement depends on the system under consideration, more precisely on the decision of what the entangled entities shall be. Mainly two different concepts of entanglement are relevant for the Bose-Hubbard model, namely the notion of quantum correlations between indistinguishable particles and the concept of mode entanglement.

If the investigated entangled entities are the indistinguishable particles themselves, *Schliemann et al.* proposed to speak of quantum correlations instead of entanglement [52, 53], in order to distinguish the existing correlations from entanglement of distinguishable particles. This distinction is necessary because entanglement theory of distinguishable particles promotes entanglement as a resource [30], in a way like energy, that may be used to do tasks that can not

be done classically. E.g. by means of an entangled state two classical bits can be encoded and sent with only one qubit [54], a phenomenom termed superdense coding. And quantum teleportation renders possible the teleportation of a quantum state to a spatially remote location via an entangled state [55]. So the resource of an entangled state allows to overcome classical restrictions, like locality in the case of quantum teleportation. However it is still unclear if the entanglement between indistinguishable particles can be used as a resource in the same way and therefore *Schliemann et al.* suggested not to talk of entanglement but of quantum correlations, the well-known term of solid-state physics, in the context of indistinguishable particles.

Unfortunately *Schliemann et al.* mainly focus on fermions [52] and later *Eckert, Schliemann et al.* consider bosons [53] but do not give an interpretational motivation for their definition of separability. Many other approaches to this topic [56, 57, 58, 59] also lack this interpretational motivation for bosons and additionally limit their explanations to only two indistinguishable particles. *Ghirardi et al.* especially focus on the interpretational aspects of entanglement in systems of indistinguishable particles [60, 61], but they do not tell how entanglement in these systems can be quantified.

A completely different discussion of many-particle entanglement in systems of indistinguishable particles emerged in the context of spin squeezing [62, 63]. Spin squeezed states enhance spectroscopy, compared to coherent states. That's why spin squeezed states can be considered entangled [64]. Experimentally spin squeezed states of ultracold atoms were for the first time realized in [65]. Spin squeezing is quantified by the spin squeezing parameter ξ [62, 63] and this parameter can often be measured experimentally. *Sørensen et al.* derived an inequality for ξ that holds for a separable state of N distinguishable bosons [66] and *Wang et al.* calculated that inequality for a separable state of N indistinguishable bosons [67]. *Estève et al.* experimentally showed that BECs can violate these inequalities and hence he proved the existence of many-particle entanglement in a BEC [9]. We remark that in [68, 69] all possible spin squeezing inequalities are derived for spin-$\frac{1}{2}$ particles.

If the investigated entangled entities are the modes of the Fock states *Zanardi* and *Wang* suggested to refer to mode entanglement [70]. E.g. in the Bose-Hubbard model it is self-evident to study entanglement between different wells understanding each well as an individual quantum system. And because the wells correspond to the modes of the Wannier Fock states one actually looks at Wannier mode entanglement. Mode entanglement obviously depends on the choice of modes [71, 72] and a change from one set of modes to another is accomplished by a unitary transformation on the creation operators. Equivalently this corresponds to the same unitary transformation on the single-particle functions that make up the Fock state. The canonical modes of the Bose-Hubbard model are the Wannier modes of the Wannier Fock states and the Bloch modes of the Bloch Fock states (c.f. Section 2.1). But Wannier mode entanglement is superior to any other mode entanglement, because entanglement between spatially separated wells represents the common notion of entanglement as a nonlocal resource. In particular, only Wannier mode entanglement allows for superdense coding and quantum teleportation. So standard entanglement is realized in our

Bose-Hubbard model as Wannier mode entanglement. This kind of directly usable entanglement will from now on be called practical entanglement.

Let us explain practical entanglement with an example. Consider the state

$$|\psi\rangle \quad = \quad \frac{1}{\sqrt{2}}(|1010\rangle_W + |0101\rangle_W)$$

which is a superposition of two Wannier Fock states. More precisely, we have $L = 4$ wells and $N = 2$ bosons and we can directly read off from the Wannier representation of $|\psi\rangle$ in which wells the two bosons sit, i.e. $|1010\rangle_W$ denotes one boson in the first well and one boson in the third well and $|0101\rangle_W$ denotes one boson in the second well and one boson in the fourth well. If we now declare the left two wells to be one quantum system and the right two wells to be a second quantum system, we have two spatially separated, and therefore distinguishable, quantum systems. This is exactly the setting of standard entanglement theory. In particular for the state above, if we define $|0\rangle := |10\rangle_W$ and $|1\rangle := |01\rangle_W$ we obtain

$$|\psi\rangle \quad = \quad \frac{1}{\sqrt{2}}(|00\rangle + |11\rangle) \qquad ,$$

which is a maximally entangled Bell state. This Bell state can now be used for superdense coding or quantum teleportation.
In contrast, consider the different state

$$|\phi\rangle \quad = \quad \frac{1}{\sqrt{2}}(|1010\rangle_B + |0101\rangle_B)$$

which is a superposition of two Bloch Fock states. Written in this Bloch representation we can not directly read off in which wells the two bosons sit. We only know that the state $|1010\rangle_B$ describes one boson having quasimomentum $k = 1$ and one boson having quasimomentum $k = 3$ and the state $|0101\rangle_B$ describes one boson having quasimomentum $k = 2$ and one boson having quasimomentum $k = 4$. Before we can do the spatial separation into two quantum systems, we have to make a basis change to Wannier Fock states. In that sense the Wannier Fock states are exceptional and Wannier mode entanglement directly leads to practical entanglement.

Mode entanglement has two fundamentally different forms. If the total particle number is unlimited, i.e. if there exists a reservoir of infinitely many particles, then mode entanglement is just the same as standard entanglement. E.g. then the state

$$|\psi\rangle \quad = \quad |01\rangle_W + |10\rangle_W$$

of one boson in two wells has exactly the same entanglement properties as a maximally entangled Bell state

$$|\beta\rangle \quad = \quad |01\rangle + |10\rangle$$

of two distinguishable qubits.
However if the total particle number is fix the possible quantum operations are

fundamentally limited and the above state $|\psi\rangle$ does not have the same entanglement properties as a maximally entangled Bell state of two distinguishable particles anymore. While *Wiseman* and *Vaccaro* discovered this phenomenon [73, 74], it was *Schuch et al.* who gave a more or less complete solution [75]. We remark that the Wannier mode entanglement present in $|\psi\rangle$ nevertheless can be swapped to a different quantum system, e.g. two atoms [76], and then it is practical entanglement. But, of course, considerations like that are not relevant for us because we restrict our studies to the sole Bose-Hubbard model, without extra quantum systems.

Schuch et al. assumed a fix total particle number and that the quantum system under consideration is split into two quantum systems A and B with corresponding Hilbert spaces $\mathcal{H}_A$ and $\mathcal{H}_B$. It is the entanglement between these two quantum systems that they investigated. They proved that any local quantum operation, $\hat{O}_A$ or $\hat{O}_B$, has to commute with the local particle number operator, $\hat{N}_A$ or $\hat{N}_B$ respectively. This means that

$$\begin{aligned} [\hat{N}_A, \hat{O}_A] &= 0 \\ [\hat{N}_B, \hat{O}_B] &= 0 \end{aligned}$$

must hold for all local quantum operations $\hat{O}_A$ and $\hat{O}_B$. They showed that the entanglement properties of asymptotically, i.e. infinitely, many copies of the quantum state under consideration are completely described by two quantities, namely the entropy of entanglement

$$EoE(|\psi\rangle) = -\sum_j \lambda_j \log(\lambda_j) \quad ,$$

where the λ_j are the so-called Schmidt coefficients that we will explain in the first section of this chapter, and the superselection induced variance

$$SiV(|\psi\rangle) = 4(\langle\psi|\hat{N}_A^2|\psi\rangle - \langle\psi|\hat{N}_A|\psi\rangle^2) \quad ,$$

which is proportional to the variance in the local particle number. These two quantities are of fundamental importance for our analysis because as already explained in Chapter 2 we will always consider our Bose-Hubbard model with a fix total particle number of N bosons.

Entanglement is expected to be important in quantum phase transitions [26, 27, 28, 29]. Because quantum phase transitions occur at zero temperature they are not driven by thermal fluctuations but by quantum fluctuations. *Buonsante* and *Vezzani* investigated mode entanglement at the superfluid to Mott insulating quantum phase transition in the periodic Bose-Hubbard Hamiltonian [28]. There they showed that mode entanglement does not allow to locate the quantum critical point as well as the static fidelity, which we thoroughly described in Chapter 3. In fact, they were only able to roughly locate the quantum critical point in the periodic Bose-Hubbard model via the minima of the second derivative of Bloch mode entanglement by making use of finite size scaling. They leave as an open question why the minima of the second derivative of Bloch mode entanglement are important for this quantum phase transition.

Practical entanglement is especially interesting for quantum computation [30]. Experimentally ultracold bosons in optical lattices can be controlled very well and so this setup is a promising candidate for quantum computation. In [13, 14, 15, 16] different schemes for quantum computation in the Bose-Hubbard model are presented.

We begin this chapter with a thorough introduction to standard entanglement theory in the first section. There we will derive the later used entanglement measures and work out the problems that come along with quantum many-body systems. We compare single-copy and asymptotic entanglement measures in the second section. In the third section we will present our own theory of quantum correlations between indistinguishable bosons. This theory will be built on an interpretational motivation and will allow the quantification of entanglement in systems of arbitrarily many bosons. We will apply our measure to the quantum phase transition. Finally we will present a novel experimentally realizable technique for the generation of practical entanglement in the Bose-Hubbard model in the fourth section.

4.1 Introduction to entanglement theory

Here we want to present an introduction to standard entanglement theory of distinguishable particles. As explained in the introduction to this chapter there exist many nice treatments of entanglement theory [30, 25, 33, 50, 51]. Unfortunately, they do not explain in simple terms what the important entanglement measures are and how they are computed. In particular, they do not cover the problems of standard entanglement theory in quantum many-body systems, where the particles are indistinguishable and the Fock formalism is the common description.

This introduction to entanglement theory serves a twofold purpose. First it shall derive the tools we will be using later on to quantify entanglement. Second it shall foreshadow the obstacles that come into play if one has identical particles. In order to fulfill these two aims we decided to give a rather long, but convincing, presentation touching all the important aspects of the field related to the quantification of entanglement. The largest part of this introduction to entanglement theory is based on the very first publications to the discussed topics.

4.1.1 Basics of entanglement theory

We begin by defining what an entanglement measure actually is. Fundamental for entanglement theory is the concept of local operations and classical communication (LOCC). These form a subset of the so-called quantum operations which cover all allowed operations on a quantum mechanical system. Entanglement monotones are then defined as scalar quantities that do not increase under LOCC and entanglement measures are entanglement monotones that fulfill additional physically motivated requirements.

Quantum operations

For any understanding of entanglement an understanding of the allowed operations on quantum mechanical systems is absolutely crucial.

Assume our system under consideration ρ_S is coupled to a second system and both systems evolve under Hamiltonian evolution described by a Schrödinger equation. It is common to call the second system environment ρ_E. Without loss of generality we can set the initial state to $\rho_S \otimes |0_E\rangle\langle 0_E|$ and then the complete system propagates according to a unitary U_{SE}. In order to get the evolution of ρ_S we now have two possibilities [77]:

1. If we are not interested in the environment, we simply trace it out:

$$\begin{aligned}\rho'_S &= \mathrm{tr}_E(U_{SE}(\rho_S \otimes |0_E\rangle\langle 0_E|)U_{SE}^\dagger) \\ &= \sum_j \langle j_E|U_{SE}(\rho_S \otimes |0_E\rangle\langle 0_E|)U_{SE}^\dagger|j_E\rangle \\ &= \sum_j \langle j_E|U_{SE}|0_E\rangle\rho_S\langle 0_E|U_{SE}^\dagger|j_E\rangle \\ &=: \sum_j M_j\rho_S M_j^\dagger \quad ;\end{aligned}$$

   here we have introduced the so-called Kraus operators $M_j := \langle j_E|U_{SE}|0_E\rangle$ and they fulfill

$$\begin{aligned}\sum_j M_j^\dagger M_j &= \sum_j \langle j_E|U_{SE}|0_E\rangle\langle 0_E|U_{SE}^\dagger|j_E\rangle \\ &= \mathbb{I} \quad .\end{aligned}$$

   This last equality assures that the above operation is trace-preserving,

$$\begin{aligned}\mathrm{tr}(\rho'_S) &= \mathrm{tr}(\sum_j M_j\rho_S M_j^\dagger) = \sum_j \mathrm{tr}(M_j\rho_S M_j^\dagger) = \sum_j \mathrm{tr}(M_j^\dagger M_j\rho_S) \\ &= \mathrm{tr}(\sum_j M_j^\dagger M_j\rho_S) = \mathrm{tr}(\mathbb{I}\rho_S) = \mathrm{tr}(\rho_S) = 1 \quad ,\end{aligned}$$

   and thus ρ'_S again is a valid density matrix.

2. We can measure the environment and thereby filter the resulting system state:
   The probability for obtaining measurement result j is

$$p_j = \mathrm{tr}(M_j\rho_S M_j^\dagger)$$

   and the state after measuring result j is

$$\rho'_S = \frac{M_j\rho_s M_j^\dagger}{\mathrm{tr}(M_j\rho_S M_j^\dagger)} \quad .$$

Both approaches are unified by the concept of a quantum operation $\mathcal{E}$,

$$\begin{aligned}\rho'_S &= \mathcal{E}(\rho_S) \\ &= \sum_j M_j\rho_S M_j^\dagger \quad ,\end{aligned}$$

which is defined through a set of Kraus operators M_j. We remark that in the literature $\mathcal{E}$ is also called quantum channel in analogy to the notion of a channel in classical communication theory [30]. In the case

$$\sum_j M_j^\dagger M_j \quad = \quad \mathbb{I}$$

the quantum operation is deterministic while in the case

$$\sum_j M_j^\dagger M_j \quad < \quad \mathbb{I}$$

it is probabilistic with $\mathrm{tr}(\mathcal{E}(\rho_S))$ being the probability for the quantum operation to occur [51].

Quantum operations - Example
Assume we have a state

$$|\psi\rangle \quad = \quad \frac{1}{\sqrt{2}}(|0\rangle + |1\rangle)$$

and want to perform a quantum operation described by the Kraus operators

$$M_1 = \begin{pmatrix} \cos(\Theta) & 0 \\ 0 & \sin(\Theta) \end{pmatrix} \qquad M_2 = \begin{pmatrix} \sin(\Theta) & 0 \\ 0 & \cos(\Theta) \end{pmatrix} \quad .$$

A quick check, $M_1^\dagger M_1 + M_2^\dagger M_2 = \mathbb{I}$, reveals that this is a correct quantum operation. Now we will measure result 1 with probability

$$p_1 = \langle\psi|M_1^\dagger M_1|\psi\rangle = 0.5$$

and the state will have changed to

$$|\psi_1\rangle = \frac{M_1|\psi\rangle}{\sqrt{\langle\psi|M_1^\dagger M_1|\psi\rangle}} = \cos(\Theta)|0\rangle + \sin(\Theta)|1\rangle \qquad .$$

We will measure result 2 with probability

$$p_2 = \langle\psi|M_2^\dagger M_2|\psi\rangle = 0.5$$

and the state will then be

$$|\psi_2\rangle = \frac{M_2|\psi\rangle}{\sqrt{\langle\psi|M_2^\dagger M_2|\psi\rangle}} = \sin(\Theta)|0\rangle + \cos(\Theta)|1\rangle \qquad .$$

Local operations and classical commmunication (LOCC)
Consider two parties, named Alice and Bob, with their laboratories far apart from each other and let them share a quantum system. You can think of Alice and Bob each having one of two qubits. On the one hand, clearly any quantum mechanical correlation between the two parts of the shared system, the two

qubits, can only be the result of a former interaction. On the other hand, what kind of quantum operations generate only classical correlations? E.g. if the two parts initially are uncorrelated, what quantum operations may Alice and Bob use such that only classical correlations arise? It is widely accepted that local operations and classical communication are exactly these quantum operations [33, 78].

Local operations cover all quantum operations that Alice and Bob can do locally in their laboratory on their part of the shared quantum system. Under such operations no quantum correlations should emerge because the two parts do not see each other. Classical communication then permits to choose the consecutive local quantum operations conditional on former results of local quantum operations. I.e. if Alice starts with a local quantum operation given by Kraus operators M_j and she measures result j, she can call Bob and tell him her measurement result. Bob can then perform a local quantum operation described by Kraus operators N_{jk} depending on Alice's measurement result j. Of course he now can call back Alice, tell her his measurement result k and she makes another local quantum operation depending on Bob's result and so on.

It can be shown that any LOCC protocol composed of rounds of measuring and communicating can be substituted by a three step protocol [30]:

1. Alice performs a local quantum operation defined by Kraus operators $\mathbf{M}_j$.
2. She calls Bob and tells him her measurement result j.
3. Depending on Alice's measurement result j Bob applies a local unitary $\mathbf{U}_j$.

We conclude that LOCC are quantum operations of the form [79]:

$$\begin{aligned}\rho'_S &= \sum_{j,k,l,\ldots} \ldots (O_{jkl}\otimes I)(I\otimes N_{jk})(M_j\otimes I)\rho_S(M_j^\dagger\otimes I)(I\otimes N_{jk}^\dagger)\ldots \\ &= \sum_j (I\otimes \mathbf{U}_j)(\mathbf{M}_j\otimes I)\rho_S(\mathbf{M}_j^\dagger\otimes I)(I\otimes \mathbf{U}_j^\dagger) \quad .\end{aligned}$$

Quantum operations and LOCC for indistinguishable particles

The correct description for indistinguishable particles is the Fock formalism [80]. Because the particles are indistinguishable only statements about the occupation of different quantum numbers can be made. So a Fock state contains all the information that one can have about a quantum system of indistinguishable particles. It is fundamentally impossible to tell which particles exactly populate the different quantum numbers.

Fock states for bosons are symmetrized products of single-particle functions and Fock states for fermions are antisymmetrized products of single-particle functions. Of course, any operation in Fock formalism can be equally expressed on these (anti-)symmmetrized products of single-particle functions and vice versa. In the Fock picture a basis change is realized by a unitary U applied to the creation operators,

$$\vec{b}^\dagger = U\vec{a}^\dagger$$

and we have used that already in Chapter 2 when we made a basis change from Wannier to Bloch Fock states. It can be easily shown that in the particle picture this corresponds to applying the same unitary U to each single-particle function in the (anti-)symmetrized product. This assures that the total wave function stays (anti-)symmetrized.

In fact, this also keeps the particles indistinguishable. Consider two indistinguishable bosons in the state

$$|0\rangle \otimes |0\rangle$$

written in the particle picture. Assume we could apply two different unitaries U_1 and U_2 to the two bosons. In fact, this already presupposes that we can address them individually which is impossible because they are indistinguishable. Nevertheless, if we choose $U_1 = \mathbb{I}$ and $U_2 = \sigma_X$, where

$$\sigma_X = \begin{pmatrix} 0 & 1 \\ 1 & 0 \end{pmatrix}$$

is the σ_X-Pauli matrix or equivalently a NOT gate, we obtain

$$U_1|0\rangle \otimes U_2|0\rangle \quad = \quad |0\rangle \otimes |1\rangle \qquad .$$

But then the particles are distinguishable by their quantum numbers.

We conclude that any quantum operation on indistinguishable particles has to make sure that the total wave function stays (anti-)symmetrized and this can be simply guaranteed by working in the Fock picture. Hence quantum operations have to be expressed in terms of annihilation and creation operators.

The concept of LOCC does not make sense for indistinguishable particles. Because the particles can not be addressed individually, local operations reduce to the same quantum operation applied to every indistinguishable particle. In the second section of this chapter we will introduce our own concept of LOCC for indistinguishable particles.

Entanglement monotones

An entanglement monotone E is a scalar function on the set of all density operators, which we denote by $\mathcal{D}$,

$$E : \mathcal{D} \to [0, \infty) \qquad ,$$

that does not increase on average under LOCC [81]:

$$E(\rho) \geq \sum_j p_j E(\frac{M_j \rho M_j^\dagger}{\mathrm{tr}(M_j \rho M_j^\dagger)}) \qquad .$$

Here the Kraus operators M_j realize the LOCC protocol and the above inequality has to hold for all possible LOCC protocols. The restriction to nonincreasing behaviour on average means that there may exist LOCC protocols such that for some measurement results the entanglement may grow but the probability for these results to occur has to be sufficiently small.

From this follows a simple necessary criterion for entanglement monotones, namely that they are invariant under local unitaries:

$$\begin{aligned} E(\rho) &\geq E((U_A \otimes U_B)\rho(U_A^\dagger \otimes U_B^\dagger)) \\ &\geq E((U_A^{-1} \otimes U_B^{-1})(U_A \otimes U_B)\rho(U_A^\dagger \otimes U_B^\dagger)(U_A^{-1^\dagger} \otimes U_B^{-1^\dagger})) \\ &= E(\rho) \quad . \end{aligned}$$

Entanglement measures
Entanglement measures are entanglement monotones that fulfill additional requirements. Among them can be [50, 51]:

- $E(\rho_{sep}) = 0$
  This can always be defined for any entanglement monotone.
- Subadditivity: $E(\rho_1 \otimes \rho_2) \leq E(\rho_1) + E(\rho_2)$
- Additivity: $E(\rho_1 \otimes \rho_2) = E(\rho_1) + E(\rho_2)$
  Additivity is particularly important for the interpretation of entanglement as a resource. Thinking of the resource energy, it is clear that the energy of two systems is given by the sum of the energies of each system. So any measure of a resource has to be additive in the above sense.
- Convexity: $E(p \cdot \rho_1 + (1-p) \cdot \rho_2) \leq p \cdot E(\rho_1) + (1-p) \cdot E(\rho_2)$
  Convexity is motivated by the intuition that the amount of entanglement of a mixture should never exceed the average amount of entanglement of the individual states.

4.1.2 Pure bipartite states

We are now in a position to derive a first entanglement measure, the entropy of entanglement, for pure bipartite states. For such states an extensive entanglement theory exists mainly because all of these states can be written in a special form, the Schmidt decomposition, and then their entanglement properties can be compared by means of the majorization criterion. Looking at only a single copy of a state, single-copy entanglement, this will lead to a partial order on the set of all entangled states. However, allowing for infinitely many copies of a state, asymptotic entanglement, will facilitate a total order.

Separability of pure bipartite states
A pure bipartite state $|\psi\rangle$ is separable iff there exist $|\phi_1\rangle$ and $|\phi_2\rangle$ such that

$$|\psi\rangle = |\phi_1\rangle \otimes |\phi_2\rangle \quad .$$

Otherwise $|\psi\rangle$ is entangled.

Separability of pure bipartite states - Examples

- Is the state $|\psi\rangle = \frac{1}{\sqrt{2}}(|00\rangle + |01\rangle)$ entangled?
  No, $|\psi\rangle$ is separable:

$$|\psi\rangle \quad = \quad |0\rangle \otimes \frac{1}{\sqrt{2}}(|0\rangle + |1\rangle) \qquad .$$

- Is the state $|\psi\rangle = \sqrt{\frac{2}{3}}|00\rangle + \frac{1}{\sqrt{3}}|11\rangle$ entangled?
  Yes, $|\psi\rangle$ is not separable.

Schmidt decomposition

Having the last example in mind, how can we be sure that $|\psi\rangle = \sqrt{\frac{2}{3}}|00\rangle + \frac{1}{\sqrt{3}}|11\rangle$ is not separable? The reason is its special form, it is already Schmidt decomposed. Remember that entanglement monotones have to be invariant under local unitaries, formalizing the intuitively clear requirement that entanglement should not depend on the local basis choice. Hence we can apply a unitary U_1 to the left qubit and a unitary U_2 to the right qubit without changing the amount of entanglement in $|\psi\rangle$, i.e.

$$|\psi'\rangle \quad = \quad \sqrt{\frac{2}{3}} U_1|0\rangle \otimes U_2|0\rangle + \frac{1}{\sqrt{3}} U_1|1\rangle \otimes U_2|1\rangle$$

has the same entanglement as $|\psi\rangle$.

Consider a general state of two qubits,

$$|\psi\rangle \quad = \quad a_{00}|00\rangle + a_{01}|01\rangle + a_{10}|10\rangle + a_{11}|11\rangle \qquad ,$$

and take a look at the coefficient matrix

$$A = \begin{pmatrix} a_{00} & a_{01} \\ a_{10} & a_{11} \end{pmatrix} \qquad .$$

For a separable state we can find two unitaries U_1 and U_2 such that the new coefficient matrix A' has only one diagonal entry a'_{00} different from zero. If you now think of the above $|\psi\rangle = \sqrt{\frac{2}{3}}|00\rangle + \frac{1}{\sqrt{3}}|11\rangle$ again where the corresponding coefficient matrix has two diagonal entries it should be clear that no unitaries U_1 and U_2 reducing A to one nonvanishing entry can be found. We conclude that the diagonal form of the coefficient matrix A allows to detect entangled states: If it has only one nonvanishing entry, the state is separable, otherwise the state is entangled. In fact, the diagonal form can be obtained easily by a singular value decomposition and this is then called the Schmidt decomposition [30].

Because of its fundamental importance for pure bipartite entanglement and because of its relevance for indistinguishable particles, we want to derive the singular value decomposition of an arbitrary matrix at this point [42].

Theorem: For any general matrix A of dimension $m \times n$, with $m \leq n$, there exist unitary matrices U and V and a real positive semidefinite diagonal matrix D such that

$$A \;=\; UDV^\dagger \qquad .$$

Proof: $A^\dagger A$ is hermitian, since $(A^\dagger A)^\dagger = A^\dagger A$, and positive semidefinite, because

$$\vec{x}^\dagger A^\dagger A \vec{x} = ||A\vec{x}|| \geq 0 \quad \forall \vec{x} \qquad .$$

But then there exists a unitary V that diagonalizes $A^\dagger A$ to a real positive semidefinite matrix $S = V^\dagger A^\dagger A V$. We define

$$S = \begin{pmatrix} s_1^2 & & \\ & s_2^2 & \\ & & \ddots \end{pmatrix} =: D^2 \qquad ,$$

and now $AV = UD = (s_1\vec{u_1} \quad s_2\vec{u_2} \quad \ldots)$ with a unitary U gives us $A = UDV^\dagger$. This ends the proof.

Note that the singular values s_j are uniquely determined by A and the unitaries U and V are not. The singular values of A are therefore the square roots of the eigenvalues of $AA^\dagger = UD^2U^\dagger$ or of $A^\dagger A = VD^2V^\dagger$. In fact, $AA^\dagger$ contains the coefficients of the reduced density matrix of system A,

$$\begin{aligned} \rho_A &= \mathrm{tr}_B(|\psi\rangle\langle\psi|) = \mathrm{tr}_B(\sum_{i,j,k,l} a_{ij}a_{kl}^*|i_A j_B\rangle\langle k_A l_B|) \\ &= \sum_x \sum_{i,j,k,l} a_{ij}a_{kl}^*|i_A\rangle\langle x_B|j_B\rangle\langle k_A|\langle l_B|x_B\rangle = \sum_{x,i,k} a_{ix}a_{kx}^*|i_A\rangle\langle k_A| \\ &= \sum_{x,i,k} a_{ix}a_{xk}^\dagger|i_A\rangle\langle k_A| \qquad , \end{aligned}$$

and $A^\dagger A$ contains the coefficients of the reduced density matrix of system B,

$$\begin{aligned} \rho_B &= \mathrm{tr}_A(|\psi\rangle\langle\psi|) = \mathrm{tr}_A(\sum_{i,j,k,l} a_{ij}a_{kl}^*|i_A j_B\rangle\langle k_A l_B|) \\ &= \sum_x \sum_{i,j,k,l} a_{ij}a_{kl}^*\langle x_A|i_A\rangle|j_B\rangle\langle k_A|x_A\rangle\langle l_B| = \sum_{x,j,l} a_{xj}a_{xl}^*|j_B\rangle\langle l_B| \\ &= \sum_{x,j,l} a_{lx}^\dagger a_{xj}|j_B\langle\rangle l_B| \qquad . \end{aligned}$$

We can now continue the above discussion on a more general footing. An arbitrary pure bipartite state $|\psi\rangle$ can be written as:

$$|\psi\rangle \;=\; \sum_{j,k} a_{jk}|j\rangle|k\rangle \qquad ,$$

where the two quantum systems may have different dimensions and so j shall run from 1 to m, k shall run from 1 to n and $m \leq n$. Now consider the singular value decomposition of the coefficient matrix $A = (a_{jk})$:

$$A \;=\; U^T DV \qquad ,$$

where U and V are unitaries and D is diagonal with nonnegative real entries,

$$\begin{aligned} a_{jk} &= \sum_i u_{ji}^T d_{ii} v_{ik} \\ &= \sum_i u_{ij} d_{ii} v_{ik} \quad . \end{aligned}$$

As we have seen, such a singular value decomposition exists for any arbitrary rectangular matrix. Then our $|\psi\rangle$ becomes:

$$\begin{aligned} |\psi\rangle &= \sum_{i,j,k} u_{ij} d_{ii} v_{ik} |j\rangle|k\rangle \\ &= \sum_i d_{ii} (\sum_j u_{ij}|j\rangle)(\sum_k v_{ik}|k\rangle) \\ &=: \sum_i \sqrt{\lambda_i}|i\rangle|i\rangle \quad . \end{aligned}$$

We conclude that for every pure bipartite state $|\psi\rangle$ there exists a decomposition

$$|\psi\rangle = \sum_i \sqrt{\lambda_i}|i\rangle|i\rangle$$

and it is called the Schmidt decomposition.

The coefficients $\sqrt{\lambda_i}$ are termed Schmidt coefficients. We have shown above that the squared Schmidt coefficients are the eigenvalues of the reduced density matrices

$$\begin{aligned} \rho_A &= \mathrm{tr}_B(|\psi\rangle\langle\psi|) \\ \rho_B &= \mathrm{tr}_A(|\psi\rangle\langle\psi|) \end{aligned}$$

and they fulfill

$$\sum_i \lambda_i = 1$$

due to the normalization of the state under consideration. Because every entanglement monotone is invariant under local unitaries, we can restrict ourselves to Schmidt decomposed states. Obviously a pure bipartite state $|\psi\rangle$ is separable iff it has only one nonvanishing Schmidt coefficient.

Pure bipartite states, separability and Schmidt decomposition of indistinguishable particles

The wave function of two indistinguishable particles is either symmetrized in the case of bosons or antisymmetrized in the case of fermions [80]. This means that the corresponding coefficient matrix $A = (a_{jk})$ of the total quantum state

$$|\psi\rangle = \sum_{j,k} a_{jk}|j\rangle|k\rangle$$

is symmetric for bosons and antisymmetric for fermions. It was shown by *Schliemann et al.* [52] that if A is a $n \times n$-dimensional complex antisymmetric matrix

there exists a decomposition $A = UDU^T$ of A where D is block diagonal with $m \leq \frac{n}{2}$ blocks of the form

$$d_j = \begin{pmatrix} 0 & z_j \\ -z_j & 0 \end{pmatrix} \quad .$$

and zero entries everywhere else. In general the z_j are complex. This decomposition was then interpreted as the Schmidt decomposition for indistinguishable fermions and *Schliemann et al.* decided to call a state entangled if $m > 1$. *Paskauskas* and *You* [56] thereupon derived the analogous decomposition for the coefficient matrix of two bosons. They proved that if A is a $n \times n$-dimensional complex symmetric matrix there exists a decomposition $A = UDU^T$ of A where D is diagonal with $m \leq n$ real nonnegative entries d_j and zero entries everywhere else. These entries d_j were then considered to be the Schmidt coefficients of the quantum state of two indistinguishable bosons and *Paskauskas* and *You* defined a state to be entangled if $m > 1$.

It is interesting to start from a separable state of two distinguishable particles, (anti-)symmetrize it and look at the above decompositions. We did this calculation for arbitrary nonorthogonal initial states $|\phi\rangle$ and $|\chi\rangle$ and because it was rather lengthy we just want to report the results.

In the case of bosons the symmetrized total quantum state reads

$$|\psi\rangle \quad = \quad \frac{1}{\sqrt{2}}(|\phi\rangle|\chi\rangle + |\phi\rangle|\chi\rangle)$$

and it turns out that the above Schmidt decomposition for two indistinguishable bosons yields $m \leq 2$ Schmidt coefficients

$$\lambda_{1,2} \quad = \quad \frac{1}{2} \pm \frac{|\langle\phi|\chi\rangle|}{|\langle\phi|\chi\rangle|^2 + 1} \quad .$$

Obviously we have only $m = 1$ Schmidt coefficient if $|\phi\rangle = |\chi\rangle$. The more orthogonal $|\phi\rangle$ and $|\chi\rangle$ are to each other the bigger is the second Schmidt coefficient. If $|\phi\rangle$ and $|\chi\rangle$ are completely orthogonal, i.e. $\langle\phi|\chi\rangle = 0$, we have $m = 2$ equal Schmidt coefficients.

In the case of fermions the antisymmetrized total quantum state reads

$$|\psi\rangle \quad = \quad \frac{1}{\sqrt{2}}(|\phi\rangle|\chi\rangle - |\phi\rangle|\chi\rangle)$$

and the nonorthogonal part of $|\phi\rangle$ and $|\chi\rangle$ directly cancels out. That is the reason why the above Schmidt decomposition for two indistinguishable fermions always only gives $m = 1$ nonvanishing block matrix

$$d_1 = \begin{pmatrix} 0 & \frac{1}{2} \\ -\frac{1}{2} & 0 \end{pmatrix} \quad .$$

We conclude that if we define separability for indistinguishable particles by looking at the corresponding wave function of distinguishable particles, then we would call a fermionic state entangled if there are $m > 1$ nonvanishing block

matrices in the Schmidt decomposition for indistinguishable fermions and this is exactly the result of *Schliemann et al.*. And we would call a bosonic state entangled if there are $m > 2$ nonvanishing Schmidt coefficients in the Schmidt decomposition for indistinguishable bosons and this is different from the result of *Paskauskas* and *You* which assign entanglement already for $m > 1$ nonvanishing Schmidt coefficients. However, in the second section of this chapter we will define separability of indistinguishable bosons in a slightly different way.

Maximally entangled states
A $m \times n$-dimensional state $|\psi\rangle$, where $m \leq n$, is maximally entangled iff it has m equivalent Schmidt coefficients $\sqrt{\frac{1}{m}}$. Maximally entangled states allow directly for:

- Superdense coding [54]
- Quantum teleportation [55]

Maximally entangled states - Example
The 2×2-dimensional maximally entangled states

$$\begin{aligned} |\Phi^+\rangle &= \frac{1}{\sqrt{2}}(|00\rangle + |11\rangle) \\ |\Phi^-\rangle &= \frac{1}{\sqrt{2}}(|00\rangle - |11\rangle) \\ |\Psi^+\rangle &= \frac{1}{\sqrt{2}}(|01\rangle + |10\rangle) \\ |\Psi^-\rangle &= \frac{1}{\sqrt{2}}(|01\rangle - |10\rangle) \end{aligned}$$

are called Bell states. As we already saw in the introduction to this thesis, the Bell states maximally violate Bell's inequalities. This should be a first hint why they are called maximally entangled, but we will come back to the notion of maximally entangled states in more detail later.

State transformations
State transformations are LOCC protocols. One differentiates

- Single-copy entanglement [82, 83]:
  Where do I get from a single entangled state?
- Asymptotic entanglement [84]:
  Where do I get from a huge number of copies of an entangled state?

and respectively

- Deterministic state transformations [85]:
  Where do I get with certainty?
- Probabilistic state transformations [86, 87]:
  Where do I get probabilistically?

Single-copy entanglement - Example
We want to introduce single-copy entanglement with an example. Assume Alice and Bob share a Bell state

$$|\psi\rangle = \frac{1}{\sqrt{2}}(|00\rangle + |11\rangle) \quad .$$

They use the following LOCC protocol:

1. Alice measures with

$$M_1 = \begin{pmatrix} \cos(\Theta) & 0 \\ 0 & \sin(\Theta) \end{pmatrix} \qquad M_2 = \begin{pmatrix} \sin(\Theta) & 0 \\ 0 & \cos(\Theta) \end{pmatrix}$$

   on her qubit.

2. If she obtains result 1 the state has become

$$|\psi_1\rangle = \cos(\Theta)|00\rangle + \sin(\Theta)|11\rangle \quad .$$

3. If she measures result 2 the state is

$$|\psi_2\rangle = \sin(\Theta)|00\rangle + \cos(\Theta)|11\rangle$$

   and A applies a NOT gate resulting in

$$|\psi_2\rangle = \sin(\Theta)|10\rangle + \cos(\Theta)|01\rangle \quad .$$

4. A now calls B and tells him her measurement result.

5. If the measurement result was 1 then B does nothing.

6. If it was 2 however B applies a NOT gate to get

$$|\psi_2\rangle = \sin(\Theta)|11\rangle + \cos(\Theta)|00\rangle \quad .$$

Finally A and B have transformed the Bell state

$$|\psi\rangle = \frac{1}{\sqrt{2}}(|00\rangle + |11\rangle)$$

into

$$|\psi\rangle = \cos(\Theta)|00\rangle + \sin(\Theta)|11\rangle$$

by LOCC deterministically.

Although we have only shown it for 2×2-dimensional systems it holds generally that from a maximally entangled state one can reach every other state by LOCC deterministically [85]. Keep in mind that we are searching for an order on the set of all states making it possible to say that one state is more or less entangled than another state for all states. This order is achieved by defining a state $|\psi\rangle$ to be more entangled than a state $|\phi\rangle$ iff there exists a deterministic

LOCC protocol that transforms $|\psi\rangle$ to $|\phi\rangle$ [87, 88]. This should justify the notion of a maximally entangled state.

Majorization criterion
Let $|\psi\rangle$ and $|\phi\rangle$ be arbitrary pure bipartite states and let $\vec{\lambda}_\psi$ and $\vec{\lambda}_\phi$ denote vectors of the respective eigenvalues of the reduced density matrices. Then $|\psi\rangle$ can be transformed to $|\phi\rangle$ by LOCC deterministically iff

$$\vec{\lambda_\psi} \prec \vec{\lambda_\phi} \quad .$$

Here $\vec{x} \prec \vec{y}$, one says $\vec{x}$ is majorized by $\vec{y}$, iff

$$\sum_{j=1}^{k} x_j^{\downarrow} \leq \sum_{j=1}^{k} y_j^{\downarrow} \qquad \forall k$$

and the $\downarrow$ means that the elements of the vector are ordered decreasingly. The majorization criterion was derived by *Nielsen* [85].

Majorization criterion - Examples

- In accordance with the above example we have:

$$\begin{pmatrix} 0.5 \\ 0.5 \end{pmatrix} \prec \begin{pmatrix} \cos^2(\Theta) \\ \sin^2(\Theta) \end{pmatrix} \quad .$$

- What about

$$\begin{pmatrix} 0.5 \\ 0.5 \\ 0 \\ 0 \end{pmatrix} \text{and} \begin{pmatrix} 0.8 \\ 0.1 \\ 0.05 \\ 0.05 \end{pmatrix} \quad ?$$

  They are incomparable.

The last example points out the main problem of ordering entangled states by looking at single copies only, namely that there exist states which can not be transformed into each other by LOCC deterministically and hence are incomparable [33]. So the majorization criterion only leads to a partial order on the set of entangled states. We will later see that taking infinitely many copies of the states we wish to compare will always enable us to transform them into each other and therefore gives a total order.

Single-copy entanglement
Eisert and *Cramer* proposed the following measure for single-copy entanglement [83]:

$$E(|\psi\rangle) \quad = \quad \log(\lfloor (\lambda_1^{\downarrow})^{-1} \rfloor) \quad .$$

Their idea is to take only the largest Schmidt coefficient into account. If it is less than $\frac{1}{m}$ the state can be transformed into a maximally entangled state with

Schmidt coefficients $\frac{1}{m}$ due to the majorization criterion. This measure was further studied in [89].

Probabilistic state transformations - Example
We will discuss probabilistic state transformations only in an example here. In the later subsection on pure multipartite states we will go into more detail and find out that probabilistic state transformations permit a classification of entangled states.

We assume a state

$$|\psi\rangle \quad = \quad \sqrt{\lambda_1}|00\rangle + \sqrt{\lambda_2}|11\rangle$$

and apply a quantum operation

$$M_1 = \begin{pmatrix} \sqrt{\frac{\lambda_2}{\lambda_1}} & 0 \\ 0 & 1 \end{pmatrix} \qquad M_2 = \begin{pmatrix} \sqrt{1-\frac{\lambda_2}{\lambda_1}} & 0 \\ 0 & 0 \end{pmatrix}$$

to the first qubit. Then with probabilitiy $2\lambda_2$ we will measure 1 and get a maximally entangled state

$$|\psi_1\rangle \quad = \quad \frac{1}{\sqrt{2}}(|00\rangle + |11\rangle) \qquad ,$$

while with probability $\lambda_1 - \lambda_2$ we will measure 2 and obtain a separable state

$$|\psi_2\rangle \quad = \quad |00\rangle \qquad .$$

This is an example of entanglement gambling: We bet our state and either win a maximally entangled state or loose all the entanglement.

Asymptotic entanglement - Example
With the majorization criterion it is not possible to compare the following two states:

$$\begin{aligned} |\psi\rangle &= \frac{1}{\sqrt{2}}(|00\rangle + |11\rangle) \\ |\phi\rangle &= \sqrt{0.8}|00\rangle + \sqrt{0.1}|11\rangle + \sqrt{0.05}|22\rangle + \sqrt{0.05}|33\rangle \qquad . \end{aligned}$$

Nevertheless, one can compare $|\phi\rangle$ with two copies of $|\psi\rangle$,

$$\begin{aligned} |\psi\rangle^{\otimes 2} &= \frac{1}{2}(|0000\rangle + |0101\rangle + |1010\rangle + |1111\rangle) \\ &=: \frac{1}{2}(|00\rangle + |11\rangle + |22\rangle + |33\rangle) \qquad , \end{aligned}$$

and

$$\begin{pmatrix} 0.25 \\ 0.25 \\ 0.25 \\ 0.25 \end{pmatrix} \prec \begin{pmatrix} 0.8 \\ 0.1 \\ 0.05 \\ 0.05 \end{pmatrix}$$

tells us that we can transform two copies of $|\psi\rangle$ into one copy of $|\phi\rangle$ by LOCC deterministically.

Asymptotic entanglement
Asymptotic entanglement determines how m copies of an arbitrary state $|\psi\rangle$ can be transformed to n copies of the maximally entangled state $|\beta\rangle$ and the other way around by LOCC in the limit $m, n \to \infty$ and defines the amount of entanglement of $|\psi\rangle$ to be the rate

$$r \quad = \quad \frac{n}{m} \qquad .$$

The motivation for this measure is the agreement on a standard unit of entanglement [50, 30], the maximally entangled state. Then the rate r is exactly the quantity under consideration in standard units. Think of measuring an unknown length x with a standard meter s and assume You have to lay m bars of length x at another to get the same length as when You lay n bars of length s at another, i.e.

$$mx = ns \qquad \Longrightarrow \qquad x = \frac{n}{m}s \qquad .$$

The following two measures canonically arise from the above definition of asymptotic entanglement [33]:

- Distillable entanglement quantifies the maximal number n of maximally entangled states that one can distill from m copies of $|\psi\rangle$ in the asymptotic limit $m, n \to \infty$.
- Entanglement cost quantifies the minimal number n of maximally entangled states that one needs to obtain m copies of $|\psi\rangle$ in the asymptotic limit $m, n \to \infty$.

Entropy of entanglement
m copies of an arbitrary state $|\psi\rangle$ can be transformed to $r \cdot m$ copies of the maximally entangled state $|\beta\rangle$ revertibly by LOCC in the asymptotic limit $m, n \to \infty$ and

$$r \quad = \quad EoE(|\psi\rangle) \qquad ,$$

where

$$EoE(|\psi\rangle) \quad := \quad -\sum_j \lambda_j \log(\lambda_j)$$

is called the entropy of entanglement. This was discovered by *Bennett et al.* [84]. For pure bipartite states distillable entanglement and entanglement cost are equal to each other and they equal the entropy of entanglement.

The proof of the entropy of entanglement is important for the discussion of indistinguishable particles. That is the reason why we present it in Appendix B. As shown there the entropy of entanglement indeed is an entanglement monotone. Moreover the entropy of entanglement is additive [50] and thus it is a

good entanglement measure.

Entropy of entanglement - Examples

- What is the entropy of entanglement of the Bell-state $|\beta\rangle = \frac{1}{\sqrt{2}}(|00> +|11>)$?

$$EoE(|\beta\rangle) = \log(2) \quad .$$

- What is the entropy of entanglement of any maximally entangled state $|\beta\rangle$ in the dimension $m \times n$ where $m \leq n$?

$$EoE(|\beta\rangle) = \log(m) \quad .$$

Entropy of entanglement for indistinguishable particles

The asymptotic interpretation of the entropy of entanglement does not make sense for indistinguishable particles. If we have asymptotically, i.e. infinitely, many copies of a quantum state of indistinguishable particles the total wave function has to be (anti-)symmetrized and this makes it impossible to discuss asymptotic entanglement for indistinguishable particles on the same lines as we did above for distinguishable particles.

Nevertheless we can use the entropy of entanglement as an entanglement measure for indistinguishable particles. We just have to put the Schmidt coefficients, that come from the above explained Schmidt decomposition of indistinguishable particles, into the formula of the entropy of entanglement. However, we have to be aware that the asymptotic interpretation underlying the entropy of entanglement does not hold for indistinguishable particles.

We are now interested in how the entropy of entanglement changes if one (anti-)symmetrizes the quantum state under consideration. We want to look at an example of two bosons which are initially distinguishable and in the quantum state

$$|\psi\rangle = \alpha|00\rangle + \beta|11\rangle + \gamma|22\rangle \quad .$$

Because the two bosons are distinguishable this state actually has to be rewritten before we can symmetrize it:

$$|\psi\rangle_{dist.} = \alpha|03\rangle + \beta|14\rangle + \gamma|25\rangle \quad .$$

We could assume that the bosons are distinguishable because they are spatially separated. Then the new quantum numbers 0 to 5 additionally specify the position of a boson. The entropy of entanglement for this quantum state of distinguishable bosons is

$$EoE(|\psi\rangle_{dist.}) = -|\alpha|^2 \log(|\alpha|^2) - |\beta|^2 \log(|\beta|^2) - |\gamma|^2 \log(|\gamma|^2) \quad .$$

Let us now symmetrize the state:

$$|\psi\rangle_{indist.} = \frac{\alpha}{\sqrt{2}}(|03\rangle + |30\rangle) + \frac{\beta}{\sqrt{2}}(|14\rangle + |41\rangle) + \frac{\gamma}{\sqrt{2}}(|25\rangle + |52\rangle) \quad .$$

Now the entropy of entanglement for this quantum state of indistinguishable bosons reads

$$\begin{aligned} EoE(|\psi\rangle_{indist.}) &= -\frac{|\alpha|^2}{2}\log(\frac{|\alpha|^2}{2}) - \frac{|\alpha|^2}{2}\log(\frac{|\alpha|^2}{2}) - \frac{|\beta|^2}{2}\log(\frac{|\beta|^2}{2}) - \\ &\quad \frac{|\beta|^2}{2}\log(\frac{|\beta|^2}{2}) - \frac{|\gamma|^2}{2}\log(\frac{|\gamma|^2}{2}) - \frac{|\gamma|^2}{2}\log(\frac{|\gamma|^2}{2}) \\ &= -|\alpha|^2\log(\frac{|\alpha|^2}{2}) - |\beta|^2\log(\frac{|\beta|^2}{2}) - |\gamma|^2\log(\frac{|\gamma|^2}{2}) \\ &= -|\alpha|^2\log(|\alpha|^2) - |\beta|^2\log(|\beta|^2) - |\gamma|^2\log(|\gamma|^2) + \\ &\quad (|\alpha|^2 + |\beta|^2 + |\gamma|^2)\log(2) \\ &= -|\alpha|^2\log(|\alpha|^2) - |\beta|^2\log(|\beta|^2) - |\gamma|^2\log(|\gamma|^2) + \log(2) \\ &= EoE(|\psi_{dist.}\rangle) + \log(2) \quad . \end{aligned}$$

In the derivation we have used that the quantum state is normalized, $|\alpha|^2 + |\beta|^2 + |\gamma|^2 = 1$. It is remarkable that the symmetrization enters into the entropy of entanglement only as an additional constant $\log(2)$. It is very easy to show that this holds in general for all quantum states of indistinguishable bosons and that the same is true for fermions where the antisymmetrization also enters into the entropy of entanglement as an additional constant $\log(2)$.

4.1.3 Mixed bipartite states of lowest dimension

In the previous chapter we have seen that for pure bipartite states in any dimension there exists an entanglement measure, the entropy of entanglement, that has a convincing interpretation and can be computed in a simple manner at the same time. In this chapter we will learn that for mixed states the situation is very different.

The generalization of the entropy of entanglement to mixed states is called entanglement of formation and can be calculated algebraically only for systems of dimension 2×2. In this case the entanglement of formation can be expressed in terms of the so-called concurrence and because it depends monotonously on the concurrence the latter is often used as an entanglement measure on its own.

The theory of positive maps leads to a separability criterion, the positive partial transpose, that is necessary and sufficient for systems of dimension up to 2×3. For higher dimensions this criterion turns out to be only necessary for separability. This criterion can be evaluated straighforwardly via an entanglement measure called negativity.

Mixed states

Mixed states appear naturally in experiments, e.g. due to imperfect state preparation or coupling to an environment [30]. They are described by a density operator ρ with the following properties:

- ρ is positive.
- $\mathrm{tr}(\rho) = 1$.

In practice, mixed states show up if one traces out part of the quantum system under consideration. E.g. in the above treatment of pure bipartite states we traced out the second quantum system B to obtain the reduced density matrix ρ_A of the first quantum system A. This reduced density matrix is a product state $\rho_A = |\psi_A\rangle\langle\psi_A|$ if the two particles were in a separable quantum state before, and it is a mixed state $\rho_A \neq |\psi_A\rangle\langle\psi_A|$ if the two particles were in an entangled quantum state before. The fundamentally important characteristic of the reduced density matrix ρ_A is that it completely describes the properties of system A if nothing is known about system B [30]. The tracing out over quantum system B corresponds to averaging over all possible quantum states that B could be in.

The mapping from the set of density operators to the set of pure state ensembles is not bijective. Two pure state ensembles $\{p_j, |\psi_j\rangle\}$ and $\{q_j, |\phi_j\rangle\}$ generate the same density operator iff there exists a unitary matrix U such that

$$\sqrt{p_j}|\psi_j\rangle = \sum_k u_{jk}\sqrt{q_k}|\phi_k\rangle \quad .$$

Mixed states - Examples

- Consider

$$\begin{aligned} |\phi_1\rangle &= \sqrt{\frac{3}{4}}|\psi_1\rangle + \sqrt{\frac{1}{4}}|\psi_2\rangle \\ |\phi_2\rangle &= \sqrt{\frac{3}{4}}|\psi_1\rangle - \sqrt{\frac{1}{4}}|\psi_2\rangle \end{aligned} \quad ,$$

  then

$$\begin{aligned} \rho &= \frac{3}{4}|\psi_1\rangle\langle\psi_1| + \frac{1}{4}|\psi_2\rangle\langle\psi_2| \\ &= \frac{1}{2}|\phi_1\rangle\langle\phi_1| + \frac{1}{2}|\phi_2\rangle\langle\phi_2| \end{aligned} \quad .$$

- The density operator

$$\rho = \frac{1}{12}\begin{pmatrix} 9 & 1 & 1 & 1 \\ 1 & 1 & 1 & 1 \\ 1 & 1 & 1 & 1 \\ 1 & 1 & 1 & 1 \end{pmatrix}$$

  fulfills

$$\begin{aligned} \rho &= p_1|\psi_1\rangle\langle\psi_1| + p_2|\psi_2\rangle\langle\psi_2| \\ &= q_1|\phi_1\rangle\langle\phi_1| + q_2|\phi_2\rangle\langle\phi_2| \end{aligned} \quad .$$

Here $p_1 = \frac{1}{3}$, $p_2 = \frac{2}{3}$,

$$\begin{aligned} |\psi_1\rangle &= \frac{1}{2\sqrt{3}}(3|00\rangle + |01\rangle + |10\rangle + |11\rangle) \\ |\psi_2\rangle &= \frac{1}{2\sqrt{3}}(3|00\rangle - |01\rangle - |10\rangle - |11\rangle) \end{aligned}$$

and $q_1 = \frac{2}{3}$, $q_2 = \frac{1}{3}$,

$$\begin{aligned} |\phi_1\rangle &= |00\rangle \\ |\phi_2\rangle &= \frac{1}{2}(|00\rangle + |01\rangle + |10\rangle + |11\rangle) \quad . \end{aligned}$$

Separability of mixed bipartite states
A mixed bipartite state ρ is called a product state iff there exist ρ_1 and ρ_2 such that

$$\rho = \rho_1 \otimes \rho_2 \quad .$$

It is called separable iff there exists a decomposition

$$\rho = \sum_j p_j \rho_1^j \otimes \rho_2^j \quad .$$

Otherwise it is entangled.

Mixed states and separability of indistinguishable particles
In quantum many-body systems one is often interested in configurations with big particle numbers, e.g. in the asymptotic limit or in order to be close to the experiment. As we will soon see in the following subsections there exists no unique measure of entanglement even for pure multipartite states of distinguishable particles. In fact, the treatment of pure four-partite states of distinguishable particles [90] is already so involved that we believe it is hopeless to follow these lines for asymptotically many particles. So what one does in quantum many-body systems of distinguishable particles is that one traces out all but two quantum systems, i.e. particles, A and B. This results in a mixed bipartite state ρ_{AB} for which the concurrence or the negativity can be used as entanglement measures, as we will see in this subsection.

In quantum many-body systems of indistinguishable particles it is not clear how to perform the partial trace over all but two particles. E.g. the Fock state of three indistinguishable bosons

$$|\psi\rangle_F = |210\rangle$$

is in the particle picture given by

$$|\psi\rangle_p = \frac{1}{\sqrt{3}}(|0\rangle_1|0\rangle_2|1\rangle_3 + |0\rangle_1|1\rangle_2|0\rangle_3 + |1\rangle_1|0\rangle_2|0\rangle_3) \quad .$$

Of course $|\psi\rangle_p$ is a symmetrized state because the bosons are indistinguishable and we included mathematically necessary indices 1, 2 and 3. In order to obtain the reduced density matrix ρ_{AB} of two bosons we could now just trace over the third boson. But in reality the three bosons are indistinguishable and so we can not address one particular boson and trace it out. What we can do, nevertheless, is trace over index 3 to obtain

$$\rho_{AB} = \frac{1}{3}(|0\rangle_1|0\rangle_2\langle 0|_1\langle 0|_2) + \frac{2}{3}|\Psi^+\rangle\langle\Psi^+|$$

where

$$|\Psi^+\rangle = \frac{1}{\sqrt{2}}(|0\rangle_1|1\rangle_2 + |1\rangle_1|0\rangle_2)$$

formally is a maximally entangled Bell state. But we have to keep in mind that this partial trace still needs a motivation.

In the third section of this chapter we will see that a completely different approach for obtaining the two-particle reduced density matrix ρ_{AB} of indistinguishable bosons will lead to exactly that trace over all but two indices in the particle picture.

Convex roof

Convex roof constructions afford to infer entanglement properties for mixed states from pure state entanglement monotones.

Let E be a pure state entanglement monotone. Then

$$\mathbf{E} = \inf\{\sum_j p_j E(|\psi_j\rangle) : \rho = \sum_j p_j|\psi_j\rangle\langle\psi_j|\}$$

is its convex roof. It can be shown that then $\mathbf{E}$ is an entanglement monotone too. The convex roof construction to the entropy of entanglement is called entanglement of formation [33] and abbreviated EoF:

$$EoF(\rho) = \inf\{\sum_j p_j EoE(|\psi_j\rangle) : \rho = \sum_j p_j|\psi_j\rangle\langle\psi_j|\}$$

We want to remark that for a long time the entanglement of formation was believed to be additive and only recently it has been shown that this is not the case [91].

Entanglement of formation

For states of dimension 2×2 the entanglement of formation can be expressed algebraically:

$$EoF(\rho) = -x(\rho)\log(x(\rho)) - (1 - x(\rho))\log(1 - x(\rho)) \quad ,$$

where

$$x(\rho) := \frac{1 + \sqrt{1 - \mathcal{C}^2(\rho)}}{2}$$

and $\mathcal{C}(\rho)$ is called the concurrence. This relation was found by *Wootters* [92].

Concurrence
It can be shown that the entanglement of formation depends monotonously on the concurrence. Therefore the concurrence is used as an entanglement measure on its own, being zero for a separable state and one for a maximally entangled state. However, we have not specified yet what the concurrence actually is.

For a pure bipartite state $|\psi\rangle$ of dimension 2×2 we define

$$|\tilde{\psi}\rangle \quad := \quad \sigma_y \otimes \sigma_y |\psi^*\rangle \qquad ,$$

where $|\psi^*\rangle$ denotes the complex conjugate of $|\psi\rangle$, and the concurrence

$$\mathcal{C}(|\psi\rangle) \quad := \quad |\langle\psi|\tilde{\psi}\rangle| \qquad .$$

For a mixed bipartite state ρ of dimension 2×2 we define

$$\tilde{\rho} \quad := \quad \sigma_y \otimes \sigma_y \rho^* \sigma_y \otimes \sigma_y \qquad ,$$

where ρ^* is the complex conjugate of ρ, and the concurrence

$$\mathcal{C}(\rho) \quad := \quad \max\{0, \lambda_1 - \lambda_2 - \lambda_3 - \lambda_4\}$$

where the λ_j are the square roots of the eigenvalues of $\rho\tilde{\rho}$ in decreasing order.

Concurrence - Examples

- What is the concurrence of $|\psi\rangle = |01\rangle$?

$$\mathcal{C}(|\psi\rangle) \quad = \quad 0 \qquad .$$

- What is the concurrence of $|\psi\rangle = \frac{1}{\sqrt{2}}(|00\rangle + |11\rangle)$?

$$\mathcal{C}(|\psi\rangle) \quad = \quad 1 \qquad .$$

- What is the concurrence of

$$|\psi\rangle \quad = \quad \sqrt{\lambda_1}|00\rangle + \sqrt{\lambda_2}|11\rangle \qquad ?$$

$$\mathcal{C}(|\psi\rangle) \quad = \quad 2\sqrt{\lambda_1\lambda_2} \qquad .$$

- What is the concurrence of

$$\rho = \frac{1}{12}\begin{pmatrix} 9 & 1 & 1 & 1 \\ 1 & 1 & 1 & 1 \\ 1 & 1 & 1 & 1 \\ 1 & 1 & 1 & 1 \end{pmatrix} \qquad ?$$

$$\mathcal{C}(\rho) \quad = \quad 0 \qquad .$$

After this brief discussion of the concurrence we want to address the negativity now. The negativity as an entanglement measure follows from a completely different approach than above.

All quantum operations that happen in nature are completely positive maps Λ_{CP} [51]. That means that they turn a positive operator ρ into a positive operator ρ and the same is true for the trivially extended map $\Lambda_{CP} \otimes \mathbb{I}$ where $\mathbb{I}$ is the one-operator in any dimension. The motivation for this extension is that the system under consideration should always be embeddable into any environment and still the quantum operation should map ρ onto a valid positive ρ'. Of course there exist maps that are positive but not completely positive. One of them is the partial transpose, which we will explain in more detail now.

Positive maps
A linear map

$$\Lambda : \mathcal{D} \to \mathcal{D}$$

acting on the space of density operators is called positive iff:

$$\forall \rho \geq 0 : \quad \Lambda(\rho) \geq 0 \qquad .$$

It is called completely positive iff:

$$\forall \rho \geq 0 : \quad (\Lambda \otimes \mathbb{I})(\rho) \geq 0 \qquad .$$

For separable states we make the following observations:

- For a separable state ρ_{sep} every positive map is completely positive:

$$\begin{aligned} (\Lambda \otimes \mathbb{I})(\rho_{sep}) &= \sum_j p_j \Lambda(\rho_1^j) \otimes \rho_2^j \\ &\geq 0 \qquad . \end{aligned}$$

- One can also show that if every positive map is completely positive, then ρ is separable [50].

Positive partial transpose (PPT) criterion
A density operator ρ of dimension 2×2 and 2×3 is separable iff the partial transposition

$$\rho^{PT} := (T \otimes \mathbb{I})(\rho)$$

is positive. The PPT criterion was discovered by *Peres* [93] and *Horodecki et al.* [94] and is also known as the Peres-Horodecki criterion.

Let us sketch a short proof of the PPT criterion:

- If ρ is separable, then

$$\begin{aligned} \rho^{PT} &= \sum_j p_j T(\rho_1^j) \otimes \rho_2^j \\ &\geq 0 \end{aligned}$$

  and hence the partial transposition is positive.

- We now assume that the partial transposition is positive. Any positive map on systems of dimension 2×2 and 2×3 can be written as

$$\Lambda = \Lambda_{CP}^1 + \Lambda_{CP}^2 \circ T$$

such that

$$(\Lambda \otimes \mathbb{I})(\rho) = (\Lambda_{CP}^1 \otimes \mathbb{I})(\rho) + (\Lambda_{CP}^2 \otimes \mathbb{I}) \circ (T \otimes \mathbb{I})(\rho)$$

and thus every positive map is completely positive.

We remark that the proof relies heavily on the knowledge of how positive maps in dimension 2×2 and 2×3 look like [94]. Moreover we infer from the proof that for density matrices of dimension bigger than 2×2 and 2×3 the PPT criterion is still necessary for separability. This is because a separable state of any dimension must have a positive partial transpose. But equivalently this gives us a sufficient criterion for entanglement because if the PPT criterion is violated, i.e. ρ^{PT} has negative eigenvalues, the state can not be separable.

Negativity
The negativity is defined as

$$\begin{aligned} \mathcal{N}(\rho) &= \frac{||\rho^{PT}|| - 1}{2} \\ &= \sum_j |\lambda_j^-| \quad , \end{aligned}$$

where the λ_j^- denote the negative eigenvalues of ρ^{PT}. The logarithmic negativity is given by

$$\mathcal{N}_L(\rho) = \log(||\rho^{PT}||) \quad .$$

Here

$$||\rho|| := \sqrt{\mathrm{tr}(\rho^2)}$$

is called trace norm of ρ and it is equal to the sum of absolute values of the eigenvalues of ρ:

$$\begin{aligned} ||\rho^{PT}|| &= \mathrm{tr}(\rho^{PT}) + 2\sum_j |\lambda_j^-| \\ &= 1 + 2\sum_j |\lambda_j^-| \quad . \end{aligned}$$

Negativity and logarithmic negativity were introduced by *Vidal* in [95] where he proved that the negativity is an entanglement monotone and that the logarithmic negativity is additive.

We note that the negativity only detects entanglement, by being nonzero for entangled states, but its exact value does not at all allow for an interpretation of the amount of entanglement present. In particular, a quantum state

having higher negativity than another quantum state can not be called more entangled. This is completely different from the concurrence, where by plugging the concurrence into the formula of the entanglement of formation one gets a reasonable interpretation in terms of the entropy of entanglement. Therefore a quantum state having higher concurrence than another quantum state can be called more entangled, because it allows to extract more maximally entangled states $|\beta\rangle$ in the asymptotic limit.

Negativity - Examples

- What is the negativity of $|\psi\rangle = |01\rangle$?

$$\mathcal{N}(|\psi\rangle) = 0 \quad .$$

- What is the negativity of $|\psi\rangle = \frac{1}{\sqrt{2}}(|00\rangle + |11\rangle)$?

$$\mathcal{N}(|\psi\rangle) = \frac{1}{2} \quad .$$

- What is the negativity of

$$|\psi\rangle = \sqrt{\lambda_1}|00\rangle + \sqrt{\lambda_2}|11\rangle \quad ?$$

$$\mathcal{N}(|\psi\rangle) = \sqrt{\lambda_1\lambda_2} \quad .$$

- What is the negativity of

$$\rho = \frac{1}{12}\begin{pmatrix} 9 & 1 & 1 & 1 \\ 1 & 1 & 1 & 1 \\ 1 & 1 & 1 & 1 \\ 1 & 1 & 1 & 1 \end{pmatrix} \quad ?$$

$$\mathcal{N}(\rho) = 0 \quad .$$

As can be seen from the examples for pure states the concurrence and the negativity differ only by a factor of 2.

4.1.4 Pure multipartite states

Pure multipartite states can be ordered by means of probabilistic state transformations. The latter are also called stochastic state transformations or SLOCC. As an example we will discuss pure states of three qubits where the so-called 3-tangle, an entanglement monotone measuring genuine tripartite entanglement, will turn out to be of importance.

Separability of pure multipartite states
A pure multipartite state $|\psi\rangle$ of N parties is separable iff there exist $|\phi_1\rangle$, $|\phi_2\rangle$, $\ldots$, $|\phi_N\rangle$ such that

$$|\psi\rangle \quad = \quad |\phi_1\rangle \otimes |\phi_2\rangle \otimes \ldots \otimes |\phi_N\rangle.$$

Otherwise $|\psi\rangle$ is entangled.

A pure multipartite state $|\psi\rangle$ of N parties is called k-separable, $k \leq N$, iff there exist $|\phi_1\rangle$, $|\phi_2\rangle$, $\ldots$, $|\phi_k\rangle$ such that

$$|\psi\rangle \quad = \quad |\phi_1\rangle \otimes |\phi_2\rangle \otimes \ldots \otimes |\phi_k\rangle.$$

Reducibilities and equivalences
We want to adopt the terminology of [87].

- Reducibility formalizes general state transformations within LOCC.
- Equivalences are reversible state transformations within LOCC.
- From now on deterministic state transformations are called exact.
- Probabilistic state transformations are called stochastic.
- Probabilistic LOCC protocols are abbreviated SLOCC.

It can be shown that arbitrary states $|\psi\rangle$ and $|\phi\rangle$ are exactly equivalent iff they can be transformed into each other by local unitaries. But then an ordering of entangled states under exact equivalence implies an infinity of parameters. E.g. two pure bipartite states are exactly equivalent iff they have the same Schmidt coefficients. We believe that this criterion is too strict.

It turns out that arbitrary states $|\psi\rangle$ and $|\phi\rangle$ are stochastically equivalent iff they can be transformed into each other by invertible local operators (ILO) [88]. Under this perspective two pure bipartite states are stochastically equivalent iff the have the same Schmidt rank, i.e. the same number of Schmidt coefficients.

Classification of entangled states
In order to get a reasonable classification of entangled states we agree on the following two axioms of *Dür et al.* [88]:

- Arbitrary states $|\psi\rangle$ and $|\phi\rangle$ are termed equivalent iff they are stochastically equivalent.
- $|\psi\rangle$ is called more entangled than $|\phi\rangle$ iff $|\phi\rangle$ can be created from $|\psi\rangle$ by using noninvertible local operations.

The second axiom allows for a hierarchy on all entangled states.

As an example consider pure bipartite states of dimension $m \times n$, $m \leq n$. For each Schmidt rank we have a class of equivalent entangled states, giving m classes and because noninvertible local operations can lower the Schmidt rank a class is more entangled if it belongs to a bigger Schmidt rank. In particular,

the most entangled states have Schmidt rank m and the least entangled states have Schmidt rank 1. Of course the latter are actually separable.

Let us now apply this formalism to the first nontrivial case, i.e. pure states of three qubits.

Tripartite states
For tripartite states of qubits there exist six classes [88]:

- Class A-B-C: Separable states

$$\mathrm{rank}(\rho_A) = \mathrm{rank}(\rho_B) = \mathrm{rank}(\rho_C) = 1 \quad ,$$

  representative:

$$|\psi_{A-B-C}\rangle \;=\; |0\rangle|0\rangle|0\rangle \quad .$$

- Class A-BC: Bipartite entanglement

$$\begin{aligned} \mathrm{rank}(\rho_A) &= 1 \\ \mathrm{rank}(\rho_B) &= 2 \\ \mathrm{rank}(\rho_C) &= 2 \end{aligned} \quad ,$$

  representative:

$$|\psi_{A-BC}\rangle \;=\; \frac{1}{\sqrt{2}}|0\rangle(|0\rangle|0\rangle + |1\rangle|1\rangle) \quad .$$

- Class B-AC: Bipartite entanglement
- Class C-AB: Bipartite entanglement
- Class ABC: Tripartite $|GHZ\rangle$-entanglement

$$\mathrm{rank}(\rho_A) = \mathrm{rank}(\rho_B) = \mathrm{rank}(\rho_C) = 2 \quad ,$$

  representative:

$$|GHZ\rangle \;=\; \frac{1}{\sqrt{2}}(|0\rangle|0\rangle|0\rangle + |1\rangle|1\rangle|1\rangle) \quad .$$

- Class ABC: Tripartite $|W\rangle$-entanglement

$$\mathrm{rank}(\rho_A) = \mathrm{rank}(\rho_B) = \mathrm{rank}(\rho_C) = 2 \quad ,$$

  representative:

$$|W\rangle \;=\; \frac{1}{\sqrt{3}}(|0\rangle|0\rangle|1\rangle + |0\rangle|1\rangle|0\rangle + |1\rangle|0\rangle|0\rangle) \quad .$$

Here ρ_X denotes the reduced density of quantum system X which is obtained by tracing out all quantum systems other than quantum system X.

It is remarkable that by no means a state belonging to the $|GHZ\rangle$-class can be transformed to a state belonging to the $|W\rangle$-class and vice versa. However, from any of the two classes of tripartite entanglement we can get to the first four classes of bipartite entanglement and separable states by noninvertible local operations, thereby obtaining a complete hierarchy. We note further that for many reasons the $|GHZ\rangle$ state is seen in the literature as the maximally entangled tripartite state, while it can be shown that the $|W\rangle$ state is the state that retains the maximal amount of entanglement in several aspects under loss of one particle [88].

In the following the 3-tangle will enable us to decide if a given state belongs to the $|GHZ\rangle$-class or to the $|W\rangle$-class.

3-tangle
Coffman et al. showed that for a pure tripartite state

$$\mathcal{C}^2_{AB} + \mathcal{C}^2_{AC} \quad \leq \quad \mathcal{C}^2_{A(BC)}$$

and defined

$$\tau_{ABC} \quad := \quad \mathcal{C}^2_{A(BC)} - \mathcal{C}^2_{AB} - \mathcal{C}^2_{AC} \qquad .$$

The latter quantity is called 3-tangle. It was shown to be an entanglement monotone [88].

3-tangle - Examples

- What is the 3-tangle of the $|W\rangle$ state?

$$\tau(|W\rangle) \quad = \quad 0 \qquad .$$

- What is the 3-tangle of the $|GHZ\rangle$ state?

$$\tau(|GHZ\rangle) \quad = \quad 1 \qquad .$$

In fact, it can be shown [88] that any state belonging to the $|W\rangle$-class has a vanishing 3-tangle while any state belonging to the $|GHZ\rangle$-class has a nonvanishing 3-tangle. So we can distinguish the states with $\text{rank}(\rho_A) = \text{rank}(\rho_B) = \text{rank}(\rho_C) = 2$ with the help of the 3-tangle: If it vanishes the state belongs to the $|W\rangle$-class, otherwise it belongs to the $|GHZ\rangle$-class.

$|W\rangle$ and $|GHZ\rangle$ for indistinguishable bosons
Here we just want to present the indistinguishable counterparts to the above $|W\rangle$ and $|GHZ\rangle$ states in the bosonic case.

Obviously $|W\rangle$ is given by the Fock state

$$|W\rangle_F \quad = \quad |21\rangle$$

because in the particle picture this state reads

$$|W\rangle_p \quad = \quad \frac{1}{\sqrt{3}}(|0\rangle|0\rangle|1\rangle + |0\rangle|1\rangle|0\rangle + |1\rangle|0\rangle|0\rangle) \qquad .$$

However this state of three indistinguishable bosons is argued to be unentangled because it can be written as a single Fock state [57]. Nevertheless our own interpretation of quantum correlations between indistinguishable particles in the third section of this chapter will call this state entangled, just as it is in the case of distinguishable particles.

The indistinguishable analogon of the $|GHZ\rangle$ is given by the Fock state

$$|GHZ\rangle_F \quad = \quad \frac{1}{\sqrt{2}}(|30\rangle + |03\rangle)$$

because in the particle picture this state reads

$$|GHZ\rangle_p \quad = \quad \frac{1}{\sqrt{2}}(|0\rangle|0\rangle|0\rangle + |1\rangle|1\rangle|1\rangle) \qquad .$$

In terms of mode entanglement this state is a maximally entangled state, and this will also be the case with our own measure of quantum correlations between indistinguishable bosons.

Four-partite states

Verstraete et al. proved that there are 9 different entanglement families under SLOCC for pure four-qubit states [90]. However, already for these pure four-qubit states the calculations are very involved and we expect that the classification of the entanglement of higher-partite states can not be done on the same lines.

4.1.5 Mixed multipartite states

Finally we want to analyze the most general case, i.e. what can be said about the entanglement of mixed multipartite states. However, there exists a plethora of measures being more or less practically computable and having a more or less sensible interpretation [96, 97, 98, 34]. We decided to mainly follow a line leading to a generalization of the concurrence to arbitrary many subsystems and dimensions. We will only briefly touch the Θ-concurrence, the I-concurrence and finally come to an approach introduced by *Mintert et al.*, that has an interpretation for entanglement and can be well approximated numerically.

Separability of mixed multipartite states

A mixed multipartite state ρ of N parties is called a product state iff there exist ρ_1, ρ_2, $\ldots$, ρ_N such that

$$\rho \quad = \quad \rho_1 \otimes \rho_2 \otimes \ldots \otimes \rho_N \qquad .$$

It is called separable iff there exists a decomposition

$$\rho \quad = \quad \sum_j p_j \rho_1^j \otimes \rho_2^j \otimes \ldots \otimes \rho_N^j \qquad .$$

Otherwise it is entangled.

Θ-concurrence
An anti-linear operator Θ, i.e.

$$\Theta(\alpha|\psi_1\rangle + \beta|\psi_2\rangle) \;=\; \alpha^*\Theta(|\psi_1\rangle) + \beta^*\Theta(|\psi_2\rangle) \qquad ,$$

that is unitary and an involution, i.e.

$$\Theta^{-1} \;=\; \Theta \qquad ,$$

is called a conjugation. The Θ-concurrence [99] is defined in terms of a conjugation Θ:

$$\mathcal{C}_\Theta(|\psi\rangle) \;=\; |\langle\psi|\Theta|\psi\rangle| \qquad .$$

Even though the Θ-concurrence reduces to the well-known concurrence for systems of dimension 2×2 and then has a clear meaning for measuring entanglement, in arbitrary dimensions this interpretation for entanglement does not exist.

I-concurrence
The I-concurrence [100] is given by:

$$\mathcal{C}_I(|\psi\rangle) \;=\; \sqrt{\langle\psi|(I_1 \otimes I_2|\psi\rangle\langle\psi|)|\psi\rangle} \qquad ,$$

where the operators I_1 and I_2 are determined uniquely by additional requirements. The I-concurrence in arbitrary dimensions lacks an interpretation for entanglement too.

Mintert's approach
In contrast to the above two examples of generalizations of the concurrence to higher-dimensional systems *Mintert et al.* derived a generalization of the concurrence to higher-dimensional and multipartite systems [101] that additionally has an interpretation for entanglement. We just want to show here one example of how Mintert's concurrence can be applied.

Mintert looks at two copies of the state $|\psi\rangle$ and defines

$$\mathcal{C}(|\psi\rangle) \;=\; \sqrt{\langle\psi| \otimes \langle\psi|A|\psi\rangle \otimes |\psi\rangle}$$

where A is a projector onto the antisymmetric subspace of the first and the second Hilbert space:

$$A \;:=\; 4P_1^- \otimes P_2^- \qquad .$$

Then two copies of a separable state $|\psi\rangle = |\phi_1\rangle \otimes |\phi_2\rangle$ have the expectation value

$$\begin{aligned}
\langle\psi|\langle\psi|A|\psi\rangle|\psi\rangle &= 4\langle\phi_1|\langle\phi_2|\langle\phi_1|\langle\phi_2|P_1^- \otimes P_2^-|\phi_1\rangle|\phi_2\rangle|\phi_1\rangle|\phi_2\rangle \\
&= 4\langle\phi_1|\langle\phi_1|P_1^-|\phi_1\rangle|\phi_1\rangle \cdot \langle\phi_2|\langle\phi_2|P_2^-|\phi_2\rangle|\phi_2\rangle \\
&= 0 \qquad .
\end{aligned}$$

The two copies of an entangled state on the other hand will have a positive expectation value.

It turns out that Mintert's approach has an obvious extension to mixed and multipartite states. Additionally his concurrence can be computed efficiently by making use of reasonable approximations.

4.1.6 Summary of entanglement theory

- Pure state entanglement is quantified by the entropy of entanglement.
- Concurrence and negativity are the appropriate entanglement measures for mixed states of dimension 2×2 and 2×3.
- Pure multipartite states are classifiable for systems comprising up to four qubits.
- The entanglement of multipartite mixed states of higher dimensions can only be approximated so far and new theoretical concepts are needed.

4.2 Single-copy vs. asymptotic entanglement

In this very short section we want to report a numerical result that we obtained concerning the difference between single-copy and asymptotic entanglement. More precisely, we found numerical evidence that the largest Schmidt coefficient alone possesses all entanglement information. However, we already want to emphasize that further studies are needed.

As explained in the above introduction to entanglement theory *Eisert* and *Cramer* used the largest Schmidt coefficient to define a measure for single-copy entanglement,

$$E(|\psi\rangle) \quad = \quad \log(\lfloor(\lambda_1^{\downarrow})^{-1}\rfloor) \qquad .$$

If one neglects the floor function one gets a new quantity

$$\begin{aligned} SCE(|\psi\rangle) &= \log((\lambda_1^{\downarrow})^{-1}) \\ &= -\log(\lambda_1^{\downarrow}) \end{aligned}$$

that depends continuously on the largest Schmidt coefficient.

We numerically compare this single-copy entanglement measure SCE with the commonly used asymptotic entanglement measure EoE by analyzing Wannier mode entanglement of two neighbouring modes with the remaining modes in the ground state of the periodic Bose-Hubbard Hamiltonian in Figure 4.1 and in a propagated state, which initially is $|\psi(t=0)\rangle = |50000\rangle_W$, that evolves with the periodic Bose-Hubbard Hamiltonian to $L = 5 = N$ and $J = 1 = U$ in Figure 4.2. We chose these two scenarios for our comparison of SCE and EoE because they represent standard scenarios in entanglement studies. We want to find out if in these two scenarios SCE and EoE imply the same conclusions.

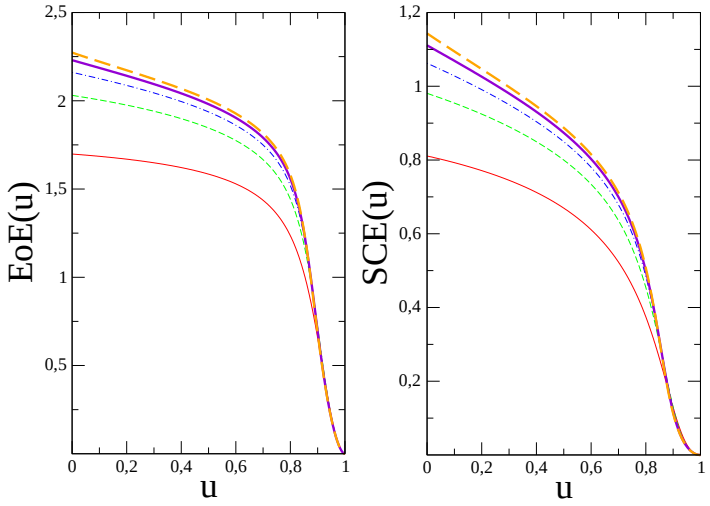

Figure 4.1: $EoE(u)$ (left) and $SCE(u)$ (right) for the entanglement between two neighbouring Wannier modes with the remaining Wannier modes of the ground state of the periodic Bose-Hubbard Hamiltonian with $L = 3 = N$ (red, thin line), $L = 4 = N$ (green, thin dashed line), $L = 5 = N$ (blue, thin dash dotted line), $L = 6 = N$ (violet, thick line) and $L = 7 = N$ (orange, thick dashed line). Obviously the single-copy entanglement measure SCE and the asymptotic entanglement measure EoE qualitatively look the same.

We conclude from Figure 4.1 that the entropy of entanglement of the ground state is high in-between $u = 0$ and $u = 0.8$ and quickly drops to zero in-between $u = 0.8$ and $u = 1$. The same is true for the single-copy entanglement. Even though quantitatively SCE and EoE differ, which they have to since they are different quantities, qualitatively they imply the same conclusion for the entanglement properties of the ground state. Their behaviour can be understood if one keeps in mind that we are looking at Wannier mode entanglement and for $u \in [0, 0.8]$ the ground state is a superposition of many Wannier Fock states, which is why the entanglement is expected to be high in this region. However at $u = 1$ the ground state is a single Wannier Fock state, which is separable, and therefore the entanglement has to vanish for $u \in [0.8, 1]$.

Figure 4.2 shows how the initially separable state $|\psi(t = 0)\rangle = |50000\rangle_W$ gets entangled while it propagates with the periodic Bose-Hubbard Hamiltonian in the chaotic regime of $J = 1 = U$. Again SCE and EoE quantitatively differ, as they have to, but qualitatively allow for the same conclusion. The entanglement grows quickly at the beginning and then shows irregular behaviour, as we expect it for the chaotic regime, around a constant value of $SCE \approx 1.0$ and $EoE \approx 2.7$.

The figures suggest that SCE, the measure for single-copy entanglement, and EoE, the measure for asymptotic entanglement, qualitatively behave in the same way. If this was true in general, we could always quantify the entanglement in terms of SCE instead of EoE. This would have two major advantages. First SCE originates from a single-copy interpretation which is favoured by experimentalists because the realization of many copies of an entangled state,

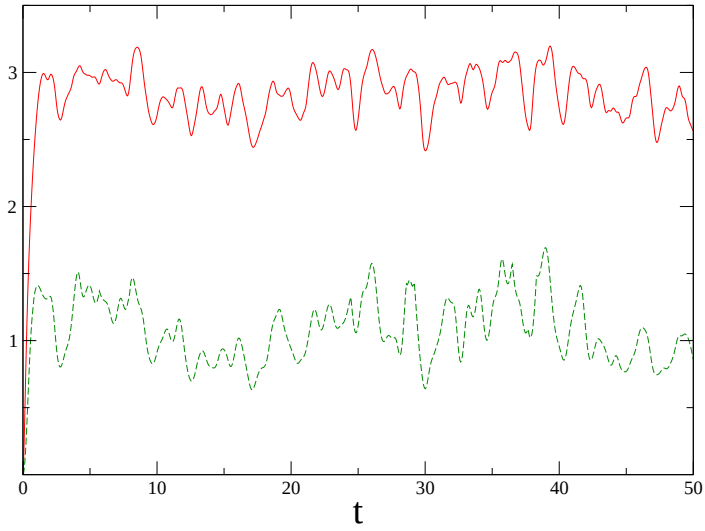

Figure 4.2: $EoE(t)$ (red, thin line) and $SCE(t)$ (green, thin dashed line) for the entanglement between two neighbouring Wannier modes with the remaining Wannier modes of the propagated state $|\psi(t=0)\rangle = |50000\rangle_W$ that evolves with the periodic Bose-Hubbard Hamiltonian to $L = 5 = N$ and $J = 1 = U$; see Section 2.1.1 for the units of time. Here the single-copy entanglement measure SCE and the asymptotic entanglement measure EoE have their local minima and maxima approximately at the same position.

necessary in the asymptotic interpretation of EoE, exceeds the state-of-the-art experimental possibilities. And second the computation of only the largest Schmidt coefficient, i.e. only the largest singular value, can often be done analytically or numerically efficient and this allows to study larger systems.

4.3 Quantum correlations between indistinguishable bosons

We have seen in the above introduction to entanglement theory that there exists no convincing theory that allows us to directly *quantify* entanglement in quantum many-body systems of indistinguishable bosons. *Paskauskas* and *You* introduced the Schmidt decomposition for two indistinguishable bosons [56], but they did not explain the use of the resulting Schmidt coefficients for entanglement. Moreover they did not show how their results can be applied to systems of more than two bosons. Later *Eckert, Schliemann et al.* derived formulas for the detection of entanglement in quantum systems of more than two indisinguishable bosons [53]. But their formulas are hard to compute and again lack a clear interpretation for entanglement.

In the context of spin squeezing, inequalities for the squeezing parameter were derived for separable states of N distinguishable bosons [66] as well as for separable states of N indistinguishable bosons [67]. *Estève et al.* then proved experimentally that BECs can violate these inequalities [9] and so they proved

the existence of entanglement, as they define it, in a quantum many-body system of indistinguishable bosons. However, their notion of separability coincides with all bosons populating the same state and they do not give a motivation for this definition of separability. Also they can only show that an inequality for the squeezing parameter is violated and by this detect entanglement, but they can not quantify it. Additionally the corresponding inequalities for the squeezing parameter exist only for systems of two wells [68, 69], because there the direct analogy to spin-$\frac{1}{2}$ particles holds and this makes the derivation of the inequalities for the squeezing parameter straightforward.

In the following we want to develop our own entanglement theory for systems of indistinguishable bosons. In analogy to *Schliemann et al.* [52, 53] we refer to quantum correlations instead of entanglement because it is still unclear if the entanglement between indistinguishable particles can be used as a resource on the same lines as the entanglement between distinguishable particles. Our measure will have a clear interpretation for entanglement and it will be applicable to any number N of indistinguishable bosons. Additionally it will turn out to be efficiently computable.

We will start by defining separability for indistinguishable bosons and then present our measure of quantum correlations. We will introduce our own concept of LOCC for indistinguishable bosons as noninteracting Hamiltonian evolution and prove the invariance of our measure under this concept. Thereupon we will extend our measure to mixed states of two bosons. In this context we will also show how the reduced density matrix of two bosons is obtained, i.e. how the partial trace over all but two indistinguishable bosons is performed. With these tools at hand we are able to investigate quantum systems comprising an arbitrary number of indistinguishable bosons. As we have argued above in the introduction to entanglement theory, it was an open question of how to perform the partial trace over indistinguishable particles. Finally we simplify our measure and apply it to the ground and to the thermal state of the Bose-Hubbard model.

4.3.1 Separability for indistinguishable bosons

It is important to distinguish between the Fock and the particle picture as we already did in the above introduction to entanglement theory. Every state of indistinguishable particles can be either written as a superposition of Fock states or as a superposition of symmetrized products of one-particle wave functions. While our approach uses the particle picture most of the time, we will justify every operation in the Fock picture, since this is the commonly accepted description for systems of indistinguishable particles.

Paskauskas and *You* have first shown that there exists a Schmidt decomposition for two indistinguishable particles [56], in total analogy to systems of two distinguishable particles. Any state of two indistinguishable bosons can be written as

$$|\psi\rangle \quad = \quad \sum_{j,k} a_{jk} |j\rangle |k\rangle$$

where $A = (a_{jk})$ is a symmetric matrix due to requirement that $|\psi\rangle$ has to be symmetrized. There exists a decomposition of the symmetric coefficient matrix $A = U^T D U$, where D is diagonal with real nonnegative entries, that allows to rewrite $|\psi\rangle$ in terms of a new basis. Using

$$\begin{aligned} a_{jk} &= \sum_i u_{ji}^T d_{ii} u_{ik} \\ &= \sum_i u_{ij} d_{ii} u_{ik} \end{aligned}$$

we get

$$\begin{aligned} |\psi\rangle &= \sum_{j,k} a_{jk}|j\rangle|k\rangle = \sum_{i,j,k} u_{ij} d_{ii} u_{ik}|j\rangle|k\rangle \\ &= \sum_i d_{ii}(\sum_j u_{ij}|j\rangle)(\sum_k u_{ik}|k\rangle) =: \sum_i \sqrt{\lambda_i}|i\rangle|i\rangle \end{aligned}$$

and the $\sqrt{\lambda_i}$ are then the Schmidt coefficients for indistinguishable bosons.

Here we want to motivate that these Schmidt coefficients indeed characterize the entanglement between two indistinguishable bosons [102]. Consider a pair of indistinguishable bosons and now detect one, without specifying which one. In fact, because they are indistinguishable it is impossible to further specify the measured particle. This detection of one particle is described by the quantum operation

$$\rho_1 = \frac{1}{N} \sum_{j=1}^{L} \hat{a}_j |\psi\rangle\langle\psi| \hat{a}_j^\dagger \quad , \tag{4.1}$$

where L is the dimension of the single-particle Hilbert space, in the Fock picture and turns out to be equivalent to performing the partial trace over one index in the particle picture. Now the degree of mixedness of the one-particle density matrix ρ_1 tells how much the measurement of one particle influences the state of the other particle. With this interpretation at hand entanglement measures for distinguishable particles can be directly used for indistinguishable particles.

So we define a pure state $|\psi\rangle$ for two indistinguishable bosons to be separable iff there exists a single-particle quantum state $|\phi\rangle$ such that

$$|\psi\rangle = |\phi\rangle \otimes |\phi\rangle \quad .$$

Such a separable state $|\psi\rangle$ has the Schmidt decomposition

$$|\psi\rangle = |00\rangle \quad .$$

In the case of distinguishable particles a separable state is of the form $|\psi\rangle = |\phi_1\rangle \otimes |\phi_2\rangle$ with two possibly different single-particle quantum states $|\phi_1\rangle$ and $|\phi_2\rangle$, and this state has the same Schmidt decomposition $|\psi\rangle = |00\rangle$.

We define a mixed state ρ for two indistinguishable bosons to be separable iff there exists a decomposition

$$\rho = \sum_j p_j \rho^j \otimes \rho^j \quad . \tag{4.2}$$

In the case of distinguishable particles a separable state is of the form

$$\rho \quad = \quad \sum_j p_j \rho_1^j \otimes \rho_2^j \qquad .$$

At the moment we believe it is reasonable that any entanglement measure for distinguishable particles can equally be applied to indistinguishable particles in the particle picture. We choose the entropy of entanglement although we lack an asymptotic interpretation for indistinguishable bosons, as we have explained in the above introduction to entanglement theory (c.f. Section 4.1.2). Another appropriate measure would be the single-copy entanglement which does not rely on many copies of the state under consideration. However, the standard entanglement measure for pure bipartite states of distinguishable particles is the entropy of entanglement and that is the reason why we choose the entropy of entanglement. Thus our measure of quantum correlations for pure states $|\psi\rangle$ of two indistinguishable bosons reads

$$EoE(|\psi\rangle) \quad = \quad -\sum_j \lambda_j \log(\lambda_j)$$

where the λ_j are the Schmidt coefficients resulting from the Schmidt decomposition for indistinguishable bosons.

4.3.2 LOCC for indistinguishable bosons

Because we can not address the particles individually, due to their indistinguishability, it does not make sense to talk about usual LOCC. This we have also argued in the above introduction to entanglement theory (c.f. Section 4.1.1). In our opinion the correct analogue is *noninteracting* Hamiltonian evolution. E.g. for two indistinguishable bosons in a two-dimensional Hilbert space the complete set of noninteracting Hamiltonians is given by

$$\hat{H}_1 \quad = \quad C_1 \hat{a}_1^\dagger \hat{a}_1 + C_2 \hat{a}_1^\dagger \hat{a}_2 + C_2^* \hat{a}_2^\dagger \hat{a}_1 + C_3 \hat{a}_2^\dagger \hat{a}_2$$

where C_1 and C_3 must be real and C_2 can be complex because $\hat{H}_1$ has to be Hermitian. Then noninteracting Hamiltonian evolution is given by

$$|\psi(t)\rangle \quad = \quad e^{-\frac{i}{\hbar}\hat{H}_1 t}|\psi(0)\rangle \qquad .$$

We demand that our entanglement measure of quantum correlations should never grow under evolution with $\hat{H}_1$, i.e.

$$EoE(|\psi(t)\rangle) \leq EoE(|\psi(0)\rangle) \quad \forall t \qquad .$$

In contrast, e.g. a Hamiltonian with two-particle interaction can look like

$$\hat{H}_2 \quad = \quad D_1 \hat{n}_1(\hat{n}_1 - 1) \qquad ,$$

where D_1 must be real because $\hat{H}_2$ has to be Hermitian. In fact, here we have just chosen the interaction part of the Bose-Hubbard model. We would expect that the Schmidt coefficients change under evolution with $\hat{H}_1 + \hat{H}_2$.

Let us first check numerically how the Schmidt coefficients behave under arbitrary noninteracting Hamiltonian evolution. For this numerical check we choose two bosons in a five-dimensional Hilbert space. We pick as an arbitrary noninteracting Hamiltonian

$$\hat{H}_1 = \begin{pmatrix} 1.0 & 1.3+1.8I & 0 & 0 & 0 \\ 1.3-1.8I & 1.5 & 1.2+2.1I & 2.1+1.5I & 3.1+1.5I \\ 0 & 1.2-2.1I & 0.9 & 1.2+3.2I & 0 \\ 0 & 2.1-1.5I & 1.2-3.2I & 1.9 & 3.2+3.2I \\ 0 & 3.1-1.5I & 0 & 3.2-3.2I & 2.9 \end{pmatrix} ,$$

where H_1^{ij} is the coefficient to $\hat{a}_i^\dagger \hat{a}_j$. The eigenstates of $\hat{H}_1$ all have either one Schmidt coefficient with value 1 or two with both being $\frac{1}{\sqrt{2}}$. We now choose as an arbitrary starting state

$$\begin{aligned} |\psi(0)\rangle &= 0.25|20000\rangle + 0.25I|10010\rangle + \frac{1}{\sqrt{8}}|10001\rangle + 0.25|02000\rangle + \\ &\quad (0.25+0.25I)|01010\rangle + 0.5|01001\rangle + \frac{1}{\sqrt{8}}|00101\rangle + 0.25|00020\rangle + \\ &\quad 0.25|00011\rangle + 0.25|00002\rangle \end{aligned}$$

and propagate it with $\hat{H}_1$. The result can be seen in the left part of Figure 4.3 and we conclude that the Schmidt coefficients S_1 to S_5 remain constant over all times t.

The situation changes if we include two-particle interaction. In order to have a realistic Hamiltonian with two-particle interaction we make use of the periodic Bose-Hubbard Hamiltonian with $L = 5$ wells and $N = 2$ bosons:

$$\hat{H} = -J \sum_{l=1}^{5} (\hat{a}_{l+1}^\dagger \hat{a}_l + \hat{a}_l^\dagger \hat{a}_{l+1}) + \frac{U}{2} \sum_{l=1}^{5} \hat{n}_l (\hat{n}_l - 1)$$

where the two-particle interaction obviously resides in the second part of the Hamiltonian. This is thoroughly explained in Chapter 2. Now we choose as an inital state a separable state

$$|\psi(0)\rangle = |00\rangle$$

which initially only has one nonvanishing Schmidt coefficient. By choosing this initial state it is particularly easy to see if the Schmidt coefficients change in time. The propagation of $|\psi(0)\rangle$ with the above periodic Bose-Hubbard Hamiltonian where we put $J = 1$ and $U = 1$ is shown in the right part of Figure 4.3. We conclude that the two-particle interaction indeed causes the Schmidt coefficients to change. More precisely, they change very irregularly with time and this is due to the fact that the propagation is done in the chaotic regime of $J = 1 = U$. We also looked at the propagation in the regular regime of $J = 1$ and $U = 10$ and in the regular regime of $J = 10$ and $U = 1$, and there the change of the Schmidt coefficients was characterized by regular oscillations.

We will now prove analytically that our entanglement measure is invariant under noninteracting Hamiltonian evolution.

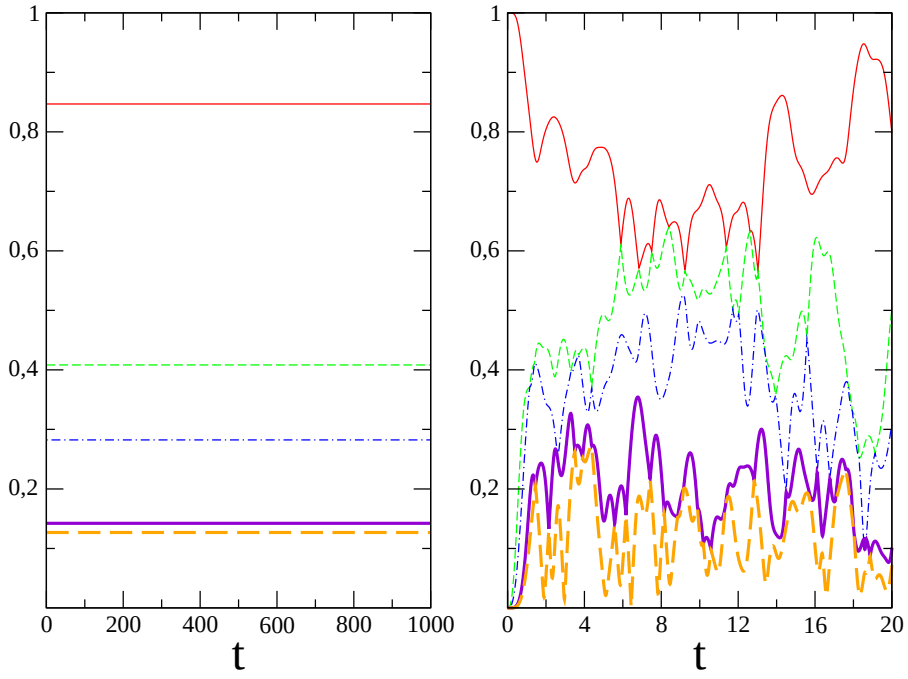

Figure 4.3: Schmidt coefficients S_1 (red, thin line), S_2 (green, thin dashed line), S_3 (blue, thin dash dotted line), S_4 (violet, thick line) and S_5 (orange, thick dashed line) of an arbitrary initial state of 2 bosons in a 5-dimensional single-particle Hilbert space under arbitrary noninteracting Hamiltonian evolution (left) and of an intially separable state of 2 bosons propagating with the periodic Bose-Hubbard Hamiltonian with $L = 5$ wells and $J = 1$ and $U = 1$ (right); see Section 2.1.1 for the units of time. We conclude that the Schmidt coefficients are invariant under noninteracting Hamiltonian evolution and they change in time if two-particle interaction is included.

Theorem:
If two indistinguishable bosons are initially in the state $|\psi(0)\rangle$ with Schmidt coefficients λ_1, λ_2, ..., λ_d and this state is propagated with a noninteracting Hamiltonian $\hat{H}_1$, then

$$|\psi(t)\rangle \quad = \quad e^{-\frac{i}{\hbar}\hat{H}_1 t}|\psi(0)\rangle$$

will have exactly the same Schmidt coefficients λ_1, λ_2, ..., λ_d for all times t.

Proof:
The general noninteracting Hamiltonian $\hat{H}_1$ has the form

$$\hat{H}_1 \quad = \quad \sum_{j,k} C_{jk}\hat{a}_j^\dagger \hat{a}_k$$

and $C_{jk} = C_{kj}^*$ because $\hat{H}_1$ is Hermitian.

We will now look at $|\psi(\Delta t)\rangle$, where Δt is an infinitesimally small time step. On the one hand, this will allow us to expand the exponential function and

neglect all higher orders of Δt, i.e. we will only consider terms up to first order in Δt. Practically this means that $(\Delta t)^2$, $(\Delta t)^3$, ... are put to zero wherever they show up in the calculation. On the other hand, if we prove that $|\psi(\Delta t)\rangle$ has the same Schmidt coefficients as $|\psi(0)\rangle$ we are done, because if the Schmidt coefficients do not change within any small amount of time then they will never change. For the correctness of this argument it is important to keep in mind that our time-evolution is unitary and that we can propagate a state to the time t by applying many successive unitaries that each propagate it over a time step Δt. If there is a contribution of higher orders $(\Delta t)^2$, $(\Delta t)^3$, ... to a Schmidt-coefficient then we just have to decrease Δt such that this contribution becomes negligible.

In the following derivation we choose the basis in which $|\psi(0)\rangle$ is Schmidt decomposed,

$$\begin{aligned} |\psi(0)\rangle &= \sum_l \lambda_l |l\rangle|l\rangle \\ &= \sum_l \lambda_l \frac{\hat{a}_l^\dagger \hat{a}_l^\dagger}{\sqrt{2}} |\Omega\rangle \end{aligned}$$

where the λ_l are the real nonnegative Schmidt coefficients of $|\psi(0)\rangle$ and $|\Omega\rangle$ denotes the vacuum. Furthermore we will often make use of the well-known bosonic commutation relations

$$\begin{aligned} [\hat{a}_j, \hat{a}_k^\dagger] &= \delta_{j,k} \\ [\hat{a}_j, \hat{a}_k] &= 0 \\ [\hat{a}_j^\dagger, \hat{a}_k^\dagger] &= 0 \end{aligned}$$

and we will frequently apply

$$\begin{aligned} \hat{a}|n\rangle &= \sqrt{n}|n-1\rangle \\ \hat{a}^\dagger|n\rangle &= \sqrt{n+1}|n+1\rangle \quad . \end{aligned}$$

With these tools at hand we can start:

$$
\begin{aligned}
|\psi(\Delta t)\rangle &= e^{-\frac{i}{\hbar}\hat{H}_1\Delta t}|\psi(0)\rangle \\
&\approx (1-\frac{i}{\hbar}\hat{H}_1\Delta t)|\psi(0)\rangle \\
&= |\psi(0)\rangle - \frac{i\Delta t}{\hbar}\sum_{j,k} C_{jk}\hat{a}_j^\dagger\hat{a}_k|\psi(0)\rangle \\
&= |\psi(0)\rangle - \frac{i\Delta t}{\hbar}\sum_{j,k} C_{jk}\hat{a}_j^\dagger\hat{a}_k\sum_l \lambda_l\frac{\hat{a}_l^\dagger\hat{a}_l^\dagger}{\sqrt{2}}|\Omega\rangle \\
&= |\psi(0)\rangle - \frac{i\Delta t}{\sqrt{2}\hbar}\sum_{j,k,l} \lambda_l C_{jk}\hat{a}_j^\dagger\hat{a}_k\hat{a}_l^\dagger\hat{a}_l^\dagger|\Omega\rangle \\
&= |\psi(0)\rangle - \frac{i\Delta t}{\sqrt{2}\hbar}\sum_{j,k,l} \lambda_l C_{jk}\hat{a}_j^\dagger(\delta_{k,l}+\hat{a}_l^\dagger\hat{a}_k)\hat{a}_l^\dagger|\Omega\rangle \\
&= |\psi(0)\rangle - \frac{i\Delta t}{\sqrt{2}\hbar}\sum_{j,k,l} \lambda_l C_{jk}\hat{a}_j^\dagger\delta_{k,l}\hat{a}_l^\dagger|\Omega\rangle - \\
&\quad \frac{i\Delta t}{\sqrt{2}\hbar}\sum_{j,k,l} \lambda_l C_{jk}\hat{a}_j^\dagger\hat{a}_l^\dagger\hat{a}_k\hat{a}_l^\dagger|\Omega\rangle \\
&= |\psi(0)\rangle - \frac{i\Delta t}{\sqrt{2}\hbar}\sum_{j,k} \lambda_k C_{jk}\hat{a}_j^\dagger\hat{a}_k^\dagger|\Omega\rangle - \\
&\quad \frac{i\Delta t}{\sqrt{2}\hbar}\sum_{j,k,l} \lambda_l C_{jk}\hat{a}_j^\dagger\hat{a}_l^\dagger(\delta_{k,l}+\hat{a}_l^\dagger\hat{a}_k)|\Omega\rangle \\
&= |\psi(0)\rangle - \frac{i\Delta t}{\sqrt{2}\hbar}\sum_{j,k} \lambda_k C_{jk}\hat{a}_j^\dagger\hat{a}_k^\dagger|\Omega\rangle - \frac{i\Delta t}{\sqrt{2}\hbar}\sum_{j,k,l} \lambda_l C_{jk}\hat{a}_j^\dagger\hat{a}_l^\dagger\delta_{k,l}|\Omega\rangle - \\
&\quad \frac{i\Delta t}{\sqrt{2}\hbar}\sum_{j,k,l} \lambda_l C_{jk}\hat{a}_j^\dagger\hat{a}_l^\dagger\hat{a}_l^\dagger\hat{a}_k|\Omega\rangle \\
&= |\psi(0)\rangle - \frac{i\sqrt{2}\Delta t}{\hbar}\sum_{j,k} \lambda_k C_{jk}\hat{a}_j^\dagger\hat{a}_k^\dagger|\Omega\rangle \\
&= \sum_k \lambda_k\frac{\hat{a}_k^\dagger\hat{a}_k^\dagger}{\sqrt{2}}|\Omega\rangle - \frac{i\sqrt{2}\Delta t}{\hbar}\sum_{j,k} \lambda_k C_{jk}\hat{a}_j^\dagger\hat{a}_k^\dagger|\Omega\rangle \\
&= \sum_k \lambda_k(\frac{\hat{a}_k^\dagger\hat{a}_k^\dagger}{\sqrt{2}} - \frac{i\sqrt{2}\Delta t}{\hbar}\sum_j C_{jk}\hat{a}_j^\dagger\hat{a}_k^\dagger)|\Omega\rangle \\
&= \sum_k \lambda_k(|k\rangle|k\rangle - \frac{i2\Delta t}{\hbar}C_{kk}|k\rangle|k\rangle - \frac{i\Delta t}{\hbar}\sum_{j\neq k} C_{jk}(|j\rangle|k\rangle + |k\rangle|j\rangle))) \\
&= \sum_k \lambda_k(|k\rangle|k\rangle - \frac{i\Delta t}{\hbar}\sum_j C_{jk}(|j\rangle|k\rangle + |k\rangle|j\rangle))) \qquad .
\end{aligned}
$$

We do a change of basis with the unitary

$$U = \begin{pmatrix} 1-\frac{i\Delta t}{\hbar}C_{11} & -\frac{i\Delta t}{\hbar}C_{21} & -\frac{i\Delta t}{\hbar}C_{31} & \dots \\ -\frac{i\Delta t}{\hbar}C_{12} & 1-\frac{i\Delta t}{\hbar}C_{22} & -\frac{i\Delta t}{\hbar}C_{32} & \dots \\ -\frac{i\Delta t}{\hbar}C_{13} & -\frac{i\Delta t}{\hbar}C_{23} & 1-\frac{i\Delta t}{\hbar}C_{33} & \dots \\ \vdots & \vdots & \vdots & \ddots \end{pmatrix} \quad ,$$

i.e.

$$\begin{aligned} u_{jj} &= 1-\frac{i\Delta t}{\hbar}C_{jj} \\ u_{jk} &= -\frac{i\Delta t}{\hbar}C_{kj} \quad \forall j \neq k \quad . \end{aligned}$$

Clearly U is unitary if one keeps in mind that $C_{jk} = C^*_{kj}$. The scalar product of one row j with itself becomes

$$\begin{aligned} \langle j|j\rangle &= 1+\frac{(\Delta t)^2}{\hbar^2}\sum_k |C_{jk}|^2 \\ &= 1+\frac{(\Delta t)^2}{\hbar^2} \\ &\approx 1 \quad , \end{aligned}$$

while the scalar product of one row j with a different row k is

$$\begin{aligned} \langle j|k\rangle &= \frac{i\Delta t}{\hbar}(C^*_{kj}-C_{jk})+\frac{(\Delta t)^2}{\hbar^2}\sum_l C^*_{lj}C_{lk} \\ &= \frac{i\Delta t}{\hbar}(C_{jk}-C_{jk})+\frac{(\Delta t)^2}{\hbar^2}\delta_{j,k} \\ &= 0 \quad , \end{aligned}$$

and the same is true for the columns. In this new basis we get

$$|k'\rangle = |k\rangle - \frac{i\Delta t}{\hbar}\sum_j C_{jk}|j\rangle$$

and

$$\begin{aligned} |k'\rangle|k'\rangle &= (|k\rangle - \frac{i\Delta t}{\hbar}\sum_j C_{jk}|j\rangle)(|k\rangle - \frac{i\Delta t}{\hbar}\sum_l C_{lk}|l\rangle) \\ &= |k\rangle|k\rangle - \frac{i\Delta t}{\hbar}(\sum_j C_{jk}|j\rangle|k\rangle + \sum_l C_{lk}|k\rangle|l\rangle) - \\ &\quad \frac{(\Delta t)^2}{\hbar^2}\sum_{j,l} C_{jk}C_{lk}|j\rangle|l\rangle \\ &= |k\rangle|k\rangle - \frac{i\Delta t}{\hbar}\sum_j C_{jk}(|j\rangle|k\rangle + |k\rangle|j\rangle) - \frac{(\Delta t)^2}{\hbar^2}\sum_{j,l} C_{jk}C_{lk}|j\rangle|l\rangle \\ &\approx |k\rangle|k\rangle - \frac{i\Delta t}{\hbar}\sum_j C_{jk}(|j\rangle|k\rangle + |k\rangle|j\rangle) \quad . \end{aligned}$$

So in this new basis the above longer calculation can be continued:

$$\begin{aligned} |\psi(\Delta t)\rangle &= \sum_k \lambda_k(|k\rangle|k\rangle - \frac{i\Delta t}{\hbar}\sum_j C_{jk}(|j\rangle|k\rangle + |k\rangle|j\rangle)) \\ &= \sum_k \lambda_k|k'\rangle|k'\rangle \end{aligned}$$

and we conclude that the Schmidt coefficients indeed stay the same. This ends the proof.

4.3.3 Mixed states of two bosons

In this subsection we want to derive how our measure is applied to systems of many indistinguishable bosons. We will show how our two-particle density matrix is obtained. This two-particle density matrix will allow us to study the quantum correlations between two indistinguishable bosons in a bulk of many indistinguishable bosons by means of the concurrence and the negativity. Here we will derive a representation of our two-particle density matrix in terms of expectation values of the two-particle correlation function. This will simplify the calculation of our two-particle density matrix in systems of many indistinguishable bosons a lot. Additionally we will prove then how the concurrence is evaluated in the Fock picture and that the negativity has to be computed in the particle picture.

Two-particle density matrix
The two-particle density matrix is obtained by generalizing (4.1), i.e. by detecting all but two bosons:

$$\begin{aligned} \rho_2 &:= \frac{1}{N(N-1)\cdot\ldots\cdot 3}\sum_{j_3=1}^{L}\hat{a}_{j_3}\Big(\sum_{j_4=1}^{L}\hat{a}_{j_4}\Big(\ldots\Big(\sum_{j_N=1}^{L}\hat{a}_{j_N}\rho_N\hat{a}_{j_N}^\dagger\Big)\ldots\Big)\hat{a}_{j_4}^\dagger\Big)\hat{a}_{j_3}^\dagger \\ &= \frac{1}{N(N-1)\cdot\ldots\cdot 3}\sum_{j_3,j_4,\ldots,j_N=1}^{L}\hat{a}_{j_3}\hat{a}_{j_4}\ldots\hat{a}_{j_N}\rho_N\hat{a}_{j_N}^\dagger\ldots\hat{a}_{j_4}^\dagger\hat{a}_{j_3}^\dagger \quad , \end{aligned} \tag{4.3}$$

where L is the dimension of the single-particle Hilbert space, in the Fock picture or, equivalently, by tracing out all but two indices in the particle picture. Hence it can be seen as a mixture of all possible two-boson states that are in ρ_N. The prefactor $\frac{1}{N(N-1)\cdot\ldots\cdot 3}$ assures that ρ_2 is a valid density matrix as we will now prove.

Proposition 1:

$$\mathrm{tr}(\rho_N) = 1 \qquad \Longrightarrow \qquad \mathrm{tr}(\rho_{N-k}) = 1 \quad \forall k < N$$

Proof of Proposition 1 by induction:
Assume we detect one boson:

$$\rho_{N-1} = \frac{1}{N}\sum_{j=1}^{L}\hat{a}_j\rho_N\hat{a}_j^\dagger \quad ,$$

then

$$\begin{aligned}\mathrm{tr}(\rho_{N-1}) &= \mathrm{tr}(\frac{1}{N}\sum_{j=1}^{L}\hat{a}_j\rho_N\hat{a}_j^\dagger) = \frac{1}{N}\sum_{j=1}^{L}\mathrm{tr}(\hat{a}_j\rho_N\hat{a}_j^\dagger)\\ &= \frac{1}{N}\sum_{j=1}^{L}\mathrm{tr}(\hat{a}_j^\dagger\hat{a}_j\rho_N) = \mathrm{tr}(\frac{1}{N}\sum_{j=1}^{L}\hat{n}_j\rho_N)\\ &= \mathrm{tr}(\rho_N) = 1 \qquad .\end{aligned}$$

In the induction step we assume the formula holds for ρ_{N-k}, i.e. $\mathrm{tr}(\rho_{N-k}) = 1$, and then show that it is also true for ρ_{N-k-1}:

$$\begin{aligned}\mathrm{tr}(\rho_{N-k-1}) &= \mathrm{tr}(\frac{1}{N-k}\sum_{j=1}^{L}\hat{a}_j\rho_{N-k}\hat{a}_j^\dagger)\\ &= 1 \qquad ,\end{aligned}$$

exactly like above. So our procedure of performing the partial trace yields correct density matrices.

Now we want to show that ρ_2 can be written in a way that simplifies its calculation.

Proposition 2:
ρ_2 can be rewritten as:

$$\rho_2 = \frac{2}{N(N-1)}\sum_{j_1+j_2+\ldots+j_L=N-2}\frac{\hat{a}_1^{j_1}}{\sqrt{j_1!}}\frac{\hat{a}_2^{j_2}}{\sqrt{j_2!}}\cdots\frac{\hat{a}_L^{j_L}}{\sqrt{j_L!}}\rho_N\frac{(\hat{a}_1^\dagger)^{j_1}}{\sqrt{j_1!}}\frac{(\hat{a}_2^\dagger)^{j_2}}{\sqrt{j_2!}}\cdots\frac{(\hat{a}_L^\dagger)^{j_L}}{\sqrt{j_L!}} \quad ,$$

where the sum runs over all L-tuple of $j_1, j_2, \ldots, j_L$ that fulfill $j_1+j_2+\ldots+j_L = N-2$.

Proof of Proposition 2:

$$\begin{aligned}\rho_2 &= \frac{1}{N(N-1)\cdot\ldots\cdot 3}\sum_{i_3,i_4,\ldots,i_N=1}^{L}\hat{a}_{i_3}\hat{a}_{i_4}\ldots\hat{a}_{i_N}\rho_N\hat{a}_{i_N}^\dagger\ldots\hat{a}_{i_4}^\dagger\hat{a}_{i_3}^\dagger\\
&= \frac{1}{N(N-1)\cdot\ldots\cdot 3}\sum_{j_1+j_2+\ldots+j_L=N-2}\binom{N-2}{j_1}\binom{N-2-j_1}{j_2}\cdots\\
&\quad\binom{N-2-j_1-j_2-\ldots-j_{L-1}}{j_L}\hat{a}_1^{j_1}\hat{a}_2^{j_2}\ldots\hat{a}_L^{j_L}\rho_N(\hat{a}_1^\dagger)^{j_1}(\hat{a}_2^\dagger)^{j_2}\ldots(\hat{a}_L^\dagger)^{j_L}\\
&= \frac{1}{N(N-1)\cdot\ldots\cdot 3}\sum_{j_1+j_2+\ldots+j_L=N-2}\frac{(N-2)(N-3)\ldots(N-2-j_1+1))}{j_1!}\\
&\quad\frac{(N-2-j_1)\ldots(N-2-j_1-j_2+1))}{j_2!}\cdots\\
&\quad\frac{(N-2-j_1-\ldots-j_{L-1})\ldots(N-2-j_1-\ldots-j_{L-1}-j_L+1))}{j_L!}\\
&\quad\hat{a}_1^{j_1}a_2^{j_2}\ldots\hat{a}_L^{j_L}\rho_N(\hat{a}_1^\dagger)^{j_1}(\hat{a}_2^\dagger)^{j_2}\ldots(\hat{a}_L^\dagger)^{j_L}\\
&= \frac{2}{N(N-1)}\sum_{j_1+j_2+\ldots+j_L=N-2}\frac{\hat{a}_1^{j_1}}{\sqrt{j_1!}}\frac{\hat{a}_2^{j_2}}{\sqrt{j_2!}}\cdots\frac{\hat{a}_L^{j_L}}{\sqrt{j_L!}}\rho_N\frac{(\hat{a}_1^\dagger)^{j_1}}{\sqrt{j_1!}}\frac{(\hat{a}_2^\dagger)^{j_2}}{\sqrt{j_2!}}\cdots\frac{(\hat{a}_L^\dagger)^{j_L}}{\sqrt{j_L!}} \quad .\end{aligned}$$

It is important to keep in mind that each of the i_3, i_4, ..., i_N run from 1 to L while j_1, j_2, ..., j_L run over all L-tuple that fulfill $j_1 + j_2 + \ldots + j_L = N - 2$.

Proposition 3:
The matrix elements of ρ_2 can be expressed as expectation values of the two-particle correlation function:

$$\begin{aligned}
\langle\Omega|\frac{\hat{a}_j^2}{\sqrt{2}}\rho_2\frac{(\hat{a}_k^\dagger)^2}{\sqrt{2}}|\Omega\rangle &= \frac{1}{N(N-1)}\mathrm{tr}((\hat{a}_k^\dagger)^2\hat{a}_j^2\rho_N) \\
\langle\Omega|\frac{\hat{a}_j^2}{\sqrt{2}}\rho_2\hat{a}_l^\dagger\hat{a}_k^\dagger|\Omega\rangle &= \frac{\sqrt{2}}{N(N-1)}\mathrm{tr}(\hat{a}_l^\dagger\hat{a}_k^\dagger\hat{a}_j^2\rho_N) \\
\langle\Omega|\hat{a}_j\hat{a}_k\rho_2\frac{(\hat{a}_l^\dagger)^2}{\sqrt{2}}|\Omega\rangle &= \frac{\sqrt{2}}{N(N-1)}\mathrm{tr}((\hat{a}_l^\dagger)^2\hat{a}_k\hat{a}_j\rho_N) \\
\langle\Omega|\hat{a}_j\hat{a}_k\rho_2\hat{a}_m^\dagger\hat{a}_l^\dagger|\Omega\rangle &= \frac{2}{N(N-1)}\mathrm{tr}(\hat{a}_m^\dagger\hat{a}_l^\dagger\hat{a}_k\hat{a}_j\rho_N) \quad .
\end{aligned} \tag{4.4}$$

Proof of Proposition 3:

$$\begin{aligned}
\langle\Omega|\frac{\hat{a}_j^2}{\sqrt{2}}\rho_2\frac{(\hat{a}_k^\dagger)^2}{\sqrt{2}}|\Omega\rangle &= \langle\Omega|\frac{\hat{a}_j^2}{\sqrt{2}}\Big(\frac{2}{N(N-1)}\sum_{j_1+j_2+\ldots+j_L=N-2}\frac{\hat{a}_1^{j_1}}{\sqrt{j_1!}}\frac{\hat{a}_2^{j_2}}{\sqrt{j_2!}}\cdots \\
&\qquad \frac{\hat{a}_L^{j_L}}{\sqrt{j_L!}}\rho_N\frac{(\hat{a}_1^\dagger)^{j_1}}{\sqrt{j_1!}}\frac{(\hat{a}_2^\dagger)^{j_2}}{\sqrt{j_2!}}\cdots\frac{(\hat{a}_L^\dagger)^{j_L}}{\sqrt{j_L!}}\Big)\frac{(\hat{a}_k^\dagger)^2}{\sqrt{2}}|\Omega\rangle \\
&= \langle\Omega|\frac{1}{N(N-1)}\sum_{j_1+j_2+\ldots+j_L=N-2}\frac{\hat{a}_1^{j_1}}{\sqrt{j_1!}}\frac{\hat{a}_2^{j_2}}{\sqrt{j_2!}}\cdots \\
&\qquad \frac{\hat{a}_L^{j_L}}{\sqrt{j_L!}}\hat{a}_j^2\rho_N(\hat{a}_k^\dagger)^2\frac{(\hat{a}_1^\dagger)^{j_1}}{\sqrt{j_1!}}\frac{(\hat{a}_2^\dagger)^{j_2}}{\sqrt{j_2!}}\cdots\frac{(\hat{a}_L^\dagger)^{j_L}}{\sqrt{j_L!}}|\Omega\rangle \\
&= \frac{1}{N(N-1)}\sum_{j_1+j_2+\ldots+j_L=N-2}\langle\Omega|\frac{\hat{a}_1^{j_1}}{\sqrt{j_1!}}\frac{\hat{a}_2^{j_2}}{\sqrt{j_2!}}\cdots \\
&\qquad \frac{\hat{a}_L^{j_L}}{\sqrt{j_L!}}\hat{a}_j^2\rho_N(\hat{a}_k^\dagger)^2\frac{(\hat{a}_1^\dagger)^{j_1}}{\sqrt{j_1!}}\frac{(\hat{a}_2^\dagger)^{j_2}}{\sqrt{j_2!}}\cdots\frac{(\hat{a}_L^\dagger)^{j_L}}{\sqrt{j_L!}}|\Omega\rangle \\
&= \frac{1}{N(N-1)}\sum_x\langle x|\hat{a}_j^2\rho_N(\hat{a}_k^\dagger)^2|x\rangle \\
&= \frac{1}{N(N-1)}\mathrm{tr}(\hat{a}_j^2\rho_N(\hat{a}_k^\dagger)^2) \\
&= \frac{1}{N(N-1)}\mathrm{tr}((\hat{a}_k^\dagger)^2\hat{a}_j^2\rho_N) \quad .
\end{aligned}$$

The other three equalities above are derived along the same lines.

In practice, we will calculate our two-particle density matrix via the equations (4.4), because it is much easier to evaluate the expectation values of the two-particle correlation function than it is to compute our initial form of the two-particle correlation function (4.3) for a large number N of bosons.

Concurrence for quantum correlations

Let us now investigate convex roof constructions

$$\mathbf{E} \quad = \quad \inf\{\sum_j p_j E(|\psi_j\rangle) : \rho = \sum_j p_j |\psi_j\rangle\langle\psi_j|\}$$

from pure-state entanglement monotones E. It is well-known that the convex roof to the entropy of entanglement, namely the entanglement of formation, can be expressed algebraically for 2×2-dimensional systems in terms of the concurrence. We remark that this also seems to be true for the convex roof of single-copy entanglement because the Schmidt coefficients can be expressed as functions of the concurrence. This is explained in more detail in the above introduction to entanglement theory.

The concurrence results from a minimization procedure over all possible representations of the density matrix in terms of pure state ensembles. Thus we have to make sure that we do not leave the symmetric subspace of the total Hilbert space during this minimization. We start from

$$\rho \quad = \quad \sum_j p_j |\psi_j\rangle\langle\psi_j| \qquad ,$$

where the $|\psi_j\rangle$ are symmetrized wave functions. Now every other representation of ρ can be written in terms of new probabilities and wave functions

$$\sqrt{q_j}|\phi_j\rangle \quad = \quad \sum_k u_{jk}\sqrt{p_k}|\psi_k\rangle$$

where $U = (u_{jk})$ is unitary. Fortunately, the $|\phi_j\rangle$ are also symmetrized. We conclude that we can directly use the concurrence in the particle picture, and how this is done is explained in Section 4.1.3. Nevertheless we want to derive the concurrence in the Fock picture because it will turn out to be a simpler formula.

The concurrence is defined via the eigenvalues of $\rho\tilde{\rho}$ where

$$\tilde{\rho} \quad = \quad \sigma_y \otimes \sigma_y \rho^* \sigma_y \otimes \sigma_y \qquad .$$

In the case of bosons the total wave function is a symmetrized product of the one-particle wave functions, such that any state of two bosons in a two-dimensional Hilbert space can be written in the basis

$$\begin{aligned} |20\rangle_F &= |00\rangle_p \\ |11\rangle_F &= \frac{1}{\sqrt{2}}(|01\rangle_p + |10\rangle_p) \\ |02\rangle_F &= |11\rangle_p \end{aligned}$$

where the subscript F denotes a Fock state and the subscript p denotes a state written in the particle picture. During the construction of the concurrence one does not leave the symmetric subspace of the total Hilbert space:

$$\begin{aligned} \sigma_y \otimes \sigma_y |20\rangle_F &= -|02\rangle_F \\ \sigma_y \otimes \sigma_y |11\rangle_F &= |11\rangle_F \\ \sigma_y \otimes \sigma_y |02\rangle_F &= -|20\rangle_F \qquad . \end{aligned}$$

Hence if we write ρ in the complete orthonormal basis $|1\rangle := |00\rangle_p$, $|2\rangle := \frac{1}{\sqrt{2}}(|01\rangle_p + |10\rangle_p)$, $|3\rangle := |11\rangle_p$, $|4\rangle := \frac{1}{\sqrt{2}}(|01\rangle_p - |10\rangle_p)$ it will have all zeros in the last column and in the last row. The same will then be true for $\tilde{\rho}$ and for $\rho\tilde{\rho}$. So we can equally consider ρ in the Fock picture.

We conclude that the concurrence is better computed in the Fock picture. A general quantum state of two indistinguishable bosons in a two-dimensional single-particle Hilbert space reads

$$\rho = \begin{pmatrix} R_1 & C_1 & C_2 \\ C_1^* & R_2 & C_3 \\ C_2^* & C_3^* & R_3 \end{pmatrix} \quad ,$$

where the R_j are real and the C_j are complex. Then we get

$$\tilde{\rho} = \begin{pmatrix} R_3 & -C_3 & C_2 \\ -C_3^* & R_2 & -C_1 \\ C_2^* & -C_1^* & R_1 \end{pmatrix} \quad .$$

If the square roots of the eigenvalues of $\rho\tilde{\rho}$ sorted in decreasing order are called λ_1, λ_2 and λ_3, then the concurrence becomes

$$\mathcal{C}(\rho) \quad = \quad \max(0, \lambda_1 - \lambda_2 - \lambda_3) \quad .$$

The standard concurrence can only be applied to mixed bipartite states ρ of dimension 2×2. Only in this case it has an interpretation for entanglement by means of the entanglement of formation. With respect to the Bose-Hubbard model the applicability of the standard concurrence is therefore limited to systems of $L = 2$ wells. If we want to study quantum correlations in the Bose-Hubbard model with $L > 2$ wells, then the negativity is the standard approach. Let us emphasize again that a nonvanishing negativity is necessary and sufficient for entanglement only in systems of dimension 2×2 and 2×3. For higher-dimensional systems, e.g. the Bose-Hubbard model with $L > 2$ wells, a nonvanishing negativity is just sufficient for entanglement. All this is explained in detail in the above introduction to entanglement theory in Section 4.1.3.

Negativity for quantum correlations

To begin with we have to formulate and prove the PPT criterion for quantum states of two indistinguishable bosons. As we defined in (4.2) a mixed state of two indistinguishable bosons is separable iff there exists a decomposition

$$\rho \quad = \quad \sum_j p_j \rho^j \otimes \rho^j \quad .$$

Then the PPT criterion reads: A density operator ρ of dimension 2×2 describing two indistinguishable bosons is separable iff the partial transposition

$$\rho^{PT} \quad := \quad (T \otimes \mathbb{I})(\rho)$$

is positive. The proof of this PPT criterion is done in exactly the same way as in our introduction to entanglement theory, only that a separable state is now of the above form.

That the PPT criterion also holds for quantum states of two indistinguishable bosons implies that we can directly compute the negativity in the particle picture. Unfortunately it is not possible to calculate the negativity in the Fock picture, because one usually leaves the symmetric subspace of the total Hilbert space by applying the partial transposition. E.g. the quantum state ρ of two indistinguishable bosons in a two-dimensional single-particle Hilbert space written in the particle picture reads

$$\begin{aligned}
\rho &= R_1|00\rangle\langle 00| + \frac{C_1}{\sqrt{2}}|00\rangle(\langle 01| + \langle 10|) + C_2|00\rangle\langle 11| + \\
&\quad \frac{C_1^*}{\sqrt{2}}(|01\rangle + |10\rangle)\langle 00| + \frac{R_2}{2}(|01\rangle + |10\rangle)(\langle 01| + \langle 10|) + \\
&\quad \frac{C_3}{\sqrt{2}}(|01\rangle + |10\rangle)\langle 11| + C_2^*|11\rangle\langle 00| + \\
&\quad \frac{C_3^*}{\sqrt{2}}|11\rangle(\langle 01| + \langle 10|) + R_3|11\rangle\langle 11| \\
&= R_1|00\rangle\langle 00| + \frac{C_1}{\sqrt{2}}|00\rangle\langle 01| + \frac{C_1}{\sqrt{2}}|00\rangle\langle 10| + C_2|00\rangle\langle 11| + \\
&\quad \frac{C_1^*}{\sqrt{2}}|01\rangle\langle 00| + \frac{R_2}{2}|01\rangle\langle 01| + \frac{R_2}{2}|01\rangle\langle 10| + \frac{C_3}{\sqrt{2}}|01\rangle\langle 11| + \\
&\quad \frac{C_1^*}{\sqrt{2}}|10\rangle\langle 00| + \frac{R_2}{2}|10\rangle\langle 01| + \frac{R_2}{2}|10\rangle\langle 10| + \frac{C_3}{\sqrt{2}}|10\rangle\langle 11| + \\
&\quad C_2^*|11\rangle\langle 00| + \frac{C_3^*}{\sqrt{2}}|11\rangle\langle 01| + \frac{C_3^*}{\sqrt{2}}|11\rangle\langle 10| + R_3|11\rangle\langle 11| \quad ,
\end{aligned}$$

which is why the partial transposition of ρ,

$$\begin{aligned}
\rho^{PT} &= R_1|00\rangle\langle 00| + \frac{C_1^*}{\sqrt{2}}|00\rangle\langle 01| + \frac{C_1}{\sqrt{2}}|00\rangle\langle 10| + \frac{R_2}{2}|00\rangle\langle 11| + \\
&\quad \frac{C_1}{\sqrt{2}}|01\rangle\langle 00| + \frac{R_2}{2}|01\rangle\langle 01| + C_2|01\rangle\langle 10| + \frac{C_3}{\sqrt{2}}|01\rangle\langle 11| + \\
&\quad \frac{C_1^*}{\sqrt{2}}|10\rangle\langle 00| + C_2^*|10\rangle\langle 01| + \frac{R_2}{2}|10\rangle\langle 10| + \frac{C_3^*}{\sqrt{2}}|10\rangle\langle 11| + \\
&\quad \frac{R_2}{2}|11\rangle\langle 00| + \frac{C_3^*}{\sqrt{2}}|11\rangle\langle 01| + \frac{C_3}{\sqrt{2}}|11\rangle\langle 10| + R_3|11\rangle\langle 11| \quad ,
\end{aligned}$$

in general is not symmetric under exchange of the two particle labels.

So we always have to compute the negativity in the particle picture. It is then given by the sum over the absolute values of the negative eigenvalues λ_j^- of ρ^{PT}:

$$\mathcal{N}(\rho) = \sum_j |\lambda_j^-| \quad .$$

In the specific case discussed above, i.e. two bosons in a two-dimensional single-particle Hilbert space, a positive partial transposition is necessary and sufficient

for separability and we have to find the negative eigenvalues of

$$\rho^{PT} = \begin{pmatrix} R_1 & \frac{C_1^*}{\sqrt{2}} & \frac{C_1}{\sqrt{2}} & \frac{R_2}{2} \\ \frac{C_1}{\sqrt{2}} & \frac{R_2}{2} & C_2 & \frac{C_3}{\sqrt{2}} \\ \frac{C_1^*}{\sqrt{2}} & C_2^* & \frac{R_2}{2} & \frac{C_3^*}{\sqrt{2}} \\ \frac{R_2}{2} & \frac{C_3^*}{\sqrt{2}} & \frac{C_3}{\sqrt{2}} & R_3 \end{pmatrix}$$

for the evaluation of the negativity.

Finally, we want to check numerically if our derived two-particle density matrix, concurrence and negativity for quantum correlations behave as expected with respect to our definiton of entanglement in systems of indistinguishable bosons. More precisely, we would expect concurrence and negativity of the two-particle density matrix to be invariant under noninteracting Hamiltonian evolution and to be changing in time if two-particle interaction is included.

We choose five bosons in a two-dimensional single-particle Hilbert space. Our noninteracting Hamiltonian shall have the random form

$$\hat{H}_1 = \begin{pmatrix} 1.0 & 1.3 + 1.8I \\ 1.3 - 1.8I & 1.5 \end{pmatrix} \quad ,$$

where H_1^{ij} is the coefficient to $\hat{a}_i^\dagger \hat{a}_j$. We propagate an arbitrary initial state

$$\begin{aligned} |\psi(0)\rangle &= (0.25 + 0.25I)|50\rangle_F + 0.5|41\rangle_F + (0.5 + 0.25I)|32\rangle_F + 0.25|23\rangle_F \\ &\quad +0.5|14\rangle_F \end{aligned}$$

with $\hat{H}_1$. The left part of Figure 4.4 depicts concurrence and negativity for the two-particle reduced density matrix and we conclude that they are indeed constant over time.

Again we include two-particle interaction by looking at a realistic system, namely the periodic Bose-Hubbard Hamiltonian with $L = 2$ wells and $N = 5$ bosons:

$$\hat{H} = -J \sum_{l=1}^{2} (\hat{a}_{l+1}^\dagger \hat{a}_l + \hat{a}_l^\dagger \hat{a}_{l+1}) + \frac{U}{2} \sum_{l=1}^{2} \hat{n}_l (\hat{n}_l - 1)$$

We choose an initally separable state

$$|\psi(0)\rangle = |00000\rangle$$

such that both concurrence and negativity should be zero at the beginning. We propagate $|\psi(0)\rangle$ with the above periodic Bose-Hubbard Hamiltonian with $J = 1$ and $U = 1$ and look at concurrence and negativity of the two-particle reduced density matrix in the right part of Figure 4.4. Both concurrence and negativity are zero at the beginning, but they change with time due to the two-particle interaction, just as it is the case with the Schmidt-coefficients in Figure

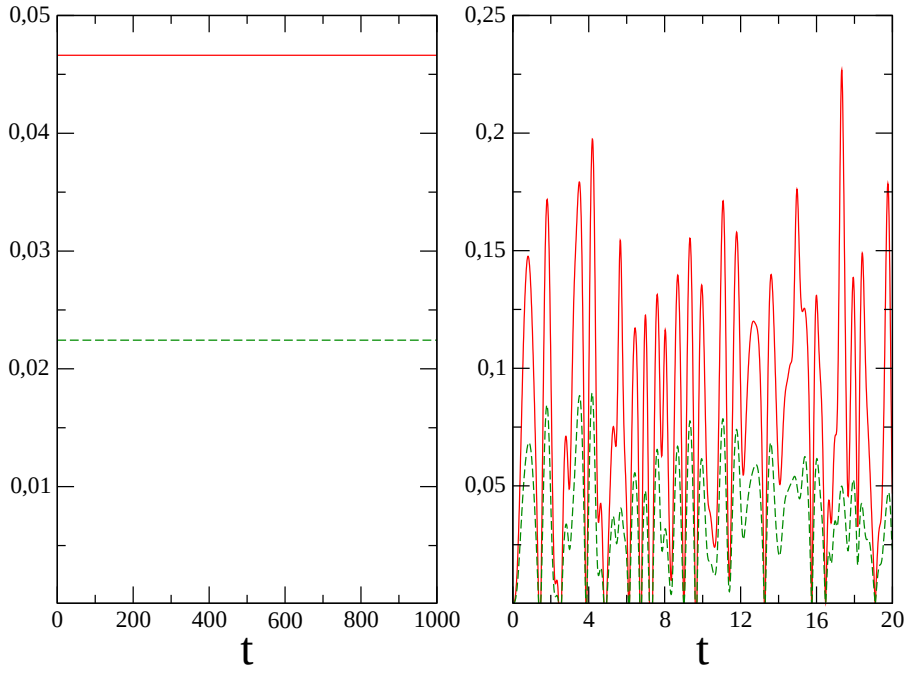

Figure 4.4: Concurrence $C(t)$ (red, thin line) and Negativity $N(t)$ (green, thin dashed line) of the two-particle density matrix obtained from an arbitrary initial state of 5 bosons in a 2-dimensional single-particle Hilbert space under arbitrary noninteracting Hamiltonian evolution (left) and obtained from an intially separable state of 5 bosons propagating with the periodic Bose-Hubbard Hamiltonian with $L = 2$ wells and $J = 1$ and $U = 1$ (right). We conclude that concurrence and negativity of our two-particle density matrix are invariant under noninteracting Hamiltonian evolution and they change in time if two-particle interaction is included.

4.3. We note that in Figure 4.4 the concurrence turns out to be twice as big as the negativity. We showed in Section 4.1.3 that this is always the case for pure states. It is completely unexpected for our two-particle reduced density matrix and needs further investigation.

4.3.4 Quantum correlations in the Bose-Hubbard model

We are now in a position to apply our formalism to the Bose-Hubbard model. In this subsection we are interested in the quantum correlations of the ground state as well as of the thermal state. In Chapter 5 we will use our measure to analyze chaotic entanglement in the Bose-Hubbard model.

Ground state

We choose periodic boundary conditions for the investigation of the ground state. Particularly interesting are systems of integer filling because they exhibit a quantum phase transition between a superfluid and a Mott insulating phase [10]. In fact, the critical point of the quantum phase transition in the

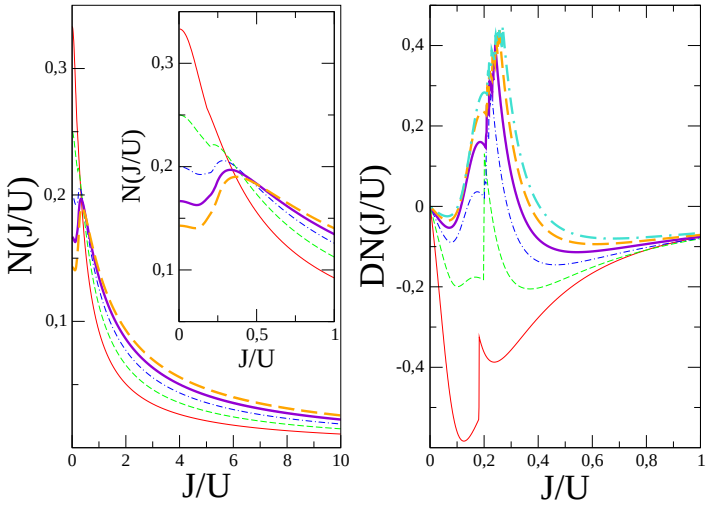

Figure 4.5: Negativity $N(J/U)$ (left) and first derivative of the negativity $DN(J/U)$ (right) for the two-particle density matrix obtained from the ground state of the periodic Bose-Hubbard Hamiltonian with $L = 3 = N$ (red, thin line), $L = 4 = N$ (green, thin dashed line), $L = 5 = N$ (blue, thin dash dotted line), $L = 6 = N$ (violet, thick line), $L = 7 = N$ (orange, thick dashed line) and $L = 8 = N$ (turquoise, thick dash dotted line). The maxima of both the negativity and the first derivative of the negativity of our two-particle density matrix wander to the quantum critical point at $(J/U)_{crit.} = 0.26$ with growing system size.

periodic Bose-Hubbard Hamiltonian with unit filling, i.e. $\frac{N}{L} = 1$, is located at $(\frac{J}{U})_{crit.} = 0.257$ [28].

In the left part of Figure 4.5 we plot the negativity of the two-particle reduced density matrix as a function of $\frac{J}{U}$. For a small system, i.e. $L = 3 = N$, we see the expected behaviour because the negativity strictly monotonously declines if the ratio $\frac{J}{U}$ grows. This is expected because quantum correlations should be large if the two-particle interaction U is large, since quantum correlations originate from the interaction of particles. As the system size grows the negativity gets a maximum in the region $\frac{J}{U} = 0.0$ to $\frac{J}{U} = 0.4$ due to the quantum critical point.

In the right part of Figure 4.5 we show the first derivative of the negativity. The results are obtained with an Arnoldi algorithm [103]. All investigated systems show discontinuities in the region of the quantum critical point. If one identifies maximal change in the negativity with the quantum critical point one can pinpoint the quantum critical point to $(\frac{J}{U})_{crit.} = 0.26 \pm 0.02$ by looking at the maximum of the curve to $L = 8 = N$. This is remarkable because we can read off the quantum critical point almost without making use of finite size scaling. However, we have to emphasize that there are small fluctuations in the maxima that we can not explain at the moment. Further investigation is needed, in particular by means of finite-size scaling.

We want to compare the ability of our quantum correlations to pinpoint the quantum critical point with standard mode entanglement. For this we obtain the

reduced two-mode density matrix of two neighbouring modes from the ground state of the periodic Bose-Hubbard Hamiltonian and calculate its negativity.

Figure 4.6 shows the negativity and the first derivative of the negativity for Wannier modes around the quantum critical point. At $\frac{J}{U} = 0$ Wannier mode entanglement vanishes because there the ground state is a single separable Wannier Fock state. $\frac{J}{U} = 1$ corresponds to the chaotic regime and since there the ground state is a superposition of many Wannier Fock states it is not surprising that also Wannier mode entanglement is high at $\frac{J}{U} = 1$. In-between $\frac{J}{U} = 0$ and $\frac{J}{U} = 1$ the quantum phase transition causes a maximum of the negativity. However, the maxima of the negativity and the minima of the first derivative of the negativity for Wannier modes wander away from the quantum critical point at $(J/U)_{crit.} = 0.26$ with growing system size.

The situation is completely different with Bloch modes as one can see in Figure 4.7. Bloch mode entanglement decays very fast as a function of $\frac{J}{U}$. Indeed, the inset reveals that it decays exponentially. This is surprising because if one takes a look at Figure 3.18 one would expect that due to the large number of avoided crossings in the region between $\frac{J}{U} = 0$ and $\frac{J}{U} = 1$ the ground state is a superposition of many Bloch Fock states. Nevertheless Figure 4.7 reveals that Bloch mode entanglement in the ground state vanishes very fast. Moreover, with growing system size Bloch mode entanglement vanishes completely which is why we conclude that it does not allow to locate the quantum critical point.

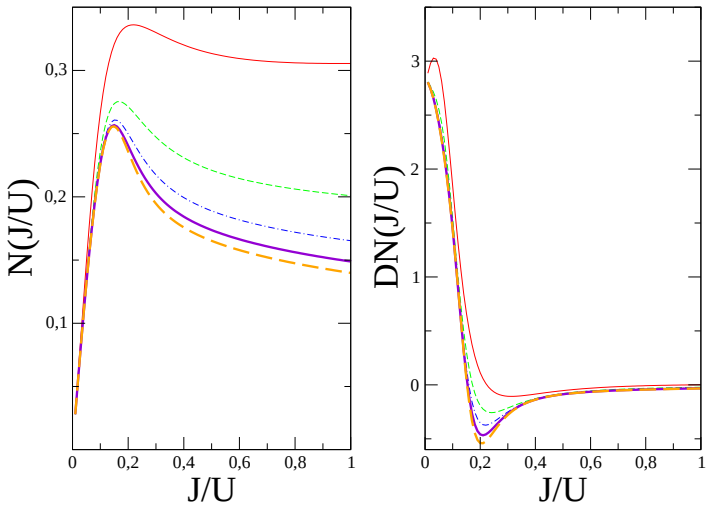

Figure 4.6: Negativity $N(J/U)$ (left) and first derivative of the negativity $DN(J/U)$ (right) for the reduced two-mode density matrix of two neighbouring Wannier modes obtained from the ground state of the periodic Bose-Hubbard Hamiltonian with $L = 3 = N$ (red, thin line), $L = 4 = N$ (green, thin dashed line), $L = 5 = N$ (blue, thin dash dotted line), $L = 6 = N$ (violet, thick line), $L = 7 = N$ (orange, thick dashed line). The maxima of the negativity and the minima of the first derivative of the negativity (of the two-mode density matrix of two neighbouring Wannier modes) wander away from the quantum critical point at $(J/U)_{crit.} = 0.26$ with growing system size.

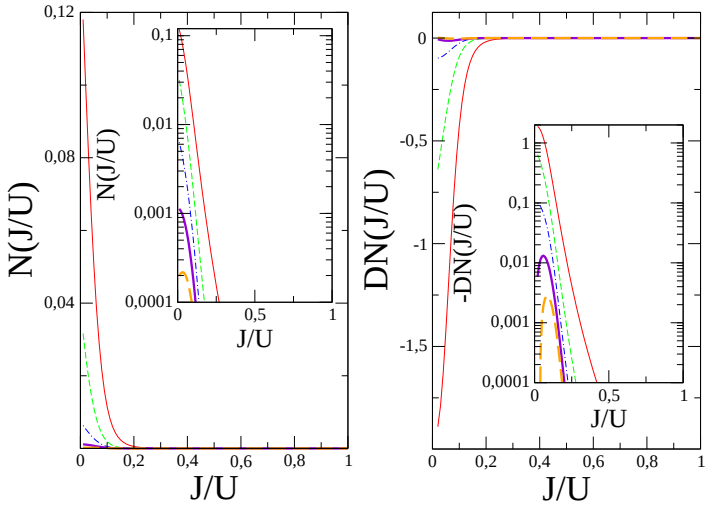

Figure 4.7: Negativity $N(J/U)$ (left) and first derivative of the negativity $DN(J/U)$ (right) for the reduced two-mode density matrix of two neighbouring Bloch modes obtained from the ground state of the periodic Bose-Hubbard Hamiltonian with $L = 3 = N$ (red, thin line), $L = 4 = N$ (green, thin dashed line), $L = 5 = N$ (blue, thin dash dotted line), $L = 6 = N$ (violet, thick line), $L = 7 = N$ (orange, thick dashed line). Neither the negativity nor the first derivative of the negativity (of the two-mode density matrix of two neighbouring Bloch modes) allow to locate the quantum critcal point because both vanish with growing system size.

Thermal state

We choose hard wall boundary conditions (in solid-state physics often called open boundary conditions, c.f. Section 2.1.2) for the investigation of the thermal state, because we want to look at experimentally interesting systems of many bosons in just a few wells and we believe that periodic boundary conditions do not make sense for a small number of wells. The thermal state that we want to consider is the equilibrium state of the canonical ensemble

$$\rho(T) = \frac{e^{-\beta \hat{H}}}{Z}$$

where $\beta = \frac{1}{k_B T}$ and

$$Z = \mathrm{tr}(e^{-\beta \hat{H}})$$

is the partition function. We put $k_B = 1$ and express the termal state in the eigenbasis to the Hamilonian, such that we get

$$\rho(T) = \frac{1}{Z} \sum_j e^{-\frac{E_j}{T}} |\psi_j\rangle\langle\psi_j|$$

and

$$Z = \sum_j e^{-\frac{E_j}{T}}$$

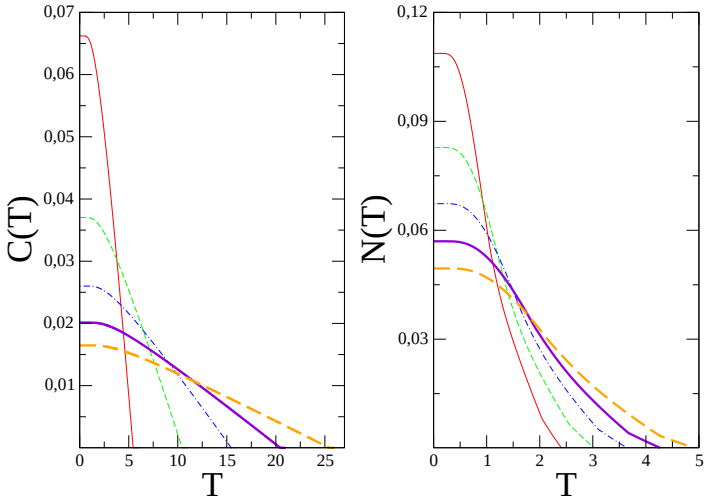

Figure 4.8: Concurrence $C(T)$ (left) and negativity $N(T)$ (right) for the two-particle density matrix obtained from the thermal state of the hard wall Bose-Hubbard Hamiltonian with $L = 2$ wells and $N = 10$ bosons (left) and $L = 3$ wells and $N = 4$ bosons (right) (red, thin line), $L = 2$ wells and $N = 20$ bosons (left) and $L = 3$ wells and $N = 6$ bosons (right) (green, thin dashed line), $L = 2$ wells and $N = 30$ bosons (left) and $L = 3$ wells and $N = 8$ bosons (right) (blue, thin dash dotted line), $L = 2$ wells and $N = 40$ bosons (left) and $L = 3$ wells and $N = 10$ bosons (right) (violet, thick line), $L = 2$ wells and $N = 50$ bosons (left) and $L = 3$ wells and $N = 12$ bosons (right) (orange, thick dashed line). It is remarkable that the concurrence for a system of $L = 2$ wells and the negativity for a system of $L = 3$ wells qualitatively behave the same.

in terms of the eigenvalues E_j and corresponding eigenfunctions $|\psi_j\rangle$ of $\hat{H}$. We remark that the thermal state is a mixed state.

First we are looking at the concurrence of the two-particle density matrix obtained from the thermal state of $L = 2$ wells being filled with different numbers of bosons. This is shown in the left part of Figure 4.8. We conclude that the ground state quantum correlations for $T = 0$ are already reached at a critical temperature $T^{(1)}_{crit.} > 0$ and this critical temperature gets bigger with growing boson number. Additionally quantum correlations vanish after a second critical temperature $T^{(2)}_{crit.} > 0$ and this critical temperature also gets bigger with growing boson number. Increasing the boson number hence saves the quantum correlations from thermal reduction. Nevertheless the ground state quantum correlations for $T = 0$ are highest for the smallest number of bosons which we would expect because then the system is more quantum. The right part of Figure 4.8 shows the negativity of the two-particle density matrix obtained from the thermal state of $L = 3$ wells being filled with different numbers of bosons. We can draw the same conclusions from this setting.

If one fixes the temperature and analyzes quantum correlations in the thermal state as a function of $\frac{J}{U}$ than one would expect that they monotonously decrease. For $L = 2$ wells and using the concurrence we obtained exactly that

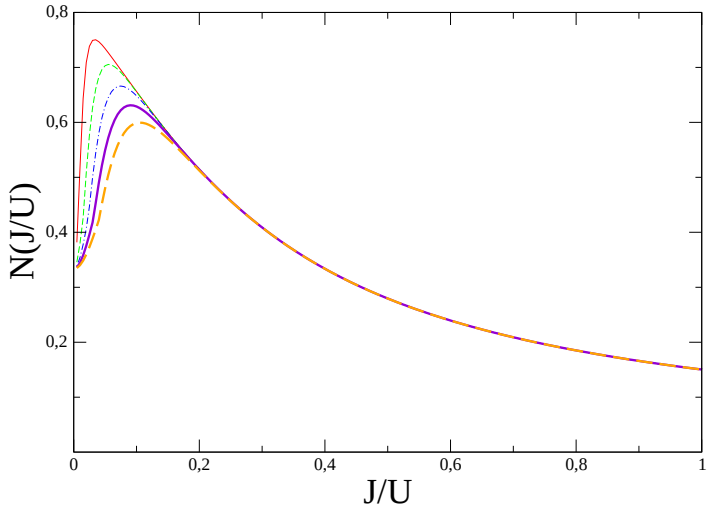

Figure 4.9: Negativity $N(J/U)$ (right) of the thermal state of the hard wall Bose-Hubbard Hamiltonian with $L = 3$ wells and $N = 2$ bosons at temperature $T = 0.01$ (red, thin line), $T = 0.02$ (green, thin dashed line), $T = 0.03$ (blue, thin dash dotted line), $T = 0.04$ (violet, thick line) and $T = 0.05$ (orange, thick dashed line). At the moment we are unable to tell if the observed maxima have any physical meaning because the negativity strictly speaking does only allow to detect but not to quantify entanglement.

behaviour of the quantum correlations. But for $L = 3$ wells and using the negativity we discovered that the negativity can have a maximum in systems of very few bosons and at low temperatures $T < 0.1$. This is shown in Figure 4.9. However it is hard to tell if this maximum has a physical meaning because the negativity does not allow to quantify entanglement in a strict sense. As explained in Section 4.1.3 the negativity just allows to detect entanglement.

Let us finally recapitulate what we have achieved in this section. We have derived a measure for quantum correlations between indistinguishable bosons that can *quantify* entanglement between two indistinguishable bosons in systems of arbitrarily many bosons. This quantification is done by calculating a reduced two-particle density matrix, which has the interpretation of detecting all but two bosons, and then applying concurrence or negativity to the resulting mixed state of two bosons. In the last part we tested this formalism in the Bose-Hubbard model and the results confirm the correctness of our approach. Moreover, they suggest that our measure of quantum correlations between indistinguishable bosons might be better suited to locate the quantum critical point than the commonly used measure of mode entanglement.

4.4 Generation of practical entanglement

In this last section we want to present a novel scheme for the generation of practical entanglement in the Bose-Hubbard model. As we have already explained in the introduction to this chapter, practical entanglement is the standard en-

tanglement [25] that may exist between distinguishable particles in the form of nonlocal correlations. Practical entanglement is the standard entanglement that is understood as a resource which may be used to overcome the restrictions of locality. Standard entanglement theory and hence the properties of practical entanglement are thoroughly discussed in the above introduction to entanglement theory. In particular, practical entanglement is necessary for superdense coding and quantum teleportation. There have been many approaches to the generation of entanglement in the Bose-Hubbard model [13, 14, 15, 16], but most of them do not consider practical entanglement, such that it remains unclear how the generated entanglement can be used practically, e.g. for quantum teleportation.

4.4.1 Practical entanglement in the Bose-Hubbard model

As argued in the introduction to this chapter practical entanglement in the Bose-Hubbard model is realized in Wannier modes. Only the Wannier Fock states render possible a spatial separation into two quantum systems which are then distinguishable and may have nonlocal correlations. The smallest possible practically entangled quantum state in the Bose-Hubbard model is

$$|\psi\rangle \quad = \quad \frac{1}{\sqrt{2}}(|1010\rangle_W + |0101\rangle_W) \qquad ,$$

where the subscript W denotes Wannier Fock states, because we can separate the left double well from the right double well and obtain two distinguishable quantum systems by raising the barrier between these two double wells. The two double wells are two distinguishable qubits and a sufficiently big distance between these qubits is modelled by a sufficiently high barrier. The practical entanglement between the two double wells can directly be used for superdense coding or quantum teleportation. In the following we will always consider Wannier Fock states and therefore drop the subscript W. Moreover we will refer to the left double well as system A, i.e. Alice, and to the right double well as system B, i.e. Bob.

Quantum states arising in studies of the Bose-Hubbard Hamiltonian are mostly superpositions of many different Wannier Fock states and so we have to define what practical entanglement is in general. E.g. the state

$$|\psi\rangle \quad = \quad \frac{1}{\sqrt{3}}(|1020\rangle + |0102\rangle + |2010\rangle)$$

has a varying local particle number in each double well and at the moment it is not clear how practical entanglement is assigned to this state. It follows from decoherence theory that if we separate the two double wells by raising the intermediate barrier then $|\psi\rangle$ very quickly decoheres into a mixture

$$\rho \quad = \quad \frac{2}{3}|\psi_1\rangle\langle\psi_1| + \frac{1}{3}|\psi_2\rangle\langle\psi_2|$$

of two states

$$|\psi_1\rangle \quad = \quad \frac{1}{\sqrt{2}}(|1020\rangle + |0102\rangle)$$

to local particle number $N = 1$ with respect to system A and

$$|\psi_2\rangle \quad = \quad |2010\rangle$$

to local particle number $N = 2$ with respect to system A. Of course we could have also done the discussion with the local particle number of system B since system A and B are on an equal footing. The point is that the initial state with varying local particle number and sufficiently separated double wells decoheres quickly into a mixture of states to fix local particle number. This implies that $|\psi\rangle$ effectively turns into the practically entangled state $|\psi_1\rangle$ with probability $p_1 = \frac{2}{3}$ and it becomes the practically separable state $|\psi_2\rangle$ with probability $p_2 = \frac{1}{3}$.

We now want to explain this decoherence to fix local particle number in system A and system B. It can be understood if one assumes that the environment reacts on a specific local particle number n by being in state $|n_E\rangle$ [102]. This state results from the interaction between the system and the environment. Let us think of the system state $|n_S\rangle$ as a quantum state of four wells, just like above, and let us think of the environment as the surrounding of this system which ideally shall be the vacuum. Without loss of generality our system shall be in a pure state and we order the superposition of Fock states to local particle number n into the state $|n_S\rangle$, then the total state of system and environment reads

$$|\psi_{SE}\rangle \quad = \quad \sum_n c_n |n_S\rangle |n_E\rangle \qquad ,$$

or equivalently

$$\begin{aligned} \rho_{SE} &= |\psi_{SE}\rangle\langle\psi_{SE}| \\ &= \sum_{m,n} c_m^* c_n |n_S\rangle |n_E\rangle\langle m_S|\langle m_E| \qquad . \end{aligned}$$

As explained in Section 4.1.1, in order to get the quantum state of our system we have to trace out the environment:

$$\rho_S \quad = \quad \mathrm{tr}_E(\rho_{SE}) \qquad .$$

If the two quantum systems, e.g. the two double wells, are sufficiently far apart from each other, then the $|n_E\rangle$ fulfill

$$\langle m_E | n_E \rangle \quad \approx \quad \delta_{m,n}$$

and we can use them to trace out the environment:

$$\begin{aligned} \rho_S &= \sum_j \langle j_E| (\sum_{m,n} c_m^* c_n |n_S\rangle |n_E\rangle\langle m_S|\langle m_E|) |j_E\rangle \\ &= \sum_{j,m,n} c_m^* c_n |n_S\rangle\langle m_S| \langle j_E|n_E\rangle\langle m_E|j_E\rangle \\ &\approx \sum_{j,m,n} c_m^* c_n |n_S\rangle\langle m_S| \cdot \delta_{j,n} \cdot \delta_{m,j} \\ &= \sum_n |c_n|^2 |n_S\rangle\langle n_S| \qquad . \end{aligned}$$

We conclude that our system state indeed decoheres into a mixture of states $|n_S\rangle$ to local particle number n.

In the derivation it is crucial that the two quantum systems having varying local particle numbers are sufficiently far apart from each other. Only then the corresponding states of the environment $|n_E\rangle$ to local particle number n are sufficiently orthogonal. The closer the two quantum systems get, the more the states of the environment coincide, i.e. $\langle n_E|m_E\rangle \approx 1$. Then, in a sense, the environment can not resolve the varying local particle number so well anymore by interacting with the system. This is the reason why the decoherence mainly affects the two double wells, that we spatially separate sufficiently, and not the two single wells of each double well which of course also have varying local particle numbers.

There also exist other arguments that the entanglement in quantum states of varying local particle number can not directly be accessed [73, 104, 74, 75, 105, 106, 107]. For our definition of practical entanglement we decide to measure the local particle number. By this we get a specific amount of practical entanglement to the state $|n_S\rangle$ with a specific probability p_n. We want to quantify the amount of practical entanglement by means of the entropy of entanglement

$$EoE(|\psi\rangle) \quad = \quad -\sum_j \lambda_j \log_2(\lambda_j)$$

where we choose the logarithm to the basis 2. The entropy of entanglement is extensively studied in Section 4.1.2 and in Appendix B. E.g. for the above state

$$|\psi\rangle \quad = \quad \frac{1}{\sqrt{3}}(|1020\rangle + |0102\rangle + |2010\rangle)$$

we get the practical entanglement of

$$|\psi_1\rangle \quad = \quad \frac{1}{\sqrt{2}}(|1020\rangle + |0102\rangle) \qquad ,$$

i.e.

$$EoE(|\psi_1\rangle) \quad = \quad 1 \qquad ,$$

with probability $p_1 = \frac{2}{3}$ and we receive the practical entanglement of

$$|\psi_2\rangle \quad = \quad |2010\rangle \qquad ,$$

i.e.

$$EoE(|\psi_2\rangle) \quad = \quad 0 \qquad ,$$

with probability $p_2 = \frac{1}{3}$.

We believe that our considerations of practical entanglement in small systems are better described by hard wall boundary conditions and so we study the hard wall Bose-Hubbard Hamiltonian in this section. More precisely, the spatial separation of two double wells is impossible if one thinks of the system being a ring, as one should for periodic boundary conditions. We explain that in Chapter 2.

4.4.2 Generation of practical entanglement

Let us now introduce our novel approach for the generation of practical entanglement in the Bose-Hubbard model. We emphasize that this method can be realized experimentally already. In fact, a group from Pisa has done this experiment, however without investigating entanglement properties [108]. The idea is to vary the lattice depth V_0 periodically in time:

$$V_0(t) = V\big(1 + \delta V \cos(\omega t)\big) \qquad .$$

We remark that the approach $V_0(t) = V\cos(\omega t))$ would violate the applicability of the one-band Bose-Hubbard model which necessitates a deep lattice to be a correct description.

So for a small modulation δV we can insert $V_0(t)$ into the equations (2.9) and (2.10) from the end of the first chapter. Before we do that we have to adapt these equations to our one-dimensional Bose-Hubbard model. Following [39] we introduce a strong transverse confining potential $V_\perp$ such that the bosons effectively have only one degree of freedom. In this case (2.9) and (2.10) read

$$\frac{J(t)}{E_R} = \frac{4}{\sqrt{\pi}}\Big(\frac{V(1+\delta V\cos(\omega t))}{E_R}\Big)^{\frac{3}{4}} \exp\Big(-2\sqrt{\frac{V(1+\delta V\cos(\omega t))}{E_R}}\Big)$$

and

$$\frac{U(t)}{E_R} = \sqrt{\frac{8}{\pi}} k a_s \Big(\frac{V(1+\delta V\cos(\omega t))V_\perp^2}{E_R^3}\Big)^{\frac{1}{4}} \qquad .$$

We adopt the setup of [39]:

$$\begin{aligned} V &= 15E_R \\ V_\perp &= 30E_R \\ \lambda &= 825\text{nm} \\ a_s &= 5.45\text{nm} \qquad . \end{aligned}$$

It turns out that the system absorbs energy only for specific values of ω. If $\hbar\omega = \frac{U}{2}$ two-photon absorption takes place and single-photon absorption happens if $\hbar\omega$ is an integer multiple of U [39].

We propagate the ground state of the hard wall Bose-Hubbard Hamiltonian with the above parameters. This propagation with a time-dependent Hamiltonian is implemented with a Fatunla algorithm [109]. It is slightly more efficient than our standard Runge-Kutta algorithm. In the left part of Figure 4.10 the energy absorption is shown for ω being out of resonance. Clearly the system does not absorb any significant amount of energy. In the right part of Figure 4.10 the energy absorption is shown for $\omega = U$ being in resonance. Obviously the system absorbs energy. It is noticeable that we observe the energy absorption with rather small systems. In contrast, in [39] they use a DMRG method to investigate the Bose-Hubbard Hamiltonian with $L = 32$ wells and $N = 32$ bosons.

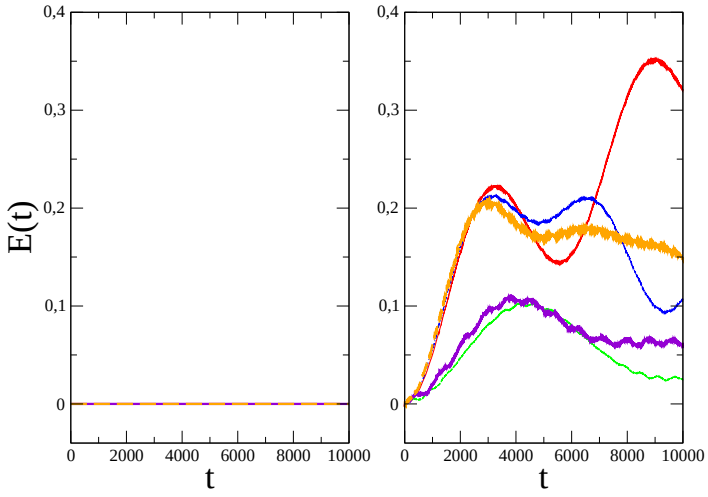

Figure 4.10: Energy absorption with ω out of resonance (left) and with $\omega = U$ in resonance (right) for the ground state of the hard wall Bose-Hubbard Hamiltonian with $L = 4 = N$ (red, thin line), $L = 5 = N$ (green, thin dashed line), $L = 6 = N$ (blue, thin dash dotted line), $L = 7 = N$ (violet, thick line) and $L = 8 = N$ (orange, thick dashed line); see Section 2.1.1 for the units of time. We conclude that energy is absorbed only in resonance. We remark that we can find the resonances with our rather small systems just as well as *Kollath et al.* in [39] where they use DMRG methods to investigate the Bose-Hubbard Hamiltonian with $L = 32$ wells and $N = 32$ bosons.

Remarkably it turns out that also only in these resonances of ω big amounts of practical entanglement arise. This surely is a manifestation of the close relationship between the resources energy and entanglement. The left part of Figure 4.11 depicts practical entanglement and probability for the ground state of the hard wall Bose-Hubbard Hamiltonian with $L = 4$ wells and $N = 2$ bosons. Obviously practical entanglement and probability oscillate but do not change significantly. This is different if we propagate the ground state in resonance for $\omega = U$, as can be seen in the right part of Figure 4.11. Now practical entanglement and probability change in time. We have to emphasize that we can not explain the period of the oscillation in Figure 4.11. We believe that this oscillation is connected to the driving frequency, but we have to further investigate that.

As we see in Figure 4.11 it is not possible to obtain the entanglement $EoE = 1$ of a Bell pair. So we are unable to generate the state

$$|\beta\rangle \quad = \quad \frac{1}{\sqrt{2}}(|1010\rangle + |0101\rangle) \qquad .$$

In fact, even by using other initial states we could not exceed the practical entanglement seen in Figure 4.11. We suspect that the system of $L = 4$ wells and $N = 2$ bosons has a natural limit in the amount of practical entanglement that can be generated from it, but this needs further investigation.

The situation is different if we consider $L = 4$ wells and $N = 4$ bosons. Here

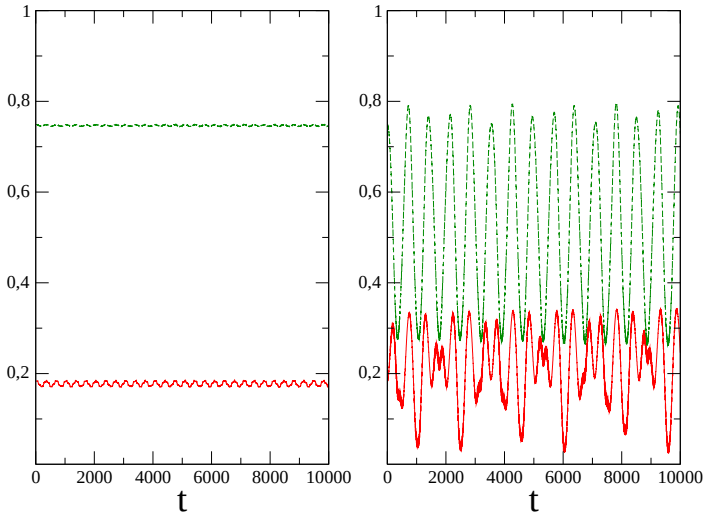

Figure 4.11: Practical entanglement quantified by the EoE to the basis 2 (red, thin line) and probability p (green, dashed line) for the propagation of the ground state of the hard wall Bose-Hubbard Hamiltonian with $L = 4$ wells and $N = 2$ bosons for ω out of resonance (left) and $\omega = U$ in resonance (right); see Section 2.1.1 for the units of time. While practical entanglement and probability do not change significantly if the system is driven out of resonance, both do change if the system is driven in resonance.

the maximally practically entangled state is

$$|\beta\rangle = \frac{1}{\sqrt{3}}(|2020\rangle + |1111\rangle + |0202\rangle)$$

with

$$\begin{aligned} EoE(|\beta\rangle) &= \log(3) \\ &\approx 1.58 \end{aligned}$$

and this amount of practical entanglement can indeed be generated as we show in Figure 4.12. Around $t = 2000$ and $t = 7000$ the generated practical entanglement gets arbitrarily close to the maximal amount of entanglement possible, which is $EoE \approx 1.58$ in this case.

Now the question is, of course, how we can access this practical entanglement around $t = 7000$. In our opinion a self-evident approach is given by stopping the periodic modulation of V_0 at the desired time t and simultaneously lowering the lattice depth V_0. By doing this the quantum state of time t should be saved. As we conclude from Figure 4.13 this indeed happens. The lowering of the lattice depth V_0 can be easily achieved experimentally by enhancing the power of the laser that creates the optical lattice. Also the separation of double wells can be easily done experimentally by imposing a second lattice [41]. Hence this complete scheme for the generation of practical entanglement in the Bose-Hubbard model can be realized experimentally.

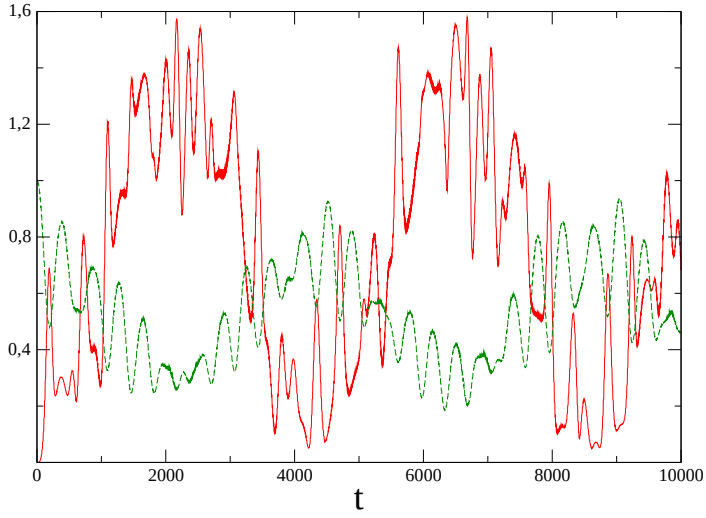

Figure 4.12: Practical entanglement quantified by the EoE to the basis 2 (red, thin line) and probability p (green, dashed line) for the propagation of the ground state of the hard wall Bose-Hubbard Hamiltonian with $L = 4$ wells and $N = 4$ bosons for $\omega = U$ in resonance. Remarkably around $t = 2000$ and around $t = 7000$ the generated practical entanglement is arbitrarily close to the maximally possible amount of entanglement $EoE \approx 1.58$.

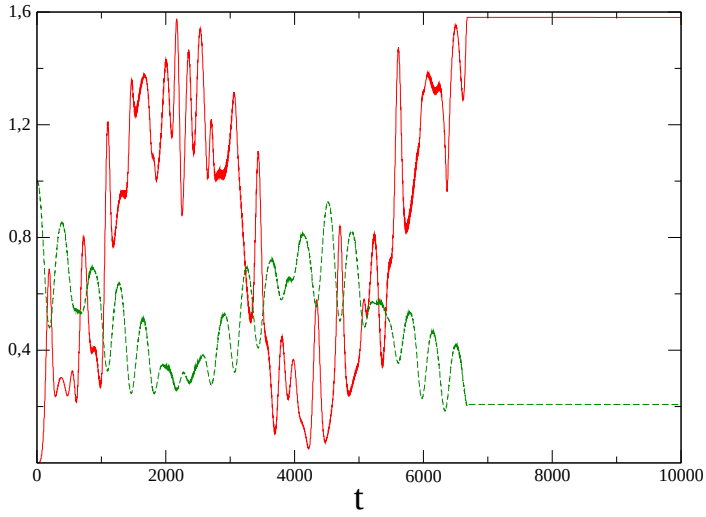

Figure 4.13: Practical entanglement quantified by the EoE to the basis 2 (red, thin line) and probability p (green, dashed line) for the propagation of the ground state of the hard wall Bose-Hubbard Hamiltonian with $L = 4$ wells and $N = 4$ bosons for $\omega = U$ in resonance, where we simultaneously stop the periodic modulation of V_0 and lower V_0 around $t = 7000$. We conclude that this scheme allows to save the generated maximally practically entangled state.

We just want to note here that we additionally implemented the setup where the next-neighbouring wells respectively moved up and down with the same frequency such that we had two lattices and two frequencies. Indeed, these two frequencies could be adjusted to produce bigger areas of constant maximal practical entanglement.

Let us briefly summarize the results obtained in this chapter. First we introduced the notion of practical entanglement as the standard kind of entanglement that can be used for quantum teleportation and superdense coding. We showed that this practical entanglement is given in the Bose-Hubbard model by Wannier mode entanglement between double wells where the local particle number is measured and hence fix. Finally we presented a novel experimentally realizable scheme that allows to generate practical entanglement in the Bose-Hubbard model. With this scheme we generated and stored the entanglement $EoE \approx 1.58$ of a maximally entangled qutrit.

Chapter 5

Chaotic entanglement in the Bose-Hubbard model

In this chapter we want to investigate in how far the methods of entanglement theory can be used to distinguish the regular and the chaotic regime of the Bose-Hubbard Hamiltonian. We propose to abbreviate entanglement arising in the chaotic regime by chaotic entanglement. While we located the regular and the chaotic regime of the Bose-Hubbard Hamiltonian by means of spectral and dynamic analysis in Chapter 3, we elaborated in how far entanglement theory can be reasonably applied to the Bose-Hubbard model in Chapter 4. Here we want to establish the link between these two chapters by studying the entanglement properties of the regular and the chaotic regime of the Bose-Hubbard Hamiltonian.

More precisely, we are interested in quantum correlations and mode entanglement, since these are the two major manifestations of entanglement in the Bose-Hubbard model. For quantum correlations between indistinguishable bosons we refer to our own approach developed in Section 4.3. For mode entanglement we refer to the work of *Schuch et al.* [75]. As already explained in the introduction to Chapter 4, *Schuch et al.* proved that asymptotic mode entanglement in systems of constant global particle number is completely described by two quantities, namely the entropy of entanglement and the superselection induced variance

$$SiV(|\psi\rangle) \quad = \quad 4(\langle\psi|\hat{N}_A^2|\psi\rangle - \langle\psi|\hat{N}_A|\psi\rangle^2) \qquad .$$

As discussed in Chapter 2 Wannier and Bloch Fock states form a canonical basis of the Bose-Hubbard Hamiltonian respectively. Additionally the Wannier occupation numbers of the different sites and the Bloch occupation numbers of the different quasimomenta are directly accessible in an experiment. This is why we will focus on Wannier and Bloch mode entanglement.

In analogy to Chapter 3, where we assigned the regular and the chaotic regime by static and dynamic arguments, a complete characterization of the entanglement properties of the regular and the chaotic regime also has to be done via static as well as dynamic considerations. We define the static part to be given by the entanglement properties of the eigenstates and the dynamic

part to coincide with the entanglement properties of propagated states.

It was shown by *Venzl et al.* that the time evolution of generic initial states with the Bose-Hubbard Hamiltonian in the chaotic regime can not be computed reliably by means of time-dependent DMRG methods [110]. Time-dependent DMRG methods apply the Schmidt decomposition to all possible bipartitions of the evolving quantum state and then cut off the parts of the basis that correspond to the smallest Schmidt coefficients [111, 112]. By doing so the calculation is performed in an effective basis that can be substantially smaller than the initial basis of the total Hilbert space. However, *Venzl et al.* found out that during the propagation in the chaotic regime all Schmidt coefficients become approximately equal to each other such that neglecting parts of the basis can lead to a considerable error in the calculation. Hence time-dependent DMRG methods can only badly simulate dynamics of the Bose-Hubbard model in the chaotic regime. On the other hand all Schmidt coefficients being equal to each other implies high entropy of entanglement. So dynamic chaotic entanglement is expected to be characterized by a high degree of mode entanglement.

Remarkably *Kubotani et al.* discovered universality of the distribution of Schmidt coefficients in the dynamics of quantum chaotic systems [113]. This implies that dynamic chaotic mode entanglement has universal properties. We expect that such universal properties exist for static and dynamic chaotic entanglement in general.

In the first half of this chapter we will study the static entanglement properties of the eigenstates of the Bose-Hubbard Hamiltonian. In particular, we will be interested in the ground state and in the average entanglement properties of all eigenstates. In the second half of this chapter we will analyze the dynamic change of entanglement during propagation with the Bose-Hubbard Hamiltonian. Here we will look at the propagation of the Fock state with highest initial energy and we will average the change of entanglement over many propagated states. By considering quantum correlations, Wannier and Bloch entropy of entanglement and Wannier and Bloch superselection induced variance we will obtain a comprehensive picture of the entanglement properties of the Bose-Hubbard Hamiltonian in the regular and in the chaotic regime.

5.1 Entanglement properties of the eigenstates

In this section we want to study the static entanglement properties of the eigenstates of the Bose-Hubbard Hamiltonian. We will first inspect single eigenstates, namely the ground state and five selected excited states. Finally we will average over all eigenstates.

5.1.1 Single eigenstates

Let us begin with the entanglement properties of the ground state of the periodic Bose-Hubbard Hamiltonian with unit filling.

Figure 5.1 depicts our measure of quantum correlations QC, which is defined in Section 4.3, applied to the ground state of the periodic Bose-Hubbard Hamiltonian with unit filling and different system sizes. At $u = 0$, where $J = 1$

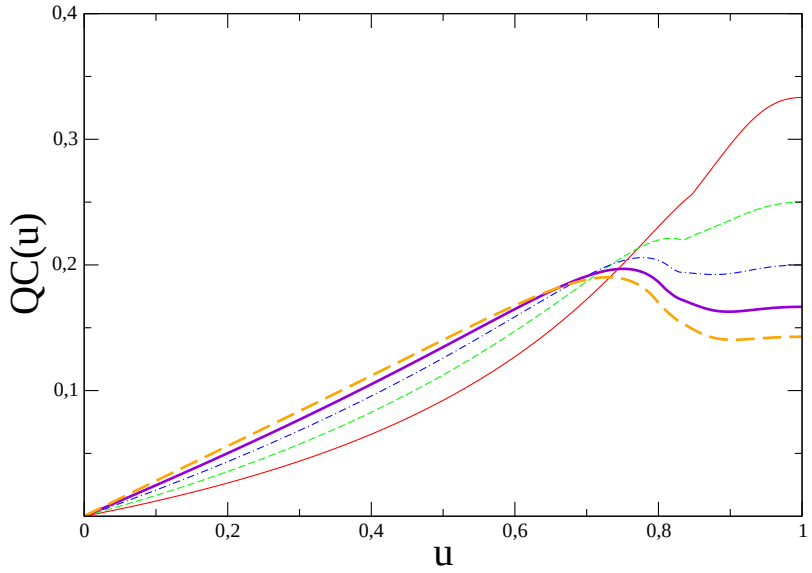

Figure 5.1: Quantum correlations $QC(u)$ applied to the ground state of the periodic Bose-Hubbard Hamiltonian with $L = 3 = N$ (red, thin line), $L = 4 = N$ (green, thin dashed line), $L = 5 = N$ (blue, thin dash dotted line), $L = 6 = N$ (violet, thick line) and $L = 7 = N$ (orange, thick dash dotted line).

and $U = 0$, our measure of quantum correlations is zero as expected because quantum correlations originate from the two-particle interaction given by U (c.f. Section 4.3). This is also the reason why QC is low for $U \ll J$ and high for $U \gg J$. The maxima of the curves are due to the quantum critical point at $u_{crit.} \approx 0.79$ and they get more pronounced with growing system size, which suggests a finite size scaling. We conclude that quantum correlations of the ground state are low in the regular regime of small u, they are high in the chaotic regime of intermediate u and they are high in the regular regime of large u.

We refer to Figure 3.5 and to Figure 3.18 from Chapter 3 for the location of the regular and the chaotic regime in the spectrum of the periodic Bose-Hubbard Hamiltonian with unit filling. While Figure 3.5 specifies the two regimes by spectral statistics, Figure 3.18 assigns the regular and the chaotic regime via the number of avoided crossings. As explained in Chapter 3 these avoided crossings are energy levels that come very close to each other but do not cross. In particular, an eigenstate corresponding to an energy level with an avoided crossing can change considerably at this avoided crossing. This will be important in the following because in the limits $u = 0$ and $u = 1$ the eigenstates are single Fock states. More precisely, for $u = 0$ the eigenstates are Bloch Fock states and for $u = 1$ the eigenstates are Wannier Fock states. But moving away from these integrable points $u = 0$ and $u = 1$ to $u \in (0, 1)$ avoided crossings cause the eigenstates to become superpositions of many Fock states. This can be also seen in Figure 3.3.

In Figure 5.2 we applied Wannier and Bloch mode entanglement, characterized by the entropy of entanglement EoE and the superselection induced

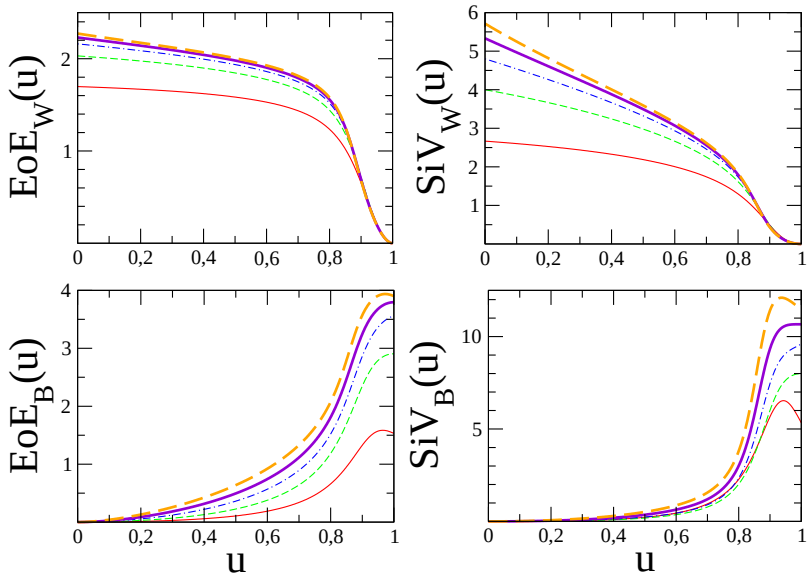

Figure 5.2: Wannier entropy of entanglement $EoE_W(u)$ and Wannier superselection induced variance $SiV_W(u)$ (upper half) and Bloch entropy of entanglement $EoE_B(u)$ and Bloch superselection induced variance $SiV_B(u)$ (lower half) between two neighbouring modes and the remaining modes applied to the setting of Figure 5.1 with the same colour code.

variance SiV, between two neighbouring modes and the remaining modes to the ground state of the periodic Bose-Hubbard Hamiltonian with unit filling and different system sizes. In the following we always summarize the two quantities entropy of entanglement EoE and superselection induced variance SiV in the notion mode entanglement. Often EoE and SiV imply the same conclusions and then we prefer to simply speak of mode entanglement, meaning both EoE and SiV.

In the regular regime of small u the ground state is expected to be a superposition of many Wannier Fock states and it is expected to be a superposition of few Bloch Fock states. This follows from Figure 3.3. We remark that Figure 3.3 shows an average over all eigenstates, but nevertheless one would expect the ground state to have the same properties. Hence it is not surprising that in the regular regime of small u Wannier mode entanglement is high and Bloch mode entanglement is low and it is the other way around in the regular regime of large u. In the chaotic regime of intermediate u both Wannier and Bloch mode entanglement are non-vanishing. We conclude that mode entanglement of the ground state can be low in the regular regime of small u and in the regular regime of high u depending on the chosen modes, but it is always high in the chaotic regime of intermediate u.

So we can identify the chaotic regime by a high degree of mode entanglement independent of the chosen modes. And we can identify the regular regime by the existence of a set of modes that has a low degree of mode entanglement. Moreover, since quantum correlations are also high in the chaotic regime it seems

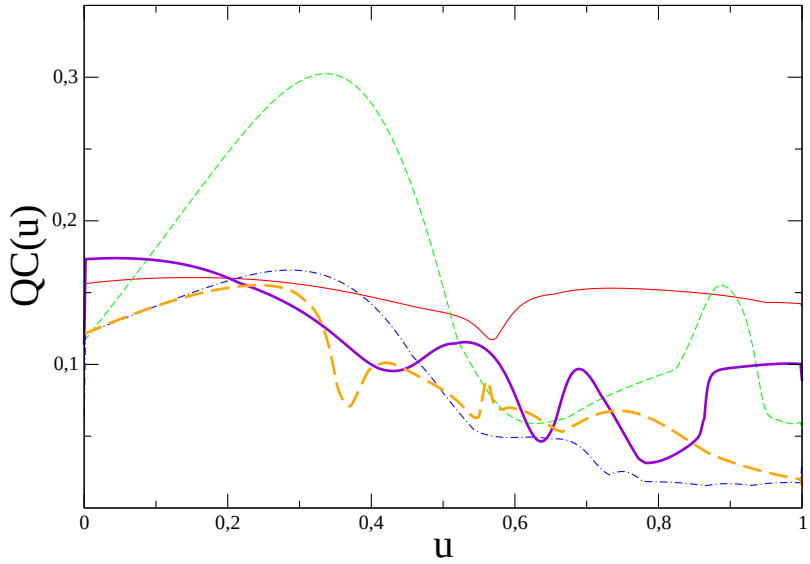

Figure 5.3: Quantum correlations $QC(u)$ applied to eigenstate 2 (red, thin line), eigenstate 7 (green, thin dashed line), eigenstate 12 (blue, thin dash dotted line), eigenstate 17 (violet, thick line) and eigenstate 22 (orange, thick dash dotted line) of the periodic Bose-Hubbard Hamiltonian with $L = 5 = N$ and quasimomentum $k = 1$.

as if any kind of entanglement is high in the chaotic regime. However, at the moment we are just talking about the entanglement properties of the ground state and it is interesting to see if the same holds for excited states. As five selected eigenstates we pick eigenstate 2, eigenstate 7, eigenstate 12, eigenstate 17 and eigenstate 22 of the periodic Bose-Hubbard Hamiltonian with $L = 5$ wells, $N = 5$ bosons and quasimomentum $k = 1$.

In Figure 5.3 we present our measure of quantum correlations applied to five eigenstates of the periodic Bose-Hubbard Hamiltonian with $L = 5 = N$ and quasimomentum $k = 1$. We can not make out any tendency of the quantum correlations of these five eigenstates, in contrast to quantum correlations of the ground state where we could find a clear tendency in Figure 5.1. The rapid changes of the curves are due to the presence of avoided crossings where the eigenstates can change considerably. We conclude that quantum correlations of eigenstates other than the ground state do not allow for a straightforward distinction between the regular and the chaotic regime. However, here we only consider the rather small system of $L = 5 = N$ and the situation might be different for larger systems. In fact, as can be seen in Figure 5.5, the average quantum correlations over all eigenstates show a clear tendency with growing system size.

Figure 5.4 is a plot of Wannier and Bloch mode entanglement between two neighbouring modes and the remaining modes applied to five eigenstates of the periodic Bose-Hubbard Hamiltonian with $L = 5 = N$ and quasimomentum $k = 1$. While Wannier entropy of entanglement EoE_W tends to get smaller with increasing u, Wannier superselection induced variance SiV_W does not show

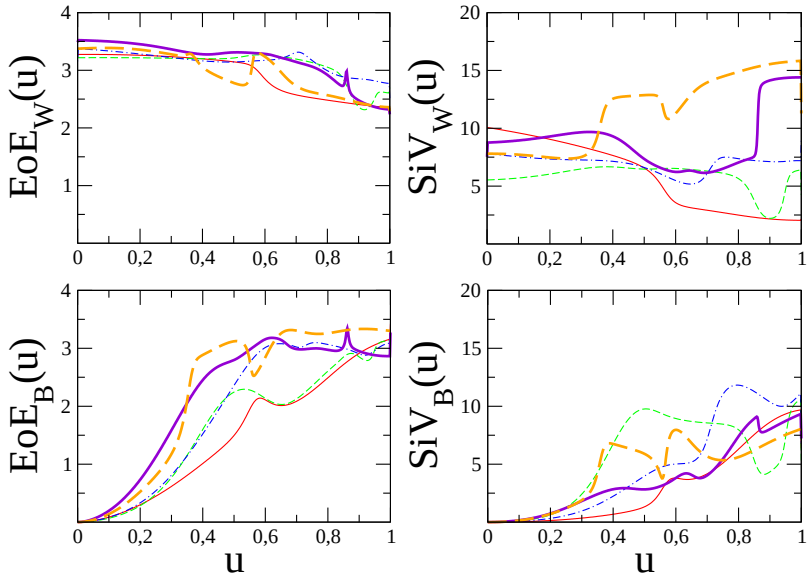

Figure 5.4: Wannier entropy of entanglement $EoE_W(u)$ and Wannier superselection induced variance $SiV_W(u)$ (upper half) and Bloch entropy of entanglement $EoE_B(u)$ and Bloch superselection induced variance $SiV_B(u)$ (lower half) between two neighbouring modes and the remaining modes applied to the setting of Figure 5.3.

a tendency. We remark that there is a discontinuous jump from $u = 1$ to $u < 1$ in EoE_W and SiV_W. As already discussed in the introduction to Chapter 2, this discontiuous jump is due to an immediate splitting up of degenerate energy levels if one goes from $u = 1$ to $u < 1$. Interestingly Bloch mode entanglement of these five eigenstates qualitatively has the same properties as Bloch mode entanglement of the ground state, i.e. it is zero at $u = 0$ and grows with increasing u. We believe that Bloch modes are exceptional because they already take the periodic boundary conditions of our Hamiltonian into account (c.f. Section 2.1.3). Let us note again that the rapid changes of the curves are due to the presence of avoided crossings where the eigenstates can change considerably.

We conclude that Wannier entropy of entanglement of eigenstates other than the ground state tends to get smaller with increasing u but does not vanish continuously in the limit $u = 1$. However, Wannier superselection induced variance of eigenstates other than the ground state does not show a clear tendency. We conclude that both Bloch entropy of entanglement and superselection induced variance of eigenstates other than the ground state tend to grow with increasing u but do not vanish continuously in the limit $u = 1$.

So also for eigenstates other than the ground state one can say that in the chaotic regime mode entanglement is high independent of the chosen modes. In the regular regime there exist modes such that mode entanglement is low, where low is meant compared to the chaotic regime. Quantum correlations did not show a clear tendency. However, we investigated a rather small system

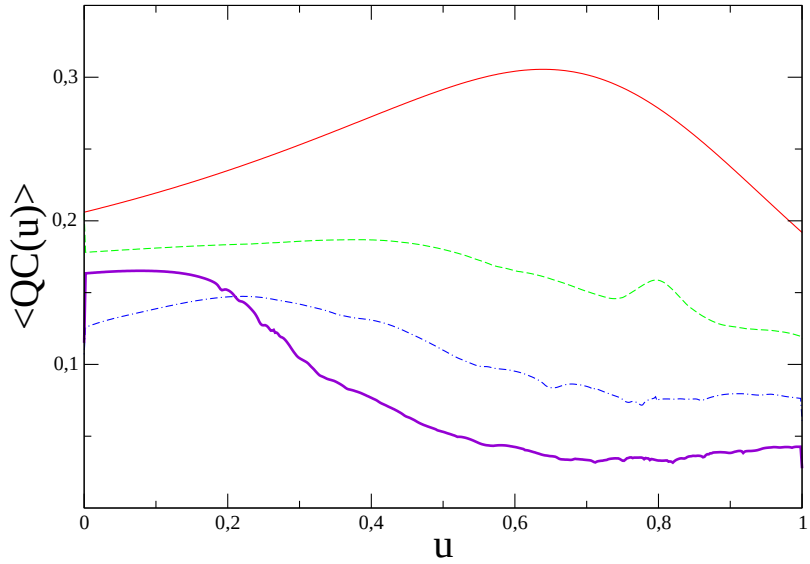

Figure 5.5: Average quantum correlations $\langle QC(u)\rangle$ of all eigenstates applied to the periodic Bose-Hubbard Hamiltonian with quasimomentum $k = 1$ and $L = 3 = N$ (red, thin line), $L = 4 = N$ (green, thin dashed line), $L = 5 = N$ (blue, thin dash dotted line) and $L = 6 = N$ (violet, thick line).

of $L = 5 = N$ and the question arises how the entanglement properties of the eigenstates change if the system grows. We want to analyze this in the following by looking at the average entanglement properties of all eigenstates.

5.1.2 Many eigenstates

Finally we address the average entanglement properties of all eigenstates of the periodic Bose-Hubbard Hamiltonian with unit filling.

Figure 5.5 depicts the average quantum correlations of all eigenstates of the periodic Bose-Hubbard Hamiltonian with quasimomentum $k = 1$, unit filling and different system sizes. With growing system size the average quantum correlations of all eigenstates are decreasing with increasing u. This is surprising because the two-particle interaction given by U determines quantum correlations and so one would expect them to be high for large u, as it is the case for the ground state in Figure 5.1. At the moment we do not have an explanation why the average quantum correlations of all eigenstates are high for small u.

Figure 5.6 is a plot of the average Wannier and Bloch mode entanglement between two neighbouring modes and the remaining modes of all eigenstates of the periodic Bose-Hubbard Hamiltonian with quasimomentum $k = 1$, unit filling and different system sizes. The plots shown in Figure 5.6 allow for the same interpretation as the plots shown in Figure 5.4 and so we are not going to repeat us here. Surprisingly the average Wannier superselection induced variance of all eigenstates is constant for all values of u and this is not the case for single eigenstates as can be seen in Figure 5.4. This certainly needs further investigation.

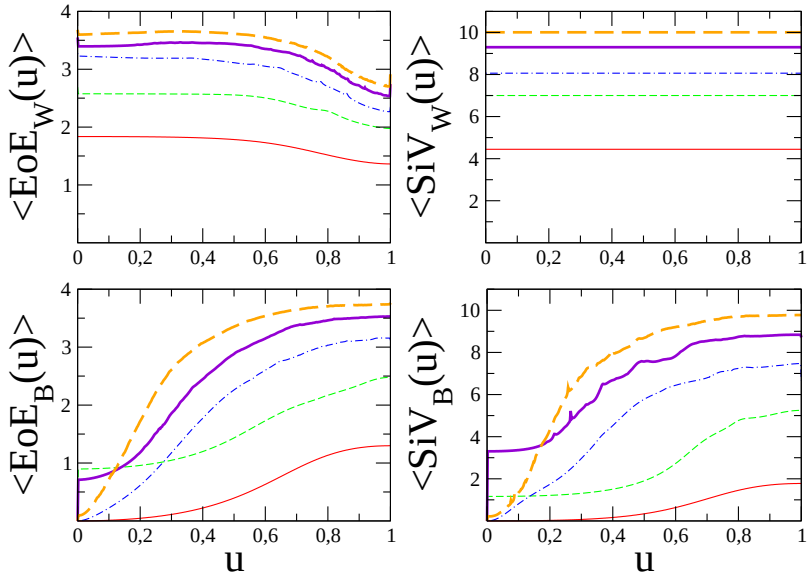

Figure 5.6: Average Wannier entropy of entanglement $\langle EoE_W(u)\rangle$ and average Wannier superselection induced variance $\langle SiV_W(u)\rangle$ (upper half) and average Bloch entropy of entanglement $\langle EoE_B(u)\rangle$ and average Bloch superselection induced variance $\langle SiV_B(u)\rangle$ (lower half) between two neighbouring modes and the remaining modes of all eigenstates applied to the setting of Figure 5.5.

Summing up our results concerning the static entanglement properties of the periodic Bose-Hubbard Hamiltonian we conclude that quantum correlations, Wannier mode entanglement and Bloch mode entanglement of all eigenstates are high in the chaotic regime of intermediate u and they can be low or high in the regular regime of small or large u. In particular, with respect to mode entanglement in the regular regime there always exists a set of modes with low mode entanglement.

5.2 Entanglement properties of propagated states

Now we want to analyze the dynamic entanglement properties of propagated states evolving with the Bose-Hubbard Hamiltonian. We will start by propagating the highly excited Fock state to highest energy. This is the setting that we also studied in the context of the dynamic fidelity in Section 3.2.1. In the second part of this section we will average over all propagated Fock states, in the same way as we averaged over all eigenstates in our above investigation of static entanglement properties. Let us emphasize that the units of time, in the following plots, are thoroughly explained in Section 2.1.1.

5.2.1 Propagation of a highly excited Fock state

Here we want to propagate the Fock state of highest energy with the periodic Bose-Hubbard Hamiltonian of $L = 5$ wells and $N = 5$ bosons and investigate

how its entanglement properties change in time. In this system the Wannier Fock state of highest energy reads $|50000\rangle_W$ because the two-particle interaction U is repulsive and hence the state of all bosons sitting in the same well must have the highest energy. The Bloch Fock state of highest energy reads $|05000\rangle_B$ and this can be calculated by means of (2.8).

We remark that we also studied the propagation of the Fock state to lowest energy, i.e. $|11111\rangle_W$ and $|00005\rangle_B$. However, it allowed for the same conclusions as the propagation of the Fock state to highest energy and so we decided not to show these results here. We just want to add that since these two states differ maximally in their energy it is expected that all Fock states exhibit the same behaviour in the different dynamic regimes.

Figure 5.7 shows the quantum correlations of the propagated Wannier Fock state $|50000\rangle_W$ of highest energy evolving with the periodic Bose-Hubbard Hamiltonian with $J = 10$ and $U = 1$ in the regular regime, with $J = 1 = U$ in the chaotic regime and with $J = 1$ and $U = 10$ in the regular regime. We refer to Figure 3.5 and Figure 3.18 for the precise location of the regular and the chaotic regime in the periodic Bose-Hubbard Hamiltonian with unit filling. As explained in Section 4.3.1 the state $|50000\rangle_W = |00000\rangle_p$, where the subscript p denotes the particle picture, is a separable state of five indistinguishable bosons. This is the reason why quantum correlations initially are zero, i.e. $QC(t = 0) = 0$. They more or less remain zero during the propagation in the regular regime of $J = 1$ and $U = 10$, and this makes sense because there the initial state $|50000\rangle_W$ is very close to an eigenstate, which is of course stationary. However, as the ratio $\frac{J}{U}$ increases also the change of quantum correlations increases. The inset of Figure 5.7 reveals that the initial growth of quantum correlations is bigger in the regular regime of $J = 10$ and $U = 1$ than it is in the chaotic regime of $J = 1 = U$. These observations can be explained because the ratio $\frac{J}{U}$ determines how far the initial state is away from a stationary eigenstate. We conclude that the quantum correlations change most in the regular regime for $J = 10$ and $U = 1$ and in the chaotic regime for $J = 1$ and $U = 1$, and they change least in the regular regime for $J = 1$ and $U = 10$.

5.8 shows the quantum correlations of the propagated Wannier Fock state $|50000\rangle_W$ of highest energy evolving with the periodic Bose-Hubbard Hamiltonian with $J = 1 - u$ and $u = U$ at a specific time $T = 100$, $T = 1000$ and $T = 10000$. Qualitatively the three curves look the same. There are huge oscillations which are due to the finite size of the system, as we will later see when we study bigger systems. We conclude that quantum correlations change most in the regular regime of small u and in the chaotic regime of intermediate u and they change least in the regular regime of large u.

In Figures 5.9 and 5.10 we applied Wannier and Bloch mode entanglement between two neighbouring modes and the remaining modes to the setting from above. Referring to Figure 5.9 we conclude that in the regular regime of $J = 10$ and $U = 1$ the change in Wannier mode entanglement is high and the change in Bloch mode entanglement is low, in the chaotic regime of $J = 1 = U$ the change in both is high and in the regular regime of $J = 1$ and $U = 10$ the change in Wannier mode entanglement is low and the change in Bloch mode entanglement is high. This makes sense if one keeps in mind that for the intial

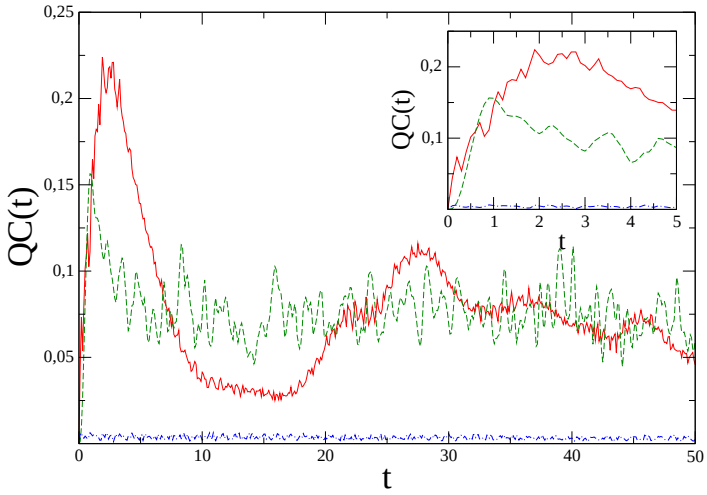

Figure 5.7: Quantum correlations $QC(t)$ of the propagated Wannier Fock state $|50000\rangle_W$ of highest energy evolving with the periodic Bose-Hubbard Hamiltonian of $L = 5 = N$ in the regular regime for $J = 10$ and $U = 1$ (red, thin line), in the chaotic regime for $J = 1$ and $U = 1$ (green, thin dashed line) and in the regular regime for $J = 1$ and $U = 10$ (blue, thin dash dotted line); note the inset which is a close-up of the beginning of the propagation. We conclude that the quantum correlations change most in the regular regime for $J = 10$ and $U = 1$ and in the chaotic regime for $J = 1$ and $U = 1$, and they change least in the regular regime for $J = 1$ and $U = 10$.

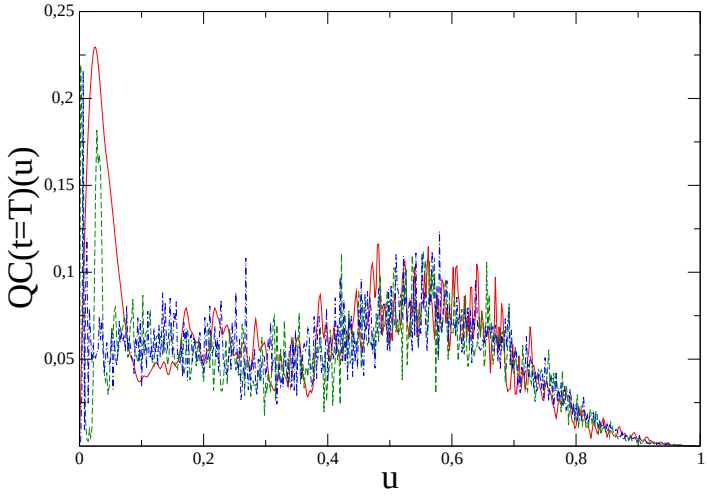

Figure 5.8: Change of quantum correlations $QC(t = T)(u)$ of the initially separable propagated Wannier Fock state $|50000\rangle_W$ of highest energy evolving with the periodic Bose-Hubbard Hamiltonian parametrized by $J = 1 - u$ and $U = u$ with $L = 5 = N$ at a time $T = 100$ (red, thin line), at a time $T = 1000$ (green, thin dashed line) and at a time $T = 10000$ (blue, thin dash dotted line).

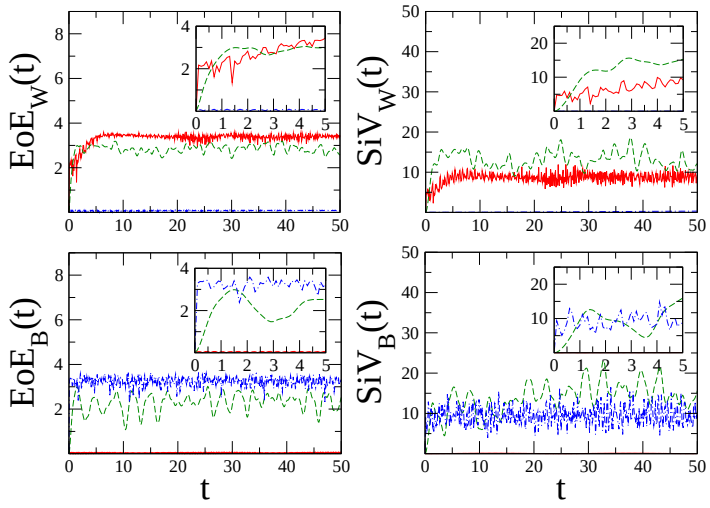

Figure 5.9: Wannier entropy of entanglement $EoE_W(t)$ and Wannier superselection induced variance $SiV_W(t)$ (upper half) and Bloch entropy of entanglement $EoE_B(t)$ and Bloch superselection induced variance $SiV_B(t)$ (lower half) between two neighbouring modes and the remaining modes applied to the setting of Figure 5.7. We conclude that in the regular regime of $J = 10$ and $U = 1$ the change in Wannier mode entanglement is high and the change in Bloch mode entanglement is low, in the chaotic regime of $J = 1 = U$ the change in both is high and in the regular regime of $J = 1$ and $U = 10$ the change in Wannier mode entanglement is low and the change in Bloch mode entanglement is high.

Wannier Fock state $|50000\rangle_W$ the ratio $\frac{J}{U}$ determines how far it is away from a stationary eigenstate and for the initial Bloch Fock state $|05000\rangle_B$ the ratio $\frac{U}{J}$ determines how far it is away from a stationary eigenstate.

Referring to Figure 5.10 we see that the mode entanglement qualitatively is the same at $T = 100$, $T = 1000$ and $T = 10000$. There are, however, huge oscillations in the superselection induced variance, which are finite size effects as we will soon see. We conclude that in the regular regime of small u Wannier mode entanglement is high while Bloch mode entanglement is low, in the chaotic regime of intermediate u both are high and in the regular regime of large u Wannier mode entanglement is low and Bloch mode entanglement is high.

Let us recapitulate the obtained results. The propagation of a highly excited state indeed allows to distinguish the regular and the chaotic regime. In the chaotic regime the change of entanglement is always high, and this is true for quantum correlations as well as mode entanglement. In the regular regime there exist modes such that the change in mode entanglement is low. Since we only considered one propagated state in a rather small system of $L = 5 = N$ it is now self-evident to study the dynamic entanglement properties of many propagated states in systems of different size. We do this in complete analogy to the above static analysis.

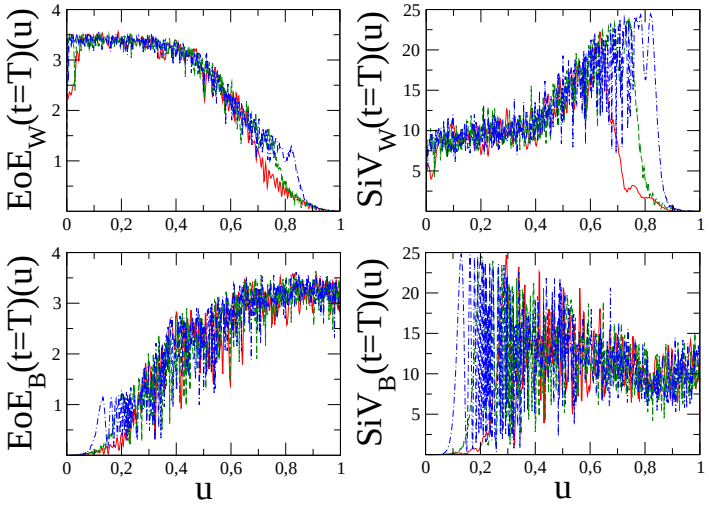

Figure 5.10: Change of Wannier entropy of entanglement $EoE_W(t = T)$ and change of Wannier superselection induced variance $SiV_W(t = T)$ (upper half) and change of Bloch entropy of entanglement $EoE_B(t = T)$ and change of Bloch superselection induced variance $SiV_B(t = T)$ (lower half) between two neighbouring modes and the remaining modes applied to the setting of Figure 5.8.

5.2.2 Many propagated states

Finally let us consider the average change of entanglement of many propagated Fock states. More precisely, for quantum correlations and Wannier mode entanglement we will propagate the complete Wannier Fock basis and for Bloch mode entanglement we will propagate the complete Bloch Fock basis.

Figure 5.11 shows the average change of quantum correlations of all propagated Wannier Fock states evolving with the periodic Bose-Hubbard Hamiltonian with unit filling and different system sizes at a sufficiently large time. This sufficiently large time is taken from Figure 5.8 to be $T = 1000$, because there we could not see a significant difference between the times $T = 100$, $T = 1000$ and $T = 10000$. Because Wannier Fock states in general have a huge amount of quantum correlations, e.g. the state $|11111\rangle_W$ is a maximally entangled state of five indistinguishable bosons according to our formalism in Section 4.3, we have to plot the quantity $|QC(t = T) - QC(t = 0)|(u)$. Only this quantity reflects the change of quantum correlations in time reasonably. We conclude that the average change of quantum correlations of all propagated Wannier Fock states is high in the regular regime of small u and in the chaotic regime of intermediate u and it is low in the regular regime of large u. This is the same result that we obtained for the single highly excited propagated state. However, in Figure 5.11 we see that as the system size grows and as the number of propagated states grows the oscillations get smaller.

In Figure 5.12 we see the average change of Wannier mode entanglement between two neighbouring modes and the remaining modes of all propagated Wannier Fock states and the average change of Bloch mode entanglement be-

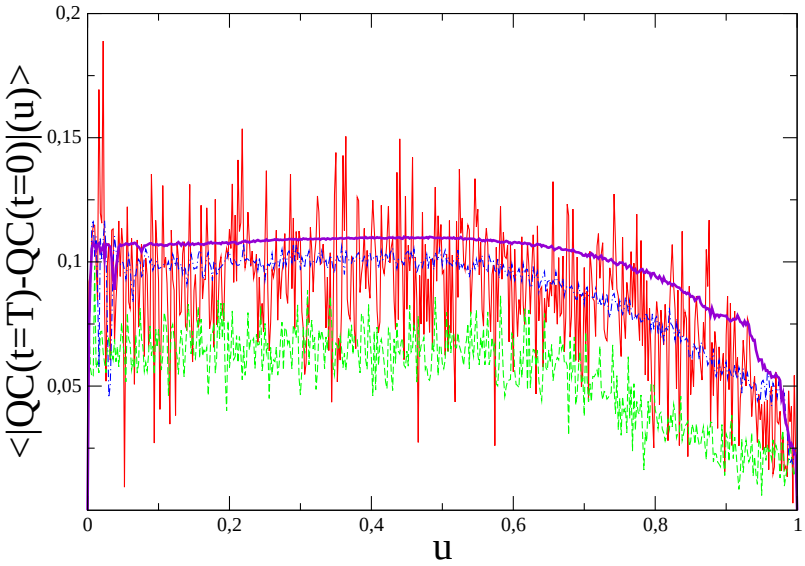

Figure 5.11: Average change of quantum correlations $\langle |QC(t=T) - QC(t=0)|(u)\rangle$ of all propagated Wannier Fock states evolving with the periodic Bose-Hubbard Hamiltonian of $L = 3 = N$ (red, thin line), $L = 4 = N$ (green, thin dashed line), $L = 5 = N$ (blue, thin dash dotted line) and $L = 6 = N$ (violet, thick line) at a time $T = 1000$.

tween two neighbouring modes and the remaining modes of all propagated Bloch Fock states in the setting from above. The sufficiently large time $T = 1000$ is justified by Figure 5.10 where no significant difference could be found between the curves to $T = 100$, $T = 1000$ and $T = 10000$. We conclude that in the regular regime of small u Wannier mode entanglement is high while Bloch mode entanglement is low, in the chaotic regime of intermediate u both are high and in the regular regime of large u Wannier mode entanglement is low and Bloch mode entanglement is high. Again this can be understood if one keeps in mind that the ratio $\frac{J}{U}$ determines how far initial Wannier Fock states are away from stationary eigenstates and the ratio $\frac{U}{J}$ determines how far initial Bloch Fock states are away from stationary eigenstates.

In summary we conclude that the change of quantum correlations, Wannier mode entanglement and Bloch mode entanglement in the propagation of a highly excited Fock state is high in the chaotic regime of intermediate u and it can be low or high in the regular regime of small or large u. The same is true for the average change of entanglement properties of all propagated Fock states. Hence we can characterize the chaotic regime by a high change of entanglement. On the other hand, in the regular regime there always exist modes such that the change in mode entanglement is low.

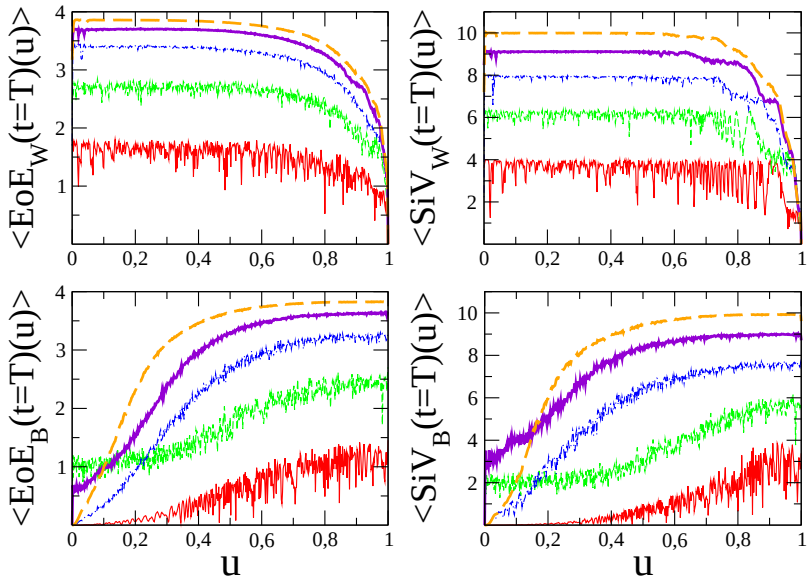

Figure 5.12: Average change of Wannier entropy of entanglement $\langle EoE_W(t = T)(u)\rangle$ and average change of Wannier superselection induced variance $\langle SiV_W(t = T)(u)\rangle$ between two neighbouring modes and the remaining modes of all initially separable propagated Wannier Fock states and average change of Bloch entropy of entanglement $\langle EoE_B(t = T)(u)\rangle$ and average change of Bloch superselection induced variance $\langle SiV_B(t = T)(u)\rangle$ between two neighbouring modes and the remaining modes of all initially separable propagated Bloch Fock states applied to the setting of Figure 5.11.

Chapter 6

Conclusions and perspectives

In this diploma thesis we studied aspects of quantum chaos and entanglement in the Bose-Hubbard model.

Concerning quantum chaos we first analyzed dynamic characteristics by means of the fidelity. Astonishingly its decay is always the same in the regular regime independent of the perturbation and this is not true in the chaotic regime. This allows for a nice analogy between quantum chaos and classical chaos, if one interprets the perturbation in the parameter of the fidelity as the initial distance between two points in classical phase space. In classical regular motion one would expect that the distance between the two resulting trajectories does not depend significantly on the initial distance. That this is true for the fidelity confirms the close connection between the fidelity in quantum chaos and the notion of classical chaos.

Then we investigated spectral properties and derived our own measure for the detection of the chaotic regime by counting avoided crossings. The standard approach for the classification of the regular and the chaotic regime is via investigation of the level spacing distribution and in general needs an unfolding of the spectrum. This unfolding can be involved and severely limits the validity of the result. Our novel method reliably and unambiguously distinguishes regular and chaotic and is easy to evaluate. Moreover, we showed that the standard approach can assign regularity to a spectrum which has a large number of dense lying avoided crossings and hence cannot be regular. This was the case with the spectrum of the periodic Bose-Hubbard Hamiltonian with $L = 37$ and $N = 3$. Hence our new measure is a necessary supplementary tool for the investigation of regular and chaotic spectra.

Concerning quantum entanglement we developed proper notions of entanglement for our system concluding that there are mainly two different perspectives. If the entangled entities under consideration are the indistinguishable bosons the entanglement is called quantum correlations between indistinguishable particles. If the entangled entities under consideration are the occupation numbers in the Fock states the entanglement is called mode entanglement. We derive our own measure for quantum correlations between indistinguishable bosons that has a reasonable interpretation and allows to quantify entanglement in systems of arbitrarily many indistinguishable bosons. Up to now there exist many ap-

proaches to entanglement between indistinguishable particles in the literature. These are, however, either formulated only for two indistinguishable particles or they are not efficiently computable. Our measure is a completely new approach, and we confirm its validity in several different scenarios. In particular, we showed that our measure pinpoints the quantum critical point of the quantum phase transition in the periodic Bose-Hubbard Hamiltonian with unit filling to $(\frac{J}{U})_{crit.} = 0.26 \pm 0.02$ without need of finite size scaling. In this context we also studied mode entanglement and showed that it does not locate this critical point comparably. Hence we conclude that the quantum phase transition manifests itself rather in entanglement between indistinguishable bosons than in entanglement between modes.

We then proposed a novel experimentally realizable method for the generation of practical entanglement in the Bose-Hubbard model. Here we introduced the notion of practical entanglement for practically useful entanglement, that is meant if one speaks about standard entanglement between distinguishable particles. This standard entanglement, due to its nonlocal properties, can be used for quantum teleportation and superdense coding. Even though there exist many works to the generation of entanglement in the Bose-Hubbard model, mostly they are not concerned with practical entanglement and so it remains an open question on how the generated entanglement can be used practically, e.g. for quantum teleportation. We show with our novel technique how a maximally entangled qutrit can be generated and stored in the Bose-Hubbard model.

Finally we addressed the question if the tools of entanglement theory can be used to separate the regular and the chaotic regime in the Bose-Hubbard model. We investigated static entanglement properties of the eigenstates and dynamic entanglement properties of propagated states. We showed that the chaotic regime is characterized by a high degree of entanglement, both quantum correlations and mode entanglement, in the eigenstates and in propagated states. Since we looked at two fundamentally different kinds of entanglement, namely quantum correlations and mode entanglement, in static and dynamic settings we conjecture that there is always a high degree of entanglement in the chaotic regime, independent of the specific kind of entanglement and independent of the specific setting. We showed that in the regular regime there always exists a set of modes such that mode entanglement is low. We conclude that mode entanglement is the proper entanglement measure to distinguish the regular and the chaotic regime. If we can not find a set of modes with low mode entanglement we are in the chaotic regime, whereas if we can find a set of modes with low mode entanglement we are in the regular regime.

We conclude that the usefulness of a specific measure depends on the precise task. Our proposed measure of quantum correlations between indistinguishable bosons locates the quantum critical point very well, but does not allow a clear separation of the regular and the chaotic regime. On the other hand mode entanglement does not pinpoint the quantum critical point very well, but it is a good tool for the specification of the regular and the chaotic regime. Nevertheless, in order to determine the regular to chaotic transition in the spectrum of the Bose-Hubbard Hamiltonian our novel method of counting avoided crossings turned out to be the best approach.

In the future we want to apply our proposed measures to larger systems. This is numerically demanding, but interesting from an experimental point of view, since in experiments usually large numbers of bosons in extended lattices are studied. In the context of quantum chaos, we want to determine the distribution of avoided crossings in the spectrum of large systems. In the context of quantum entanglement, we further want to analyze the quantum phase transition with our new measure of quantum correlations between indistinguishable bosons by means of finite size scaling.

We believe that the relation between single-copy and asymptotic entanglement measures is an interesting topic for further studies. In Section 4.2 we showed numerical evidence that a single-copy entanglement measure proposed by *Eisert* qualitatively behaves the same as the asymptotic entanglement measure entropy of entanglement. However, while *Eisert's* measure needs only the largest Schmidt coefficient the entropy of entanglement needs all Schmidt coefficients. Since numerically the largest Schmidt coefficient can be obtained more efficiently than all Schmidt coefficients, single-copy entanglement can be evaluated for larger systems. Addtionally single-copy entanglement is favored by experimentalists because its interpretation relies on only one copy of the state under consideration, while the interpretation of asymptotic entanglement requires infinitely many copies of the state under consideration.

Another exciting subject is multipartite entanglement in the Bose-Hubbard model. *Mintert* introduced a measure for multipartite entanglement that can be computed efficiently [101]. While we thoroughly studied bipartite entanglement in this thesis, we are now in a position to address multipartite entanglement. E.g. in this context an interesting question is the importance of multipartite entanglement in the quantum phase transition.

Appendix A

Quantum teleportation

This chapter on quantum teleportation is especially important for the proof of the entropy of entanglement in Appendix B. Unfortunately in the literature only the simplest form of quantum teleportation is explained [30], and so we derive here our own procedure for the quantum teleportation of an arbitrary quantum state.

Quantum teleportation is about sending the state of a quantum system over a quantum channel represented by a maximally entangled state shared between sender and receiver. As usual in quantum information theory the communicating parties are called Alice and Bob, and they are sufficiently far away from each other. We will explain the simplest settings first for the reader to become acquainted with the subject, but in the end we will teach a constructive method to teleport the entanglement present in an arbitrary finite-dimensional state over a maximally entangled state.

First Alice and Bob share a Bell state $|\beta\rangle = \frac{1}{\sqrt{2}}(|00\rangle + |11\rangle)$ and Alice has a qubit $|\psi\rangle = \alpha|0\rangle + \beta|1\rangle$ that she wants to teleport to Bob. Thus their entire state reads

$$\begin{aligned} |\psi\rangle \otimes |\beta\rangle &= (\alpha|0\rangle + \beta|1\rangle) \otimes (\frac{1}{\sqrt{2}}(|00\rangle + |11\rangle)) \\ &= \frac{\alpha}{\sqrt{2}}(|000\rangle + |011\rangle) + \frac{\beta}{\sqrt{2}}(|100\rangle + |111\rangle) \quad . \end{aligned}$$

It is important to have in mind that the first two kets correspond to Alice's qubit $|\psi\rangle$ and Alice's half of the shared maximally entangled state $|\beta\rangle$ while the third ket is Bob's half of $|\beta\rangle$. We rewrite the state as

$$\begin{aligned} |\psi\rangle \otimes |\beta\rangle &= \frac{1}{2}(\frac{1}{\sqrt{2}}(|00\rangle + |11\rangle)(\alpha|0\rangle + \beta|1\rangle) + \\ &\quad \frac{1}{\sqrt{2}}(|00\rangle - |11\rangle)(\alpha|0\rangle - \beta|1\rangle) + \\ &\quad \frac{1}{\sqrt{2}}(|01\rangle + |10\rangle)(\beta|0\rangle + \alpha|1\rangle) + \\ &\quad \frac{1}{\sqrt{2}}(|01\rangle - |10\rangle)(-\beta|0\rangle + \alpha|1\rangle)) \end{aligned}$$

to find that if Alice does a projective measurement, a so-called von Neumann measurement, in the Bell basis on her two qubits the state of Bob's qubit immediately alters and suddenly depends on α and β. Obviously the following LOCC protocol allows Alice to teleport $|\psi\rangle$ to Bob:

1. Alice does a projective measurement in the Bell basis on her two qubits.

2. She uses a classical channel, e.g. a telephone, to communicate her measurement result to Bob.

3. Finally Bob applies a unitary to his qubit conditional on Alice's measurement outcome, i.e.
   if Alice measured $\frac{1}{\sqrt{2}}(|00\rangle + |11\rangle)$ Bob does nothing,
   if Alice measured $\frac{1}{\sqrt{2}}(|00\rangle - |11\rangle)$ Bob applies a

$$\sigma_Z = \begin{pmatrix} 1 & 0 \\ 0 & -1 \end{pmatrix}$$

   to his qubit,
   if Alice measured $\frac{1}{\sqrt{2}}(|01\rangle + |10\rangle)$ Bob applies a

$$\sigma_X = \begin{pmatrix} 0 & 1 \\ 1 & 0 \end{pmatrix}$$

   to his qubit,
   if Alice measured $\frac{1}{\sqrt{2}}(|01\rangle - |10\rangle)$ Bob applies $\sigma_Z\sigma_X$ to his qubit.

In the end Bob's qubit will always be in the state $|\psi\rangle = \alpha|0\rangle + \beta|1\rangle$.

At first glance this looks like a possibility to superluminal communication. But Bob does not know the state of his qubit until Alice has used a classical channel to send her measurement result to him. And the classical channel prohibits messages to travel faster than light.

Second Alice and Bob share a Bell state $|\beta\rangle = \frac{1}{\sqrt{2}}(|00\rangle + |11\rangle)$, Alice additionally has two qubits in the state $|\psi\rangle = \alpha|00\rangle + \beta|11\rangle$ and she wants to teleport them to Bob. Again let us have a look at the total state:

$$\begin{aligned} |\psi\rangle \otimes |\beta\rangle &= (\alpha|00\rangle + \beta|11\rangle) \otimes (\frac{1}{\sqrt{2}}(|00\rangle + |11\rangle)) \\ &= \frac{\alpha}{\sqrt{2}}(|00\rangle|00\rangle + |00\rangle|11\rangle) + \frac{\beta}{\sqrt{2}}(|11\rangle|00\rangle + |11\rangle|11\rangle) \quad . \end{aligned}$$

In this notation the first two kets denote the two qubits Alice additionally has, the third ket is Alice's qubit from the shared Bell state and the fourth ket stands for Bob's qubit from the shared Bell state. We now change this order such that kets two and three become ket one and two and kets one and four become kets three and four. Still the first three kets correspond to Alice's qubits. We have

then:

$$\begin{aligned}
|\psi\rangle \otimes |\beta\rangle &= \frac{\alpha}{\sqrt{2}}(|00\rangle|00\rangle + |01\rangle|01\rangle) + \frac{\beta}{\sqrt{2}}(|10\rangle|10\rangle + |11\rangle|11\rangle) \\
&= \frac{1}{2}(\frac{1}{\sqrt{2}}(|00\rangle + |11\rangle)(\alpha|00\rangle + \beta|11\rangle) + \\
&\quad \frac{1}{\sqrt{2}}(|00\rangle - |11\rangle)(\alpha|00\rangle - \beta|11\rangle) + \\
&\quad \frac{1}{\sqrt{2}}(|01\rangle + |10\rangle)(\beta|10\rangle + \alpha|01\rangle) + \\
&\quad \frac{1}{\sqrt{2}}(|01\rangle - |10\rangle)(-\beta|10\rangle + \alpha|01\rangle)) \qquad .
\end{aligned}$$

Clearly the following LOCC protocol does the job:

1. Alice does a projective measurement in the Bell basis on her first two qubits, i.e. those that belong to the first two kets.

2. She uses a classical channel, e.g. a telephone, to communicate her measurement result to Bob.

3. Finally Bob applies a unitary to his qubit conditional on Alice's measurement outcome, i.e.
   if Alice measured $\frac{1}{\sqrt{2}}(|00\rangle + |11\rangle)$ Bob does nothing,
   if Alice measured $\frac{1}{\sqrt{2}}(|00\rangle - |11\rangle)$ Bob applies a

$$\sigma_Z = \begin{pmatrix} 1 & 0 \\ 0 & -1 \end{pmatrix}$$

   to his qubit,
   if Alice measured $\frac{1}{\sqrt{2}}(|01\rangle + |10\rangle)$ Bob applies a

$$\sigma_X = \begin{pmatrix} 0 & 1 \\ 1 & 0 \end{pmatrix}$$

   to his qubit,
   if Alice measured $\frac{1}{\sqrt{2}}(|01\rangle - |10\rangle)$ Bob applies $\sigma_Z\sigma_X$ to his qubit.

In the end Alice and Bob will share the state $|\psi\rangle = \alpha|00\rangle + \beta|11\rangle$.

In order to teleport states of dimension greater than two Alice has to be able to measure projectively in a new orthonormal complete basis other than the Bell basis. We choose the Fourier transform since we already know it very well from the transition of Wannier states $\psi_l(x)$ to Bloch states $\phi_k(x)$, as it is explained in Chapter 2:

$$\phi_k(x) = \frac{1}{\sqrt{L}} \sum_{l=1}^{L} e^{i\frac{2\pi k}{L}l} \psi_l(x) \qquad .$$

Here L is set equal to the Schmidt rank of the maximally entangled state and k runs from 1 to L. E.g. in the case $d = 2$ we define as new basis states

$$\begin{aligned}
|0\rangle &:= \frac{1}{\sqrt{2}}(e^{i\pi}|00\rangle + e^{i2\pi}|11\rangle) \\
&= \frac{1}{\sqrt{2}}(-|00\rangle + |11\rangle) \\
|1\rangle &:= \frac{1}{\sqrt{2}}(e^{i2\pi}|00\rangle + e^{i4\pi}|11\rangle) \\
&= \frac{1}{\sqrt{2}}(|00\rangle + |11\rangle) \\
|2\rangle &:= \frac{1}{\sqrt{2}}(e^{i\pi}|01\rangle + e^{i2\pi}|10\rangle) \\
&= \frac{1}{\sqrt{2}}(-|01\rangle + |10\rangle) \\
|3\rangle &:= \frac{1}{\sqrt{2}}(e^{i2\pi}|01\rangle + e^{i4\pi}|10\rangle) \\
&= \frac{1}{\sqrt{2}}(|01\rangle + |10\rangle)
\end{aligned}$$

and this is essentially the Bell basis. But we can equally construct a proper basis for Alice to do her projective measurement in any dimension, enabling us to do general quantum teleportation. The following third and last example gives a constructive procedure for quantum teleportation of arbitrary finite-dimensional states.

So third and finally Alice and Bob share a maximally entangled state $|\beta\rangle = \frac{1}{\sqrt{3}}(|00\rangle + |11\rangle + |22\rangle)$, Alice additionally has two qutrits in the state $|\psi\rangle = \alpha|00\rangle + \beta|11\rangle + \gamma|22\rangle$ and she wants to teleport their state. Hence the entire state reads

$$\begin{aligned}
|\psi\rangle \otimes |\beta\rangle &= (\alpha|00\rangle + \beta|11\rangle + \gamma|22\rangle) \otimes (\frac{1}{\sqrt{3}}(|00\rangle + |11\rangle + |22\rangle)) \\
&= \frac{\alpha}{\sqrt{3}}(|00\rangle|00\rangle + |00\rangle|11\rangle + |00\rangle|22\rangle) + \\
&\quad \frac{\beta}{\sqrt{3}}(|11\rangle|00\rangle + |11\rangle|11\rangle + |11\rangle|22\rangle) + \\
&\quad \frac{\gamma}{\sqrt{3}}(|22\rangle|00\rangle + |22\rangle|11\rangle + |22\rangle|22\rangle) \quad .
\end{aligned}$$

Again we place kets two and three at positions one and two and kets one and four at positions three and four:

$$\begin{aligned}
|\psi\rangle \otimes |\beta\rangle &= \frac{\alpha}{\sqrt{3}}(|00\rangle|00\rangle + |01\rangle|01\rangle + |02\rangle|02\rangle) + \\
&\quad \frac{\beta}{\sqrt{3}}(|10\rangle|10\rangle + |11\rangle|11\rangle + |12\rangle|12\rangle) + \\
&\quad \frac{\gamma}{\sqrt{3}}(|20\rangle|20\rangle + |21\rangle|21\rangle + |22\rangle|22\rangle) \quad .
\end{aligned}$$

We rewrite this state with the help of our new basis:

$$
\begin{aligned}
|\psi\rangle \otimes |\beta\rangle \;=\; & \frac{1}{3}\Big(\frac{1}{\sqrt{3}}(e^{i\frac{2\pi}{3}}|00\rangle + e^{i\frac{4\pi}{3}}|11\rangle + |22\rangle)(e^{-i\frac{2\pi}{3}}\alpha|00\rangle + e^{-i\frac{4\pi}{3}}\beta|11\rangle + \gamma|22\rangle) + \\
& \frac{1}{\sqrt{3}}(e^{i\frac{4\pi}{3}}|00\rangle + e^{i\frac{8\pi}{3}}|11\rangle + |22\rangle)(e^{-i\frac{4\pi}{3}}\alpha|00\rangle + e^{-i\frac{8\pi}{3}}\beta|11\rangle + \gamma|22\rangle) + \\
& \frac{1}{\sqrt{3}}(|00\rangle + |11\rangle + |22\rangle)(\alpha|00\rangle + \beta|11\rangle + \gamma|22\rangle) + \\
& \frac{1}{\sqrt{3}}(e^{i\frac{2\pi}{3}}|01\rangle + e^{i\frac{4\pi}{3}}|12\rangle + |20\rangle)(e^{-i\frac{2\pi}{3}}\alpha|01\rangle + e^{-i\frac{4\pi}{3}}\beta|12\rangle + \gamma|20\rangle) + \\
& \frac{1}{\sqrt{3}}(e^{i\frac{4\pi}{3}}|01\rangle + e^{i\frac{8\pi}{3}}|12\rangle + |20\rangle)(e^{-i\frac{4\pi}{3}}\alpha|01\rangle + e^{-i\frac{8\pi}{3}}\beta|12\rangle + \gamma|20\rangle) + \\
& \frac{1}{\sqrt{3}}(|01\rangle + |12\rangle + |20\rangle)(\alpha|01\rangle + \beta|12\rangle + \gamma|20\rangle) + \\
& \frac{1}{\sqrt{3}}(e^{i\frac{2\pi}{3}}|02\rangle + e^{i\frac{4\pi}{3}}|10\rangle + |21\rangle)(e^{-i\frac{2\pi}{3}}\alpha|02\rangle + e^{-i\frac{4\pi}{3}}\beta|10\rangle + \gamma|21\rangle) + \\
& \frac{1}{\sqrt{3}}(e^{i\frac{4\pi}{3}}|02\rangle + e^{i\frac{8\pi}{3}}|10\rangle + |21\rangle)(e^{-i\frac{4\pi}{3}}\alpha|02\rangle + e^{-i\frac{8\pi}{3}}\beta|10\rangle + \gamma|21\rangle) + \\
& \frac{1}{\sqrt{3}}(|02\rangle + |10\rangle + |21\rangle)(\alpha|02\rangle + \beta|10\rangle + \gamma|21\rangle)\Big) \qquad ,
\end{aligned}
$$

and choose the following LOCC protocol:

1. Alice does a projective measurement in the new orthonormal complete basis on her first two qubits, i.e. those that belong to the first two kets.

2. She uses a classical channel, e.g. a telephone, to communicate her measurement result to Bob.

3. Finally Bob applies a unitary to his qubit conditional on Alice's measurement outcome. We do not want to write out all resulting unitaries but rather give an example that illustrates the general procedure. E.g. if Alice measures $\frac{1}{\sqrt{3}}(e^{i\frac{4\pi}{3}}|02\rangle + e^{i\frac{8\pi}{3}}|10\rangle + |21\rangle)$ Bob uses

$$
U = \begin{pmatrix} 0 & 0 & e^{i\frac{2\pi}{3}} \\ e^{i\frac{4\pi}{3}} & 0 & 0 \\ 0 & 1 & 0 \end{pmatrix} \qquad .
$$

In the end Alice and Bob will share the state $|\psi\rangle = \alpha|00\rangle + \beta|11\rangle + \gamma|22\rangle$.

Appendix B

Entropy of entanglement

The entropy of entanglement is the entanglement measure for pure bipartite states. Because the complete proof is given nowhere in the literature and because it is relevant for the discussion of identical particles, we want to present it here.

Theorem: m copies of an arbitrary state $|\psi\rangle$ can be transformed into $r \cdot m$ copies of the maximally entangled state $|\beta\rangle$ revertibly by LOCC in the asymptotic limit $m, n \to \infty$ and

$$r \quad = \quad EoE(|\psi\rangle) \qquad ,$$

where

$$EoE(|\psi\rangle) \quad := \quad -\sum_j \lambda_j \log(\lambda_j)$$

is called the entropy of entanglement. For pure bipartite states distillable entanglement and entanglement cost are equal to each other and they equal the entropy of entanglement.

Proof: Our goal is on the one hand to specify a LOCC protocol that transforms m copies of our state $|\psi\rangle$ into $EoE(|\psi\rangle) \cdot m$ copies of the maximally entangled state $|\beta\rangle$ in the asymptotic limit. This process is called entanglement distillation, because maximally entangled states are distilled from partly entangled states. On the other hand we have to derive a LOCC protocol that transforms $EoE(|\psi\rangle) \cdot m$ maximally entangled states $|\beta\rangle$ into m copies of our state $|\psi\rangle$ in the asymptotic limit. This is called entanglement dilution, since the maximally entangled states are diluted to partly entangled states. In short we will have to prove

$$|\psi\rangle^{\otimes m} \overset{LOCC}{\rightleftharpoons} |\beta\rangle^{\otimes n = EoE(|\psi\rangle) \cdot m} \quad m, n \to \infty \qquad .$$

Finally we have to show that both given protocols are optimal, i.e. it is not possible to distill more entanglement than with our protocol of entanglement distillation and it is not possible to dilute more entanglement than with our protocol of entanglement dilution. By this we then have also proved that distillable entanglement equals entanglement cost equals entropy of entanglement.

The following proof uses ϵ-typical sequences and quantum teleportation. While we will discuss ϵ-typical sequences now, quantum teleportation is extensively explained in Appendix A.

Assume we have a source that produces letters from an alphabet $\{0, 1, \ldots, d-1\}$ with probabilities $p_0, p_1, \ldots, p_{d-1}$, such that after we have used the source N times we have a string $\vec{x}$ of N letters. The typical sequence is such a string $\vec{x}_{typ}$ where the letters 0, 1, ..., $d-1$ appear exactly with absolute frequencies $Np_0, Np_1, \ldots, Np_{d-1}$. An ϵ-typical sequence is a string $\vec{x}_{\epsilon-typ}$ where the letters 0, 1, ..., $d-1$ appear approximately with absolute frequencies Np_0, Np_1, ..., Np_{d-1}. Of course a mathematically strict definition of ϵ-typical sequences can be given and has to be used in a correct proof. However, this is done in most of the literature and so we refuse to do it here because it complicates the subject and does not lead to any deeper understanding. We believe that it suffices to see a set of ϵ-typical sequences for a certain small ϵ to comprise all sequences that are near to the typical sequence where the nearness is given by ϵ, i.e. the smaller ϵ the less sequences are ϵ-typical. Thinking of our source again, for large N it will mostly produce ϵ-typical sequences due to the central limit theorem.

There exists a nice analogy for $d = 2$. If we have N particles in a box of volume V and bipartite the box into two volumes V_1 and $V - V_1$, then the probability for a gas particle to be in volume V_1 is $p_1 = \frac{V_1}{V}$. The probability for exactly n specific gas particles to be in V_1 and $N - n$ to be in $V - V_1$ reads $P_1{}'(n) = {p_1}^n(1 - p_1)^{N-n}$. However asking for any n gas particles we have to sum over all configurations:

$$P_1(n) = \binom{N}{n} p_1^n (1 - p_1)^{N-n} \quad .$$

It follows from the central limit theorem that in the limit of large N this probability P_1 converges to a normal distribution with mean $\mu = Np_1$ and standard deviation $\sigma = \sqrt{Np_1(1 - p_1)}$,

$$N \to \infty : \quad P_1(n) \to \frac{1}{\sqrt{2\pi N p_1(1 - p_1)}} e^{-\frac{(n - Np_1)}{2Np_1(1-p_1)}} \quad ,$$

and the relative width scales as

$$N \to \infty : \quad \frac{\sigma}{\mu} \to \frac{1}{\sqrt{N}} \quad .$$

In fact the applicability of the central limit theorem can be easily seen by attaching a random variable X to each gas particle, where X takes on the value $x_1 = x_{V_1}$ with probability $p_1 = \frac{V_1}{V}$ and $x_2 = x_{V-V_1}$ with probability $p_2 = (1 - p_1) = \frac{V - V_1}{V}$. Hence we have N independent and identically binomially distributed random variables.

Let us call the configuration where Np_1 gas particles are in V_1 a typical configuration, then the above result means that in the limit of large N we will have a typical configuration in most of the times. It turns out that we could have also divided the box into more than two volumes and would have arrived at the same conclusion, only that then the typical configuration would be made up

of $Np_1 = N\frac{V_1}{V}$ gas particles in V_1, $Np_2 = N\frac{V_2}{V}$ gas-particles in V_2, $Np_3 = N\frac{V_3}{V}$ gas-particles in V_3, and so on.

Returning to our more abstract treatment it should be clear now that the probability for obtaining a ϵ-typical sequence is

$$p(\vec{x}_{\epsilon-typ}) \;=\; p_0^{Np_0} \cdot p_1^{Np_1} \cdot \ldots \cdot p_{d-1}^{Np_{d-1}}$$

and

$$\begin{aligned} \log_d(p(\vec{x}_{\epsilon-typ})) &= \log_d(p_0^{Np_0} \cdot p_1^{Np_1} \cdot \ldots \cdot p_{d-1}^{Np_{d-1}}) \\ &= N(p_0 \log_d(p_0) + p_1 \log_d(p_1) + \ldots + p_{d-1} \log_d(p_{d-1}) \\ &=: -NH_d(X) \end{aligned}$$

implies

$$p(\vec{x}_{\epsilon-typ}) \;=\; d^{-NH_d(X)} \qquad .$$

Here X is a random variable with the above probability distribution and H_d is the Shannon entropy on dits. As for large N almost all sequences are ϵ-typical we can say that there are approximately $d^{NH_d(X)}$ ϵ-typical sequences.

After this excursion to ϵ-typical sequences we can now come back to our initial concern, the proof of the entropy of entanglement. We remark again that quantum teleportation is a necessary ingredient for this proof and it is explained thoroughly in Appendix A. Suppose Alice and Bob share m copies of a $d \times d$-dimensional entangled state

$$|\psi\rangle \;=\; \sum_x \sqrt{p(x)}|x_A\rangle|x_B\rangle \qquad ,$$

i.e.

$$|\psi\rangle^{\otimes m} \;=\; \sum_{x_1,x_2,\ldots,x_m} \sqrt{p(x_1)p(x_2)\ldots p(x_m)}|x_1x_2\ldots x_m\rangle_A \otimes |x_1x_2\ldots x_m\rangle_B \qquad ,$$

in the asymptotic limit $m \to \infty$. We adopt the point of view that the squared Schmidt coefficients are interpreted as probabilities.

We will now explain a LOCC protocol that allows to distill n copies of the maximally entangled pair from $|\psi\rangle^{\otimes m}$, entanglement distillation, and then give a protocol that transforms n copies of the maximally entangled pair into m copies of $|\psi\rangle$, entanglement dilution. The remarkable thing about asymptotic entanglement is that the ratios $r = \frac{n}{m}$ in the asymptotic limit $m, n \to \infty$ are equal in both protocols,

$$r \;=\; EoE(|\psi\rangle) \qquad ,$$

and this is actually the maximum ratio achievable.

Entanglement distillation protocol:
Alice and Bob share $|\psi\rangle^{\otimes m}$. Now Alice measures the absolute frequencies of 0, 1, $\ldots$, $d-1$ without specifying which of her quantum systems have that quantum

numbers. This last point is very important: If she would measure both quantum number and corresponding quantum system the total state would collapse to only one ket, a separable state. With very high probability she will measure an ϵ-typical sequence, i.e. she will measure quantum number 0 $m \cdot p(0)$ times, quantum number 1 $m \cdot p(1)$ times, ... and quantum number $d-1$ $m \cdot p(d-1)$ times. Then the state will have reduced to a sum of $d^{EoE(|\psi\rangle)\cdot m}$ summands with equal coefficients $\sqrt{d^{-EoE(|\psi\rangle)\cdot m}}$. And this state is equivalent, up to local unitaries, to sharing $n = EoE(|\psi\rangle) \cdot m$ maximally entangled pairs.

Entanglement dilution protocol:
Alice and Bob share $|\beta\rangle^{\otimes n=EoE(|\psi\rangle)\cdot m}$. Alice additionally has $|\psi\rangle^{\otimes m}$ in her laboratory. Now she prepares the ϵ-typical subspace of $|\psi\rangle^{\otimes m}$ locally and teleports Bob's part to Bob. This she can do because she only needs $n = EoE(|\psi\rangle) \cdot m$ maximally entangled pairs for the quantum teleportation of the reduced $|\psi\rangle^{\otimes m}$.

Together with Appendix A, we have shown that

$$|\psi\rangle^{\otimes m} \overset{LOCC}{\rightleftharpoons} |\beta\rangle^{\otimes n=EoE(|\psi\rangle)\cdot m} \quad m,n \to \infty \qquad .$$

and it remains to be proved that both proposed protocols are also optimal.

Assume there existed a distillation protocol that would distill $r^{'} \cdot m > EoE(|\psi\rangle) \cdot m$ maximally entangled pairs from $|\psi\rangle^{\otimes m}$. Then we could start with $EoE(|\psi\rangle) \cdot m$ Bell pairs, dilute $|\psi\rangle^{\otimes m}$ and then distill $r^{'} \cdot m > EoE(|\psi\rangle) \cdot m$ Bell pairs. So by LOCC only we would have enlarged the Schmidt number. But this is forbidden by the majorization criterion. This ends the proof of the entropy of entanglement.

We want to emphasize that with this proof we have shown that the entropy of entanglement indeed is an entanglement monotone. It can be easily shown that the entropy of entanglement is additive [50] and therefore it is a good entanglement measure.

Bibliography

[1] E. A. Cornell and C. E. Wieman, *Nobel lecture: Bose-Einstein condensation in a dilute gas, the first 70 years and some recent experiments*, Rev. Mod. Phys. **74** (2002).

[2] A. J. Leggett, *Bose-Einstein condensation in the alkali gases: Some fundamental concepts*, Rev. Mod. Phys. **73** (2001).

[3] I. Bloch, J. Dalibard, and W. Zwerger, *Many-body physics with ultracold gases*, Rev. Mod. Phys. **80** (2008).

[4] C. Liu, Z. Dutton, C. H. Behroozi, and L. V. Hau, *Observation of coherent optical information storage in an atomic medium using halted light pulses*, Nature **409** (2001).

[5] W. Hänsel, P. Hommelhoff, T. W. Hänsch, and J. Reichel, *Bose-Einstein condensation on a microelectronic chip*, Nature **413** (2001).

[6] M. Greiner, O. Mandel, T. Rom, A. Altmeyer, A. Widera, T. W. Hänsch, and I. Bloch, *Quantum phase transition from a superfluid to a Mott insulator in an ultracold gas of atoms*, Physica B: Condensed Matter **329-333** (2003).

[7] C. A. Regal, M. Greiner, and D. S. Jin, *Observation of resonance condensation of fermionic atom pairs*, Phys. Rev. Lett. **92** (2004).

[8] M. Fleischhauer, *Quantum physics: Indistinguishable from afar*, Nature **445** (2007).

[9] J. Esteve, C. Gross, A. Weller, S. Giovanazzi, and M. K. Oberthaler, *Squeezing and entanglement in a Bose-Einstein condensate*, Nature **455** (2008).

[10] M. P. A. Fisher, *Boson localization and the superfluid-insulator transition*, Symposium on quantum fluids and solids **194** (1989).

[11] D. Jaksch, C. Bruder, J. I. Cirac, C. W. Gardiner, and P. Zoller, *Cold bosonic atoms in optical lattices*, Phys. Rev. Lett. **81** (1998).

[12] R. P. Feynman, *Simulating physics with computers*, Int. J. Theo. Phys. **21** (1982).

[13] R. Ionicioiu and P. Zanardi, *Quantum information processing in bosonic lattices*, Phys. Rev. A **66** (2002).

[14] S. Bose, *Entanglement from the dynamics of an ideal Bose gas in a lattice*, preprint, arXiv:cond-mat/0610024 (2006).

[15] N. Teichmann and C. Weiss, *Coherently controlled entanglement generation in a binary Bose-Einstein condensate*, Europhys. Lett. **78** (2007).

[16] O. Romero-Isart, K. Eckert, C. Rodo, and A. Sanpera, *Transport and entanglement generation in the Bose-Hubbard model*, Mathematical Systems Theory **40** (2007).

[17] A. R. Kolovsky and A. Buchleitner, *Quantum chaos in the Bose-Hubbard model*, Europhys. Lett. **68** (2004).

[18] M.-J. H. Giannoni and N. Balázs, *Les Houches lectures 1989: Chaos et physique quantique*, North-Holland, Amsterdam, 1991.

[19] E. A. Jackson, *Perspectives of nonlinear dynamics*, Cambridge Univ. Press, Cambridge, 1992.

[20] M. V. Berry and M. Tabor, *Level clustering in the regular spectrum*, Proc. R. Soc. Lond. A **356** (1977).

[21] O. Bohigas, M. J. Giannoni, and C. Schmit, *Characterization of chaotic quantum spectra and universality of level fluctuation laws*, Phys. Rev. Lett. **52** (1984).

[22] F. Haake, *Quantum signatures of chaos*, Springer, Berlin; Heidelberg, 2001.

[23] J. E. Bayfield, *Quantum evolution: An introduction to time-dependent quantum mechanics*, Wiley VCH, 1999.

[24] T. Gorin, T. Prosen, T. H. Seligman, and M. Znidaric, *Dynamics of Loschmidt echoes and fidelity decay*, Phys. Rep. **435** (2006).

[25] R. Horodecki, P. Horodecki, M. Horodecki, and K. Horodecki, *Quantum entanglement*, preprint, arXiv:quant-ph/0702225 (2007).

[26] T. J. Osborne and M. A. Nielsen, *Entanglement in a simple quantum phase transition*, Phys. Rev. A **66** (2002).

[27] A. Osterloh, L. Amico, G. Falci, and R. Fazio, *Scaling of entanglement close to a quantum phase transition*, Nature **416** (2002).

[28] P. Buonsante and A. Vezzani, *Ground-state fidelity and bipartite entanglement in the Bose-Hubbard model*, Phys. Rev. Lett. **98** (2007).

[29] F. Mintert, A. M. Rey, I. I. Satija, and C. W. Clark, *Phase transitions, entanglement and quantum noise interferometry in cold atoms*, preprint, arXiv:0803.0760 (2008).

[30] M. A. Nielsen and I. L. Chuang, *Quantum computation and quantum information*, Cambridge Univ. Press, Cambridge, 2004.

[31] E. Schrödinger, *Discussion of probability relations between separated systems*, Math. Proc. Camb. Phil. Soc. **31** (1935).

[32] J. S. Bell, *On the Einstein-Podolsky-Rosen paradox*, Physics (US) (1964).

[33] M. B. Plenio and S. Virmani, *An introduction to entanglement measures*, Quant. Inf. Comp. **7** (2007).

[34] L. Amico, R. Fazio, A. Osterloh, and V. Vedral, *Entanglement in many-body systems*, Rev. Mod. Phys. **80** (2008).

[35] A. R. Kolovsky and A. Buchleitner, *Floquet-Bloch operator for the Bose-Hubbard model with static field*, Phys. Rev. E **68** (2003).

[36] A. Tomadin, R. Mannella, and S. Wimberger, *Many-body interband tunneling as a witness for complex dynamics in the Bose-Hubbard model*, Phys. Rev. Lett. **98** (2007).

[37] A. Buchleitner and A. R. Kolovsky, *Interaction-induced decoherence of atomic Bloch oscillations*, Phys. Rev. Lett. **91** (2003).

[38] W. Zwerger, *Mott-Hubbard transition of cold atoms in optical lattices*, Quant. Semicl. Opt. **5** (2003).

[39] C. Kollath, A. Iucci, T. Giamarchi, W. Hofstetter, and U. Schollwöck, *Spectroscopy of ultracold atoms by periodic lattice modulations*, Phys. Rev. Lett. **97** (2006).

[40] W.-K. Tung, *Group theory in physics*, World Scientific, New Jersey, 2008.

[41] M. Oberthaler, *Private communication.*

[42] W. H. Press, S. A. Teukolsky, W. T. Vetterling, and B. P. Flannery, *Numerical recipes in fortran 90*, Cambridge Univ. Press, Cambridge, 1996.

[43] M. Hiller, T. Kottos, and T. Geisel, *Complexity in parametric Bose-Hubbard hamiltonians and structural analysis of eigenstates*, Phys. Rev. A **73** (2006).

[44] J. Liu, W. Wang, C. Zhang, Q. Niu, and B. Li, *Fidelity of a Bose-Einstein condensate*, Phys. Rev. A **72** (2005).

[45] P. Zanardi, M. Cozzini, and P. Giorda, *Ground state fidelity and quantum phase transitions in free Fermi systems*, J. Stat. Mech. (2007).

[46] M. Wilkinson, *Diffusion and dissipation in complex quantum systems*, Phys. Rev. A **41** (1990).

[47] P. Zanardi and N. Paunkovic, *Ground state overlap and quantum phase transitions*, Phys. Rev. E **74** (2006).

[48] P. Plötz, *Private communication.*

[49] W.-L. You, Y.-W. Li, and S.-J. Gu, *Fidelity, dynamic structure factor, and susceptibility in critical phenomena*, Phys. Rev. E **76** (2007).

[50] M. M. Wolf, *Lecture notes: Quantum information theory.*

[51] F. Mintert, *Lecture notes: Introduction to entangled states and entanglement measures.*

[52] J. Schliemann, J. I. Cirac, M. Kus, M. Lewenstein, and D. Loss, *Quantum correlations in two-fermion systems*, Phys. Rev. A **64** (2001).

[53] K. Eckert, J. Schliemann, D. Bruss, and M. Lewenstein, *Quantum correlations in systems of indistinguishable particles*, Ann. Phys. **299** (2002).

[54] C. H. Bennett and S. J. Wiesner, *Communication via one- and two-particle operators on Einstein-Podolsky-Rosen states*, Phys. Rev. Lett. **69** (1992).

[55] C. H. Bennett, G. Brassard, C. Crépeau, R. Jozsa, A. Peres, and W. K. Wootters, *Teleporting an unknown quantum state via dual classical and Einstein-Podolsky-Rosen channels*, Phys. Rev. Lett. **70** (1993).

[56] R. Paskauskas and L. You, *Quantum correlations in two-boson wavefunctions*, Phys. Rev. A **64** (2001).

[57] Y. S. Li, B. Zeng, X. S. Liu, and G. L. Long, *Entanglement in a two-identical-particle system*, Phys. Rev. A **64** (2001).

[58] Y. Shi, *Quantum entanglement of identical particles*, Phys. Rev. A **67** (2003).

[59] X.-G. Wang and B. C. Sanders, *Canonical entanglement for two indistinguishable particle*, Math. Gen. **38** (2005).

[60] G. Ghirardi, L. Marinatto, and T. Weber, *Entanglement and properties of composite quantum systems: a conceptual and mathematical analysis*, J. Stat. Phys. **108** (2002).

[61] G. Ghirardi and L. Marinatto, *Identical particles and entanglement*, Opt. Spec. **99** (2005).

[62] M. Kitagawa and M. Ueda, *Squeezed spin states*, Phys. Rev. A **47** (1993).

[63] D. J. Wineland, J. J. Bollinger, W. M. Itano, and D. J. Heinzen, *Squeezed atomic states and projection noise in spectroscopy*, Phys. Rev. A **50** (1994).

[64] A. S. Sørensen and K. Mølmer, *Entanglement and extreme spin squeezing*, Phys. Rev. Lett. **86** (2001).

[65] J. Hald, J. L. Sørensen, C. Schori, and E. S. Polzik, *Spin squeezed atoms: A macroscopic entangled ensemble created by light*, Phys. Rev. Lett. **83** (1999).

[66] A. Sorensen, L.-M. Duan, I. Cirac, and P. Zoller, *Many-particle entanglement with Bose–Einstein condensates*, Nature **409** (2001).

[67] X. Wang and B. C. Sanders, *Spin squeezing and pairwise entanglement for symmetric multiqubit states*, Phys. Rev. A **68** (2003).

[68] J. K. Korbicz, O. Guhne, M. Lewenstein, H. Haeffner, C. F. Roos, and R. Blatt, *Generalized spin squeezing inequalities in N-qubit systems: theory and experiment*, Phys. Rev. A **74** (2006).

[69] G. Toth, C. Knapp, O. Guhne, and H. J. Briegel, *Spin squeezing and entanglement*, preprint, arXiv:0806.1048 (2008).

[70] P. Zanardi and X. Wang, *Fermionic entanglement in itinerant systems*, J. Phys. A **35** (2002).

[71] S. J. van Enk, *Entanglement of photons*, Phys. Rev. A **67** (2003).

[72] V. Vedral, *Entanglement in the second quantization formalism*, Centr. Eur. J. Phys. **1** (2003).

[73] H. M. Wiseman and J. A. Vaccaro, *The entanglement of indistinguishable particles shared between two parties*, Phys. Rev. Lett. **91** (2003).

[74] J. A. Vaccaro, F. Anselmi, and H. M. Wiseman, *Entanglement of identical particles and reference phase uncertainty*, Int. J. Quant. Inf. **1** (2003).

[75] N. Schuch, F. Verstraete, and J. I. Cirac, *Quantum entanglement theory in the presence of superselection rules*, Phys. Rev. A **70** (2004).

[76] S. J. van Enk, *Single-particle entanglement*, Phys. Rev. A **72** (2005).

[77] A. Salles, F. Melo, M. P. Almeida, M. Hor-Meyll, S. P. Walborn, P. H. S. Ribeiro, and L. Davidovich, *Experimental investigation of the dynamics of entanglement: Sudden death, complementarity, and continuous monitoring of the environment*, Phys. Rev. A **78** (2008).

[78] F. Mintert, A. R. R. Carvalho, M. Kus, and A. Buchleitner, *Measures and dynamics of entangled states*, PhD thesis, University of Munich.

[79] C. H. Bennett, D. P. DiVincenzo, C. A. Fuchs, T. Mor, E. Rains, P. W. Shor, J. A. Smolin, and W. K. Wootters, *Quantum nonlocality without entanglement*, Phys. Rev. A **59** (1999).

[80] W. Nolting, *Viel-Teilchen-Theorie*, Springer, Berlin; Heidelberg, 2005.

[81] G. Vidal, *Entanglement monotones*, J. Mod. Opt. **47** (2000).

[82] G. Vidal, *Entanglement of pure states for a single copy*, Phys. Rev. Lett. **83** (1999).

[83] J. Eisert and M. Cramer, *Single-copy entanglement in critical spin chains*, Phys. Rev. A **72** (2005).

[84] C. H. Bennett, H. J. Bernstein, S. Popescu, and B. Schumacher, *Concentrating partial entanglement by local operations*, Phys. Rev. A **53** (1996).

[85] M. A. Nielsen, *Conditions for a class of entanglement transformations*, Phys. Rev. Lett. **83** (1999).

[86] G. Vidal, *Optimal local preparation of an arbitrary mixed state of two qubits. closed expression for the single copy case*, Phys. Rev. A **62** (2000).

[87] C. H. Bennett, S. Popescu, D. Rohrlich, J. A. Smolin, and A. V. Thapliyal, *Exact and asymptotic measures of multipartite pure-state entanglement*, Phys. Rev. A **63** (2000).

[88] W. Dür, G. Vidal, and J. I. Cirac, *Three qubits can be entangled in two inequivalent ways*, Phys. Rev. A **62** (2000).

[89] I. Peschel and J. Zhao, *On single-copy entanglement*, J. Stat. Mech. (2005).

[90] F. Verstraete, J. Dehaene, B. De Moor, and H. Verschelde, *Four qubits can be entangled in nine different ways*, Phys. Rev. A **65** (2002).

[91] M. B. Hastings, *A counterexample to additivity of minimum output entropy*, preprint, arXiv:0809.3972 (2008).

[92] W. K. Wootters, *Entanglement of formation of an arbitrary state of two qubits*, Phys. Rev. Lett. **80** (1998).

[93] A. Peres, *Separability criterion for density matrices*, Phys. Rev. Lett. **77** (1996).

[94] M. Horodecki, P. Horodecki, and R. Horodecki, *Separability of mixed states: Necessary and sufficient conditions*, Phys. Lett. A **223** (1996).

[95] G. Vidal and R. F. Werner, *A computable measure of entanglement*, Phys. Rev. A **65** (2002).

[96] J. Eisert and H. J. Briegel, *The Schmidt measure as a tool for quantifying multi-particle entanglement*, Phys. Rev. A **64** (2001).

[97] J. Eisert and D. Gross, *Multi-particle entanglement*, preprint, arXiv:quant-ph/0505149 (2006).

[98] R. Demkowicz-Dobrzanski, A. Buchleitner, M. Kus, and F. Mintert, *Evaluable multipartite entanglement measures: are multipartite concurrences entanglement monotones?*, Phys. Rev. A **74** (2006).

[99] A. Uhlmann, *Fidelity and concurrence of conjugated states*, Phys. Rev. A **62** (2000).

[100] P. Rungta, V. Bužek, C. M. Caves, M. Hillery, and G. J. Milburn, *Universal state inversion and concurrence in arbitrary dimensions*, Phys. Rev. A **64** (2001).

[101] F. Mintert, M. Kus, and A. Buchleitner, *Concurrence of mixed multipartite quantum states*, Phys. Rev. Lett. **95** (2005).

[102] F. Mintert, *Private communication.*

[103] R. B. Lehoucq, D. C. Sorensen, and C. Yang, *ARPACK User's Guide*, Soc. for Ind. and Appl. Math., 1998.

[104] F. Verstraete and J. I. Cirac, *Quantum nonlocality in the presence of superselection rules and data hiding protocols*, Phys. Rev. Lett. **91** (2003).

[105] M. R. Dowling, A. C. Doherty, and H. M. Wiseman, *Entanglement of indistinguishable particles in condensed matter physics*, Phys. Rev. A **73** (2006).

[106] S. J. Jones, H. M. Wiseman, S. D. Bartlett, J. A. Vaccaro, and D. T. Pope, *Entanglement and symmetry: A case study in superselection rules, reference frames, and beyond*, Phys. Rev. A **74** (2006).

[107] S. D. Bartlett, T. Rudolph, and R. W. Spekkens, *Reference frames, superselection rules, and quantum information*, Rev. Mod. Phys. **79** (2007).

[108] E. Arimondo, *Private communication.*

[109] J. Madroñero, *Private communication.*

[110] H. Venzl, A. J. Daley, F. Mintert, and A. Buchleitner, *Simulability and regularity of complex quantum systems*, preprint, arXiv:0808.3911 (2008).

[111] U. Schollwöck, *The density-matrix renormalization group*, Rev. Mod. Phys. **77** (2005).

[112] A. J. Daley, C. Kollath, U. Schollwöck, and G. Vidal, *Time-dependent density-matrix renormalization-group using adaptive effective Hilbert spaces*, Theor. Exp. (2004).

[113] H. Kubotani, S. Adachi, and M. Toda, *Exact formula of the distribution of Schmidt eigenvalues for dynamical formation of entanglement in quantum chaos*, Phys. Rev. Lett. **100** (2008).

Acknowledgements

Finally I would like to thank everybody who supported me during my work on this thesis. In particular, I would like to thank

- my thesis supervisor Sandro Wimberger for suggesting a very interesting topic and for his helpful guidance throughout the year. I especially want to thank him for giving me the opportunity to travel to the group of Andreas Buchleitner in Freiburg, to the group of Javier Madroñero in Munich and for inviting both Florian Mintert and Norbert Schuch to Heidelberg.
- my whole group for the nice atmosphere, for the many funny winetastings and, of course, for very valuable discussions concerning physics. I especially want to thank Patrick Plötz for always being reachable and the useful discussions, and I want to thank him and Tobias for proofreading my thesis.
- Florian Mintert for teaching me the fundamentals of entanglement theory.
- Andreas Buchleitner and his group for my stay in Freiburg and the many exciting discussions.
- Javier Madroñero for my stay in Munich and his help with the Fatunla-algoritm and numerical questions in general.
- Norbert Schuch for coming to Heidelberg and explaining difficult subjects of entanglement theory.
- all people from the Institute for Theoretical Physics for the enjoyable atmosphere and the interesting discussions over lunch or coffee: especially my group and Fabian Rühle, Johannes Held and Michael Bach.

Last but not least, I thank my parents for their support during and before my studies.

Erklärung:

Ich versichere, dass ich diese Arbeit selbstständig verfasst und keine anderen als die angegebenen Quellen und Hilfsmittel benutzt habe.

Heidelberg, den 13. März 2009

.....
(Unterschrift)